

Realistic LOCA Evaluation Methodology Applied to the Full Spectrum of Break Sizes (FULL SPECTRUM LOCA Methodology)

Volume III FULL SPECTRUM LOCA Uncertainty Methodology and Demonstration Plant Analysis

WCAP-16996-NP-A
Revision 1

**Realistic LOCA Evaluation Methodology Applied to the
Full Spectrum of Break Sizes
(FULL SPECTRUM LOCA Methodology)**

Jeffrey R. Kobelak	LOCA Integrated Services
Dr. Katsuhiro Ohkawa	LOCA Integrated Services
Dr. Liping Cao	LOCA Integrated Services
Aaron M. Everhard	LOCA Integrated Services
Dr. Jun Liao	LOCA Integrated Services
Nikolay P. Petkov	LOCA Integrated Services
Michael A. Shockling	LOCA Integrated Services

November 2016

Prepared by: Jeffrey R. Kobelak*
LOCA Integrated Services

Reviewer: Michael A. Shockling*
LOCA Integrated Services

Approved: Amy J. Colussy*, Manager
LOCA Integrated Services

AP1000, FSLOCA, FULL SPECTRUM, ZIRLO, and Optimized ZIRLO are trademarks or registered trademarks of Westinghouse Electric Company LLC, its affiliates and/or its subsidiaries in the United States of America and may be registered in other countries throughout the world. All rights reserved. Unauthorized use is strictly prohibited. Other names may be trademarks of their respective owners.

*Electronically approved records are authenticated in the electronic document management system.

Westinghouse Electric Company LLC
1000 Westinghouse Drive
Cranberry Township, PA 16066, USA

© 2016 Westinghouse Electric Company LLC
All Rights Reserved

TABLE OF CONTENTS

LIST OF TABLES	v
----------------------	---

LIST OF FIGURES	vii
-----------------------	-----

VOLUME III

25	PLANT SOURCES OF UNCERTAINTY	25-1
25.1	PLANT PHYSICAL CONFIGURATION	25-1
25.2	PLANT INITIAL OPERATING CONDITIONS	25-7
25.2.1	Core Power Parameters	25-8
25.2.2	Plant Fluid Conditions	25-25
25.3	REACTOR ACCIDENT BOUNDARY CONDITIONS	25-45
25.4	MODEL PARAMETERS	25-49
25.5	OPERATOR ACTIONS	25-49
25.5.1	EOP Sequences for a Small Break LOCA	25-50
25.5.2	Variability of Plant Conditions Due to Operation Actions	25-51
25.6	CONTAINMENT RESPONSE	25-57
25.7	PUMP LOCKED ROTOR	25-58
25.8	REFERENCES	25-62
26	<u>W</u> COBRA/TRAC-TF2 MODEL OF PILOT PLANTS	26-1
26.1	MODELING APPROACH	26-1
26.1.1	Introduction	26-1
26.1.2	Modeling Consistency	26-2
26.1.3	Conclusions	26-5
26.2	V. C. SUMMER NUCLEAR POWER PLANT	26-10
26.2.1	V. C. Summer <u>W</u> COBRA/TRAC-TF2 Nodalization	26-10
26.2.2	V. C. Summer Reference Case and Allowable Plant Operating Conditions	26-17
26.2.3	Plant Operating Range	26-21
26.3	BEAVER VALLEY UNIT 1 NUCLEAR POWER PLANT	26-34
26.3.1	Beaver Valley Unit 1 <u>W</u> COBRA/TRAC-TF2 Nodalization	26-34
26.3.2	Beaver Valley Unit 1 Reference Case and Allowable Plant Operating Conditions	26-41
26.3.3	Plant Operating Range	26-45
26.4	STEADY STATE CALCULATION/CALIBRATION	26-64
26.5	REFERENCES	26-67

27	REFERENCE BREAK SPECTRUM ANALYSIS	27-1
27.1	LARGE, INTERMEDIATE, AND SMALL BREAK SPECTRA	27-1
27.1.1	V. C. Summer (CGE) Break Spectra	27-1
27.1.2	Beaver Valley Unit 1 (DLW) Break Spectra.....	27-26
27.2	V. C. SUMMER (CGE) REFERENCE TRANSIENTS	27-49
27.2.1	CGE Large Break Reference Transient Description.....	27-49
27.2.2	CGE Intermediate Break Reference Transient Description.....	27-64
27.2.3	CGE Small Break Reference Transient Description.....	27-76
27.3	BEAVER VALLEY UNIT 1 (DLW) REFERENCE TRANSIENTS	27-91
27.3.1	DLW Large Break Reference Transient Description	27-91
27.3.2	DLW Intermediate Break Reference Transient Description	27-106
27.3.3	DLW Small Break Reference Transient Description.....	27-118
28	SCOPING AND SENSITIVITY STUDIES	28-1
28.1	LARGE BREAK SCOPING STUDY RESULTS	28-3
28.1.1	Axial Power Distributions – LBLOCA	28-3
28.1.2	Offsite Power Availability – LBLOCA	28-17
28.1.3	Time Step and Convergence Criteria Studies – LBLOCA	28-32
28.1.4	Break Path Resistance – LBLOCA	28-43
28.1.5	Treatment of Accumulator Elevation – LBLOCA.....	28-82
28.1.6	Steam Generator Hydraulics: Tube Plugging – LBLOCA	28-93
28.2	SMALL BREAK SCOPING STUDY RESULTS	28-108
28.2.1	Small Break Reference Transient	28-108
28.2.2	Axial Power Distributions – SBLOCA	28-108
28.2.3	Initial and Accident Boundary Conditions and Offsite Power – SBLOCA	28-128
28.2.4	Time Step and Convergence Criteria Studies – SBLOCA	28-150
28.2.5	Treatment of Accumulator Elevation – SBLOCA	28-157
28.2.6	Break Location in the Accumulator and SI Lines – SBLOCA	28-161
28.2.7	Break Orientation Studies – SBLOCA	28-171
28.2.8	Interfacial Drag in the Core (Level Swell) – SBLOCA	28-187
28.2.9	Steam Generator Hydraulics: Tube Plugging – SBLOCA	28-205
28.2.10	Steam Generator Hydraulics: Interfacial Drag – SBLOCA	28-219
28.2.11	Loop Seal Clearance – SBLOCA	28-236
28.2.12	Horizontal Stratified Flow (HS_SLUG) – SBLOCA	28-244
29	ASSESSMENT OF UNCERTAINTY ELEMENTS	29-1
29.1	GENERATION OF MODEL UNCERTAINTY PARAMETERS AND RANGING DISTRIBUTIONS	29-12
29.1.1	Break Flow – [29-12
] ^{a,c}	29-12
29.1.2	Broken Cold-Leg Nozzle Flow Resistance (KN) and Broken Loop Pump Resistance	29-21
29.1.3	Delivery and Bypassing of ECC – Bounding Approach	29-23

TABLE OF CONTENTS (cont.)

29.1.4	Condensation in the Downcomer	29-23
29.1.5	Interfacial Drag in the Core Region [$J^{a,c}$]	29-24
29.1.6	Cold Leg Condensation (KCOSI).....	29-32
29.1.7	Horizontal Stratified Flow Regime Transition Boundary (HS_SLUG).....	29-33
29.1.8	Minimum Film Boiling Temperature (T_{min}).....	29-33
29.1.9	Steam Binding and Entrainment – Bounding Approach.....	29-42
29.1.10	Non Condensable Gases/Accumulator Nitrogen – Bounding Approach.....	29-42
29.1.11	Uncertainty in Loop Seal Clearance Phenomenon	29-42
29.1.12	Steam Generator Thermal-Hydraulics	29-46
29.2	BREAK LOCATION, TYPE (SPLIT VS. DEGCL) AND SPLIT BREAK AREA	29-47
29.2.1	[$J^{a,c}$]	29-48
29.2.2	Determination of the Minimum Break Area (A_{min})	29-49
29.2.3	Break Type and Split Break Area Uncertainty Methodology	29-49
29.2.4	Modeling of DEGCL Breaks and Break Flow Uncertainty.....	29-54
29.2.5	Modeling of Split Breaks and Break Flow Uncertainty	29-57
29.2.6	Compliance with Regulatory Guide 1.157 on Break Type and Size	29-61
29.3	REVIEW OF PLANT SCOPING STUDIES AND UNCERTAINTY IN PLANT INPUT PARAMETERS	29-62
29.3.1	Bounded Parameters	29-62
29.3.2	Initial and Boundary Conditions (Ranged Parameters)	29-64
29.3.3	Uncertainty Associated with Maximum Time Step Size	29-67
29.4	CORE AND FUEL ROD MODEL UNCERTAINTIES	29-68
29.4.1	Initial Reactor State Uncertainties.....	29-68
29.4.2	Hot Rod Local Models Uncertainty.....	29-90
29.4.3	Fuel Rod: Uncertainty on Heat Transfer to the Fluid	29-118
29.5	EVALUATION MODEL BIASES AND UNCERTAINTY (EMDAP STEP 20)	29-137
29.5.1	Fuel Rod	29-137
29.5.2	Core	29-138
29.5.3	Upper Head.....	29-140
29.5.4	Upper Plenum.....	29-141
29.5.5	Steam Generator	29-142
29.5.6	Pump Suction Piping/Loop Seal.....	29-143
29.5.7	Pump.....	29-143
29.5.8	Cold Leg/Safety Injection.....	29-144
29.5.9	Accumulator	29-146
29.5.10	Downcomer	29-146
29.5.11	Lower Plenum	29-148
29.5.12	Break.....	29-148
29.6	EXPERIMENTAL UNCERTAINTIES (EMDAP STEP 9).....	29-149
29.7	REFERENCES	29-150

TABLE OF CONTENTS (cont.)

30	TECHNICAL BASIS OF STATISTICAL PROCEDURES APPLIED IN FULL SPECTRUM LOCA UNCERTAINTY METHODOLOGY	30-1
30.1	STATISTICAL METHODOLOGY ROADMAP	30-1
30.2	STATISTICAL SAMPLING APPROACH (MONTE CARLO)	30-4
30.3	NON-PARAMETRIC ORDER-STATISTICS TOLERANCE LIMITS FORMULATION	30-5
30.3.1	Tolerance Intervals and Sample Size	30-10
30.4	[.....] ^{a,c}	30-10
30.5	OVERVIEW OF FULL SPECTRUM LOCA STATISTICAL PROCEDURE	30-11
30.6	CONCLUSIONS ON COMPLIANCE WITH 10 CFR 50.46 ACCEPTANCE CRITERIA	30-13
30.6.1	[.....] ^{a,c}	30-13
30.6.2	[.....] ^{a,c}	30-13
30.7	REFERENCES	30-15
31	FULL SPECTRUM LOCA DEMONSTRATION ANALYSIS	31-1
31.1	DEVELOPMENT OF INITIAL MATRIX	31-1
31.1.1	Break Area Ranges	31-2
31.1.2	Plant Operating Range	31-2
31.2	ANALYSIS EXECUTION	31-6
31.2.1	[.....] ^{a,c}	31-7
31.2.2	[.....] ^{a,c}	31-13
31.2.3	Conclusion	31-14
31.3	ANALYSIS OF RESULTS [.....] ^{a,c}	31-14
31.4	ANALYSIS OF RESULTS [.....] ^{a,c}	31-41
31.5	SUMMARY REPORT AND COMPLIANCE WITH 10 CFR 50.46 CRITERIA	31-56
32	METHODOLOGY SUMMARY	32-1
32.1	COMPLIANCE WITH 10 CFR 50.46	32-1
32.2	COMPLIANCE WITH REGULATORY GUIDE 1.203	32-2
32.2.1	Regulatory Position 1, "Evaluation Model Development and Assessment Process"	32-2
32.2.2	Regulatory Position 2, "Quality Assurance"	32-15
32.2.3	Regulatory Position 3, "Documentation"	32-15
32.2.4	Regulatory Position 4, "General Purpose Computer Programs"	32-16
32.2.5	Regulatory Position 5, "Graded Approach to Applying the EMDAP Process"	32-17
32.3	COMPLIANCE WITH REGULATORY POSITION WITH RESPECT TO THE UNCERTAINTY METHODOLOGY	32-17
32.3.1	Regulatory Position 4, "Estimation of Overall Calculational Uncertainty"	32-17
32.4	METHODOLOGY LIMITATIONS	32-21
32.5	REFERENCES	32-21

LIST OF TABLES

VOLUME III

Table 25.2-1	Hot Assembly Rod Power Census Summary for Westinghouse Fuel.....	25-29
Table 25.2-2	Peaking Factor Uncertainties.....	25-29
Table 25.2-3	Rod Bow F_Q Uncertainties.....	25-30
Table 25.2-4	Typical Westinghouse Plant Operation Parameters	25-30
Table 25.5-1	Condensed EOPs for Indian Point Unit 2, Short-Term Portion	25-54
Table 26.1-1	Core Section Axial Cell Lengths	26-7
Table 26.1-2	Hot Leg Noding Comparison	26-8
Table 26.1-3	Steam Generator Noding Comparison.....	26-8
Table 26.1-4	Crossover Leg Noding.....	26-8
Table 26.1-5	Cold Leg Noding	26-9
Table 26.2-1	Key LOCA Parameters and Scoping Study Values for V. C. Summer	26-22
Table 26.3-1	Key LOCA Parameters and Scoping Study Values for Beaver Valley Unit 1	26-46
Table 26.4-1	Criteria for an Acceptable Steady-State.....	26-66
Table 28.1.3-1	DTMAX Values used in LBLOCA Timestep Sensitivity	28-33
Table 28.1.3-2	PCT Results When Varying DTMAX, CGE LBLOCA Sensitivity.....	28-33
Table 28.1.3-3	PCT Results When Varying DTMAX, DLW LBLOCA Sensitivity	28-34
Table 28.1.4-1	Scenarios for Break Path Resistance Sensitivity Study	28-43
Table 28.2.9-1	[] ^{a,c}	28-206
Table 28.2.12-1	Flow Regime Flags.....	28-246
Table 28.2.12-2	[] ^{a,c}	28-247
Table 28.2.12-3	[] ^{a,c}	28-248
Table 29-1	Uncertainty Elements – Break Location, Type, Orientation and Area Sampling Methodology.....	29-5
Table 29-2	Uncertainty Elements – Thermal-Hydraulic Models.....	29-6
Table 29-3a	Uncertainty Elements – Local Models [] ^{a,c}	29-7
Table 29-3b	Burst Strain for [] ^{a,c}	29-9
Table 29-4	Uncertainty Elements – Power-Related Parameters Defined in Section 29.4.1	29-10
Table 29-5	Uncertainty Elements - Initial and Boundary Conditions Considered in Uncertainty Methodology Defined in Section 29.3.2	29-11
Table 29.1.2-1	Nozzle Loss Coefficient Assessment Data Base.....	29-22

LIST OF TABLES (cont.)

Table 29.2.3-1	[$J^{a,c}$	29-52
Table 29.3.2-1	Comparison of Measured and Calculated Accumulator Line Resistances		29-66
Table 29.4.1-1	[$J^{a,c}$	29-77
Table 29.4.2-1	Packing Fractions Using Various Measurements.....		29-108
Table 29.4.2-2a	Zircaloy Rate Constants (Total Oxygen)		29-112
Table 29.4.2-2b	[$J^{a,c}$	29-112
Table 29.4.2-3	Predictions Using Equation 29.4.2-8 and Cathcart-Pawel.....		29-113
Table 29.4.3-1	[$J^{a,c}$	29-124
Table 29.4.3-2	[$J^{a,c}$	29-124
Table 30-1	[$J^{a,c}$	30-16
Table 30-2	[$J^{a,c}$	30-17
Table 30-3	Generic Rod Power Census Used for Core-Wide Oxidation Assessment		30-18
Table 31.1-1	Nominal and Uncertainty Range of Plant Specific Uncertainty Contributors		31-3
Table 31.1-2a	[$J^{a,c}$	31-4
Table 31.1-2b	[$J^{a,c}$	31-4
Table 31.1-2c	[$J^{a,c}$	31-4
Table 31.1-3	[$J^{a,c}$	31-5
Table 31.2-1	[$J^{a,c}$	31-8
Table 31.2-2a	[$J^{a,c}$	31-13
Table 31.2-2b	[$J^{a,c}$	31-13
Table 31.3-1a	Uncertainty Attributes [$J^{a,c}$	31-17
Table 31.3-1b	Results for [$J^{a,c}$	31-18
Table 31.4-1a	Uncertainty Attributes [$J^{a,c}$	31-43
Table 31.4-1b	Results [$J^{a,c}$	31-44
Table 31.5-1	[$J^{a,c}$	31-57
Table 32-1	Summary of Assessment Results and Uncertainty Treatment for High PIRT Ranked Phenomena		32-4

LIST OF FIGURES

VOLUME III

Figure 25.2-1	Typical Assembly Power Map and Assembly Power Distribution, Beginning of Cycle	25-31
Figure 25.2-2	Typical Assembly Power Map and Assembly Power Distribution, End of Cycle.....	25-32
Figure 25.2-3	Typical Hot Assembly Fuel Rod Power Distribution.....	25-33
Figure 25.2-4	Hot Assembly Rod Power Census for Typical Westinghouse Fuel Designs	25-34
Figure 25.2-5	Relative Axial Power Distribution near Beginning of Cycle, Middle of Cycle and End of Cycle During Full Power Steady-State Conditions	25-35
Figure 25.2-6	Typical Transient Axial Power Distributions near Beginning of Cycle	25-36
Figure 25.2-7	Typical Transient Axial Power Distributions near Middle of Cycle	25-37
Figure 25.2-8	Typical Transient Axial Power Distributions near End of Cycle	25-38
Figure 25.2-9	[$\int^{a,c}$	25-39
Figure 25.2-10	Effect of Load Follow Maneuver Period on Decay Heat Equilibrium Fraction for Various Times After Trip	25-40
Figure 25.2-11	Typical Measurement of Enthalpy Rise Hot Channel Factor $F_{\Delta H}$	25-41
Figure 25.2-12	Typical Measurement of Total Peaking Factor F_Q	25-42
Figure 25.2-13	[$\int^{a,c}$	25-43
Figure 25.2-14	Typical WCOBRA/TRAC-TF2 Axial Power Distribution	25-44
Figure 25.7-1	Comparison of Analysis and Experiment for Scale Model Flywheel Tests	25-60
Figure 25.7-2	[$\int^{a,c}$	25-61
Figure 26.2-1	Virgil C. Summer Vessel Profile	26-23
Figure 26.2-2	Virgil C. Summer Vessel Component Elevations.....	26-24
Figure 26.2-3	Virgil C. Summer Vessel Model Noding Diagram.....	26-25
Figure 26.2-4	Virgil C. Summer Vessel Sections 1 through 3	26-26
Figure 26.2-5	Virgil C. Summer Vessel Sections 4 through 6	26-27
Figure 26.2-6	Virgil C. Summer Vessel Sections 7 through 9	26-28
Figure 26.2-7	Virgil C. Summer Upper Plenum Structure Map	26-29

LIST OF FIGURES (cont.)

Figure 26.2-8	Virgil C. Summer Loop Model Noding Diagram	26-30
Figure 26.2-9	Virgil C. Summer Steam Generator Component Noding Diagram.....	26-31
Figure 26.2-10a	Virgil C. Summer Reference Case Axial Power Distribution for LBLOCA and IBLOCA	26-32
Figure 26.2-10b	Virgil C. Summer Reference Case Axial Power Distribution for SBLOCA	26-33
Figure 26.3-1	Beaver Valley Unit 1 Vessel Profile	26-47
Figure 26.3-2	Beaver Valley Unit 1 Vessel Component Elevations.....	26-48
Figure 26.3-3	Beaver Valley Unit 1 Vessel Model Noding Diagram.....	26-49
Figure 26.3-4	Beaver Valley Unit 1 Vessel Section 1	26-50
Figure 26.3-5	Beaver Valley Unit 1 Vessel Section 2	26-51
Figure 26.3-6	Beaver Valley Unit 1 Vessel Section 3	26-52
Figure 26.3-7	Beaver Valley Unit 1 Vessel Section 4	26-53
Figure 26.3-8	Beaver Valley Unit 1 Vessel Section 5	26-54
Figure 26.3-9	Beaver Valley Unit 1 Vessel Section 6	26-55
Figure 26.3-10	Beaver Valley Unit 1 Vessel Section 7	26-56
Figure 26.3-11	Beaver Valley Unit 1 Vessel Section 8	26-57
Figure 26.3-12	Beaver Valley Unit 1 Vessel Section 9	26-58
Figure 26.3-13	Beaver Valley Unit 1 Upper Plenum Structure Map	26-59
Figure 26.3-14	Beaver Valley Unit 1 Loop Model Noding Diagram	26-60
Figure 26.3-15	Beaver Valley Unit 1 Steam Generator Component Noding Diagram.....	26-61
Figure 26.3-16a	Beaver Valley Unit 1 Reference Case Axial Power Distribution for LBLOCA and IBLOCA	26-62
Figure 26.3-16b	Beaver Valley Unit 1 Reference Case Axial Power Distribution for SBLOCA.....	26-63
Figure 27.1.1.1-1	Hot Rod Peak Cladding Temperature, CGE LBLOCA.....	27-3
Figure 27.1.1.1-2	Hot Rod Peak Cladding Temperature Elevation, CGE LBLOCA	27-4
Figure 27.1.1.1-3	Break Flow, CGE LBLOCA	27-5
Figure 27.1.1.1-4	RCS Pressure, CGE LBLOCA.....	27-6
Figure 27.1.1.1-5	Accumulator Mass Flow Rate, CGE LBLOCA.....	27-7
Figure 27.1.1.1-6	Vessel Fluid Mass, CGE LBLOCA.....	27-8

LIST OF FIGURES (cont.)

Figure 27.1.1.1-7	Safety Injection Flow Rate, CGE LBLOCA.....	27-9
Figure 27.1.1.1-8	Containment Pressure, CGE LBLOCA.....	27-10
Figure 27.1.1.2-1	Hot Rod Peak Cladding Temperature, CGE IBLOCA.....	27-12
Figure 27.1.1.2-2	Break Flow, CGE IBLOCA	27-13
Figure 27.1.1.2-3	RCS Pressure, CGE IBLOCA.....	27-14
Figure 27.1.1.2-4	Accumulator Mass Flow Rate, CGE IBLOCA	27-15
Figure 27.1.1.2-5	Vessel Fluid Mass, CGE IBLOCA.....	27-16
Figure 27.1.1.3-1	Break Void Fraction, CGE SBLOCA.....	27-18
Figure 27.1.1.3-2	RCS Pressure, CGE SBLOCA.....	27-19
Figure 27.1.1.3-3	Upper Head Collapsed Liquid Level, CGE SBLOCA	27-20
Figure 27.1.1.3-4	Break Flow, CGE SBLOCA	27-21
Figure 27.1.1.3-5	Hot Rod Peak Cladding Temperature, CGE SBLOCA.....	27-22
Figure 27.1.1.3-6	Loop 1 Loop Seal Differential Pressure, CGE SBLOCA	27-23
Figure 27.1.1.3-7	Loop 2 Loop Seal Differential Pressure, CGE SBLOCA	27-24
Figure 27.1.1.3-8	Loop 3 Loop Seal Differential Pressure, CGE SBLOCA	27-25
Figure 27.1.2.1-1	Hot Rod Peak Cladding Temperature, DLW LBLOCA.....	27-27
Figure 27.1.2.1-2	Hot Rod Peak Cladding Temperature Elevation, DLW LBLOCA.....	27-28
Figure 27.1.2.1-3	Break Flow, DLW LBLOCA	27-29
Figure 27.1.2.1-4	RCS Pressure, DLW LBLOCA.....	27-30
Figure 27.1.2.1-5	Accumulator Mass Flow Rate, DLW LBLOCA	27-31
Figure 27.1.2.1-6	Vessel Fluid Mass, DLW LBLOCA.....	27-32
Figure 27.1.2.1-7	Safety Injection Flow Rate, DLW LBLOCA	27-33
Figure 27.1.2.1-8	Containment Pressure, DLW LBLOCA.....	27-34
Figure 27.1.2.2-1	Hot Rod Peak Cladding Temperature, DLW IBLOCA.....	27-36
Figure 27.1.2.2-2	Break Flow, DLW IBLOCA.....	27-37
Figure 27.1.2.2-3	RCS Pressure, DLW IBLOCA.....	27-38
Figure 27.1.2.2-4	Accumulator Mass Flow Rate, DLW IBLOCA	27-39
Figure 27.1.2.2-5	Vessel Fluid Mass, DLW IBLOCA	27-40
Figure 27.1.2.3-1	RCS Pressure, DLW SBLOCA	27-42

LIST OF FIGURES (cont.)

Figure 27.1.2.3-2	Upper Head Collapsed Liquid Level, DLW SBLOCA	27-43
Figure 27.1.2.3-3	Break Flow, DLW SBLOCA.....	27-44
Figure 27.1.2.3-4	Hot Rod Peak Cladding Temperature, DLW SBLOCA	27-45
Figure 27.1.2.3-5	Loop 1 Loop Seal Differential Pressure, DLW SBLOCA	27-46
Figure 27.1.2.3-6	Loop 2 Loop Seal Differential Pressure, DLW SBLOCA	27-47
Figure 27.1.2.3-7	Loop 3 Loop Seal Differential Pressure, DLW SBLOCA	27-48
Figure 27.2.1-1	Peak Cladding Temperatures, CGE LBLOCA Reference Transient	27-51
Figure 27.2.1-2	Hot Rod Peak Cladding Temperature Elevation, CGE LBLOCA Reference Transient.....	27-52
Figure 27.2.1-3	Vessel Side Break Flow, CGE LBLOCA Reference Transient	27-53
Figure 27.2.1-4	Pump Side Break Flow, CGE LBLOCA Reference Transient	27-54
Figure 27.2.1-5	Lower Plenum Collapsed Liquid Level, CGE LBLOCA Reference Transient.....	27-55
Figure 27.2.1-6	Vapor Mass Flow Rate in Hot Assembly Near PCT Elevation, CGE LBLOCA Reference Transient.....	27-56
Figure 27.2.1-7	RCS Pressure, CGE LBLOCA Reference Transient.....	27-57
Figure 27.2.1-8	Accumulator Mass Flow Rate, CGE LBLOCA Reference Transient	27-58
Figure 27.2.1-9	Containment Pressure, CGE LBLOCA Reference Transient.....	27-59
Figure 27.2.1-10	Vessel Fluid Mass, CGE LBLOCA Reference Transient.....	27-60
Figure 27.2.1-11	Core Collapsed Liquid Levels, CGE LBLOCA Reference Transient.....	27-61
Figure 27.2.1-12	Downcomer Collapsed Liquid Level, CGE LBLOCA Reference Transient.....	27-62
Figure 27.2.1-13	Safety Injection Flow, CGE LBLOCA Reference Transient.....	27-63
Figure 27.2.2-1	Break Flow, CGE IBLOCA Reference Transient.....	27-65
Figure 27.2.2-2	Void Fraction at the Break, CGE IBLOCA Reference Transient	27-66
Figure 27.2.2-3	RCS Pressure, CGE IBLOCA Reference Transient.....	27-67
Figure 27.2.2-4	Core Collapsed Liquid Levels, CGE IBLOCA Reference Transient (2=Low Power, 3=OH/SC/FSM, 4=Guide Tube, 5=Hot Assembly)	27-68
Figure 27.2.2-5	Downcomer Collapsed Liquid Levels, CGE IBLOCA Reference Transient	27-69
Figure 27.2.2-6	Peak Cladding Temperatures, CGE IBLOCA Reference Transient	27-70
Figure 27.2.2-7	Vapor Flowrate in the Hot Assembly, CGE IBLOCA Reference Transient.....	27-71
Figure 27.2.2-8	Accumulator Mass Flow Rate, CGE IBLOCA Reference Transient	27-72

LIST OF FIGURES (cont.)

Figure 27.2.2-9	Vessel Fluid Mass, CGE IBLOCA Reference Transient	27-73
Figure 27.2.2-10	Safety Injection Flow, CGE IBLOCA Reference Transient.....	27-74
Figure 27.2.2-11	Safety Injection and Break Flow, CGE IBLOCA Reference Transient	27-75
Figure 27.2.3-1	Void Fraction at the Break, CGE SBLOCA Reference Transient	27-78
Figure 27.2.3-2	Safety Injection Flow, CGE SBLOCA Reference Transient.....	27-79
Figure 27.2.3-3	RCS and Steam Generator Secondary Side Pressure, CGE SBLOCA Reference Transient.....	27-80
Figure 27.2.3-4	Upper Head Collapsed Liquid Level, CGE SBLOCA Reference Transient	27-81
Figure 27.2.3-5	Break Flow, CGE SBLOCA Reference Transient.....	27-82
Figure 27.2.3-6	Core Collapsed Liquid Levels, CGE SBLOCA Reference Transient (2=Low Power, 3=OH/SC/FSM, 4=Guide Tube, 5=Hot Assembly)	27-83
Figure 27.2.3-7	Hot Rod Cladding Temperature, CGE SBLOCA Reference Transient.....	27-84
Figure 27.2.3-8	Loop 1 Loop Seal Differential Pressure, CGE SBLOCA Reference Transient.....	27-85
Figure 27.2.3-9	Loop 2 Loop Seal Differential Pressure, CGE SBLOCA Reference Transient.....	27-86
Figure 27.2.3-10	Loop 3 Loop Seal Differential Pressure, CGE SBLOCA Reference Transient.....	27-87
Figure 27.2.3-11	Accumulator Mass Flow Rate, CGE SBLOCA Reference Transient	27-88
Figure 27.2.3-12	Vessel Fluid Mass, CGE SBLOCA Reference Transient	27-89
Figure 27.2.3-13	Safety Injection and Break Flow, CGE SBLOCA Reference Transient.....	27-90
Figure 27.3.1-1	Peak Cladding Temperatures, DLW LBLOCA Reference Transient	27-93
Figure 27.3.1-2	Hot Rod Peak Cladding Temperature Elevation, DLW LBLOCA Reference Transient.....	27-94
Figure 27.3.1-3	Vessel Side Break Flow, DLW LBLOCA Reference Transient	27-95
Figure 27.3.1-4	Pump Side Break Flow, DLW LBLOCA Reference Transient	27-96
Figure 27.3.1-5	Lower Plenum Collapsed Liquid Level, DLW LBLOCA Reference Transient.....	27-97
Figure 27.3.1-6	Vapor Mass Flow in Hot Assembly Near PCT Elevation, DLW LBLOCA Reference Transient.....	27-98
Figure 27.3.1-7	RCS Pressure, DLW LBLOCA Reference Transient	27-99
Figure 27.3.1-8	Accumulator Mass Flow Rate, DLW LBLOCA Reference Transient	27-100

LIST OF FIGURES (cont.)

Figure 27.3.1-9	Containment Pressure, DLW LBLOCA Reference Transient	27-101
Figure 27.3.1-10	Vessel Fluid Mass, DLW LBLOCA Reference Transient	27-102
Figure 27.3.1-11	Core Collapsed Liquid Levels, DLW LBLOCA Reference Transient	27-103
Figure 27.3.1-12	Downcomer Collapsed Liquid Level, DLW LBLOCA Reference Transient...	27-104
Figure 27.3.1-13	Safety Injection Flow, DLW LBLOCA Reference Transient.....	27-105
Figure 27.3.2-1	Break Flow, DLW IBLOCA Reference Transient.....	27-107
Figure 27.3.2-2	Void Fraction at the Break, DLW IBLOCA Reference Transient	27-108
Figure 27.3.2-3	RCS Pressure, DLW IBLOCA Reference Transient	27-109
Figure 27.3.2-4	Core Collapsed Liquid Levels, DLW IBLOCA Reference Transient (2=Low Power, 3=OH/SC/FSM, 4=Guide Tube, 5=Hot Assembly)	27-110
Figure 27.3.2-5	Downcomer Collapsed Liquid Levels, DLW IBLOCA Reference Transient ..	27-111
Figure 27.3.2-6	Peak Cladding Temperatures, DLW IBLOCA Reference Transient	27-112
Figure 27.3.2-7	Vapor Flowrate in Hot Assembly Channel, DLW IBLOCA Reference Transient.....	27-113
Figure 27.3.2-8	Accumulator Mass Flow Rate, DLW IBLOCA Reference Transient.....	27-114
Figure 27.3.2-9	Vessel Fluid Mass, DLW IBLOCA Reference Transient	27-115
Figure 27.3.2-10	Safety Injection Flow, DLW IBLOCA Reference Transient.....	27-116
Figure 27.3.2-11	Safety Injection and Break Flow, DLW IBLOCA Reference Transient.....	27-117
Figure 27.3.3-1	Void Fraction at the Break, DLW SBLOCA Reference Transient	27-120
Figure 27.3.3-2	Safety Injection Flow, DLW SBLOCA Reference Transient	27-121
Figure 27.3.3-3	RCS and Steam Generator Secondary Side Pressure, DLW SBLOCA Reference Transient.....	27-122
Figure 27.3.3-4	Upper Head Collapsed Liquid Level, DLW SBLOCA Reference Transient ...	27-123
Figure 27.3.3-5	Break Flow, DLW SBLOCA Reference Transient.....	27-124
Figure 27.3.3-6	Core Collapsed Liquid Levels, DLW SBLOCA Reference Transient (2=Low Power, 3=OH/SC/FSM, 4=Guide Tube, 5=Hot Assembly)	27-125
Figure 27.3.3-7	Hot Rod Cladding Temperature, DLW SBLOCA Reference Transient	27-126
Figure 27.3.3-8	Loop 1 Loop Seal Differential Pressure, DLW SBLOCA Reference Transient.....	27-127
Figure 27.3.3-9	Loop 2 Loop Seal Differential Pressure, DLW SBLOCA Reference Transient.....	27-128

LIST OF FIGURES (cont.)

Figure 27.3.3-10	Loop 3 Loop Seal Differential Pressure, DLW SBLOCA Reference Transient.....	27-129
Figure 27.3.3-11	Accumulator Mass Flow Rate, DLW SBLOCA Reference Transient.....	27-130
Figure 27.3.3-12	Vessel Fluid Mass, DLW SBLOCA Reference Transient	27-131
Figure 27.3.3-13	Safety Injection Flow and Break Flow, DLW SBLOCA Reference Transient.....	27-132
Figure 28.1.1-1	Axial Power Distribution, CGE Axial Power Distribution Sensitivity	28-5
Figure 28.1.1-2	Rod 1 Peak Cladding Temperatures, CGE Axial Power Distribution Sensitivity	28-6
Figure 28.1.1-3	Peak Cladding Temperature Location, CGE Axial Power Distribution Sensitivity	28-7
Figure 28.1.1-4	Lower Plenum Collapsed Liquid Level, CGE Axial Power Distribution Sensitivity	28-8
Figure 28.1.1-5	Hot Assembly Collapsed Liquid Level, CGE Axial Power Distribution Sensitivity	28-9
Figure 28.1.1-6	Vessel Fluid Mass, CGE Axial Power Distribution Sensitivity	28-10
Figure 28.1.1-7	Axial Power Distribution, DLW Axial Power Distribution Sensitivity	28-11
Figure 28.1.1-8	Peak Cladding Temperatures, DLW Axial Power Distribution Sensitivity	28-12
Figure 28.1.1-9	Peak Cladding Temperature Location, DLW Axial Power Distribution Sensitivity	28-13
Figure 28.1.1-10	Lower Plenum Collapsed Liquid Level, DLW Axial Power Distribution Sensitivity	28-14
Figure 28.1.1-11	Hot Assembly Collapsed Liquid Level, DLW Axial Power Distribution Sensitivity	28-15
Figure 28.1.1-12	Vessel Fluid Mass, DLW Axial Power Distribution Sensitivity	28-16
Figure 28.1.2-1	Safety Injection Flow, CGE Offsite Power Availability Sensitivity.....	28-19
Figure 28.1.2-2	Intact Loop Pump Speed, CGE Offsite Power Availability Sensitivity	28-20
Figure 28.1.2-3	Broken Loop Pump Speed, CGE Offsite Power Availability Sensitivity.....	28-21
Figure 28.1.2-4	Accumulator and Safety Injection Flow Rates, CGE Offsite Power Availability Sensitivity.....	28-22
Figure 28.1.2-5	Hot Assembly Vapor Mass Flow Rate, CGE Offsite Power Availability Sensitivity.....	28-23
Figure 28.1.2-6	Peak Cladding Temperatures, CGE Offsite Power Availability Sensitivity	28-24

LIST OF FIGURES (cont.)

Figure 28.1.2-7	Safety Injection Flow, DLW Offsite Power Availability Study.....	28-25
Figure 28.1.2-8	Intact Loop Pump Speed, DLW Offsite Power Availability Study	28-26
Figure 28.1.2-9	Broken Loop Pump Speed, DLW Offsite Power Availability Study.....	28-27
Figure 28.1.2-10	Peak Cladding Temperature, DLW Offsite Power Availability Study.....	28-28
Figure 28.1.2-11	Hot Assembly Vapor Mass Flow Rate, DLW Offsite Power Availability Study.....	28-29
Figure 28.1.2-12	Accumulator and Safety Injection Flow Rates, DLW Offsite Power Availability Sensitivity.....	28-30
Figure 28.1.2-13	Lower Plenum Collapsed Liquid Level, DLW Offsite Power Availability Study.....	28-31
Figure 28.1.3-1	Vessel Fluid Mass, run010 of CGE Timestep Sensitivity Study (DTMAX).....	28-35
Figure 28.1.3-2	Peak Cladding Temperature, run010 of CGE Timestep Sensitivity Study (DTMAX)	28-36
Figure 28.1.3-3	Vessel Fluid Mass, run008 of CGE Timestep Sensitivity Study (DTMAX).....	28-37
Figure 28.1.3-4	Peak Cladding Temperature, run008 of CGE Timestep Sensitivity Study (DTMAX)	28-38
Figure 28.1.3-5	Vessel Fluid Mass, run004 of DLW Timestep Sensitivity Study (DTMAX)	28-39
Figure 28.1.3-6	Peak Cladding Temperature, run004 of DLW Timestep Sensitivity Study (DTMAX)	28-40
Figure 28.1.3-7	Vessel Fluid Mass, run010 of DLW Timestep Sensitivity Study (DTMAX)	28-41
Figure 28.1.3-8	Peak Cladding Temperature, run010 of DLW Timestep Sensitivity Study (DTMAX)	28-42
Figure 28.1.4-1	[] ^{a,c}	28-46
Figure 28.1.4-2	[] ^{a,c}	28-47
Figure 28.1.4-3	[] ^{a,c}	28-48
Figure 28.1.4-4	[] ^{a,c}	28-49
Figure 28.1.4-5	[] ^{a,c}	28-50

LIST OF FIGURES (cont.)

Figure 28.1.4-6	[] ^{a,c}	28-51
Figure 28.1.4-7	[] ^{a,c}	28-52
Figure 28.1.4-8	[] ^{a,c}	28-53
Figure 28.1.4-9	[] ^{a,c}	28-54
Figure 28.1.4-10	[] ^{a,c}	28-55
Figure 28.1.4-11	[] ^{a,c}	28-56
Figure 28.1.4-12	[] ^{a,c}	28-57
Figure 28.1.4-13	[] ^{a,c}	28-58
Figure 28.1.4-14	[] ^{a,c}	28-59
Figure 28.1.4-15	[] ^{a,c}	28-60
Figure 28.1.4-16	[] ^{a,c}	28-61
Figure 28.1.4-17	[] ^{a,c}	28-62
Figure 28.1.4-18	[] ^{a,c}	28-63
Figure 28.1.4-19	[] ^{a,c}	28-64
Figure 28.1.4-20	[] ^{a,c}	28-65
Figure 28.1.4-21	[] ^{a,c}	28-66
Figure 28.1.4-22	[] ^{a,c}	28-67
Figure 28.1.4-23	[] ^{a,c}	28-68

LIST OF FIGURES (cont.)

Figure 28.1.4-24	[] ^{a,c}	28-69
Figure 28.1.4-25	[] ^{a,c}	28-70
Figure 28.1.4-26	[] ^{a,c}	28-71
Figure 28.1.4-27	[] ^{a,c}	28-72
Figure 28.1.4-28	[] ^{a,c}	28-73
Figure 28.1.4-29	[] ^{a,c}	28-74
Figure 28.1.4-30	[] ^{a,c}	28-75
Figure 28.1.4-31	[] ^{a,c}	28-76
Figure 28.1.4-32	[] ^{a,c}	28-77
Figure 28.1.4-33	[] ^{a,c}	28-78
Figure 28.1.4-34	[] ^{a,c}	28-79
Figure 28.1.4-35	[] ^{a,c}	28-80
Figure 28.1.4-36	[] ^{a,c}	28-81
Figure 28.1.5-1	[] ^{a,c}	28-84
Figure 28.1.5-2	[] ^{a,c}	28-85
Figure 28.1.5-3	[] ^{a,c}	28-86
Figure 28.1.5-4	[] ^{a,c}	28-87
Figure 28.1.5-5	[] ^{a,c}	28-88
Figure 28.1.5-6	[] ^{a,c}	28-89

LIST OF FIGURES (cont.)

Figure 28.1.5-7	[] ^{a,c}	28-90
Figure 28.1.5-8	[] ^{a,c}	28-91
Figure 28.1.5-9	[] ^{a,c}	28-92
Figure 28.1.6-1	[] ^{a,c}	28-95
Figure 28.1.6-2	[] ^{a,c}	28-96
Figure 28.1.6-3	[] ^{a,c}	28-97
Figure 28.1.6-4	[] ^{a,c}	28-98
Figure 28.1.6-5	[] ^{a,c}	28-99
Figure 28.1.6-6	[] ^{a,c}	28-100
Figure 28.1.6-7	[] ^{a,c}	28-101
Figure 28.1.6-8	[] ^{a,c}	28-102
Figure 28.1.6-9	[] ^{a,c}	28-103
Figure 28.1.6-10	[] ^{a,c}	28-104
Figure 28.1.6-11	[] ^{a,c}	28-105
Figure 28.1.6-12	[] ^{a,c}	28-106
Figure 28.1.6-13	[] ^{a,c}	28-107
Figure 28.2.2-1	[] ^{a,c}	28-110
Figure 28.2.2-2	[] ^{a,c}	28-111
Figure 28.2.2-3	[] ^{a,c}	28-112
Figure 28.2.2-4	[] ^{a,c}	28-113

LIST OF FIGURES (cont.)

Figure 28.2.2-5	[] ^{a,c}	28-114
Figure 28.2.2-6	[] ^{a,c}	28-115
Figure 28.2.2-7	[] ^{a,c}	28-116
Figure 28.2.2-8	[] ^{a,c}	28-117
Figure 28.2.2-9	[] ^{a,c}	28-118
Figure 28.2.2-10	[] ^{a,c}	28-119
Figure 28.2.2-11	[] ^{a,c}	28-120
Figure 28.2.2-12	[] ^{a,c}	28-121
Figure 28.2.2-13	[] ^{a,c}	28-122
Figure 28.2.2-14	[] ^{a,c}	28-123
Figure 28.2.2-15	[] ^{a,c}	28-124
Figure 28.2.2-16	[] ^{a,c}	28-125
Figure 28.2.2-17	[] ^{a,c}	28-126
Figure 28.2.2-18	[] ^{a,c}	28-127
Figure 28.2.3-1	[] ^{a,c}	28-130
Figure 28.2.3-2	[] ^{a,c}	28-131
Figure 28.2.3-3	[] ^{a,c}	28-132

LIST OF FIGURES (cont.)

Figure 28.2.3-4	[] ^{a,c}	28-133
Figure 28.2.3-5	[] ^{a,c}	28-134
Figure 28.2.3-6	[] ^{a,c}	28-135
Figure 28.2.3-7	[] ^{a,c}	28-136
Figure 28.2.3-8	[] ^{a,c}	28-137
Figure 28.2.3-9	[] ^{a,c}	28-138
Figure 28.2.3-10	[] ^{a,c}	28-139
Figure 28.2.3-11	[] ^{a,c}	28-140
Figure 28.2.3-12	[] ^{a,c}	28-141
Figure 28.2.3-13	[] ^{a,c}	28-142
Figure 28.2.3-14	[] ^{a,c}	28-143
Figure 28.2.3-15	[] ^{a,c}	28-144
Figure 28.2.3-16	[] ^{a,c}	28-145
Figure 28.2.3-17	[] ^{a,c}	28-146
Figure 28.2.3-18	[] ^{a,c}	28-147
Figure 28.2.3-19	[] ^{a,c}	28-148
Figure 28.2.3-20	[] ^{a,c}	28-149
Figure 28.2.4-1	[] ^{a,c}	28-151

LIST OF FIGURES (cont.)

Figure 28.2.4-2	[] ^{a,c}	28-152
Figure 28.2.4-3	[] ^{a,c}	28-153
Figure 28.2.4-4	[] ^{a,c}	28-154
Figure 28.2.4-5	[] ^{a,c}	28-155
Figure 28.2.4-6	[] ^{a,c}	28-156
Figure 28.2.5-1	[] ^{a,c}	28-158
Figure 28.2.5-2	[] ^{a,c}	28-159
Figure 28.2.5-3	[] ^{a,c}	28-160
Figure 28.2.6-1	[] ^{a,c}	28-162
Figure 28.2.6-2	[] ^{a,c}	28-163
Figure 28.2.6-3	[] ^{a,c}	28-164
Figure 28.2.6-4	[] ^{a,c}	28-165
Figure 28.2.6-5	[] ^{a,c}	28-166
Figure 28.2.6-6	[] ^{a,c}	28-167
Figure 28.2.6-7	[] ^{a,c}	28-168
Figure 28.2.6-8	[] ^{a,c}	28-169
Figure 28.2.6-9	[] ^{a,c}	28-170
Figure 28.2.7-1	[] ^{a,c}	28-172
Figure 28.2.7-2	[] ^{a,c}	28-173
Figure 28.2.7-3	[] ^{a,c}	28-174

LIST OF FIGURES (cont.)

Figure 28.2.7-4	[] ^{a,c}	28-175
Figure 28.2.7-5	[] ^{a,c}	28-176
Figure 28.2.7-6	[] ^{a,c}	28-177
Figure 28.2.7-7	[] ^{a,c}	28-178
Figure 28.2.7-8	[] ^{a,c}	28-179
Figure 28.2.7-9	[] ^{a,c}	28-180
Figure 28.2.7-10	[] ^{a,c}	28-181
Figure 28.2.7-11	[] ^{a,c}	28-182
Figure 28.2.7-12	[] ^{a,c}	28-183
Figure 28.2.7-13	[] ^{a,c}	28-184
Figure 28.2.7-14	[] ^{a,c}	28-185
Figure 28.2.7-15	[] ^{a,c}	28-186
Figure 28.2.8-1	[] ^{a,c}	28-189
Figure 28.2.8-2	[] ^{a,c}	28-190
Figure 28.2.8-3	[] ^{a,c}	28-191
Figure 28.2.8-4	[] ^{a,c}	28-192
Figure 28.2.8-5	[] ^{a,c}	28-193
Figure 28.2.8-6	[] ^{a,c}	28-194
Figure 28.2.8-7	[] ^{a,c}	28-195
Figure 28.2.8-8	[] ^{a,c}	28-196
Figure 28.2.8-9	[] ^{a,c}	28-197

LIST OF FIGURES (cont.)

Figure 28.2.8-10	[$]^{a,c}$	28-198
Figure 28.2.8-11	[$]^{a,c}$	28-199
Figure 28.2.8-12	[$]^{a,c}$	28-200
Figure 28.2.8-13	[$]^{a,c}$	28-201
Figure 28.2.8-14	[$]^{a,c}$	28-202
Figure 28.2.8-15	[$]^{a,c}$	28-203
Figure 28.2.8-16	[$]^{a,c}$	28-204
Figure 28.2.9-1	[$]^{a,c}$	28-207
Figure 28.2.9-2	[$]^{a,c}$	28-208
Figure 28.2.9-3	[$]^{a,c}$	28-209
Figure 28.2.9-4	[$]^{a,c}$	28-210
Figure 28.2.9-5	[$]^{a,c}$	28-211
Figure 28.2.9-6	[$]^{a,c}$	28-212
Figure 28.2.9-7	[$]^{a,c}$	28-213
Figure 28.2.9-8	[$]^{a,c}$	28-214
Figure 28.2.9-9	[$]^{a,c}$	28-215
Figure 28.2.9-10	[$]^{a,c}$	28-216

LIST OF FIGURES (cont.)

Figure 28.2.9-11	[] ^{a,c}	28-217
Figure 28.2.9-12	[] ^{a,c}	28-218
Figure 28.2.10-1	[] ^{a,c}	28-220
Figure 28.2.10-2	[] ^{a,c}	28-221
Figure 28.2.10-3	[] ^{a,c}	28-222
Figure 28.2.10-4	[] ^{a,c}	28-223
Figure 28.2.10-5	[] ^{a,c}	28-224
Figure 28.2.10-6	[] ^{a,c}	28-225
Figure 28.2.10-7	[] ^{a,c}	28-226
Figure 28.2.10-8	[] ^{a,c}	28-227
Figure 28.2.10-9	[] ^{a,c}	28-228
Figure 28.2.10-10	[] ^{a,c}	28-229
Figure 28.2.10-11	[] ^{a,c}	28-230
Figure 28.2.10-12	[] ^{a,c}	28-231
Figure 28.2.10-13	[] ^{a,c}	28-232
Figure 28.2.10-14	[] ^{a,c}	28-233
Figure 28.2.10-15	[] ^{a,c}	28-234
Figure 28.2.10-16	[] ^{a,c}	28-235
Figure 28.2.11-1	[] ^{a,c}	28-237

LIST OF FIGURES (cont.)

Figure 28.2.11-2	[] ^{a,c}	28-238
Figure 28.2.11-3	[] ^{a,c}	28-239
Figure 28.2.11-4	[] ^{a,c}	28-240
Figure 28.2.11-5	[] ^{a,c}	28-241
Figure 28.2.11-6	[] ^{a,c}	28-242
Figure 28.2.11-7	[] ^{a,c}	28-243
Figure 28.2.12-1	[] ^{a,c}	28-249
Figure 28.2.12-2	[] ^{a,c}	28-250
Figure 28.2.12-3	[] ^{a,c}	28-251
Figure 28.2.12-4	[] ^{a,c}	28-252
Figure 28.2.12-5	[] ^{a,c}	28-253
Figure 28.2.12-6	[] ^{a,c}	28-254
Figure 28.2.12-7	[] ^{a,c}	28-255
Figure 28.2.12-8	[] ^{a,c}	28-256
Figure 28.2.12-9	[] ^{a,c}	28-257
Figure 28.2.12-10	[] ^{a,c}	28-258
Figure 28.2.12-11	[] ^{a,c}	28-259
Figure 28.2.12-12	[] ^{a,c}	28-260
Figure 28.2.12-13	[] ^{a,c}	28-261
Figure 28.2.12-14	[] ^{a,c}	28-262
Figure 29.1.1-1	[] ^{a,c}	29-14
Figure 29.1.1-2	[] ^{a,c}	29-15
Figure 29.1.1-3	[] ^{a,c}	29-16

LIST OF FIGURES (cont.)

Figure 29.1.1-4	[] ^{a,c}	29-17
Figure 29.1.1-5	Branchline Quality Versus Mainline Liquid Level for Horizontal Configuration	29-19
Figure 29.1.1-6	Branchline Quality Versus Mainline Liquid Level for Downward-Vertical Configuration	29-20
Figure 29.1.5-1	Predicted Versus Measured Level Swell for the G-1 and G-2 Boil-off Simulations with [] ^{a,c}	29-28
Figure 29.1.5-2	Predicted Versus Measured Level Swell for the G-2 Boil-off Simulations with [] ^{a,c}	29-29
Figure 29.1.5-3	Differential Pressure in the Test Bundle for [FLECHT-SEASET Test 31504	29-30
Figure 29.1.5-4	Quench Profile for [FLECHT-SEASET Test 31504	29-31
Figure 29.1.8-1	Dispersed Flow Cooling.....	29-36
Figure 29.1.8-2	Inverted Annular Cooling.....	29-36
Figure 29.1.8-3	Histogram of T_{min} Values Based on G-1 and G-2 Test Data [] ^{a,c}	29-37
Figure 29.1.8-4	T_{min} Variation with Re (From Appendix N, Boyack et al., 1989).....	29-38
Figure 29.1.8-5	T_{min} Variation with Pressure (From Appendix N, Boyack et al., 1989).....	29-38
Figure 29.1.8-6	Method for Determining Quench Temperature [] ^{a,c}	29-39
Figure 29.1.8-7a	Predicted vs. Measured Quench Temperatures from G-1 Blowdown Simulations	29-39
Figure 29.1.8-7b	Predicted vs. Measured Quench Temperatures from G-1 Blowdown Simulations with TMIN Set to Homogeneous Nucleation Temperature.....	29-40
Figure 29.1.8-8	Predicted vs. Measured Quench Temperatures from FLECHT SEASET Forced Reflood Test Simulations.....	29-40
Figure 29.1.8-9	Predicted vs. Measured Quench Temperatures from FLECHT Low Flooding Rate Forced Reflood Test Simulations	29-41
Figure 29.1.8-10	Predicted vs. Measured Quench Temperatures from FLECHT Skewed Forced Reflood Test Simulations.....	29-41
Figure 29.1.11-1	Residual Liquid Level from UPTF Loop Seal HS_SLUG Study	29-45

LIST OF FIGURES (cont.)

Figure 29.1.11-2	Break Spectrum Studies (3-loop PWR) Segregated Based on the Number and Which Loop Seals Clear.....	29-45
Figure 29.2.3-1	LOCA Frequency Evaluation Obtained using Expert Elicitation Presented by Tregoning, et al. (2007)	29-53
Figure 29.2.4-1	DEGCL Break Noding Scheme	29-55
Figure 29.2.4-2	Guillotine Break Noding Used in <u>W</u> COBRA/TRAC-TF2.....	29-56
Figure 29.2.5-1	Split Break Noding Scheme	29-59
Figure 29.2.5-2	Split Break Noding Used in <u>W</u> COBRA/TRAC-TF2	29-60
Figure 29.2.5-3	Demonstration of CD1/CD2 Application for SPLIT Breaks.....	29-60
Figure 29.4.1-1	Maximum Rod Average Power at a Given Rod Burnup at Various Times During a Typical Cycle	29-78
Figure 29.4.1-2	[.....] ^{a,c}	29-79
Figure 29.4.1-3	Fuel Pellet Average Temperatures as a Function of Rod Average Burnup for 0.422-inch Outer Diameter Fuel	29-80
Figure 29.4.1-4	Effect of Load Follow on F_Q	29-81
Figure 29.4.1-5	[.....] ^{a,c}	29-82
Figure 29.4.1-6	[.....] ^{a,c}	29-83
Figure 29.4.1-7	[.....] ^{a,c}	29-84
Figure 29.4.1-8	[.....] ^{a,c}	29-85
Figure 29.4.1-9	Example Bottom Skewed Axial Power Distribution [.....] ^{a,c}	29-86
Figure 29.4.1-10	Example Top Skewed Axial Power Distribution [.....] ^{a,c}	29-87
Figure 29.4.1-11	[.....] ^{a,c}	29-88

LIST OF FIGURES (cont.)

Figure 29.4.1-12	[$\beta^{a,c}$	29-89
Figure 29.4.2-1	ZIRLO® Cladding Burst Temperature Data and Correlation		29-95
Figure 29.4.2-2	[$\beta^{a,c}$	29-99
Figure 29.4.2-3	[$\beta^{a,c}$	29-100
Figure 29.4.2-4	[$\beta^{a,c}$	29-101
Figure 29.4.2-5	[$\beta^{a,c}$	29-102
Figure 29.4.2-6	[$\beta^{a,c}$	29-103
Figure 29.4.2-7	[$\beta^{a,c}$	29-104
Figure 29.4.2-8	[$\beta^{a,c}$	29-105
Figure 29.4.2-9	[$\beta^{a,c}$	29-106
Figure 29.4.2-10	[$\beta^{a,c}$	29-107
Figure 29.4.2-11	[$\beta^{a,c}$	29-109
Figure 29.4.2-12	Distribution of Packing Fraction Data		29-109
Figure 29.4.2-13	[$\beta^{a,c}$	29-114
Figure 29.4.2-14	[$\beta^{a,c}$	29-115
Figure 29.4.3-1	[$\beta^{a,c}$	29-125
Figure 29.4.3-2	[$\beta^{a,c}$	29-125
Figure 29.4.3-3	Heat Transfer Coefficient vs. Time from FLECHT 31805, 6 ft		29-126
Figure 29.4.3-4	Predicted vs. Measured Heat Transfer Coefficients from Forced Reflood Tests.....		29-127

LIST OF FIGURES (cont.)

Figure 29.4.3-5	[] ^{a,c}29-127
Figure 29.4.3-6	FLECHT 31203 6-ft Elevation Cladding Temperature Comparison for [] ^{a,c} Heat Transfer Multiplier of [] ^{a,c}29-128
Figure 29.4.3-7	FLECHT 31203 6-ft Elevation Cladding Temperature Comparison for [] ^{a,c} Heat Transfer Multiplier of [] ^{a,c}29-128
Figure 29.4.3-8	FLECHT 31203 8-ft Elevation Cladding Temperature Comparison for [] ^{a,c} Heat Transfer Multiplier of [] ^{a,c}29-129
Figure 29.4.3-9	FLECHT 31203 8-ft Elevation Cladding Temperature Comparison for [] ^{a,c} Heat Transfer Multiplier of [] ^{a,c}29-129
Figure 29.4.3-10	FLECHT 31203 10-ft Elevation Cladding Temperature Comparison for [] ^{a,c} Heat Transfer Multiplier of [] ^{a,c}29-130
Figure 29.4.3-11	FLECHT 31203 10-ft Elevation Cladding Temperature Comparison for [] ^{a,c} Heat Transfer Multiplier of [] ^{a,c}29-130
Figure 29.4.3-12	FLECHT 31504 6-ft Elevation Cladding Temperature Comparison for [] ^{a,c} Heat Transfer Multiplier of [] ^{a,c}29-131
Figure 29.4.3-13	FLECHT 31504 6-ft Elevation Cladding Temperature Comparison for [] ^{a,c} Heat Transfer Multiplier of [] ^{a,c}29-131
Figure 29.4.3-14	FLECHT 31504 8-ft Elevation Cladding Temperature Comparison for [] ^{a,c} Heat Transfer Multiplier of [] ^{a,c}29-132
Figure 29.4.3-15	FLECHT 31504 8-ft Elevation Cladding Temperature Comparison for [] ^{a,c} Heat Transfer Multiplier of [] ^{a,c}29-132
Figure 29.4.3-16	FLECHT 31504 10-ft Elevation Cladding Temperature Comparison for [] ^{a,c} Heat Transfer Multiplier of [] ^{a,c}29-133
Figure 29.4.3-17	FLECHT 31504 10-ft Elevation Cladding Temperature Comparison for [] ^{a,c} Heat Transfer Multiplier of [] ^{a,c}29-133
Figure 29.4.3-18	FLECHT 31805 6-ft Elevation Cladding Temperature Comparison for [] ^{a,c} Heat Transfer Multiplier of [] ^{a,c}29-134
Figure 29.4.3-19	FLECHT 31805 6-ft Elevation Cladding Temperature Comparison for [] ^{a,c} Heat Transfer Multiplier of [] ^{a,c}29-134
Figure 29.4.3-20	FLECHT 31805 8-ft Elevation Cladding Temperature Comparison for [] ^{a,c} Heat Transfer Multiplier of [] ^{a,c}29-135
Figure 29.4.3-21	FLECHT 31805 8-ft Elevation Cladding Temperature Comparison for [] ^{a,c} Heat Transfer Multiplier of [] ^{a,c}29-135

LIST OF FIGURES (cont.)

Figure 29.4.3-22	FLECHT 31805 10-ft Elevation Cladding Temperature Comparison for [] ^{a,c} Heat Transfer Multiplier of [] ^{a,c}29-136
Figure 29.4.3-23	FLECHT 31805 10-ft Elevation Cladding Temperature Comparison for [] ^{a,c} Heat Transfer Multiplier of [] ^{a,c}29-136
Figure 31.1-1	Description of Break Area Regions..... 31-5
Figure 31.2-1	[] ^{a,c} 31-9
Figure 31.2-2	[] ^{a,c}31-10
Figure 31.2-3	[] ^{a,c} 31-11
Figure 31.2-4	[] ^{a,c}31-12
Figure 31.3-1	[] ^{a,c} 31-19
Figure 31.3-2	[] ^{a,c}31-20
Figure 31.3-3	[] ^{a,c} 31-21
Figure 31.3-4	[] ^{a,c} 31-22
Figure 31.3-5	[] ^{a,c} 31-23
Figure 31.3-6	[] ^{a,c}31-24
Figure 31.3-7	[] ^{a,c} 31-25
Figure 31.3-8	[] ^{a,c} 31-26
Figure 31.3-9	[] ^{a,c}31-27
Figure 31.3-10	[] ^{a,c} 31-28
Figure 31.3-11	[] ^{a,c} 31-29
Figure 31.3-12	[] ^{a,c}31-30

LIST OF FIGURES (cont.)

Figure 31.3-13	[] ^{a,c}	31-31
Figure 31.3-14	[] ^{a,c}	31-32
Figure 31.3-15	[] ^{a,c}	31-33
Figure 31.3-16	[] ^{a,c}	31-34
Figure 31.3-17	[] ^{a,c}	31-35
Figure 31.3-18	[] ^{a,c}	31-36
Figure 31.3-19	[] ^{a,c}	31-37
Figure 31.3-20	[] ^{a,c}	31-38
Figure 31.3-21	[] ^{a,c}	31-39
Figure 31.3-22	[] ^{a,c}	31-40
Figure 31.4-1	[] ^{a,c}	31-45
Figure 31.4-2	[] ^{a,c}	31-46
Figure 31.4-3	[] ^{a,c}	31-47
Figure 31.4-4	[] ^{a,c}	31-48
Figure 31.4-5	[] ^{a,c}	31-49
Figure 31.4-6	[] ^{a,c}	31-50
Figure 31.4-7	[] ^{a,c}	31-51
Figure 31.4-8	[] ^{a,c}	31-52
Figure 31.4-9	[] ^{a,c}	31-53
Figure 31.4-10	[] ^{a,c}	31-54
Figure 31.4-11	[] ^{a,c}	31-55

25 PLANT SOURCES OF UNCERTAINTY

We have, to this point, assessed the ability of WCOBRA/TRAC-TF2 to simulate the key phenomena identified in the Phenomena Identification and Ranking Table (PIRT). In addition, it has been demonstrated that compensating errors or bias, due to the increase in scale from the experiments to the Pressurized Water Reactor (PWR), result in a more conservative estimate of the Loss-of-Coolant Accident (LOCA) analysis results relative to several key phenomena. However, there may be differences in PWR response to the LOCA, which may result in some models being more important for the PWR than for the experiment. In addition, variability in plant initial and boundary conditions introduce additional uncertainty. In this section, these additional aspects are discussed. The objective of this section is to develop a plan for performing various sensitivity or scoping studies with the PWR models described in Section 26, in order to identify those parameters which have an important influence on the calculation of the Peak Cladding Temperature (PCT) and Maximum Local Oxidation (MLO) in the PWR, and to make decisions about which variables should be considered for uncertainty propagation.

For some parameters, the uncertainty will be explicitly treated within the uncertainty analysis. For other parameters, a conservative approach may be employed (such as for the containment back-pressure).

25.1 PLANT PHYSICAL CONFIGURATION

The plant physical configuration consists of those parameters which define the geometrical and hydraulic configuration of the reactor at the time the LOCA occurs. These parameters are listed and defined below:

1. Dimensions
2. Flow resistances
3. Pressurizer location, relative to broken loop
4. Accumulator Tank Elevation
5. Hot assembly location, relative to vessel upper internals
6. Hot assembly type
7. Steam generator tube plugging level

Dimensions

Reactor dimensions, volumes, and surface areas are obtained directly from component drawings. Some variability exists in these dimensions due to tolerances and approximations which may have been made in geometrical calculations. Dimensions also vary from nominal due to thermal expansion. Thermal expansion is estimated to increase volumes by about [

]^{a,c}

Fuel assembly grids, control rod guide tubes, and steam generator tubes may be affected, in some cases, by high stresses resulting from the combination of seismic and LOCA loads, an assumption required by the Code of Federal Regulations (CFR) 10 CFR 50, Appendix A, General Design Criterion 4. A dynamic analysis of the Reactor Coolant System (RCS) under combined seismic and LOCA loads is performed to demonstrate that key RCS components will continue to perform their safety function. Structural analyses

performed as part of the original plant design basis have confirmed that Emergency Core Cooling System (ECCS) safety function and core shutdown capability are maintained. These analyses have also indicated that for some plants, the pressure differentials and structural movements which are predicted may result in minor deformation of fuel assembly grids, control rod guide tubes, and/or steam generator tubes. In the case of the fuel assembly, some deformation of the grids in assemblies at the periphery of the core may be calculated. This may push fuel rods closer together, reducing the available flow area. Steam generator tubes may be slightly deformed at support plate locations, reducing the flow area through the tube bundle and increasing the flow resistance during reflood. For larger breaks, control rod guide tubes may be displaced from their nominal positions, preventing control rod insertion and causing the core to shutdown on voids early in the LOCA, and to remain shut down due to boron alone. These deformations, while not compromising safety functions, were found to affect the LOCA analysis results.

The combined effects of LOCA and seismic loads may potentially lead to some degree of grid deformation in the core, due to the baffle plates impacting the peripheral assemblies. If the impact on the peripheral assemblies is large enough, these assemblies may subsequently impact in-board assemblies, and so on. If the loads are large enough for grid damage to occur, test data and analyses show that the damage is typically limited to no more than two rows of rods per assembly, with elevations towards the mid-plane of the core.

[

] ^{a,c}

[

] ^{a,c}

[

] ^{a,c}

Modeling Approach

[

] ^{a,c}

Flow Resistance

The flow resistance in the vessel and loops during a LOCA is as much a function of the models used to calculate the friction factor, as it is the plant configuration. However, flow resistance is included in this category because some changes in plant configuration affect this parameter. The steady-state hydraulic resistance of virtually all the major components in a PWR was determined from scaled testing.

The accuracy of the loss coefficients obtained from these tests has, over the years, been confirmed by the accurate prediction of steady-state flow and temperature conditions of operating reactors during numerous plant startup cycles. The accuracy of these predictions, using loss coefficients for subcomponents which are typically subject to large uncertainties may also be a result of the fact that the pressure distribution in a reactor circuit consists of many components. [

] ^{a,c} The uncertainty in

the pressure drop under LOCA transient conditions is discussed in Section 29.1.2.

When the LOCA occurs, reverse flow through some components and two-phase flow may significantly increase the uncertainty of the predicted flow resistance. One area in particular where reverse flow introduces additional resistance not present during normal operation is the broken cold leg inlet nozzle. Another area where additional resistance is introduced is the broken loop pump.

During several large scale ECCS tests conducted in the past years, it was observed that there was a significant pressure drop across the inlet nozzle of the broken cold leg. In the Cylindrical Core Test Facility (CCTF) reflood tests, this pressure drop was observed to result in a significant pressurization of the downcomer during reflood, resulting in increased reflood rates (Akimoto et al., 1984). Part of this loss was attributed to the increased dynamic head resulting from the reverse flow from a large reservoir, the reactor vessel, to the cold leg nozzle. Other contributors were losses associated with two-phase flow. A review of recent Upper Plenum Test Facility (UPTF) data has confirmed this finding as described in Section 29.1.2.

During a cold leg break, the flow rate through the broken loop pump increases substantially, to the point where the pump acts as a resistance. The effect of this additional flow resistance must also be taken into account, and is a source of additional uncertainty. The flow in the intact loop typically continues in the same direction at lower flow rates, therefore the predicted pressure drop is less subject to uncertainty.

Modeling Approach

[

$J^{a,c}$

Pressurizer Location

The pressurizer may be on the broken loop or one of the unbroken loops. Its location arises as a source of uncertainty because it may introduce some asymmetry into the reactor configuration at the time of the LOCA. Sensitivity studies have shown that: [

$J^{a,c}$

Modeling Approach

[

$J^{a,c}$

Accumulator Tank Elevation

The accumulator tanks may sit below, at, or above the cold leg elevation. The elevation of the accumulator relative to the cold leg will impact the maximum flow during accumulator injection, the duration of accumulator injection, and the amount of liquid which remains in the accumulator after accumulator injection into the cold leg terminates.

Modeling Approach

The modeling of the accumulator tank elevations is discussed in Section 29.2.1, Volume 3.

Hot Assembly Location

Approximately 40 percent of the fuel assemblies in the core of a PWR lie beneath control rod guide tubes which extend into the upper head. These guide tubes, arranged in an approximate checkerboard pattern, house reactor control rods used for reactor control and shutdown, and extend into the reactor vessel upper head. The remaining fuel assemblies lie below open holes in the core plate, flow mixers attached to the core plate, or support columns of several possible designs (Section 26). As a result, for larger breaks (during the blowdown phase) the fuel assemblies will receive varying amounts of flow from the upper head and upper plenum depending on their position. [

]^{a,c}

Modeling Approach

The configuration of the guide tubes is such that specific modeling of these flowpaths is considered necessary, particularly in view of the connection to the upper head, which contains a large volume of water. Consequently, the core and upper plenum geometry in the WCOBRA/TRAC-TF2 model is designed to specifically include separate channels for guide tubes and core plate open hole locations. As described in Section 26, each reactor internal layout is examined, and the hot assembly is located where reduced direct flow is expected to occur.

Hot Assembly Type

The basic design of a PWR fuel assembly has remained essentially unchanged through the years; the standard Westinghouse fuel assembly, for example, consists of an array of fuel rods in a 14x14, 15x15, 16x16 or 17x17 square matrix. Approximately 90 percent of the matrix is occupied by fuel rods; the remainder is occupied by thimble tubes. Five or more spacer grids hold the array together; some or all of the grids contain mixing vanes which serve to enhance flow turbulence, improving heat transfer during normal operation.

Variations in this standard design may occur to achieve improved fuel utilization. Typical changes made to a fuel assembly design are the following:

1. Changes in Fuel Rod Diameter – The fuel rod may be “optimized” by reducing its diameter, thus reducing the overall amount of fuel required. These changes are marginal in nature. For example, the standard Westinghouse 14x14 fuel rod diameter is 0.422 inches. For the optimized designs the diameter is 0.400 inches. Since smaller rods are designed to the same linear powers as standard rods, their surface heat fluxes and adiabatic heating rates are slightly higher. On the other hand, the amount of coolant in the core is also higher, because of the larger flow area.

2. Changes in Grid Design – The grid may be made of stainless steel, Inconel, or zirconium alloys. Typically, if the fuel rod diameter has been changed, the grids are modified slightly such that the overall hydraulic loss is the same as the standard design.

An additional design improvement is to incorporate additional mixing vane grids along portions of the rod, which further improve heat transfer characteristics, and offset reductions in departure from nucleate boiling (DNB) margin brought about by a smaller rod.

3. Changes in Fuel Enrichment – Axial and radial “blankets” are sometimes provided to reduce neutron leakage from the core. These blankets consist of regions of low reactivity fuel, or annular fuel. These blankets affect the axial and radial power distribution in the core, and are explicitly considered when these distributions are calculated.
4. Burnable Absorbers – Burnable absorbers are often used to reduce soluble boron requirements and improve power distributions. Burnable poisons may be discrete (i.e., loaded in thimbles) or integral (i.e., coatings or dopings of the fuel). Burnable absorbers affect axial and radial power distributions in the core, and are explicitly accounted for in core design calculations. Integral absorbers may also cause the internal pressure of the fuel rod, which generally increases with burnup, to increase at a different rate. Rod internal pressure causes swelling and possible burst during the LOCA.
5. Changes in Cladding Material – New alloys more resistant to corrosion are being developed. Their plastic strain characteristics may be different, and may therefore affect the LOCA results.
6. Other Changes – Minor modifications in upper and lower fuel assembly tie plates, mixing vane grid design, and removal of thimble plugging devices, are other changes which may occur from reload to reload, but which are not expected to change the LOCA results significantly.

Modeling Approach

[

] ^{a,c}

Steam Generator Tube Plugging Level

Steam generator tubes may require plugging for various reasons. Typically, tube plugging takes place during a normal outage. Plugs are inserted into each end of the degraded tube. This removes the tube completely from the RCS volume, and reduces the total flow area through the steam generator. The increased resistance and reduced volume may affect the blowdown transient and reflood behavior for larger breaks or the loop seal clearing in small breaks, and is a variation which must be considered in the LOCA analysis.

Modeling Approach

[

] ^{a,c}

25.2 PLANT INITIAL OPERATING CONDITIONS

Reactor operating conditions and their variations are described by two groups of parameters:

1. Core power parameters. These parameters define the core power distribution and fuel stored energy at the time of the LOCA.
 - a. Total core power
 - b. Peak linear heat rate (PLHR)
 - c. Hot assembly peak linear heat rate
 - d. Hot rod average power
 - e. Hot assembly average power
 - f. Axial power distribution
 - g. Low power region relative power
 - h. Time-in-Cycle
 - i. Reactor operating power history
 - j. Moderator temperature coefficient (MTC)
 - k. Hot full power (HFP) boron concentration

2. Reactor primary fluid conditions. These parameters describe the primary fluid thermodynamic state at the time of the LOCA.
 - a. Core average fluid temperature
 - b. Pressurizer pressure
 - c. Loop flow rate
 - d. Upper head fluid temperature
 - e. Pressurizer level
 - f. Accumulator water temperature
 - g. Accumulator pressure
 - h. Accumulator water volume
 - i. Accumulator line resistance
 - j. Accumulator boron concentration

The basis for the choice of these parameters is discussed in the following sections.

25.2.1 Core Power Parameters

A summary of the core modeling is given below. There are four core channels and [

] ^{a,c} simulation the following fuel rods are modeled:

- Rod 1: The rod with the highest linear heat rate [^{a,c} assumed to also have the highest average power and to reside in the assembly with the highest average power.
- Rod 2: All the other (average) rods in the highest power assembly [^{a,c}
- Rod 3: All the average rods in the assemblies residing under non-guide tube structures (e.g., support columns, free standing mixers, orifice plates, and open holes).
- Rod 4: All the average rods in the assemblies residing under guide tubes.
- Rod 5: All the average rods in the assemblies residing on the periphery of the core.
- [

] ^{a,c}

There are three distinct regions (the hot assembly, the two average channels, and the low power channel) which serve to resolve the radial power distribution in the core.

Each fuel rod group has parameters describing the peak linear heat rate, the average linear heat rate, the axial distribution of power, and the number of physical rods modeled by the rod group. [

] ^{a,c}

The axial and radial core power distributions are of basic importance to the uncertainty analysis. The parameters which affect these distributions, and their variations, are described in the following section.

25.2.1.1 Core Power Distributions

The nuclear design of the reactor core meets constraints on the local power distribution in the fuel. Power distributions are typically characterized in terms of hot channel factors. These factors relate peak pellet power and hot rod power to core average quantities. These factors and other terms which will be used are defined below:

- Core average heat flux (AFLUX) is the average thermal power produced per unit length of active fuel, kW/ft.

- Peak linear heat rate is the maximum linear heat rate produced in the reactor, kW/ft.
- Hot assembly peak heat rate (HAPHR) is the peak linear heat rate of an average rod in the hot assembly, kW/ft.
- Hot assembly average power (HAFLUX) is the average power per unit length in the hot assembly, kW/ft.
- Hot rod average power (HRFLUX) is the average power per unit length in the hot rod, kW/ft.
- Total peaking factor (F_Q) is the ratio of the peak linear heat rate to the core average linear heat rate (PLHR/AFLUX).
- Enthalpy rise peaking factor (F_{AH}) is the ratio of hot rod average power to core average linear heat rate (HRFLUX/AFLUX).

PWR power distributions are often separated into their respective radial and axial components. The radial component is sensitive to the fuel and absorber loading pattern and the presence of control rods. Radial distributions change slowly with time and fuel depletion and are relatively insensitive to power level, xenon concentration/distribution, axial burnup distribution, and axial fuel design feature. By contrast, PWR axial distributions are relatively insensitive to the loading pattern but are quite sensitive to control bank position, xenon concentration/distribution, coolant density distribution, and reactor power.

The existence of this radial/axial power distribution separability has historically been utilized by the nuclear designer. As noted above, PWR radial power distributions are slowly varying in time, provided that the presence of control rods is accounted for accurately. Axial power distributions are dependent on cycle time as well as plant operating parameters such as current power level, recent changes in power level/distribution, prior operating history, control bank position (or operating strategy), and the time during a transient power maneuver (or the xenon distribution). These characteristics allow the analysis of transient three-dimensional power distributions to be performed by superposition of transient axial power distributions on steady-state, appropriately rodded, radial power distributions rather than the rigorous direct solution for the three-dimensional power distribution. While the methods and calculations used to design reload cores are extremely reliable, and have been confirmed by measurements taken in many operating reactors, it is a normal practice to design cores with some margin, such that measured power distributions will always fall below the core power limits, even when measurement uncertainties are added. These core power limits are determined from the body of safety analyses which support the final safety analysis report (FSAR) and Technical Specifications, and ensure that regulatory limits will not be exceeded for any postulated transient.

Assembly power distributions in a typical Westinghouse designed PWR reload core are shown in Figures 25.2-1 and 25.2-2. The radial power distribution can typically be divided into three core regions: a low power peripheral region, high power assemblies distributed throughout the core (feed or non-feed), and average power regions also distributed throughout the core. These figures show the predicted power of assemblies in a reload core. This is a typical low leakage core loading pattern, in which low power assemblies are situated around the periphery of the core, while high power assemblies are in the interior of the core.

[

] ^{a,c}

Within the fuel assembly, individual fuel rods vary in power due to the presence of burnable absorbers and water holes near the thimble tubes. Figure 25.2-3 is a histogram showing the distribution of rod powers within the high power assembly of several different Westinghouse fuel designs. The powers are expressed as a fraction of the maximum power allowed by the Technical Specifications. The maximum calculated rod power is therefore more than [] ^{a,c} lower than the maximum allowed value, to accommodate measurement uncertainties during surveillance and up to additional [] ^{a,c} for “good measure” or operational allowance. It can be seen that most of the fuel rods are at powers near the middle of the distribution, and that the hot assembly power distribution can be modeled with a single average rod and a single hot rod. The cumulative distribution is shown in Figure 25.2-4, and the average hot assembly power calculated from these distributions summarized in Table 25.2-1, and is seen to lie approximately [] ^{a,c} below the maximum calculated (hot rod) value.

The steady-state axial power distribution also varies as a function of time. Figure 25.2-5 shows the core average axial power distribution near the beginning of cycle, near the middle of cycle and near the end of cycle for a typical reload core. During the cycle, the steady-state axial peak moves away from the center of the core as the core is depleted. The depletion of the center of the core also affects any transient axial power distributions.

While a PWR is designed to easily follow load demand, the most likely state of the reactor is full power and equilibrium conditions. Under these conditions, the axial peaking is relatively low. Measurements taken of the maximum peaking factor at HFP, nominal conditions are usually well below the Technical Specification limits. The margin to peaking factor limits is intended to allow for the less frequent occurrence of transient reactor operation, usually consisting of power reductions and increases to follow load. [] ^{a,c}

In summary, it is seen that the design of a core (its geometry, fuel enrichment, and loading pattern) establishes the maximum radial peaking in the core. The radial distribution is determined almost entirely by the core loading, and cannot be easily changed by external controls in normal operation. Hence, to assure that the measured hot rod power will always lie below the limit, core designs are set allowing for additional margin beyond the four percent required by Technical Specifications.

25.2.1.2 Transient Power Distributions

Short term changes in reactor power distributions are typically attributable to changes in reactor power level. Changes in power level may require control rod motion, and result in changes in coolant density profiles and xenon distribution. Changes in xenon distribution are a strong function of the magnitude and duration of the power change maneuver as well as the operating strategy used during the maneuver.

Westinghouse and Combustion Engineering (CE) core design methodologies used to generate axial power distributions have been previously reviewed by the United States Nuclear Regulatory Commission (USNRC). Distinct methods are employed in design based on the axial flux difference (AFD) Technical Specifications employed. (AFD is a measure of the axial power distribution, and is the axial flux difference between the top and bottom halves of the core.)

Westinghouse plants use the Constant Axial Offset Control (CAOC) or Relaxed Axial Offset Control (RAOC) core design method. The CAOC methodology (Morita et al., 1974) requires the core designer to simulate various types of load follow maneuvers throughout the cycle to establish the limiting axial power distributions. The approach taken is conservative in that daily load follow swings to various power levels are assumed throughout the cycle. This method is used with plants whose AFD Technical Specification is defined as an allowable band (typically ± 5 percent) about a target AFD.

Another approach is used for plants with a fixed AFD Technical Specification. The RAOC methodology (Miller et al., 1983) considers the core parameters (power level, xenon distribution, and control rod position) that can affect power distributions and establishes the maximum variability possible in these parameters throughout a given cycle. These parameters are then treated as independent variables and all possible combinations are checked. Any axial shapes that are found to be within the AFD operating space defined by the Technical Specifications are taken to be possible.

CE plants do not control via AFD. Instead their monitoring and protective systems use the concept of axial shape index (ASI) (Combustion Engineering, 1986; Combustion Engineering, 1998; Combustion Engineering, 1975). ASI is similar to AFD, in that ASI is also a measure of the axial power distribution, and is the negative of percent axial offset divided by 100.

Typical transient distributions generated by the CAOC methodology are shown in Figures 25.2-6 through 25.2-8 for different times throughout the cycle. [

]^{a,c}

An additional characteristic of these transient power shapes is that fission products do not have sufficient time to build up in the high power region of the fuel rod. Consequently, if the reactor was shut down for any reason at the time the maximum transient linear shapes occurred, the decay heat generated is substantially lower at the peak power location than if the core had been operating indefinitely at these PLHR's. This phenomenon is not credited in the **FULL SPECTRUM™ LOCA (FSLOCA™)** methodology.

The reactor heat source is made up of three major constituents. Fission energy is by far the largest component of the heat, comprising from roughly 93 to 100 percent of the total heat source for full power

operation. The stored energy contribution to the LOCA transient is, therefore, directly related to the fission rate distribution at the time of the LOCA. The magnitudes of the decay and actinide heat sources make them a small contribution to the stored energy component. The decay and actinide components are, however, the principal contributors to core heat generation later in the LOCA transient since the fission rate during this portion of the transient is negligible. The decay and actinide heat sources are independent of the instantaneous fission rate at any given point in time but dependent upon the fission rate time history. Their concentrations determine the decay power available since the decay power for radionuclide decay is determined by the product of the energy release per decay, the decay constant, and the concentration. The concentration of a non-absorbing fission product is dependent upon the fission rate time history, the fission product yield per fission, and the decay constant. Since the yield and time constant for a given fission product are constant for a specified isotope, the time dependent fission product concentration depends only upon the fission rate time history.

Decay heat is the result of a multitude of radionuclide decays (approximately 350 isotopes). These decay processes have been simplified in the ANSI/ANS 5.1-1979 decay heat standard to a summation of 23 exponentials for each fissile isotope. In the absence of significant absorption or isotope decay chain cross-coupling, the ANSI/ANS 5.1-1979 decay heat standard is a 23 group “pseudo-nuclide” representation of the fission product decay process. The magnitude of the decay heat source at any given point in the reactor, therefore, depends on the time history of the fission rate. The decay heat source for a given point in the reactor will be in effective equilibrium (production rate = decay rate) only if the fission rate has been maintained for the period of time corresponding to ten to twenty time constants for that nuclide. Figure 25.2-10 illustrates a point evaluation of decay equilibrium fraction versus sinusoidal fission rate period. [

] ^{a,c}

25.2.1.3 Power Distribution Uncertainties

After a core has been designed and loaded, it is monitored to confirm that the core operates as designed, and to ensure that the reactor is operating within specified limits. The detailed reactor power distribution is monitored by means of in-core detectors. (There are several other core monitoring systems as well.) The readings from these detectors (which are fission chambers and convert the local neutron flux to a current signal) are transformed to fission rate distributions using analytical factors, based on the specific core design (Spier et al., 1988).

The core power distribution is measured during steady-state operation at regular intervals. The following quantities are typically obtained as the result of measurement and data processing:

- $F_{\Delta H}$ The enthalpy rise hot channel factor is the ratio of the integral of local power along the rod (pin) with the highest integrated power in the core to the average rod power.
- $F_{xy}(z)$ The elevation dependent radial peaking factor is the maximum local power density in the plane at elevation z divided by the average power density of the plane.

$F_Q(z)$ The elevation dependent heat flux hot channel factor is the maximum local linear power density at elevation z divided by core average linear power density.

Because the above peaking factors are derived from a combination of instrument measurements and analytical model calculation, the uncertainty associated with these factors is a combination of the two factors.

The peaking factors defined above are typically measured on a monthly basis. In addition to the peaking factors defined above, the core axial flux difference is measured on a continual basis by the ex-core nuclear detectors. This measurement is equivalent to the axial flux difference discussed previously, and provisions are incorporated in the plant computer to provide alarms if limits are exceeded.

The calculational uncertainty on radial power distribution ($F_{\Delta H}$) has been shown (Spier et al., 1988) to be bounded by a factor of []^{a,c} through benchmarks to critical experiments and other data. There is also an additional uncertainty associated with measuring the radial power distribution, which is bounded by a factor of four percent. It is desirable to assure that the plant will not routinely experience flux map measurements which exceed the $F_{\Delta H}$ limit after a four percent uncertainty is applied due to combined effects of calculational and measurement uncertainties. To accomplish this, Westinghouse standard practice is to design the core such that it is predicted to be at least []^{a,c} below the ($F_{\Delta H}$) limit on a best-estimate basis. With this approach, the most probable condition is for the core to be measured at least []^{a,c} below the Technical Specification limit after measurement uncertainty is applied. Typical measurements shown in Figure 25.2-11 show this is indeed the case.

The margin inherent in the design as it relates to the total peaking factor $F_Q(z)$ is also reflected in typical measurements. Design calculations are performed to conservatively calculate the possible effects of adverse xenon distributions on the maximum total peaking factor. These penalty factors are generated assuming xenon transients are initiated in the core and shift the axial distribution to the full range allowed by the AFD Technical Specifications. The most probable condition for the core is at an equilibrium xenon condition which will produce F_Q values well below the limits. The total peaking factor measurement for a typical core during a cycle is shown in Figure 25.2-12. The maximum measured values include an uncertainty of 8.15 percent when compared to the Technical Specification.

Nuclear design calculations are performed assuming nominal pellet diameter, density, etc. These calculations form the basis of the analytic factors used to convert in-core measurements to rod power. Manufacturing uncertainties such as pellet diameter and the effects of rod bow introduce an additional uncertainty to point measurements. These uncertainties are accounted for in the FSLOCA methodology.

Rod bow and manufacturing uncertainties are both applied to the hot rod peaking factor measurement as described in the following paragraphs. These factors are not applied to measurements of the hot assembly and hot rod power. Local linear heat rate depends on the local mass of UO_2 per unit length, or more specifically, per pellet and also on the local channel geometry. The local mass varies as a result of manufacturing variations in pellet dimensions and fuel enrichment. []

[]^{a,c}

A similar statement can be made for rod bow. [

] ^{a,c}

A detailed study of the in-core flux mapping system and its accuracy was performed by Westinghouse (Spier et al., 1988). Because the “measured” values of $F_{\Delta H}$ and F_Q are actually inferred values obtained from the raw measurement using core model group constants, error contributions from both measurement and modeling sources were considered. Two uncertainties are defined: a measurement uncertainty, to be applied to the inferred peaking factor during normal core surveillance such that the true values are bounded at a high confidence level, and a calculational uncertainty, to be applied to the calculated peaking factors during the core design such that the true values are bounded at a high confidence level. The two uncertainties contain several common components, and so are similar in magnitude. In the best-estimate LOCA methodology, we are concerned with the calculational uncertainty of the predicted peaking factors.

The calculational uncertainty is composed of several independent subcomponents which are summarized in Table 25.2-2. Some of these components are related to uncertainties which should be applied only to the hot rod. In subsequent application of these uncertainties (Section 29.4), these components will be applied separately when considering the calculational uncertainties associated with groups of fuel rods such as the hot assembly. [

] ^{a,c}

A final uncertainty related to the power distribution is that associated with the total core power. Core power is inferred from an energy balance using feedwater flow and temperature, and steam flow and pressure. The maximum error from this measurement is typically ± 2 percent, [^{a,c}. Some plants have employed improved uncertainty measurement systems which reduce this uncertainty below 2 percent.

25.2.1.4 Power Distribution Modeling Approach

Summarizing the preceding sections, the core power distribution is seen to exhibit the following characteristics:

1. The radial power distribution is primarily controlled by core geometry, fuel enrichment, burnable absorber loading, and core loading patterns. It is relatively insensitive to operational procedures such as load follow.

-
2. Clarification on the determination of the rod bow uncertainty component was provided as part of RAID-6.4 in (Bajorek et al., 1998) for prior Westinghouse best-estimate LOCA evaluation models.

2. The axial power distribution is sensitive to operational procedures (such as load follow), which produce non-equilibrium xenon distributions in the core, and core burnup. Large axial power distribution variations have a small effect on the radial power distribution. Axial power distributions which produce the limiting F_Q occur during transient operation. []^{a,c}
3. The power distribution in the core is well described by the following parameters: the average linear heat rate, the hot assembly linear heat rate, the low power assembly linear heat rate, and the peak linear heat rate.
4. The average power of the rods in the assembly which contains the hot rod is typically []^{a,c} or more lower than the hot rod.
5. The axial peak power may occur at any location within approximately two feet from the ends of the core, during both transient and steady-state conditions.

As described in Section 26, the PWR core is modeled with sufficient detail to resolve both the radial and axial power distributions present in the core. The radial power distribution is resolved using []^{a,c}

There are several parameters which play a role in the calculation of rod power in WCOBRA/TRAC-TF2. Each parameter, in turn, contributes some uncertainty. Based on the general discussion of power distributions, the parameters as used in WCOBRA/TRAC-TF2 are described in more detail below. A final summary of uncertainty contributors is presented later in this section, after the discussion of the fuel rod model.

As described previously, there are four core channels and []^{a,c} are defined as:

- Rod 1: The rod with the highest linear heat rate []^{a,c} assumed to also have the highest average power and to reside in the assembly with the highest average power.
- Rod 2: All the other (average) rods in the highest power assembly []^{a,c}
- Rod 3: All the average rods in the assemblies residing under non-guide tube structures (e.g., support columns, free standing mixers, orifice plates, and open holes).
- Rod 4: All the average rods in the assemblies residing under guide tubes.
- Rod 5: All the average rods in the assemblies residing on the periphery of the core.
- []^{a,c}

Each fuel rod has input parameters describing the average linear heat rate, and the axial distribution of power relative to the core average linear heat rate. The important parameters used in WCOBRA/TRAC-TF2 for these fuel rods are described below. The “0” designates initial, or steady-state values of parameters which will change during the LOCA transient.

The reactor power parameters described below are directly related to several quantities which are also measured in the plant during normal operation. These are the total peaking factor (F_Q), the hot channel factor ($F_{\Delta H}$), and the AFD. Other quantities of lesser importance are the MTC and the coolant boron concentration. The Technical Specifications call for specific uncertainties and margins to be applied to the measured values of some of these quantities before they are compared to the Technical Specification limit. In the discussion below, these quantities will normally be described in terms of calculated or expected values, without local uncertainties, and will be designated with subscript BE (Best-Estimate).

Initial Core Average Linear Heat Rate

The parameter defining core power in WCOBRA/TRAC-TF2 is the core average linear heat rate, calculated by:

$$AFLUX(0) = P(0)/(NFR * L) \quad (25-1)$$

where,

L	=	nominal active fuel length
P(0)	=	initial core power
NFR	=	total number of fuel rods

There is a tendency for the fuel pellet stack (L) to shrink during the cycle, which would increase AFLUX based on Equation 25-1. However, [

]^{a,c} The only uncertainty affecting AFLUX is the core power measurement uncertainty, which results from calorimetric errors in measuring feedwater flow and temperature. As noted in Section 25.2.1.3, the range of this error is estimated as [

]^{a,c}

The axial power distributions of the core average rods (Rods 3, 4, and 5) are [

]^{a,c} These distributions will be illustrated later in the section, when the power distribution modeling is described.

Peak Linear Heat Rate

The PLHR for the hot rod (Rod 1) [

[

]^{a,c} defined by:

]

(25-2)

[

] ^{a,c}

For the hot rod, the PLHR can also be expressed as,

[

]

^{a,c}

(25-3)

[

] ^{a,c}

The variation due to transient operation is the result of assumed load follow operations and other operational transients, which introduce relatively short lived skewed power shapes with relatively high peaking factors compared to equilibrium conditions, when the plant returns to full power. Limiting transient power distributions are generated during the core design analysis to confirm that maximum values remain below limits established in the Technical Specifications. The calculated maximum peaking factor is obtained from the core design analysis using approved core design methods.

[

] ^{a,c}

Hot Assembly Rod Peak Linear Heat Rate

The hot assembly rod peak linear heat rate is defined as:

[

] ^{a,c}

(25-4)

[

] ^{a,c}

Therefore HAPHR(0) can be written as:

$$\left[\frac{P_{\text{hot rod}}}{P_{\text{hot assembly}}} \right]^{a,c} \quad (25-5)$$

Typically, the relationship in power of the hottest rod in an assembly to the assembly average will depend upon details in the design of that assembly, such as the location of the hot rod in the assembly. In this analysis, it is conservatively assumed that the [

$\left[\frac{P_{\text{hot rod}}}{P_{\text{hot assembly}}} \right]^{a,c}$ and the peak power is offset by a constant factor equal to the difference in average power. Further discussion of the validity of this assumption is provided in the next subsection.

There are two items to consider when developing the relationship between the hot rod, which is a single rod, and the hot assembly rod, which represents the average of all the rods in the hot assembly minus the hot rod. The first item is the actual difference between the hot rod and the hot assembly rod powers. The second is the difference in the uncertainty associated with various quantities for the hot rod and the hot assembly rod.

Examination of rod census data indicates that the minimum difference between the hot rod and the hot assembly average rod is $\left[\frac{P_{\text{hot rod}}}{P_{\text{hot assembly}}} \right]^{a,c}$. Absent all uncertainties, this is a conservative estimate of the relationship which will exist between the hot rod and the hot assembly average rod during normal operation for the entire fuel cycle. As a general approach, the hot assembly average rod power will be calculated using the $\left[\frac{P_{\text{hot rod}}}{P_{\text{hot assembly}}} \right]^{a,c}$ difference. However, if additional information is available in the form of a core design limit, an alternative and less conservative approach may be taken to bound the hot assembly average power. In Equations 25-4 and 25-5 and the discussion that follows, it is assumed that the general approach (where the difference is $\left[\frac{P_{\text{hot rod}}}{P_{\text{hot assembly}}} \right]^{a,c}$) is taken.

A second consideration is the uncertainty associated with the hot rod and with the hot assembly average rod. For a single rod at a single axial location, the following uncertainties exist:

1. Uncertainty in the actual linear heat rate, relative to what is predicted.
2. Uncertainty in the actual fuel pellet geometry. The pellet at a particular location may be slightly larger or be slightly more enriched than the value intended during manufacture.
3. Uncertainty in the hot rod subchannel geometry. The subchannel may be slightly distorted due to rod bow.

The overall uncertainty for the hot assembly average rod peaking factor should be less than that for the hot rod, since we are concerned with the average value over a number of rods, $\left[\frac{P_{\text{hot rod}}}{P_{\text{hot assembly}}} \right]^{a,c}$. This is indicated in Table 25.2-2.

For a single axial location on a single rod, all of these uncertainties must be considered. Since the local axial linear heat rate as specified by F_Q is defined at a single location, all of these uncertainties must be considered for the hot rod, hence the full column of numbers in Table 25.2-2 for the hot rod F_Q . For integral quantities such as the rod total power as specified by $F_{\Delta H}$, local uncertainties such as pellet dimensions should not contribute significantly to the integral uncertainty. $\left[\frac{P_{\text{hot rod}}}{P_{\text{hot assembly}}} \right]^{a,c}$

[]^{a,c}

[]^{a,c}

(25-6)

[

]^{a,c}

[]^{a,c}

(25-7)

[]^{a,c}

[]^{a,c}

(25-8)

[

] ^{a,c}

The result of the application of these different uncertainties is that the uncertainty associated with the power on the hot rod is typically larger than the uncertainty associated with the power in the hot assembly average rod. These uncertainties are discussed in Sections 29.4.1.2 and 29.4.2.1.

Hot Rod Average Linear Heat Rate

Since the hot rod has a very small effect on the hot assembly fluid conditions (it is only one rod among about 150), its total power is not as important as the power in the hot assembly rod. However, total power will affect hot rod gap pressure and cladding burst times.

[

] ^{a,c}

[

] ^{a,c}

(25-9)

where,

[

] ^{a,c}

therefore,

[

] ^{a,c}

(25-10)

$F_{\Delta H, BE}$ is defined as the maximum expected average linear heat rate of the highest power rod [] ^{a,c} relative to the core average linear heat rate. Typically, the calculated $F_{\Delta H, BE}$ for a core design is augmented by four percent to account for calculational and measurement uncertainties and up to an additional [] ^{a,c} for “good measure” or operational allowance. The reason for the application of additional margin in $F_{\Delta H}$ is that, unlike total peaking factor, there are few alternatives short of reducing power if the measured value exceeds the Technical Specification.

Hot Assembly Average Linear Heat Rate

The hot assembly rod (Rod 2) average linear heat rate during steady-state is defined as:

$$\left[\frac{P_{\text{rod}}}{L_{\text{rod}}} \right]^{a,c} \quad (25-11)$$

[

$$\left[\frac{P_{\text{rod}}}{L_{\text{rod}}} \right]^{a,c} \quad (25-12)$$

The actual thermal power produced in the hot assembly rod relative to its nuclear power may be slightly different from the hot rod, due to different levels of redistribution. [

] ^{a,c}

As discussed in Section 25.2.1.1, a review of a large number of core designs indicates that the minimum difference between the hot rod and the hot assembly average rod is [] ^{a,c} lower (Figure 25.2-4). This is a conservative estimate of the relationship which will exist between the hot rod and the hot assembly average rod during normal operation, during the entire fuel cycle. The relative nuclear power generated in the hot assembly average rod is therefore assumed to be [] ^{a,c} lower than the best-estimate value of the hot rod relative nuclear power, $F_{\Delta H, BE}$. As previously discussed, however, if additional information is available in the form of a core design limit, an alternative and less conservative approach may be taken to bound the hot assembly average power.

Axial Power Distribution

Axial power distributions vary widely due to burnup and transient operation. The distributions have been considered in prior evaluation models using [

] ^{a,c}

[

] ^{a,c}

Low Power Region (PLOW)

The power in the rod (Rod 5) representing the low power peripheral region of assemblies is determined from the core design and usually varies from [

]^{a,c} If this region has a low average power, the interior channels (Rods 3 and 4) have a higher power. A relative power []^{a,c} of the core average is typical of current and future low leakage loading patterns. An average value expected for future cycles is assumed as discussed in Section 29.3.1.

Time-in-Cycle

The time-in-cycle impacts a number of different parameters significant to the LOCA transient behavior. The fuel peaking factors, initial stored energy, rod internal pressure, corrosion, axial power distribution and decay heat are several examples of burnup dependent parameters. The impact of the time-in-cycle is considered in the uncertainty analysis as discussed in Section 29.4.1.1, Volume 3 of this topical.

Prior Operating History

As discussed previously, the power distributions which generate high peaking factors are relatively short lived. A detailed accounting of the buildup of fission products would show that after shutdown, the axial power distribution would revert back to the original, steady-state distribution. This effect will be [

]^{a,c}

Transient Power Maneuver

[

]^{a,c}

25.2.1.5 Moderator Temperature Coefficient

The MTC affects reactor shutdown during the first few seconds of blowdown. The larger (more positive) this value, the less responsive the reactor is to the increased fluid temperature which occurs in the first second or two of the LOCA. [

]^{a,c}

25.2.1.6 Hot Full Power Boron Concentration

The initial primary fluid boron concentration coupled with the moderator temperature coefficient discussed previously dictate the core power response during the blowdown phase of a LOCA transient. The initial HFP boron concentration is modeled [

$$I^{a,c}$$

25.2.1.7 Summary of Core Power Parameters

The consideration of the various core power distribution parameters described above is summarized as follows. [

$I^{a,c}$ (More details on this uncertainty treatment are provided in Section 29.4.) In Figure 25.2-14, a possible axial power distribution as input into the WCOBRA/TRAC-TF2 PWR model is shown. The hot rod peak power is offset by [$I^{a,c}$ from the hot assembly average rod power (assuming the general approach), and is offset from the average rod power by the total axial peaking ($F_{\Delta H}$). The low power rod is offset from the average rod power, in turn, by the factor PLOW.

25.2.2 Plant Fluid Conditions

The plant fluid conditions listed at the beginning of this section are those which are sufficient to define an overall thermodynamic state of the fluid. Since WCOBRA/TRAC-TF2 calculates a steady-state condition prior to the LOCA, the thermodynamic state cannot be over-specified. Thus, four basic quantities are defined for the primary fluid; its average temperature, pressure, volume, and flow rate. Then, the states of significant fluid regions which are isolated from the RCS during steady-state, but which subsequently become part of the RCS during the LOCA, such as the upper head and the accumulator, are defined. The section below is a brief description of how fluid conditions typically are controlled in a PWR.

25.2.2.1 Overview of Plant Fluid Conditions

A nuclear power plant is equipped with a variety of control systems. For example, the reactor control system in conjunction with the electric load demand program controls the neutron generation rate within the core such that core heat generation rates are proportional to the demanded electric power output. Other control systems are available for control of plant response to rapid disturbances arising from abnormal conditions and for the control of processes which maintain the plant in an economically desirable operating condition.

The static and dynamic behavior of the power production process can only be determined by reliable and accurate measurements of process variables. The application of these measurements by the control and protection systems is then accomplished in a manner which assures proper corrective action and provides protection for the plant and public against extreme accidents. This is normally accomplished by the feedback process where process variables are controlled to a predetermined value, commonly referred to as a setpoint. When measurements deviate from the setpoint, the deviation is noted as an error by the controller(s) and action is taken to restore the process to its correct state point or condition.

Setpoints generally represent either a desired, or “target,” value for a process control variable, or a limit or bounding value, that a process control variable may have. In the case of a “target” or control setpoint, variation from the desired value will result in some corrective action to return the plant to the control setpoint. For example, the pressurizer water level control setpoint is approximately 35 percent of the full-scale reading of the measurement span, with either heaters or spray being actuated with a ± 5 percent variation of full span from the 35 percent span. Violation of limiting or bounding setpoints results in a more radical plant response.

From the preceding example of the pressurizer, it is readily seen that relatively small variations from control setpoints will result in plant control systems initiating corrective action. These small spans are called control bands. Thus, for a plant maintained at equilibrium conditions, the process control parameters may be taken to vary from their respective setpoints by no more than the bounds of their respective control bands. In particular, for process parameters which are subject to automatic control, such as the pressurizer level, the likelihood of the process parameter being significantly different from the target value is extremely small. For those process parameters subject to less frequent surveillance, the potential variation may be larger.

Trip setpoints define the limits within which the plant may operate. Again referring to the example of the pressurizer, the plant will continue to operate temporarily with a pressurizer water level between 17 and 92 percent of full-scale of the measured span, with the plant control systems acting to achieve a level of between 30 to 40 percent of full-scale reading. Owing to operator and/or automatic actions however, prolonged operation outside the control bands is extremely unlikely. The trip setpoints are established to allow the plant flexibility in responding to changes in operating conditions while providing for the health and safety of the public.

Plant operation parameter variations that are significant for LOCA analyses are listed in Table 25.2-4 for a typical PWR. All but primary side loop flow may be considered process control parameters for a nuclear power plant; direct controlling of primary coolant flow rate is not provided for. For a typical plant, the variability of these parameters about their nominal or setpoint values is seen to be small, with a control band of about []^{a,c} on primary loop pressure and fluid temperature, []^{a,c} on core power, and about []^{a,c} on water volumes.

25.2.2.2 Fluid Conditions Modeling Approach

In addition to the process parameters identified in Table 25.2-4, additional RCS fluid conditions have been found to be important in past LOCA analyses. The reactor vessel upper head is supplied by a small bypass flow from the upper downcomer. While the incoming fluid is at the temperature of the cold leg (T_{cold}), the upper head fluid may be at a different average temperature because of the low bypass flow rate which results in some flow from the upper plenum, which is at a higher temperature (T_{hot}). The initial temperature of the fluid in the upper head (T_{UH}) has been found to strongly affect the blowdown PCT in other evaluation models (for LBLOCA). Typically, plants can be separated into two categories: those with sufficient bypass flow to maintain (T_{UH}) near (T_{cold}), and those with low bypass flow, in which (T_{UH}) remains close to T_{hot} .

The bypass flow mentioned above is one component of several bypass flows, which reduce the core flow rate relative to the loop flow rate by about four to eight percent. This bypass flow has an indirect effect on the LOCA transient by affecting the fluid temperature rise through the core, but is not expected to affect the LOCA transient directly by virtue of the different steady-state fluid conditions.

Not all the process parameters described in Section 25.2.2.1 are independent. Typically, if core power, primary flow, and secondary temperature and pressure are specified, the primary fluid temperature and pressure will seek appropriate levels consistent with these boundary conditions. In the modeling of these parameters, the secondary side conditions are adjusted as required to obtain primary side conditions consistent with the Technical Specifications and planned operation. Since the secondary-side model is rather detailed, the secondary-side conditions required to achieve the appropriate primary-side conditions are generally consistent with expected operational values.

Although the accumulator is isolated from the RCS by a check valve during normal operation, it is considered part of the RCS in this methodology. The performance of the accumulator during the LOCA depends on several factors including the water and cover gas initial pressure, temperature, and volume. These are all subject to some variation. Typically, pressure and volume are controlled to within plus or minus 10 percent or less. Since the accumulators reside within containment, the long term temperature of the containment atmosphere will affect the accumulator water temperature. The variation in containment temperature is likely to be seasonal to some degree, and is limited in most plants to a maximum value to avoid problems with equipment degradation. In general, therefore, the accumulator temperature range is plant specific. The accumulator line is subject to the same uncertainties as identified earlier for flow resistance; however, plant startup tests reduce this uncertainty to some extent as discussed in Section 29.3.2, Volume 3.

While accumulator boron concentration is not likely to have a significant effect on the LOCA PCT, it is modeled to ensure that recriticality does not occur in the short-term following a LOCA.

The parameters chosen to represent the reactor initial fluid conditions are:

1. Average fluid temperature (T_{avg}), degrees F
2. Pressurizer pressure (P_{RCS}), psia
3. Loop flow rate (W_{loop}), gpm per loop
4. Upper head fluid temperature (T_{UH}), degrees F

5. Pressurizer level (L_p), percent of full span
6. Accumulator temperature (T_{ACC}), degrees F
7. Accumulator pressure, (P_{ACC}) psia
8. Accumulator water volume, (V_{ACC}) cubic feet
9. Accumulator line fl/D (K_{ACC})
10. Accumulator boron concentration, (C_{ACC}) ppm

The effects that the above parameters have on the LOCA transient are considered as part of the uncertainty analysis. The treatment of the fluid condition uncertainties is discussed in Section 29.3.2, Volume 3.

Table 25.2-1 Hot Assembly Rod Power Census Summary for Westinghouse Fuel

a,c

Table 25.2-2 Peaking Factor Uncertainties

Notes: 1. Spier et al. (1988) 2. [] 3. Uncertainties are given in terms of one standard deviation divided by average value (coefficient of variation), percent. The total uncertainty is the square root sum of squares of the components.				

a,c

] a,c

Table 25.2-3 Rod Bow F_Q Uncertainties

Notes:

1. Uncertainties are given in terms of one standard deviation divided by average value (coefficient of variation).
2. Argall et al. (1979)
3. []^{a,c}

Table 25.2-4 Typical Westinghouse Plant Operation Parameters

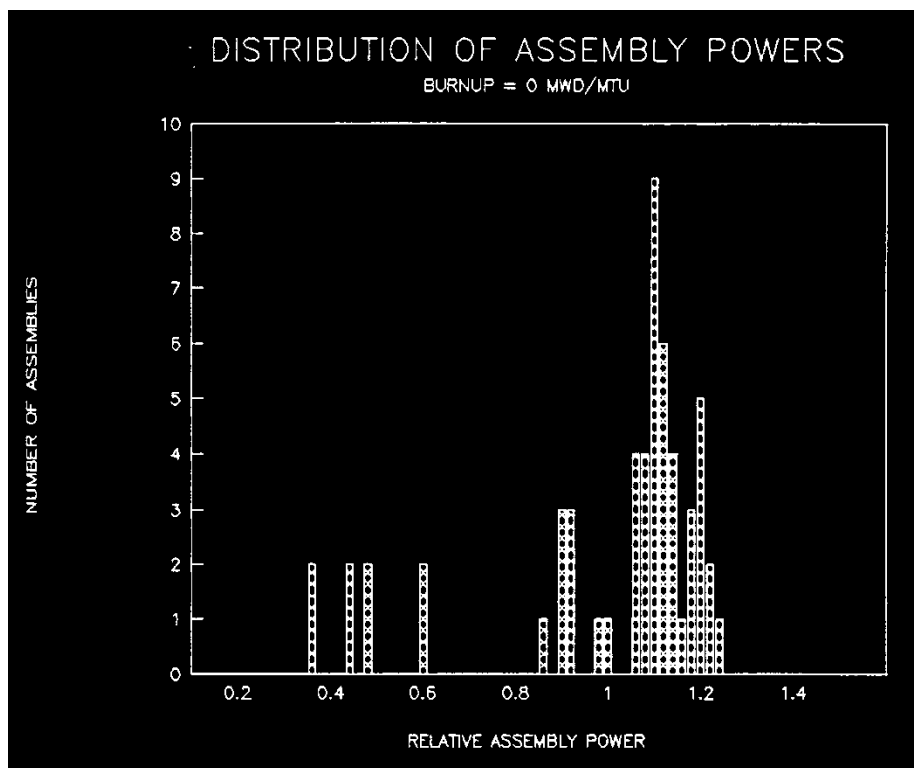
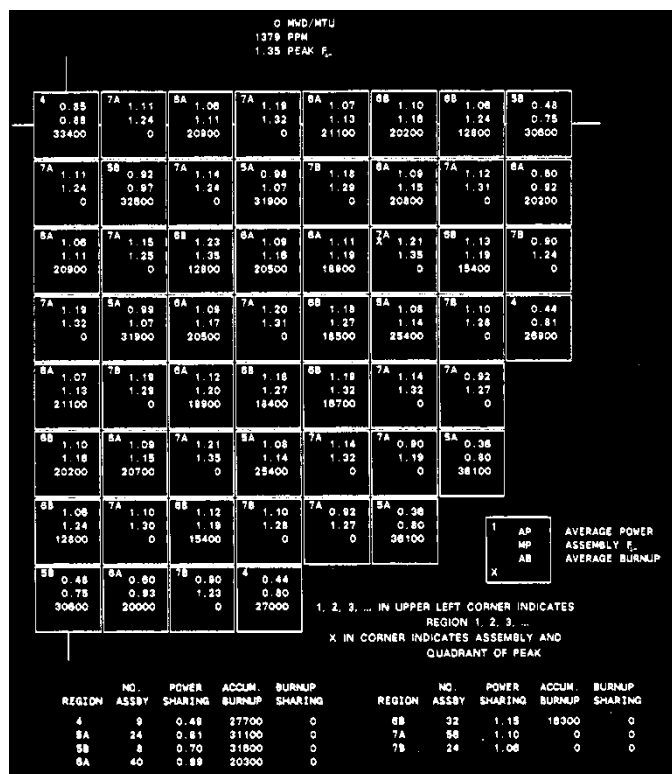


Figure 25.2-1 Typical Assembly Power Map and Assembly Power Distribution, Beginning of Cycle

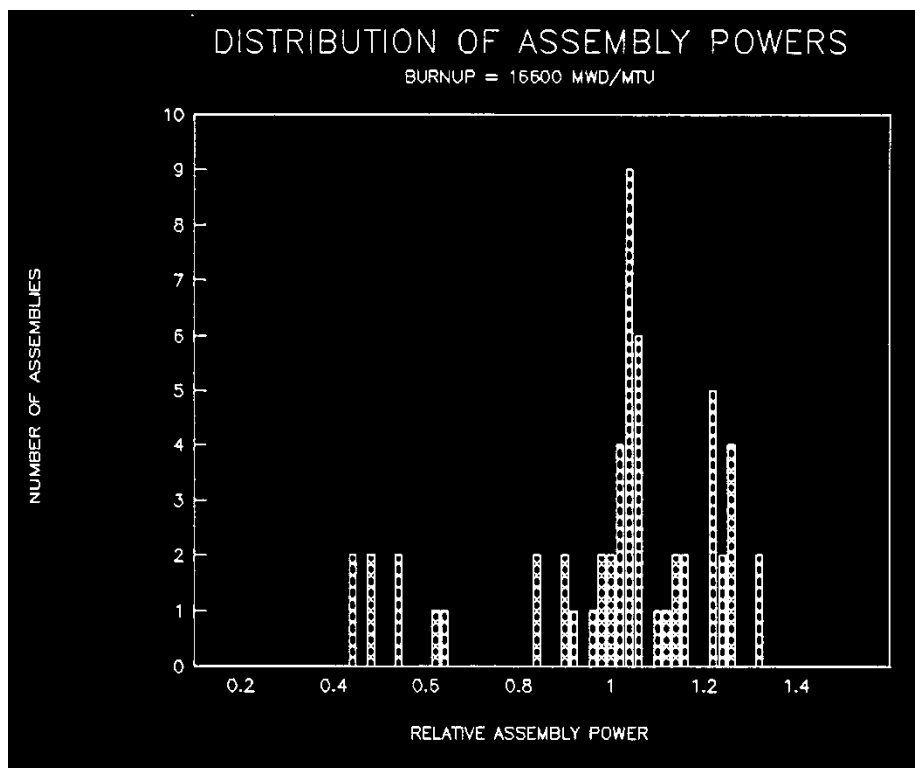
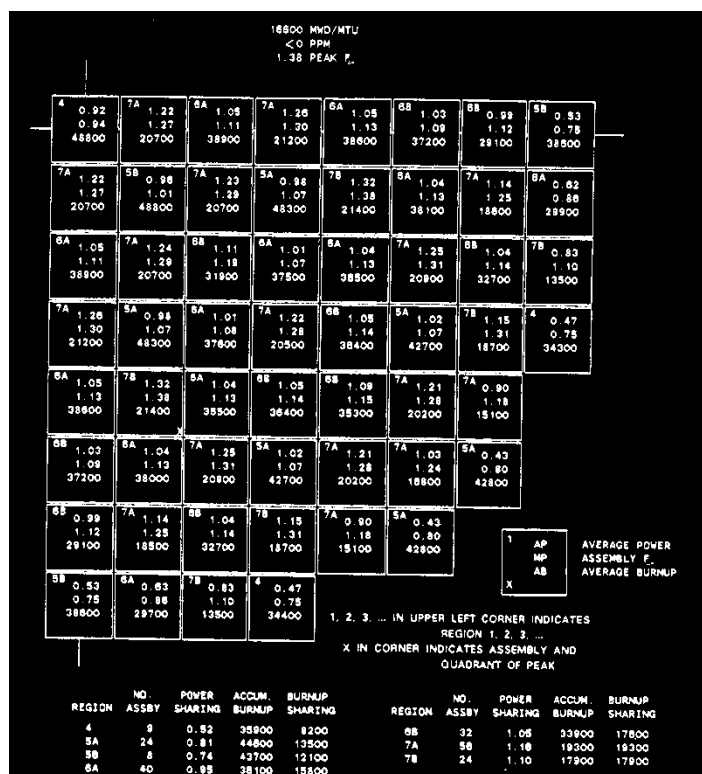


Figure 25.2-2 Typical Assembly Power Map and Assembly Power Distribution, End of Cycle

Figure 25.2-3 Typical Hot Assembly Fuel Rod Power Distribution

Figure 25.2-4 Hot Assembly Rod Power Census for Typical Westinghouse Fuel Designs

Figure 25.2-5 Relative Axial Power Distribution near Beginning of Cycle, Middle of Cycle and End of Cycle During Full Power Steady-State Conditions

Figure 25.2-6 Typical Transient Axial Power Distributions near Beginning of Cycle

Figure 25.2-7 Typical Transient Axial Power Distributions near Middle of Cycle

Figure 25.2-8 Typical Transient Axial Power Distributions near End of Cycle

a,c

Figure 25.2-9 [

] ^{a,c}

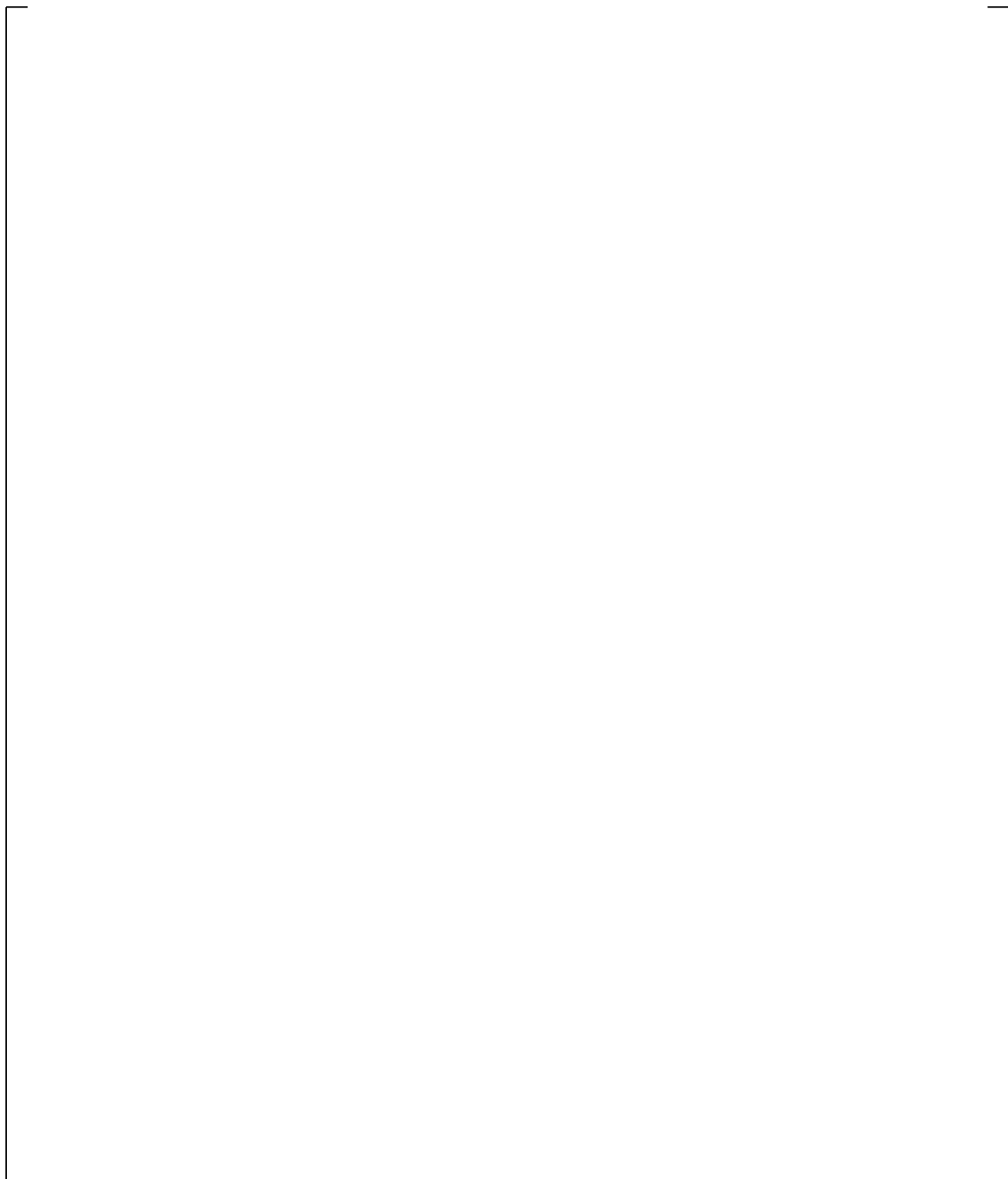


Figure 25.2-10 Effect of Load Follow Maneuver Period on Decay Heat Equilibrium Fraction for Various Times After Trip

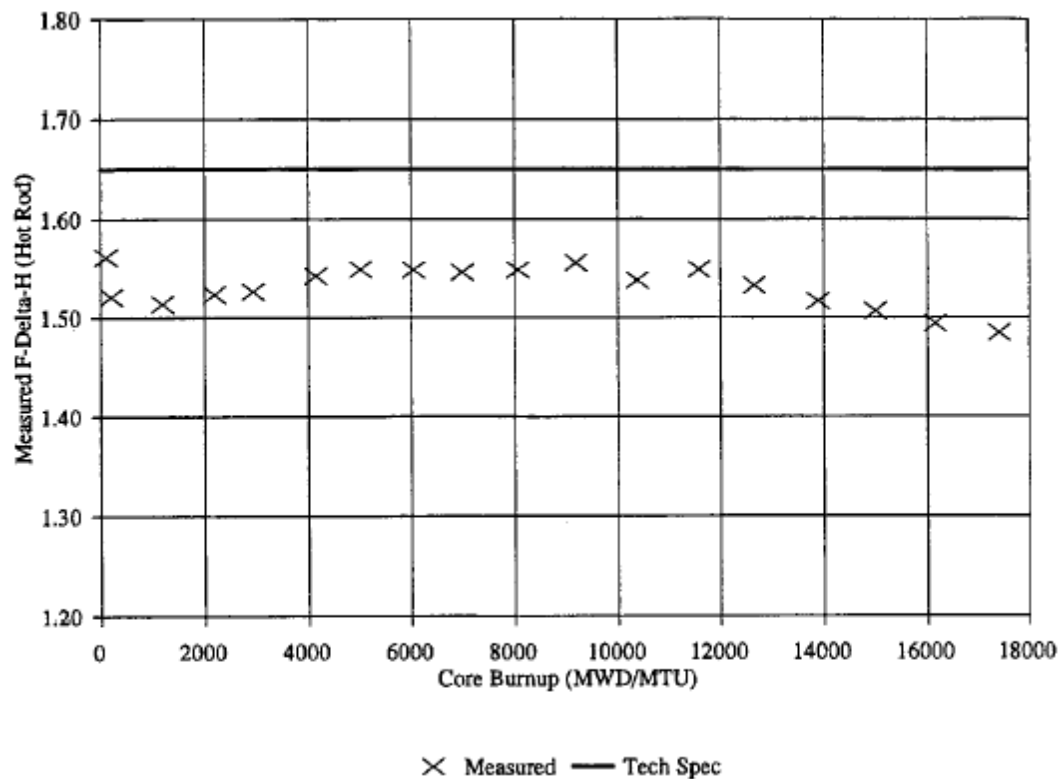


Figure 25.2-11 Typical Measurement of Enthalpy Rise Hot Channel Factor $F_{\Delta H}$

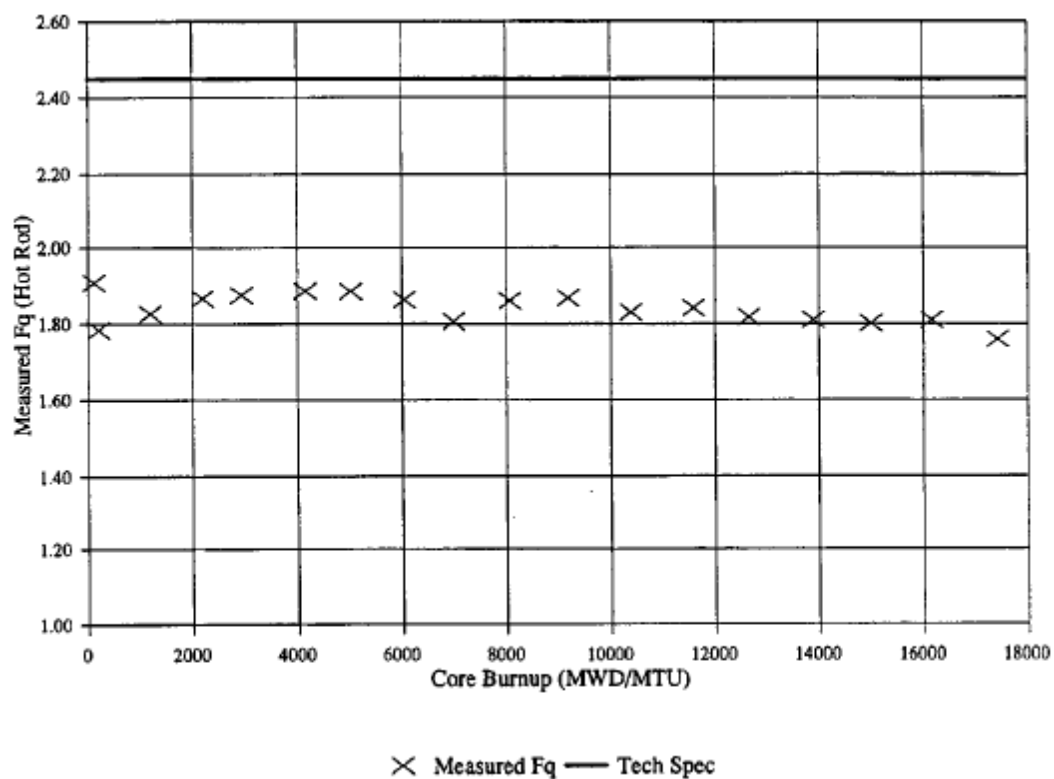


Figure 25.2-12 Typical Measurement of Total Peaking Factor F_Q

a,c

Figure 25.2-13 [

] a,c

Figure 25.2-14 Typical WCOBRA/TRAC-TF2 Axial Power Distribution

25.3 REACTOR ACCIDENT BOUNDARY CONDITIONS

The reactor accident boundary conditions are defined as those conditions outside the RCS pressure boundary which affect the LOCA transient. The break itself is considered a boundary condition. The following parameters are included in this category:

1. Break Location
2. Break Type
3. Break Size
4. Offsite Power
5. Safety Injection Flow
6. Safety Injection Temperature
7. Safety Injection Delay
8. Containment Pressure
9. Single Failure
10. Control Rod Drop/Drop Time
11. Steam Generator Secondary Side

One of the key accident boundary conditions is the postulated break. In a realistic sense, the pipe is not expected to fail. However, for the plant safety analysis and the assessment of the ECCS performance, it is postulated that the main reactor coolant piping will fail. The break parameters are discussed below.

Break Location

Break Type

Break Size

Once it is postulated that the reactor coolant pipe can fail, then all points on the piping have equal probability of failure. If a complete circumferential crack is postulated, piping analysis calculations show that the ends of the severed pipe would separate approximately one inch with a limited lateral displacement of one-half of the pipe wall thickness (Mendler, 1975). This limited displacement is the result of pipe and structural constraints. The time history of axial and lateral displacement of the piping are computed by loop dynamic analysis models.

The mechanical analysis indicates that if the reactor coolant pipe fails, the most probable break geometry is a limited displacement circumferential split break in which the flow comes out of the break in a circumferential direction. The only way that a limited displacement circumferential break can open up into a full double-ended guillotine break is by substantial lateral movement of the piping. The larger lateral displacement can only occur if the pump supports fail for the cold leg break, or the steam generator supports fail for the hot leg break. Additional mechanical analysis indicates that there is insufficient pipe whip energy to crimp the ends of the pipes to create guillotine breaks of smaller area. This is due to the rigidity of the pipes and limited axial displacement of the pipe. Therefore, based on the above mechanical considerations, the range of most probable breaks that should be investigated are the limited displacement breaks or split breaks. The only guillotine break that is possible is the full double-ended guillotine which is caused by larger lateral displacement of the reactor coolant pipes.

For smaller split breaks, the orientation of the break becomes increasingly significant to the LOCA transient behavior. As such, the orientation of the break relative to the pipe must be considered for smaller break sizes.

Modeling Approach

[

] ^{a,c}

Offsite Power

Offsite power determines whether RCS pumps initially remain on, and whether pumped safety injection (and containment safeguards) come on with only valve opening and alignment delays. The effect of the RCS pumps on the LOCA transient may be significantly different, depending on whether they are assumed to coast down or continue running (until operator action is taken, if applicable).

Modeling Approach

Sensitivity studies have shown that [

] ^{a,c}

Safety Injection Flow

Safety injection (SI) flow varies depending on the single failure assumed, and on the specific plant pump and injection line configuration. Current methods, which are also used in currently accepted evaluation models, provide conservative estimates of minimum and maximum flow, which take into account several uncertainties.

Additionally, for smaller break sizes there is the potential for switchover to recirculation mode to occur prior to meeting the transient termination criteria. The safety injection flow rate in recirculation mode may differ from the injection mode flow rate, and there may be a period of safety injection interruption during switchover.

Modeling Approach

[

] ^{a,c}

³ The approach described in Section 30.4 to determine the [^{a,c} is superseded by limitation and condition #15 from the safety evaluation report (SER).

[

] ^{a,c}

Safety Injection Temperature

SI temperature may vary, depending on the location of the refueling water storage tank (RWST), and on controls imposed by Technical Specifications. The safety injection temperature may also change as a result of switching to recirculation mode.

Modeling Approach

[

] ^{a,c}

Safety Injection Delay

SI delays vary depending on whether loss-of-offsite power is assumed to occur.

Modeling Approach

Scoping study results will be used to examine the effect of delayed injection, resulting from delayed diesel start or other delays. [

] ^{a,c}

Containment Pressure

The containment pressure is dependent on the mass and energy release from the RCS during the LOCA. Studies have shown that the containment pressure response is most highly sensitive to the value of the heat transfer coefficient used for heat transfer to passive heat sinks. In the computer codes used to calculate the pressure transient, this heat transfer coefficient is set at an upper bound to minimize calculated containment pressure.

Modeling Approach

A minimum containment pressure is calculated considering run-specific mass and energy releases (for dry containment designs) or mass and energy releases from a reference transient (for ice condenser containment designs) as discussed in Section 25.6.

Single Failure Assumption

There are two types of single failures which may have an effect on the LOCA transient. If loss of an entire train is assumed, then the flow to the RCS is minimized, since this assumption results in the loss of both high and low head pumped flows. However, this assumption also leads to reduced cooling of the containment, since the train includes containment sprays and fan coolers. If the assumed single failure is

the loss of a low head pump only, this results in a higher flow to the RCS, but also increases containment cooling, which reduces containment pressure. The negative effect of lower containment pressure may offset the positive effect of higher pumped flow to the RCS.

Modeling Approach

In order to simplify the analysis, the loss of a train may be assumed for the determination of pumped ECCS flow during the LOCA, while the train will be assumed to operate in the calculation of containment backpressure. This will result in a conservatively low containment backpressure. Alternatively, a more complete analysis using consistent assumptions may be performed on a plant-by-plant basis.

Control Rod Drop/Drop Time

If it is demonstrated that combined seismic and LOCA loads do not distort the control rod guide tubes, then the control rods may be assumed to drop during the LOCA. While this assumption has a negligible effect on the LOCA PCT/MLO transient for larger breaks, advantage may be taken of the negative reactivity introduced by the control rods when determining boron requirements to prevent short term recriticality. This, in turn, may affect the boron concentration assumed in the LOCA analysis. For smaller breaks, control rod insertion is necessary to preclude re-criticality in the core. In addition, slightly higher core flow rates would occur, since the thimble tubes would no longer be empty. [

] ^{a,c}

Modeling Approach

[

] ^{a,c}

Steam Generator Secondary Side

Downstream of the main steam isolation valve (MSIV), a steam turbine stop valve can halt the flow from the secondary side. For LBLOCA applications, it is conservative to assume the steam generator (SG) secondary side is isolated early, maximizing the secondary side pressure and temperature and eliminating the steam generator as a heat removal path during the early part of the transient. [

] ^{a,c}

For Small Break LOCA (SBLOCA) applications, the main steam safety valve (MSSV) actuates to relieve the building secondary side pressure resulting from heat transfer from the primary side during the natural circulation phase. [

] ^{a,c}

Modeling Approach

[

] ^{a,c}

25.4 MODEL PARAMETERS

The assessment studies of Volume 2 were performed such that all models and correlations were used within ranges expected to occur during analysis of a PWR. Many of the experiments were of sufficient complexity that the appropriate model interactions would also occur. The resulting comparisons between data and prediction yielded the basis for the uncertainty methodology detailed in Section 29, Volume 3.

The Westinghouse methodology for combining biases and uncertainties considers the effect of all medium and high-ranked phenomena from the Phenomena Identification Ranking Table, as detailed earlier in Table 2-1. A discussion of how each of the phenomena is considered is provided in Section 29.5, Volume 3.

25.5 OPERATOR ACTIONS

Upon the initiation of a transient in a plant, the operators use the plant's Emergency Operating Procedures (EOPs) to sequentially verify that automatic safeguards features are functioning correctly and follow prescribed operations to restore any malfunctioning systems. Eventually, the EOPs are used to begin plant recovery or to secure operations. Operator actions must be examined to determine the different transient scenarios that could develop and affect the severity of a small break LOCA transient and/or challenge the assumptions made in the LOCA analysis calculations.

The EOPs have been developed to direct the operators to analyze and respond to symptoms ascertained from measured plant parameters or trends of those parameters. During the initial stages of an accident or transient, the plant response can be similar for different events. The large number of changing parameters and their rates of change may prevent immediate diagnosis of the exact type of event; for example, LOCA, steam generator tube rupture, and steam line breaks. Therefore, the EOPs are based upon a hierarchy directing that important, common actions are performed early, based upon the symptoms observed; eventually, the EOPs branch to increasingly specific categories of accidents or transients.

The EOPs are formulated to handle many different events, including beyond design basis accident scenarios. [

] ^{a,c} Upon first review, there appear to be numerous actions that could be followed leading to a variety of outcomes. However, when the event is a design basis small break LOCA involving no more than the limiting single failure, implementation of the EOPs can be significantly streamlined because certain actions, verifications, or branch points and their outcomes are already known. The EOPs can even be further streamlined for specific small break LOCA scenarios. For example, when analyzing a given case for an assumed failure of a diesel generator or a train of safety injection (consistent with the FSLOCA methodology single failure assumption), the

symptoms that the operator will observe and the system responses to the operator's actions are known. The EOPs can then be reduced to only a few pages when operations that are unnecessary for the specific small break LOCA scenario are eliminated because key plant symptoms are known a priori.

25.5.1 EOP Sequences for a Small Break LOCA

Table 25.5-1 is a condensation of the EOPs relevant to the short-term portion of a small break LOCA at the Indian Point Unit 2 plant. While Table 25.5-1 is specific to Indian Point Unit 2, plants typically follow a generic template for the generation of EOPs, and plant-to-plant differences in the EOP structure are not expected to be important for the purpose of performing a LOCA safety analysis. [

] ^{a,c}

25.5.1.1 Adverse Containment Conditions

In adverse containment conditions, a few parameters are evaluated against specifications that are dependent upon containment conditions. The values to use when adverse containment conditions exist are given in parentheses throughout the rest of this section. Adverse containment conditions are defined as:

Containment pressure (P_{CONT}) > 4 psig

or

Containment radiation level > 10^5 R/hr

Either or both of these conditions would probably be met at some time during the small break LOCA transients of interest. Actions are based upon measurement comparisons against the adverse conditions criteria.

25.5.1.2 Continuously Monitored Conditions

In addition to the sequential steps prescribed in the EOPs, there are a few key items continuously monitored as the procedures are followed. These are listed in "Foldouts" to a given procedure where they apply. Two of these items, both of which are in procedure [] ^{a,c} of Table 25.5-1, are important to the boundary conditions assumed for small break LOCA analysis calculations. They are as follows (values in parentheses are typical values for adverse containment conditions):

[

] ^{a,c}

- [

] ^{a,c}

25.5.1.3 Inadequate Core Cooling

Another condition the operator will monitor following a small break LOCA event is to verify that the core is being adequately cooled. To establish that adequate core cooling exists, the EOPs require that the temperature readings of the core exit thermocouples do not exceed 1200°F. If this criterion is not met, the operator will enter the Inadequate Core Cooling Procedure FR-C.1, which directs the operator to depressurize the steam generator secondary side. If this depressurization is performed, it may significantly affect the small break LOCA transient, [

] ^{a,c}

25.5.2 Variability of Plant Conditions Due to Operation Actions

The condensed procedures in Table 25.5-1 show the importance of operator actions in defining the conditions during the short-term phases of a small break LOCA. The process is summarized chronologically as follows:

[

] ^{a,c}

A review of the operations in Table 25.5-1 shows that the majority of the efforts undertaken by the operators are categorized as “verify operation or status.” Although the operators continuously analyze

equipment status and respond to failures throughout the entire operation, selected equipment failures are prescribed as boundary conditions to any given LOCA analysis calculation and the responses may, therefore, be defined a priori for an analysis. It may be assumed that an operator will spend more or less time on a given EOP step attempting to remedy an equipment failure. However, given an assumption concerning the failure of certain equipment for a defined analysis scenario, that equipment will still be unavailable as far as the LOCA analysis boundary conditions are concerned. Furthermore, the operators have little latitude in the operations that may be attempted while working through the EOPs during the response to an accident. The possibility of various equipment failures is addressed within the procedures. When a failure is noted during a given step in the EOPs, the operators are directed immediately to an alternate action under a “Response Not Obtained” column. There, specific actions such as verifying or cycling a switch position or sending an operator into the field to perform a manual action are listed to attempt to remedy the failure. If the failure remains after the alternate action is taken, the operators note the failure and return to the subsequent actions directed by the EOPs.

Although some variability in the overall response times may occur from the operators spending time attempting to rectify individual failures – for example, time spent attempting to restart a failed safety injection pump – the net result is manifested only in terms of a few boundary conditions to a LOCA analysis. The only ones with potentially significant variability that could affect the ECCS performance prior to the time of PCT during a given small break LOCA calculation, are as follows:

[

] ^{a,c}

[

] ^{a,c}

a,c

7

25.6 CONTAINMENT RESPONSE

The containment pressure analyzed in the FSLOCA methodology is calculated using either the COCO code (Bordelon and Murphy, 1974) for dry containment designs or the LOTIC code (Hsieh and Raymond, 1976) for ice condenser containments. The COCO containment code was integrated into the WCOBRA/TRAC-TF2 thermal-hydraulic code. The mass and energy releases from WCOBRA/TRAC-TF2 are passed into COCO every timestep. COCO then calculates the containment pressure based on the containment model and the mass and energy releases, and passes the pressure back to WCOBRA/TRAC-TF2 as a boundary condition at the break. The COCO or LOTIC code is used to calculate the containment pressure [

] ^{a,c}

The containment model is designed to calculate a conservatively low containment pressure, including the effects of all the installed pressure reducing systems and processes. The previous Appendix K approach for calculating the containment pressure using the COCO or LOTIC code was described in Appendix A of (Bordelon et al., 1974). The same approach is generally followed within the FULL SPECTRUM LOCA methodology, with some exceptions as described herein.

Consistent values are used for inputs shared between the WCOBRA/TRAC-TF2 model and COCO model (such as the safety injection temperature), with the exception of the single failure assumption. The failure of a single-train of ECCS is assumed for the LOCA transient calculation, but all trains of containment spray, fan coolers, etc. are generally assumed to be in operation for the calculation of the containment pressure in order to further reduce the calculated containment pressure. The values for inputs pertinent only to the containment model are typically selected to provide a minimum containment pressure (e.g., maximum heat transfer areas and volumes are modeled for containment heat sinks).

[

] ^{a,c}

The LOTIC containment code is not integrated into the WCOBRA/TRAC-TF2 thermal-hydraulic code. [

] ^{a,c}

25.7 PUMP LOCKED ROTOR

The pump model includes transfer of momentum from the pump to the fluid, as described by Equation 10-1. Variable pump speed is taken into account through Equation 10-10. The pressure difference through the pump, and the torque applied by the fluid on the pump rotor are calculated using empirically determined single and two-phase homologous curves. The data used to obtain these curves is described in Section 10.4, Volume 1.

If the pumps lose power during the LOCA, the broken loop pump rotation will accelerate, while the intact loop pumps will coast down. Such an acceleration will impose centripetal stresses on the pump's flywheel. If the flywheel fails, there is a small chance that the rotor will become locked. [

$$[\quad]^{a,c}$$

[

$$]^{a,c}$$

[

] ^{a,c}

Figure 25.7-1 Comparison of Analysis and Experiment for Scale Model Flywheel Tests

a,c

Figure 25.7-2 [

] ^{a,c}

25.8 REFERENCES

1. American Nuclear Society, 1979, "American National Standard for Decay Heat Power in Light Water Reactors," ANSI/ANS-5.1-1979.
2. Akimoto, H., et al., 1984, "Pressure Drop through Broken Cold Leg During Reflood Phase of Loss-of-Coolant Accident of PWR," *Journal of Nuclear Science and Technology*, 21 [16].
3. Argall, B. M., et al., 1979, "Fuel Rod Bow Evaluation," WCAP-8691, Revision 1.
4. Bajorek, S. M., et al., 1998, "Code Qualification Document for Best Estimate LOCA Analysis," Volume 1 Revision 2, and Volumes 2 through 5, Revision 1, WCAP-12945-P-A (Proprietary).
5. Bordelon, F. M. and Murphy, E. T., 1974, "Containment Pressure Analysis Code (COCO)," WCAP-8327 (Proprietary), WCAP-8326 (Non-Proprietary).
6. Bordelon, F. M., et al., 1974, "Westinghouse Emergency Core Cooling System Evaluation Model – Summary," WCAP-8339.
7. Bordelon, F. M., et al., 1975, "The Westinghouse ECCS Evaluation Model: Supplementary Information," WCAP-8471-P-A (Proprietary).
8. Combustion Engineering, 1975, "Assessment of the Accuracy of PWR Safety System Actuation as Performed by the Core Protection Calculators (CPC)," CENPD-170-P.
9. Combustion Engineering, 1986, "C-E Setpoint Methodology, C-E Local Power Density and DNB LSSS and LCO Setpoint Methodology for Analog Protection Systems," CENPD-199-P, Rev.1-P-A.
10. Combustion Engineering, 1998, "C-E Setpoint Methodology," CENPD-199-P, Rev.1-P-A, Supplement 2-P-A.
11. Hsieh, T. and Raymond, M., 1976, "Long Term Ice Condenser Containment Code – LOTIC Code," WCAP-8354-P-A, Supplement 1 (Proprietary), WCAP-8355-A, Supplement 1 (Non-Proprietary).
12. Johnson, W. J., 1990, "Steam Generator Tube Deformation," NS-NRC-90-3557.
13. Mendler, O. J., 1975, "Method of Analysis and Evaluation of Jet Impingement Loads from Postulated Pipe Breaks," WCAP-8951.
14. Miller, R. W., et al., 1983, "Relaxation of Constant Axial Offset Control/ F_q Surveillance Technical Specification," WCAP-10216-P-A.
15. Morita, T., et al., 1974, "Power Distribution Control and Load Following Procedures," WCAP-8385-P-A.

16. Nissley, M. E., et al., 2005, "Realistic Large-Break LOCA Evaluation Methodology Using the Automated Statistical Treatment Of Uncertainty Method (ASTRUM)," WCAP-16009-P-A and WCAP-16009-NP-A.
17. Salvatori, R., 1973, "Topical Report, Reactor Coolant Pump Integrity in LOCA," WCAP-8163.
18. Spier, E. M., et al., 1988, "Evaluation of Nuclear Hot Channel Factor Uncertainties," WCAP-7308-L-P-A.
19. U.S. Nuclear Regulatory Commission, 1989, "Best-Estimate Calculations of Emergency Core Cooling System Performance," Regulatory Guide 1.157.

26 WCOBRA/TRAC-TF2 MODEL OF PILOT PLANTS

26.1 MODELING APPROACH

26.1.1 Introduction

All U.S. designed light water Pressurized Water Reactors (PWRs) have the same fundamental design. The functions of the major system components such as the reactor vessel, pressurizer, steam generators, and pumps are the same, and most have similar design features. Differences between PWR systems are primarily due to loop design and the Emergency Core Cooling System (ECCS) configuration. Operating Westinghouse units, for example, have loop designs that are 2x2 (two-loop), 3x3 (three-loop), and 4x4 (four-loop), while Combustion Engineering units, Westinghouse advanced plants (AP600 plant, **AP1000**[®] plant), and Babcock and Wilcox (B&W) units have a 2x4 loop arrangement. With the exception of size, and the B&W once-through steam generator, individual loop flow paths in each type of system are similar.

At a higher level, the reactor vessel internals for various PWRs are also similar. However, there are differences in the design details of the internal structures in various vessel regions. In some older Westinghouse plants for example, the lower support plate is curved while in other plants it is flat. Within the core, there are differences in fuel design. Some plants have a thermal shield in the downcomer, while others have a neutron pad attached to the core barrel. B&W plants include vent valves in their core barrels. The upper plenums and upper heads contain control rod guide tubes and support structures that may have slightly different designs and arrangements.

The differences in the various PWR designs lead to differences in flow areas, volumes, and surface areas within various regions of the PWR primary system. The WCOBRA/TRAC-TF2 nodalization for a PWR Reactor Coolant System (RCS) must model specific flow paths and regions within the system. Thus, the PWR design itself dictates, to an extent, the specific nodalization and inputs for a plant model.

[

]^{a,c}

The following sections describe how a RCS is modeled using WCOBRA/TRAC-TF2. Two three-loop plant models are described in detail to show a consistent modeling approach that can accommodate different plants. The relationship between the plant nodalizations and the nodalizations for the experimental tests is discussed.

Noding Strategy and Modeling Philosophy

Given that a degree of noding sensitivity to the results is unavoidable, there must be a specific relationship between the noding scheme used for the PWR compared to the noding scheme for the experiment simulations (since these simulations form the validation basis for the physical models in the code). Reinforcing noding consistency to the extent practical between the Separate Effects Tests (SETs), Integral Effects Tests (IETs) and the PWR will ensure that same conclusions with respect to biases and uncertainties derived from the code and model assessments will be applicable to the PWR LOCA simulations for which the Evaluation Model (EM) was designed. Exceptions to this noding philosophy are discussed on a case-by-case basis.

The definition of an optimal nodding strategy to apply to a specific region or component is ideally an iterative process between a realistic modeling of the test features while maintaining consistency across tests facilities and the PWR which span over a full range of scales. [

] ^{a,c}

The result of this process is the generation of modeling guidelines which were applied in the modeling the SETs, IETS and PWR presented in Volume 2 of this Topical Report.

[

] ^{a,c}

The resulting consistency in the application of the modeling guidelines for the PWR relative to the test facilities is presented in Section 26.1.2.

26.1.2 Modeling Consistency

Volume 2 documented simulations of experimental tests in a broad range of facilities using WCOBRA/TRAC-TF2. These tests were modeled so that a consistent nodding methodology could be established for use in PWRs and other experimental facilities. This section compares the experimental test and RCS nodding in various regions. The RCS nodding is described in detail for both V. C. Summer (CGE) and Beaver Valley Unit 1 (DLW) in subsequent sub-sections.

Core Axial Noding

The axial noding in a PWR core and in tests with simulated cores is established by the overall heated length and the location of spacer grids. Table 26.1-1 lists input parameters used in modeling experimental tests with heated bundles, and the PWR models. The table lists the number of grids, the number of axial hydraulic cells used to model the core, and the range of cell heights. As can be seen in this table, the average cell heights for all of the test models and the plant models fall within a narrow range.

Core Lateral Noding

The grouping of assemblies in WCOBRA/TRAC-TF2 models for the large scale experimental tests and PWRs depends on the relative radial power distribution in addition to the potential flow delivery from the upper plenum. Three large scale experimental test facilities having heated cores were modeled: Cylindrical Core Test Facility (CCTF) (Section 19.6), Rig-of-Safety Assessment (ROSA) (Section 21), and LOFT (Section 22). Consistency between the lateral core nodalization in these tests and the PWR models can be characterized as follows:

- Hot Assembly – A hot assembly is modeled in the PWR, with plant-specific input determining the possible lateral power distributions. The hot assembly in the PWR is surrounded by one of the average assembly channels. A hot assembly was modeled in each of these experimental facilities based on the radial power profile imposed on the test bundles. For LOFT, the central assembly was the hot assembly. This assembly was cross-connected to an average core channel. In CCTF, test bundles 29 to 32 were approximately one-fourth the size of a typical PWR bundle and all had the same relative high power. These four bundles were grouped and modeled as a single hot assembly, which was connected laterally to the low and medium powered assemblies below open holes and guide tubes. The ROSA hot assembly modeled a total of 8 high-power bundles, which represent one-third of the entire heated core. The ROSA hot assembly had crossflow links to both the average and low power channels (bundles).
- Upper Plenum Structures – The PWR hot assembly is assumed to reside in a location in which the flow is restricted from above. Other channels represent the core regions below support columns and guide tubes, or the low power peripheral assemblies. In LOFT, the hot channel was the central bundle, which had the highest power. The LOFT core had two other channels; one representing the four bundles beneath guide tubes, and another representing the four corner assemblies. The corner bundles were located below structures similar to support columns. In CCTF, the core was modeled by four channels; a hot channel, a channel for the bundles below guide tubes, a channel for bundles beneath open core plate holes, and a channel representing the eight low power bundles on the core perimeter beneath support columns. In the ROSA model, the hot assembly is modeled as being located below open holes and guide tubes. The ROSA model had two other channels; one representing the average power assemblies and another for the outer lower power assemblies.
- Radial Power Distribution – The radial power distribution is accounted for in both the PWR models and in the LOFT, CCTF, and ROSA models by representing various regions with several WCOBRA/TRAC-TF2 nuclear or heated rods.

Hot Leg Noding

Only the LOFT, CCTF, and ROSA experimental tests included hot legs that connected scaled upper plenums to functional steam generators. Table 26.1-2 lists the cell sizes in these test models and the PWR models. [

] ^{a,c}

Steam Generator Noding

Table 26.1-3 compares the primary side hydraulic cell lengths in the experimental test models and the PWR models. Because the LOFT and CCTF steam generators were less than full-scale in height, fewer cells are used. While in the CCTF steam generator the cell length remained very similar to that of the PWR, the LOFT value became small. Increasing the cell size in LOFT would result in excessively coarse noding for that test. The ROSA steam generator noding and the noding for the two pilot plants are similar. The ROSA facility and both pilot plants used the same number of nodes, resulting in roughly the same cell lengths for the steam generator tubes.

Crossover Leg Noding

Only the LOFT and ROSA facilities had crossover legs connecting the steam generator to actual pumps. The crossover leg noding from LOFT and ROSA is compared to the plant model noding in Table 26.1-4. As can be seen in this table, the hydraulic cell lengths are similar in the PWR models. In LOFT, the number of cells was reduced to increase cell size so the cell length is closer to the PWR models. In the ROSA model, the number of cells was increased to model the deeper loop seal and decrease the cell length.

While the UPTF facility used simulators for the steam generator and pump components, [

] ^{a,c}

Pump Noding

The pump is modeled as a two-cell component, with pump curves supplied as input. The LOFT pump and the plant model pumps are modeled the same way, with the exception of the pump curves. LOFT-specific pump curves are used for that facility, while pump curves appropriate for the plant-specific pump design are used in the plant models. Similar to LOFT, the ROSA pump model had two cells with ROSA-specific homologous curves.

Cold Leg Noding

Table 26.1-5 lists the separate effects and integral effects test facilities in which cold leg models were used. [

] ^{a,c}

26.1.3 Conclusions

A set of guidelines has been established so that nodalization of test facilities and full-scale plants is done in a consistent fashion. Axial noding in the core is based on the bundle heated length and the location of spacer grids, which defines the cell height to be approximately 10 inches. Lateral noding in the core is determined by the radial power distribution and the likelihood of flow delivery due to the upper plenum internals arrangement, with a hot assembly explicitly modeled.

In the upper and lower plena, the plant models and large scale integral tests are modeled consistently. A counter-current flow limitation (CCFL) region, which extends from the top of the active fuel to the upper core support plate, is modeled explicitly in the PWRs as well as in the UPTF, CCTF, ROSA, and LOFT models. In this region, channels are used to model the flow area through the fuel assembly nozzles extended up to the upper core plate. These channels are referred to as jet channels. The remainder of the volume in this region is modeled in a global or several global channels. The regions below the lower core support plate and above the upper core support plate are also modeled in a similar manner, with differences in noding used to account for physical differences in the various designs.

In the loop components, the number of cells and/or cell sizes used in the test models and in the PWR models are approximately the same. Differences in cell size or the number of cells, such as those in the LOFT and ROSA models, are due to unique features of the facility. In cases where the facility design required a deviation from the general guidelines, additional detail was put into the model.

While a close connection is maintained between noding for the test facilities and PWRs, an important feature of WCOBRA/TRAC-TF2 modeling is its flexibility. The noding with WCOBRA/TRAC-TF2 is not prescribed as was the noding in Appendix K type Evaluation Models. With WCOBRA/TRAC-TF2, additional noding detail is added as the actual hardware being modeled requires. Thus, additional sections can be added in the upper plenum, for example, if behavior is expected to be non-uniform as in the case of a plant with core deluge jets.

In some plants, the hot assembly location may differ. The assembly location in a PWR which leads to the highest peak cladding temperature depends not only on the core design, but also on the upper plenum internals arrangement, which determines the amount of downflow cooling, and the crossflow from surrounding assemblies. The PWR hot assembly location must then be determined from review of the internals layout and the technical assessment described in subsequent sections for the specific plants to be analyzed.

Table 26.1-2 Hot Leg Noding Comparison

a,c

Table 26.1-3 Steam Generator Noding Comparison

a,c

Table 26.1-4 Crossover Leg Noding

a,c

Table 26.1-5 Cold Leg Noding

a,c

26.2 V. C. SUMMER NUCLEAR POWER PLANT

The vessel and loop portions of a PWR are modeled with significant detail for WCOBRA/TRAC-TF2 within the Westinghouse FULL SPECTRUM LOCA (FSLOCA) Evaluation Model.

V. C. Summer is a three-loop plant containing Westinghouse 17x17 VANTAGE PLUS (V+) fuel with IFMs and **ZIRLO**[®] cladding. The nominal core power for this plant is 2,900 MWt. V. C. Summer also has Westinghouse DELTA-75 replacement steam generators.

26.2.1 V. C. Summer WCOBRA/TRAC-TF2 Nodalization

The CGE vessel geometry as modeled in WCOBRA/TRAC-TF2 is described in Section 26.2.1.1; a description of the core modeling is provided in Section 26.2.1.2, the loop geometry is described in Section 26.2.1.3, and the ECCS modeling is detailed in Section 26.2.1.4.

26.2.1.1 Vessel Model

Figure 26.2-1 shows the vessel drawing for the V. C. Summer three-loop PWR. Figure 26.2-2 shows the vessel major internal component elevation layout. The elevations shown on the right are relative to the inside bottom of the vessel. This elevation layout contains most of the information needed to divide the vessel into nine vertical sections. These sections are described in turn starting at the bottom of the vessel.

The bottom of vessel Section 1 is the inside vessel bottom. The bottom of vessel Section 2 is the bottom of the upper tie plate. The bottom of vessel Section 3 is defined as the beginning of the active fuel. The bottom of vessel Section 4 is the top of the active fuel. The bottom of vessel Section 5 is the elevation at the bottom of the upper core plate. The bottom of vessel Section 6 is equal to the elevation of the bottom of the hot leg inner wall. The bottom of vessel Section 7 is the elevation of the inside top of the hot leg. The bottom of vessel Section 8 is the elevation at the top of the upper support plate. The bottom of vessel Section 9 is the elevation at the top of the upper guide tube in the upper head. The top of vessel Section 9 is the inside top of the vessel upper head.

After defining the elevations for each section, a noding scheme is defined following the same basic philosophy applied to the SET and IET facilities as described in Section 26.1.1 of this document.

[

]^{a,c}

Figures 26.2-3 through 26.2-6 illustrate the V. C. Summer vessel noding. Figure 26.2-3 is a vertical section noding diagram. Figures 26.2-4 through 26.2-6 are the horizontal “plan” views of each section. In these figures, the numbers within the squares are the channel numbers and the numbers within the circles with arrows attached to them are the gap numbers. A gap is used to define a horizontal flow path between channels. Positive flow is in the direction indicated by the arrow. It is assumed within WCOBRA/TRAC-TF2 that a vertical flow path for vertically stacked channels exists unless specified otherwise in the input. Upward axial flow is considered as positive flow.

As can be seen in Figures 26.2-3 through 26.2-6, 89 channels and 89 gaps are used for V. C. Summer to define the vessel. It can be seen in Figure 26.2-3 that several of the nine vertical sections are sub-divided into two or more levels. For example, the active fuel region, vessel Section 3, is divided into 14 vertical levels. By accounting for the vertical sub-division within vessel Sections 2, 3, 5 and 7, the vessel model for V. C. Summer has a total of 309 fluid cells.

Vessel Section 1 models the vertical section of the vessel from the inside bottom of the vessel to the bottom of the upper tie plate. The modeling of this section is relatively simple since there is one channel with one vertical cell and no horizontal flow gaps (Figures 26.2-3 and 26.2-4). Channel 1 completely represents Section 1 of the vessel. The top flow area of this channel/section was computed based on the net flow area at the bottom of the tie plate.

Vessel Section 2 models the vertical section of the vessel from the bottom of the upper tie plate to the bottom of the active fuel region. This section contains two vertical cells for ten channels (designated 2 through 5 and 52 through 57) and horizontal flow gaps (numbered 1 through 6 and 46 through 57). Figures 26.2-3 and 26.2-4 provide an illustration for the vertical and radial representation of this section of the vessel model.

Channels 2, 3, 4, 52, 53, 54, 55, 56, and 57 each represent one-ninth of the annulus volume between the vessel inner wall and the core barrel outer wall, and are connected by Gaps 4 through 6 and 52 through 57. Channel 5 is the lower plenum volume between the upper tie plate and the fuel nozzle elevation.

[

]^{a,c}

The area at the top of Channel 5 is equal to the sum of the areas modeled at the bottom of Channels 9 through 13 in vessel Section 3. Area variation inputs are used to vary the flow area between the lower and upper cells of Channel 5 to account for the change in flow area within this channel due to the lower support plate. The radial flow gaps modeled in vessel Section 2 are illustrated in Figures 26.2-3 and 26.2-4 with positive flow in the direction indicated in the figure. Gaps 1, 2, 3, 46, 47, 48, 49, 50, and 51 model a radial flow gap in the lower cell of vessel Section 2, with the core barrel extension blocking radial flow from the upper cell of the downcomer channels into the upper cell of lower plenum Channel 5.

Vessel Section 3 models the vertical section of the vessel from the bottom to the top of the active fuel region. The modeling is accomplished using fourteen vertical cells in fourteen channels (designated 6 through 13 and 58 through 63) and thirteen horizontal flow gaps (designated 7 through 13 and 58 through 63). Figures 26.2-3 and 26.2-4 provide an illustration for the vertical and radial representation of this section of the vessel model.

Channels 6 through 8 and 58 through 63 each represent one-ninth of the downcomer annulus volume between the vessel inner wall and the core barrel outer wall. The neutron pads are modeled in this section. Channel 9 is the volume between the core barrel inner wall and the baffle plates, which is designated as the barrel/baffle channel. For V. C. Summer, flow travels upward through this region during normal operation which is referred to as an upflow barrel/baffle design.

Channels 10 through 13, combined, represent the total volume within the baffle plates, i.e., the entire core active fuel region for all 157 assemblies. Channel 10 includes assemblies on the periphery of the core which have relatively low power. [

]^{a,c}

[]^{a,c} A map of the different structures in the upper plenum is presented in Figure 26.2-7. There are six types of upper internals in the V. C. Summer upper plenum: guide tubes, open holes, orifice plates, support columns, free-standing flow mixers, and support columns with flow mixers. [

] ^{a,c}

The gaps modeled in vessel section 3 are illustrated in Figure 26.2-4. The 144-inch active fuel length is divided into fourteen axial cells. The grids and their associated form losses are modeled within this length range at their specified elevations. [

] ^{a,c}

Vessel Section 4 includes the vertical section of the vessel from the top of the active fuel to the bottom of the upper core plate. This section has one vertical cell and uses fourteen channels (designated 14 through 21 and 64 through 69) and thirteen horizontal flow gaps (17 through 23 and 64 through 69) to model this portion of the vessel. Figures 26.2-3 and 26.2-5 illustrate the vertical and radial representation of this section of the vessel model.

Section 4 of the model is referred to as the CCFL region, where CCFL is the acronym for counter-current flow limitation. [

] ^{a,c}

Channels 14, 15, 16, 64, 65, 66, 67, 68, and 69 each represent one-ninth of the downcomer annulus volume between the vessel inner wall and the core barrel outer wall. [

] ^{a,c} Channel 17 is modeled with no vertical flow path into or out of the top of the channel. The gaps within vessel Section 4 are illustrated in Figure 26.2-5.

Vessel Section 5 extends vertically from the bottom of the upper core plate to the inner bottom of the hot leg. This section contains two vertical cells for fifteen channels (designated 22 through 29, 51, and 70 through 75) and fourteen horizontal flow gaps (24 through 30, 45, and 70 through 75). Figures 26.2-3 and 26.2-5 provide an illustration of the vertical and radial representation of this section of the vessel model.

Channels 22, 23, 24, 70, 71, 72, 73, 74, and 75 each represent one-ninth of the downcomer annulus volume between the vessel inner wall and the core barrel outer wall. [

] ^{a,c} There is no flow into the bottom of Channel 25 from vessel Section 4. Since these Channels (27, 28, and 29) are all surrounded by the inner global upper plenum Channel 25, this region constitutes another area where CCFL may be calculated. [

] ^{a,c} Similar to Channel 25, there is no flow into the bottom of Channel 51 from vessel Section 4. Figure 26.2-5 defines the gaps for vessel Section 5.

Vessel Section 6 models the vertical section of the vessel from the bottom to the top of the hot leg (inner diameter). One vertical cell in sixteen channels (designated 30 through 39 and 76 through 81) and fourteen horizontal flow gaps (designated 31 through 38 and 76 through 81) are used to model this section. Figures 26.2-3 and 26.2-5 provide an illustration for the vertical and radial representation of this section of the vessel model.

Channels 30, 31, 32, 76, 77, 78, 79, 80, and 81 each represent one-ninth of the downcomer annulus volume between the vessel inner wall and the core barrel outer wall, excluding the volume of the hot leg which passes through this region. Note that the cold legs of the loop model connect to vessel downcomer Channels 30, 76, and 79. [

] ^{a,c}

Gaps 36, 37, and 38 are added to model the radial flow into the hot leg channels from the outer global Channel 34. Channels 37, 38, and 39 complete vessel Section 6, modeling the hot leg nozzles and serving as an interface to the hot legs in the loop model.

Vessel Section 7 extends vertically from the top of the hot leg to the top of the upper support plate, and is divided into two levels. This section contains two vertical cells for thirteen channels (designated 40 through 46 and 82 through 87) and eleven horizontal flow gaps (39 through 43 and 82 through 87). Figures 26.2-3 and 26.2-6 illustrate the vertical and radial representation of this section of the vessel model. The interface at the top of the downcomer in Vessel Section 7 with the upper head is via the spray nozzles; a loss coefficient is modeled to reflect the flow through this interface.

Channels 40, 41, 42, 82, 83, 84, 85, 86, and 87 each represent one-ninth of the downcomer annulus volume between the vessel inner wall and the core barrel outer wall. Channel 45 is a vertical extension of Channel 35 in vessel Section 6. [

] ^{a,c} and is a vertical extension of Channel 36 from vessel Section 6. Channel 43 is the inner global region and is a vertical extension of Channel 33 from vessel Section 6. Channel 44 is the outer global region and is a vertical extension of Channel 34 from vessel Section 6. There is no vertical flow connection between Channels 43, 44, and 45 to vessel Section 8 above. Channels 40 through 42 and 82 through 87, however, connect vertically to vessel Section 8 via the upper head spray nozzles. Guide tube Channel 46 also connects vertically to vessel Section 8 through the guide tube extension. The eleven gaps in vessel Section 7 are illustrated in Figure 26.2-6.

Vessel Section 8 extends vertically from the top of the upper support plate to the top of the upper guide tube. This section has one vertical cell for five channels (designated 47 through 49, 88, and 89) and six horizontal flow gaps (14 through 16, 44, 88, and 89). Figures 26.2-3 and 26.2-6 illustrate the vertical and radial representation of this section of the vessel model.

The boundary between outer Channels 47, 88, and 89 and inner Channel 48 is formed by the cylinder which intersects the inside of the upper head sphere at the top of the upper guide tube (Figure 26.2-3). Channels 47, 88, and 89 each include one-third of the volume in the upper head outside this boundary while Channel 48 models the volume inside this boundary, excluding the volume of the upper guide tubes. There is no flow into Channel 48 from below since the upper support plate prevents direct flow communication between the upper head and the upper plenum. Channel 49 models the volume inside of the upper guide tubes. There is no flow communication between the fluid inside the upper guide tube enclosure and Channel 48 in Section 8 of the vessel.

Vessel Section 9 models the vertical section of the vessel extending from the top of the upper guide tubes to the inside top of the vessel head. Similar to Section 1 of the vessel, vessel Section 9 is modeled as one channel (50) containing one vertical cell with no horizontal flow gaps (Figures 26.2-3 and 26.2-6). The flow area at the bottom of Channel 50 (vessel Section 9) is equal to the sum of the flow area at the top of Channels 48 and 49 from vessel Section 8.

26.2.1.2 Core Model

Rod 1 is the [

] ^{a,c} It is located in the hot assembly (Channel 13) which is an assembly under a support column with a flow mixer. Rod 2 represents the remaining 263 fuel rods in the hot assembly and has a power equivalent to the hot assembly average fuel rods.

Rod 5 represents the 28 assemblies in the outer low powered region (Channel 10) and contains (28 assemblies) * (264 fuel rods/assembly) fuel rods. The fuel rods in the remaining 128 assemblies are divided up in proportion to the number of assemblies used in Channels 11 and 12 in the core. The guide tube channel contains (53 assemblies) * (264 fuel rods/assembly) fuel rods that are represented by fuel rod 3. The OH/SC/FSM channel contains (75 assemblies) * (264 fuel rods/assembly) fuel rods that are represented by fuel rod 4.

The nuclear fuel rods are initialized with internal gas compositions, and fuel average temperatures from the PAD5 code (Crede et al., 2013).

[

] ^{a,c}

26.2.1.3 Loop Model

The V. C. Summer loop model is presented in Figure 26.2-8, with a more detailed noding for the steam generators shown in Figure 26.2-9. As with the vessel inputs, each component in the one-dimensional loop has various cells to allow for specific changes in geometry along the component. Each component is identified by a module title, a unique component number, and connections to numbered junctions. The three loops are defined using 37 components and 41 junctions. Components and junctions are indicated by rectangles (squares) and circles, respectively, in Figures 26.2-8 and 26.2-9.

Loop 1 is the loop which contains the pressurizer. Component 11 is the hot leg and was modeled with a TEE module. Component 19, the pressurizer (PRIZER module) is connected to the secondary branch of the hot leg TEE. [

] ^{a,c}

The primary side of the steam generator is modeled as Component 12; with the secondary side consisting of several components. TEE Component 112 is the shell of the steam generator secondary side. The feedwater connection is modeled as TEE Component 113, and the downcomer of the steam generator is PIPE Component 114. The feedwater is injected through FILL Component 17, and the steam flows through TEE Component 118 and then exits via either the Main Steam Isolation Valve (MSIV) (VALVE Component 218 and BREAK Component 18) or the Main Steam Safety Valve (MSSV) (VALVE Component 318 and BREAK Component 418). [

] ^{a,c}

Continuing around the loop are the crossover leg (PIPE Component 13) and reactor coolant pump (PUMP Component 14). It is noted that flow stratification is allowed in the loop seal bends via the use of the STRTX input. The cold leg is next, divided into two TEE components in order to model safety injection (FILL Component 63) and accumulator injection (accumulator PIPE Component 62). Component 15 is the pump-side cold leg safety injection TEE and Component 16 is the vessel-side cold leg accumulator TEE. The accumulator line is modeled as a VALVE module (Component 61) which simulates the check valve. The accumulator tank itself (Component 62) is modeled with a PIPE component and an associated input which causes an accumulator module to be invoked.

The accumulators and pressurizer components have two junctions, although they only have a single communication path with the RCS. As such, zero FILL Components 119 and 162 are provided as boundary conditions for the junction not in communication with the RCS.

Loop 2 is set up much the same way, except that the hot leg (Component 21) is modeled as a PIPE module in the absence of the pressurizer and the safety injection (SI) and accumulator injection points are reversed based on the actual plant ECCS configuration. Loop 3 is modeled the same as Loop 2.

[

] ^{a,c} BREAK Component(s) 4 and/or 6 are used to model containment conditions for the transient (depending on the break type, either one or both of the components are required). [

] ^{a,c}

Finally, thimble bypass is modeled using three separate PIPE modules (loop Components 50-52) connected to the bottom cells of the low power, guide tube, and OH/SC/FSM core channels in vessel Section 3 and the corresponding CCFL channels in vessel Section 4.

26.2.1.4 Emergency Core Cooling Safety Injection Model

The Safety Injection System (SIS) for V. C. Summer consists of three accumulator tanks, two charging/safety injection pumps, and two low head Residual Heat Removal (RHR) pumps. Each pump is connected to injection lines which inject directly into each cold leg. The accumulators are modeled to inject at a nominal pressure, a nominal temperature, and a nominal water volume. The pumped safety injection flow is modeled assuming a nominal temperature and the loss of one train of safety injection pumps (one SI and one RHR). The loss of one train of safety injection is considered as the limiting single failure assumption.

[

]^{a,c}

26.2.2 V. C. Summer Reference Case and Allowable Plant Operating Conditions

The best-estimate methodology establishes a sampling of the distribution of potential uncertainty contributors which occur due to changes in plant or model variables (Section 29). The following paragraphs describe the assumptions in the key LOCA parameters for V. C. Summer.

The reference case input values for V. C. Summer are listed in Table 26.2-1. The input values fall under three categories: 1) plant physical description, 2) plant initial operating conditions, and 3) accident boundary conditions. The values used for the reference case for each of these parameters are discussed in the following subsections.

For most of the parameters, the nominal value is assumed for the reference case. For others, a bounding or conservative value is assumed. The uncertainty associated with these parameters is accounted for in the uncertainty analysis, as shown in Section 31.

26.2.2.1 Plant Physical Description

[

]^{a,c}

26.2.2.2 Plant Initial Operating Conditions – Reactor Power

1. **Initial Core Average Linear Heat Rate** – The core power assumed for the Region I reference case is 102 percent of the power level, and for the Region II reference case is 100 percent of the power level (2900 MWt).
2. **Hot Rod Peak Linear Heat Rate** – The total peaking factor (FQ) for the reference case is derived from [^{a,c}].
3. **Hot Rod Average Linear Heat Rate ($F_{\Delta H}$)** – In the reference case, $F_{\Delta H}$ is derived from [^{a,c}].
4. **Hot Assembly Average Linear Heat Rate** – The minimum difference between the power generated in the hot rod and that in the hot assembly average rod is conservatively assumed. The hot assembly average rod is assumed to be [^{a,c}] lower in power than the hot rod.

5. **Hot Assembly Peak Linear Heat Rate** – Consistent with the average linear heat rates, the peaking factor used to calculate the peak linear heat rate generated in the hot assembly average rod is []^{a,c} lower than the value assumed in the hot rod.
6. **Axial Power Distribution** – The power distributions represented by the power shapes assumed for the reference cases are presented in Figure 26.2-10, and correspond to []^{a,c}
7. **Low-Power Region (PLOW)** – Current and expected core designs for V. C. Summer result in a range of PLOW from []^{a,c} is selected as the value for the reference case.
8. **Burnup** – The burnup is selected from the time-in-cycle, which is a sampled attribute within the uncertainty analysis. For the reference case, a nominal cycle burnup equal to []^{a,c} is assumed.
9. **Prior Operating History** – The power distribution assumed to exist at the time of the LOCA is conservatively assumed to have existed since plant startup when determining fission product inventories.
10. **Moderator Temperature Coefficient (MTC)** – The maximum value specified in the Technical Specifications for hot full power is assumed, to conservatively estimate core reactivity and fission power.
11. **Hot Full-Power (HFP) Boron Concentration** – A value typical of those used in current cores is assumed.

26.2.2.3 Plant Initial Operating Conditions – Fluid Conditions

1. **Average Fluid Temperature (T_{avg})** – The nominal value during normal full-power operation of 572.0°F is used for V. C. Summer.
2. **RCS Pressure** – The nominal value (2250 psia) is assumed for the V. C. Summer reference case.
3. **Loop Flowrate** – []^{a,c} loop flow is assumed for the reference case.
4. **Upper Head Temperature (T_{UH})** – The appropriate best estimate value of T_{UH} is assumed.
5. **Pressurizer Level** – The nominal value of pressurizer level is assumed.
6. **Accumulator Water Temperature** – A nominal (midpoint) value within the range established for V. C. Summer is assumed.
7. **Accumulator Pressure** – A minimum value of accumulator pressure is assumed for Region I, and a nominal (midpoint) value of accumulator pressure is assumed for Region II.

8. **Accumulator Water Volume** – A nominal (midpoint) value of accumulator water volume is assumed.
9. **Accumulator Line Resistance** – A best-estimate value of accumulator line resistance is assumed.
10. **Accumulator Boron Concentration** – The Technical Specification minimum value is assumed.

26.2.2.4 Accident Boundary Conditions

1. **Break Location** – [

] ^{a,c}

6. **Safety Injection Temperature** – Nominal (midpoint) values are assumed.
7. **Safety Injection Delay** – Maximum values consistent with the offsite-power assumption (offsite power available) are used.
8. **Containment Pressure** – A conservatively low value is assumed.

¹ The approach described in Section 30.4 to determine the [^{a,c} is superseded by limitation and condition #15 from the safety evaluation report (SER).

9. **Single-Failure Assumption – [**

]^{a,c}

26.2.3 Plant Operating Range

The [^{a,c} developed by the best-estimate methodology are valid for a range of plant operating conditions. Several parameters in the reference calculation are at nominal values. The range of variation of the operating parameters is accounted for in the uncertainty analysis. This is accomplished by assuring that, in the sampling of the attributes for each scenario (Section 31), [^{a,c}. Westinghouse has processes in place with the utilities to ensure that the analyzed ranges bound the plant operation.

a,c

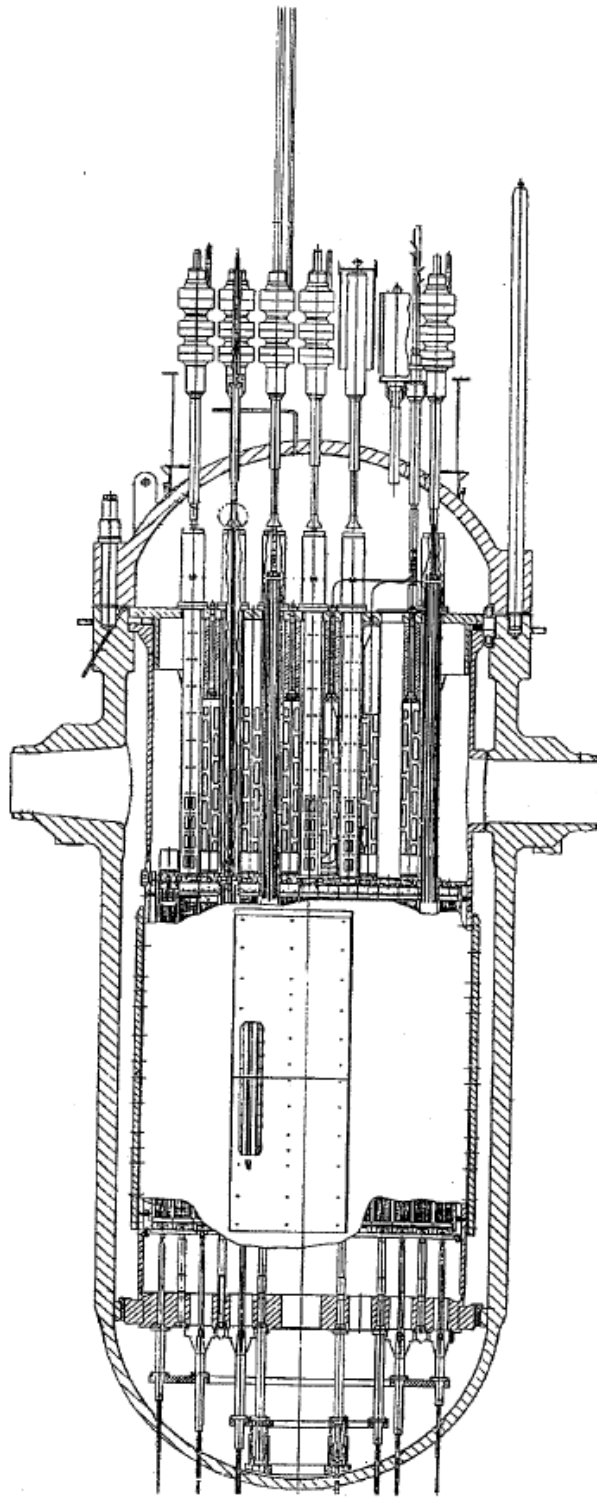


Figure 26.2-1 Virgil C. Summer Vessel Profile

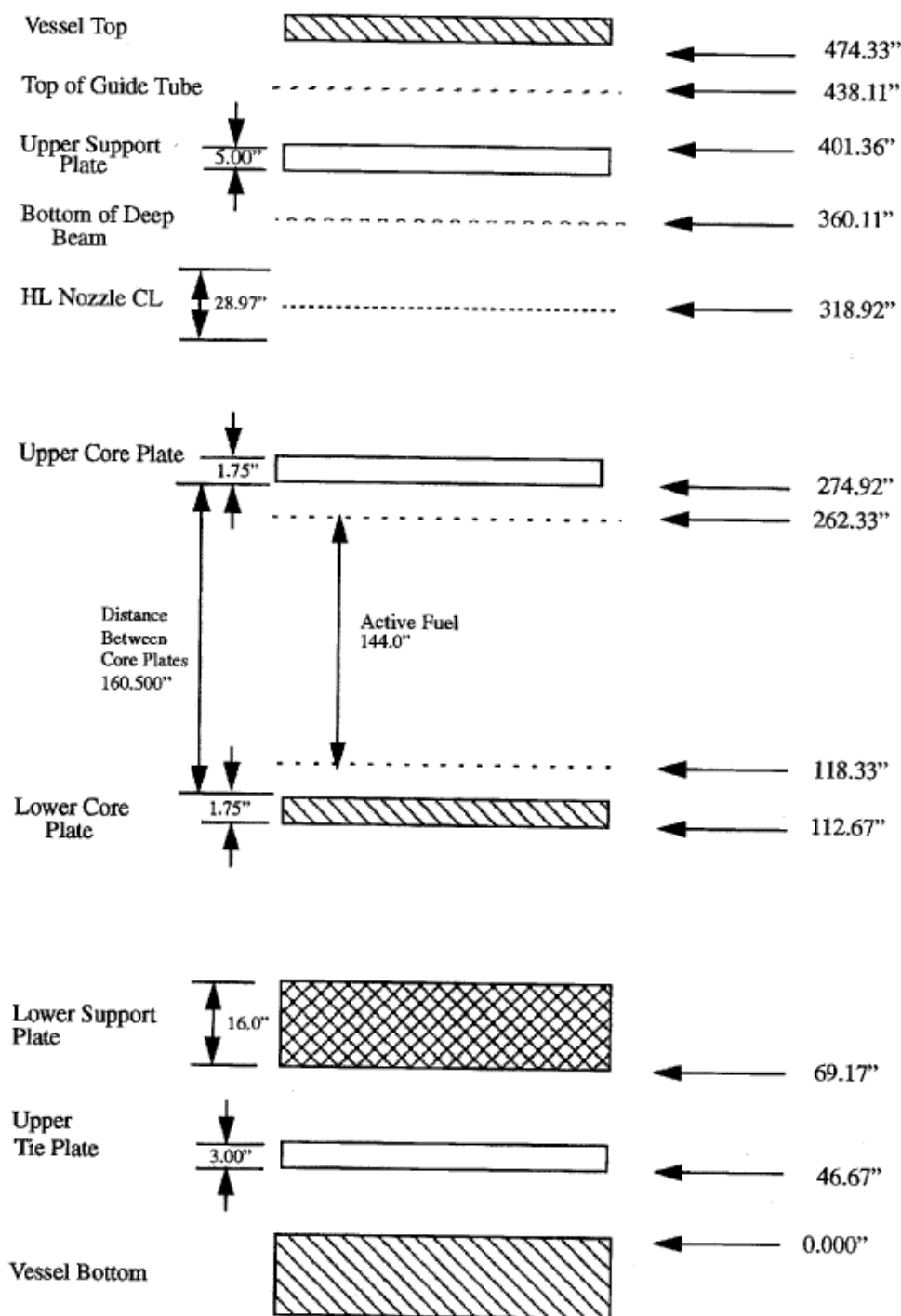


Figure 26.2-2 Virgil C. Summer Vessel Component Elevations

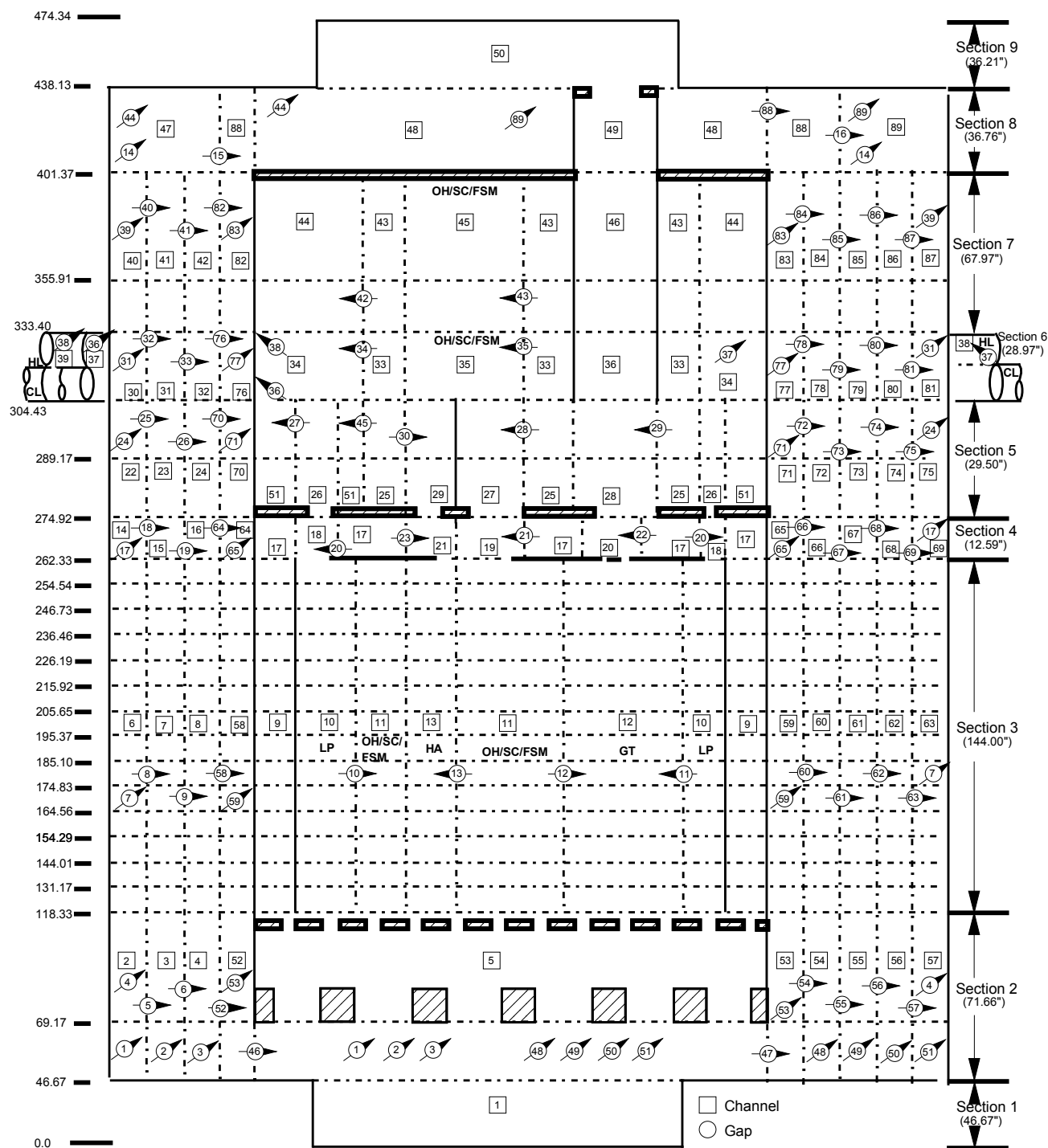
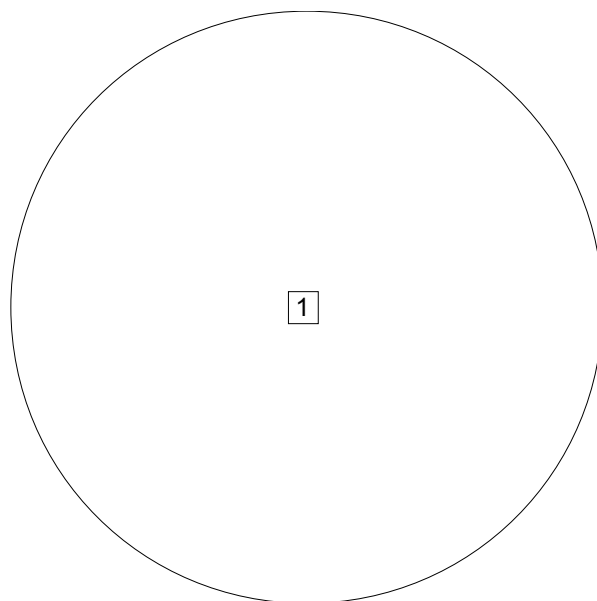


Figure 26.2-3 Virgil C. Summer Vessel Model Noding Diagram

**SECTION 1: LOWER HEAD**

□ Channel
○ Gap

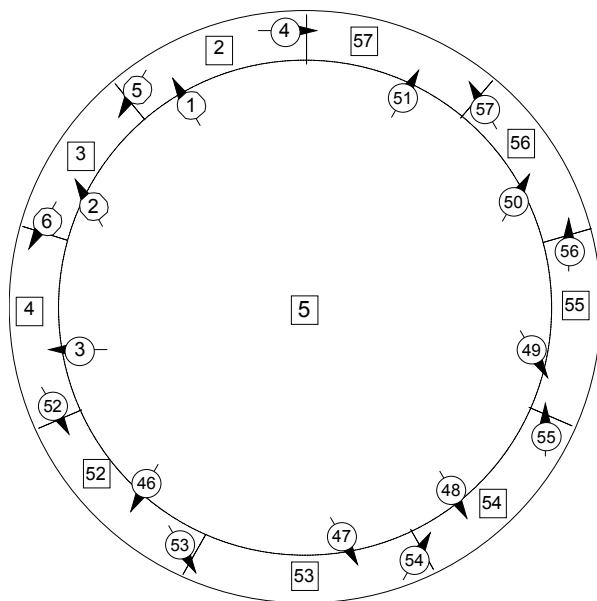
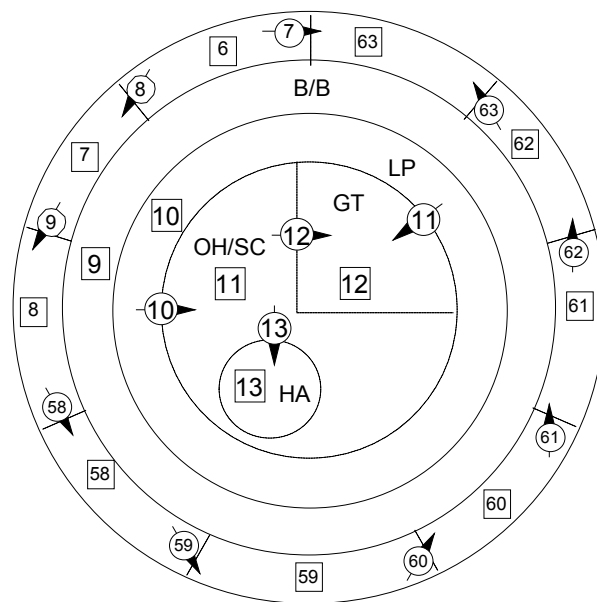
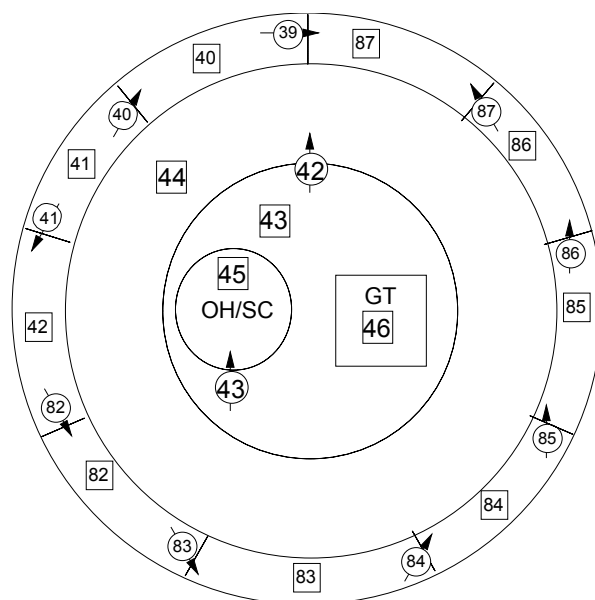
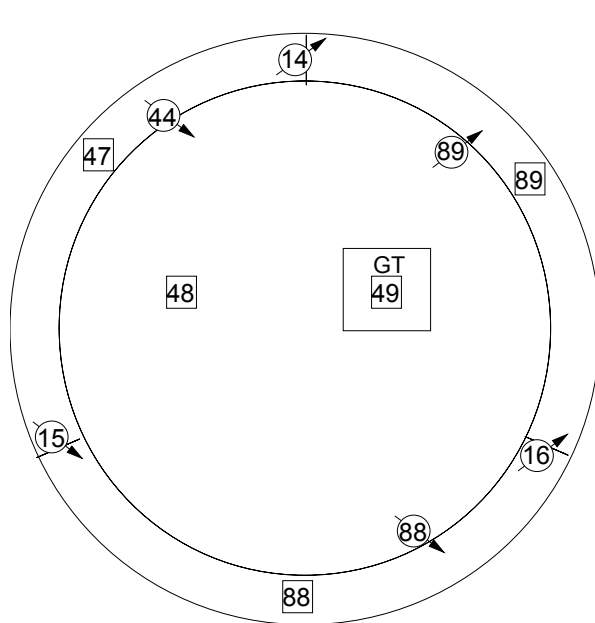
**SECTION 2: LOWER PLENUM****SECTION 3: CORE REGION****Figure 26.2-4 Virgil C. Summer Vessel Sections 1 through 3**

Figure 26.2-5 Virgil C. Summer Vessel Sections 4 through 6

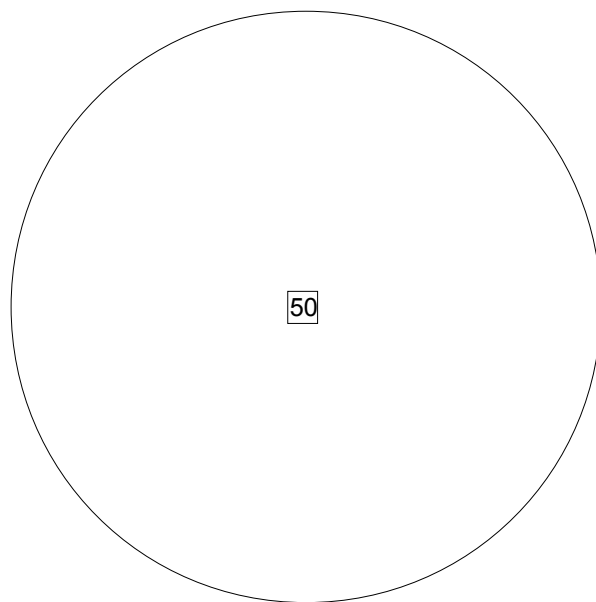


**SECTION 7: UPPER PLENUM
ABOVE NOZZLES**

□ Channel
○ Gap



**SECTION 8: UPPER HEAD UP TO
TOP OF GUIDE TUBES**



**SECTION 9: UPPER HEAD ABOVE
GUIDE TUBES**

Figure 26.2-6 Virgil C. Summer Vessel Sections 7 through 9

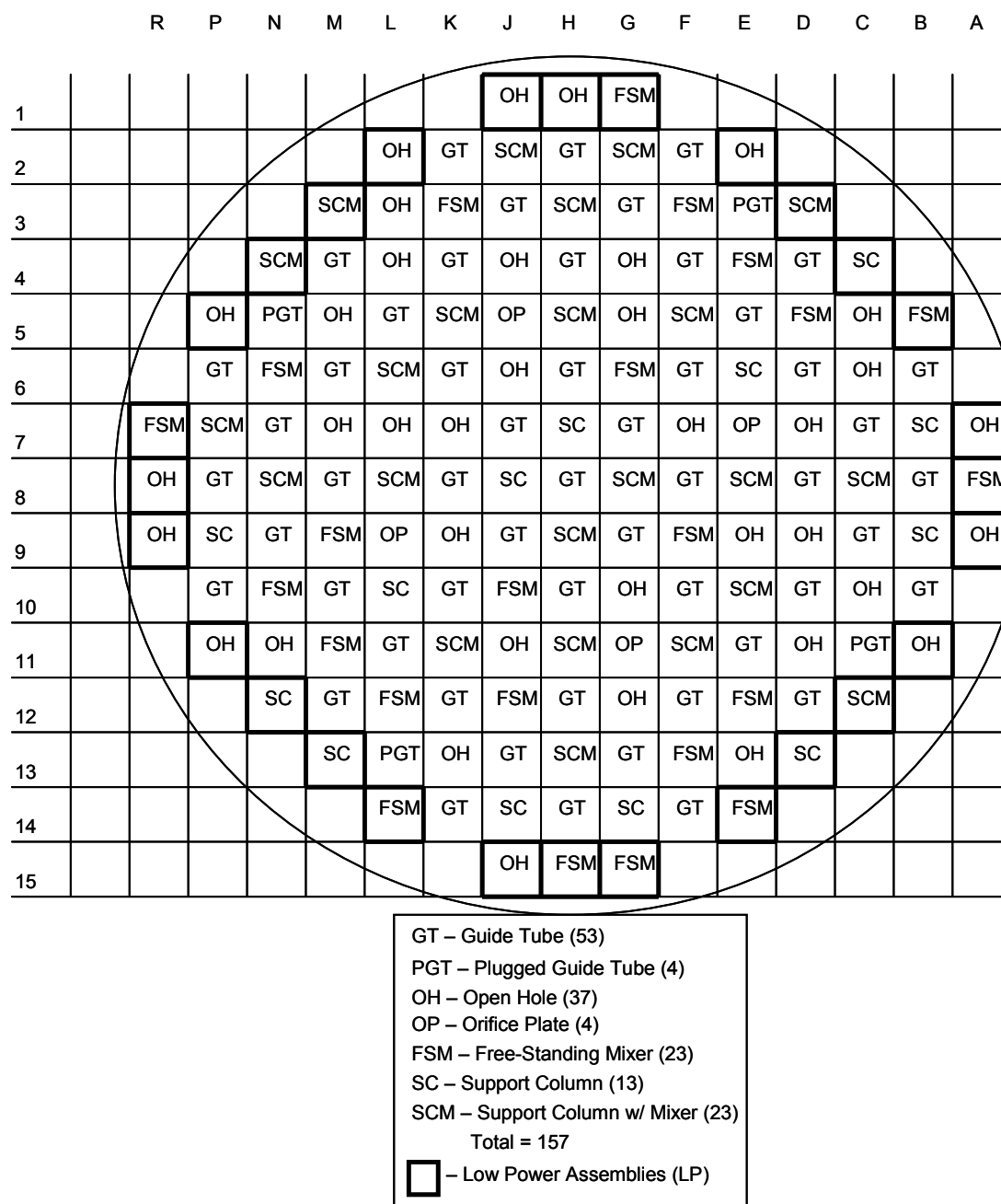


Figure 26.2-7 Virgil C. Summer Upper Plenum Structure Map

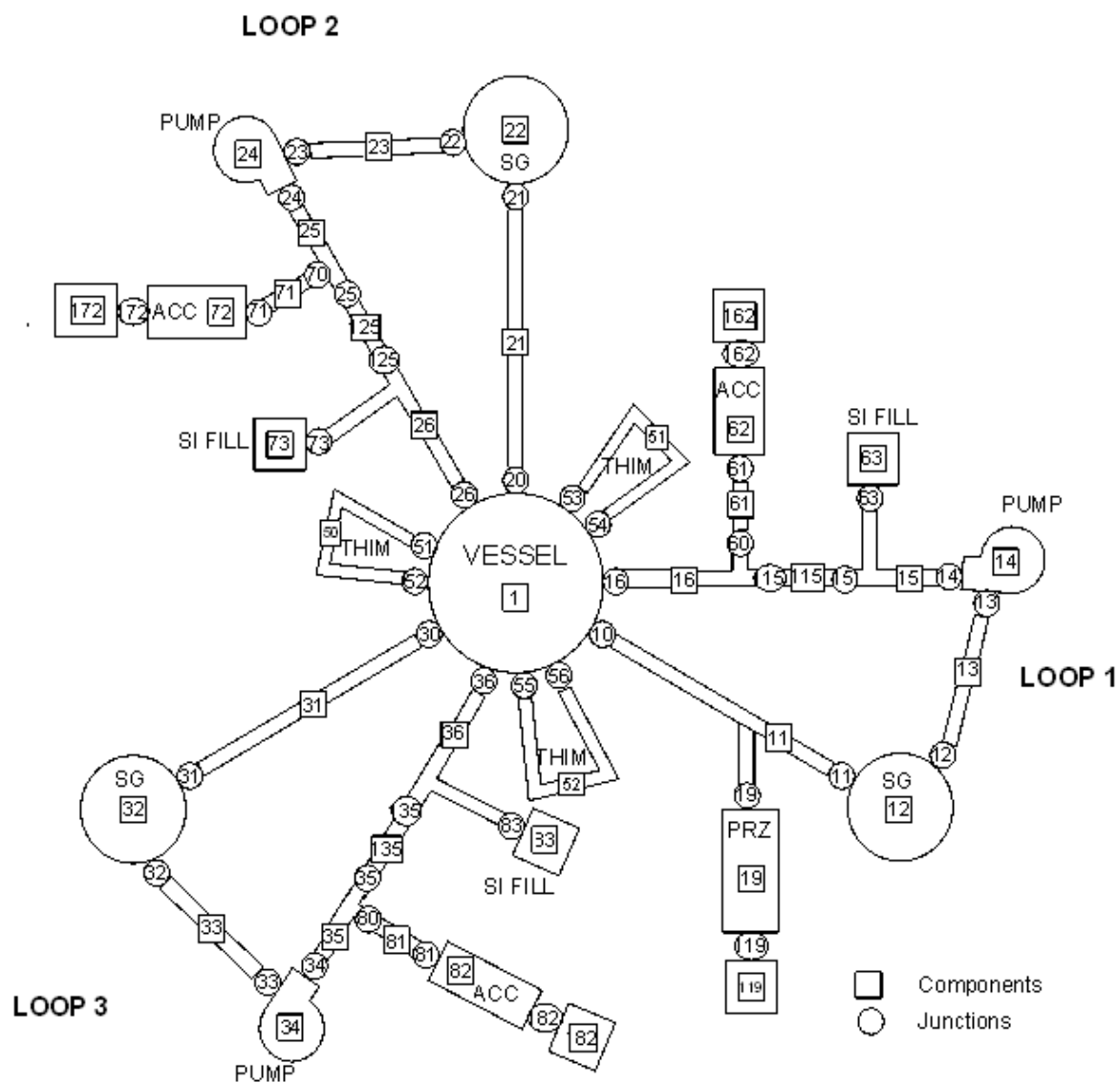


Figure 26.2-8 Virgil C. Summer Loop Model Noding Diagram

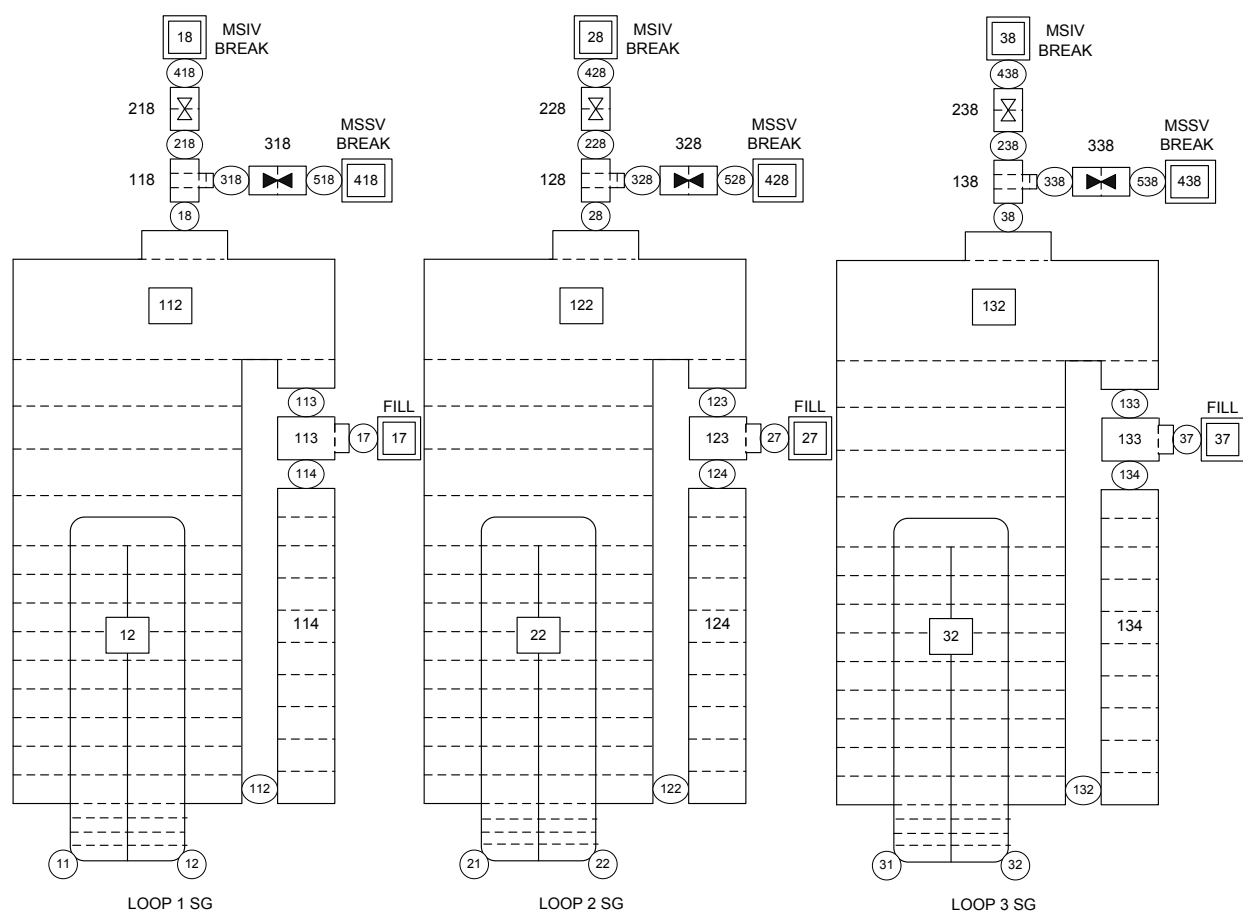


Figure 26.2-9 Virgil C. Summer Steam Generator Component Noding Diagram

**Figure 26.2-10a Virgil C. Summer Reference Case Axial Power Distribution for
LBLOCA and IBLOCA**

Figure 26.2-10b Virgil C. Summer Reference Case Axial Power Distribution for SBLOCA

26.3 BEAVER VALLEY UNIT 1 NUCLEAR POWER PLANT

Beaver Valley Unit 1 is a three-loop plant containing Westinghouse 17x17 Robust Fuel Assembly (RFA-2) fuel with IFMs and ZIRLO cladding. The nominal core power for this plant is 2,900 MWt. Beaver Valley Unit 1 also has Westinghouse 54F replacement steam generators.

26.3.1 Beaver Valley Unit 1 WCOBRA/TRAC-TF2 Nodalization

The vessel geometry as modeled in WCOBRA/TRAC-TF2 is described in Section 26.3.1.1; while a description of the core modeling is provided in Section 26.3.1.2, the loop geometry is described in Section 26.3.1.3 and the ECCS modeling is detailed in Section 26.3.1.4.

26.3.1.1 Vessel Model

Figure 26.3-1 shows the vessel drawing for the Beaver Valley Unit 1 three-loop PWR. Figure 26.3-2 shows the vessel major internal component elevation layout. The elevations shown on the right are relative to the inside bottom of the vessel. This elevation layout contains most of the information needed to divide the vessel into nine vertical sections. These sections are described in turn starting at the bottom of the vessel.

The bottom of vessel Section 1 is the inside vessel bottom. The bottom of vessel Section 2 is the bottom of the upper tie plate. The bottom of vessel Section 3 is defined as the beginning of the active fuel. The bottom of vessel Section 4 is the top of the active fuel. The bottom of vessel Section 5 is the elevation at the bottom of the upper core plate. The bottom of vessel Section 6 is equal to the elevation of the bottom of the hot leg inner wall. The bottom of vessel Section 7 is the elevation of the inside top of the hot leg. The bottom of vessel Section 8 is the elevation at the top of the upper support plate. The bottom of vessel Section 9 is the elevation at the top of the upper guide tube in the upper head. The top of vessel Section 9 is the inside top of the vessel upper head.

After defining the elevations for each section, a noding scheme is defined following the same basic philosophy applied to the SET and IET facilities are described in Section 26.1.1. [

J^{a,c}

Figures 26.3-3 through 26.3-12 illustrate the Beaver Valley Unit 1 vessel noding. Figure 26.3-3 is a vertical section noding diagram. Figures 26.3-4 through 26.3-12 are the horizontal “plan” views of each section. In these figures, the numbers within the squares are the channel numbers and the numbers within the circles with arrows attached to them are the gap numbers. A gap is used to define a horizontal flow path between channels. Positive flow is in the direction indicated by the arrow. It is assumed within WCOBRA/TRAC-TF2 that a vertical flow path for vertically stacked channels exists unless specified otherwise in the input. Upward axial flow is considered as positive flow.

As can be seen in Figures 26.3-3 through 26.3-12, 89 channels and 89 gaps are used for Beaver Valley Unit 1 to define the vessel. It can be seen in Figure 26.3-3 that several of the nine vertical sections are sub-divided into two or more levels. For example, the active fuel region, vessel Section 3, is divided into 14 vertical levels. By accounting for the vertical sub-division within vessel Sections 2, 3, 5 and 7, the vessel model for Beaver Valley Unit 1 has a total of 309 fluid cells.

Vessel Section 1 models the vertical section of the vessel from the inside bottom of the vessel to the bottom of the upper tie plate. The modeling of this section is relatively simple since there is one channel with one vertical cell and no horizontal flow gaps (Figures 26.3-3 and 26.3-4). Channel 1 completely represents Section 1 of the vessel. The top flow area of this channel/section was computed based on the net flow area at the top of the tie plate.

Vessel Section 2 models the vertical section of the vessel from the bottom of the upper tie plate to the bottom of the active fuel region. This section contains two vertical cells for ten channels (designated 2 through 5 and 52 through 57) and horizontal flow gaps (numbered 1 through 6 and 46 through 57). Figures 26.3-3 and 26.3-5 provide an illustration for the vertical and radial representation of this section of the vessel model.

Channels 2, 3, 4, 52, 53, 54, 55, 56, and 57 each represent one-ninth of the annulus volume between the vessel inner wall and the core barrel outer wall, and are connected by Gaps 4 through 6 and 52 through 57. Channel 5 is the lower plenum volume between the upper tie plate and the fuel nozzle elevation.

[

]^{a,c}

The area at the top of Channel 5 is equal to the sum of the areas modeled at the bottom of Channels 9 through 13 in vessel Section 3. Area variation inputs are used to vary the flow area between the lower and upper cells of Channel 5 to account for the change in flow area within this channel due to the lower support plate. The radial flow gaps modeled in vessel Section 2 are illustrated in Figures 26.3-3 and 26.3-5 with positive flow in the direction indicated in the figure. Gaps 1, 2, 3, 46, 47, 48, 49, 50, and 51 model a radial flow gap in the lower cell of vessel Section 2, with the core barrel extension blocking radial flow from the upper cell of the downcomer channels into the upper cell of lower plenum Channel 5.

Vessel Section 3 models the vertical section of the vessel from the bottom to the top of the active fuel region. The modeling is accomplished using fourteen vertical cells in fourteen channels (designated 6 through 13 and 58 through 63) and thirteen horizontal flow gaps (designated 7 through 13 and 58 through 63). Figures 26.3-3 and 26.3-6 provide an illustration for the vertical and radial representation of this section of the vessel model.

Channels 6 through 8 and 58 through 63 each represent one-ninth of the downcomer annulus volume between the vessel inner wall and the core barrel outer wall. Thermal shield is modeled in this section. Channel 9 is the volume between the core barrel inner wall and the baffle plates, which is designated as the barrel/baffle channel. For Beaver Valley Unit 1, flow travels upward through this region during normal operation which is referred to as an upflow barrel/baffle design.

Channels 10 through 13, combined, represent the total volume within the baffle plates, i.e., the entire core active fuel region for all 157 assemblies. Channel 10 includes assemblies on the periphery of the core which have relatively low power. [

] ^{a,c} There are five types of upper internals in the Beaver Valley Unit 1 upper plenum: guide tubes, orifice holes, support columns, free-standing flow mixers, and support columns with flow mixers. The locations of these structures in the upper plenum are presented in Figure 26.3-13. [

] ^{a,c}

The gaps modeled in vessel Section 3 are illustrated in Figure 26.3-6. The 144-inch active fuel length is divided into fourteen axial cells. The grids and their associated form losses are modeled within this length range at their specified elevations. [

] ^{a,c}

Vessel Section 4 includes the vertical section of the vessel from the top of the active fuel to the bottom of the upper core plate. This section has one vertical cell and uses fourteen channels (designated 14 through 21 and 64 through 69) and thirteen horizontal flow gaps (17 through 23 and 64 through 69) to model this portion of the vessel. Figures 26.3-3 and 26.3-7 illustrate the vertical and radial representation of this section of the vessel model.

Section 4 of the model is referred to as the CCFL region, where CCFL is the acronym for counter-current flow limitation. [

] ^{a,c}

Channels 14, 15, 16, 64, 65, 66, 67, 68, and 69 each represent one-ninth of the downcomer annulus volume between the vessel inner wall and the core barrel outer wall. [

] ^{a,c} Channel 17 is modeled with no vertical flow path into or out of the top of the channel. The gaps within section 4 are illustrated in Figure 26.3-7.

Vessel Section 5 extends vertically from the bottom of the upper core plate to the inside bottom of the hot leg. This section contains two vertical cells for fifteen channels (designated 22 through 29, 51, and 70 through 75) and fourteen horizontal flow gaps (24 through 30, 45, and 70 through 75). Figures 26.3-3 and 26.3-8 provide an illustration of the vertical and radial representation of this section of the vessel model.

Channels 22, 23, 24, 70, 71, 72, 73, 74, and 75 each represent one-ninth of the downcomer annulus volume between the vessel inner wall and the core barrel outer wall. [

] ^{a,c} There is no flow into the bottom of Channel 25 from vessel Section 4. Since these Channels (27, 28, and 29) are all surrounded by the inner global upper plenum Channel 25, this region constitutes another area where CCFL may be calculated. [

] ^{a,c} Similar to Channel 25, there is no flow into the bottom of Channel 51 from vessel Section 4. Figure 26.3-8 defines the gaps for vessel Section 5.

Vessel Section 6 models the vertical section of the vessel from the bottom to the top of the hot leg (inner diameter). One vertical cell in sixteen channels (designated 30 through 39 and 76 through 81) and fourteen horizontal flow gaps (designated 31 through 38 and 76 through 81) are used to model this section. Figures 26.3-3 and 26.3-9 provide an illustration for the vertical and radial representation of this section of the vessel model.

Channels 30, 31, 32, 76, 77, 78, 79, 80, and 81 each represent one-ninth of the downcomer annulus volume between the vessel inner wall and the core barrel outer wall, excluding the volume of the hot leg which passes through this region. Note that the cold legs of the loop model connect to vessel downcomer Channels 30, 76, and 79. [

]^{a,c}

Gaps 36, 37, and 38 are added to model the radial flow into the hot leg channels from the outer global Channel 34. Channels 37, 38, and 39 complete vessel Section 6, modeling the hot leg nozzles and serving as an interface to the hot legs in the loop model.

Vessel Section 7 extends vertically from the inside top of the hot leg to the top of the upper support plate, and is divided into two levels. This section contains two vertical cells for thirteen channels (designated 40 through 46 and 82 through 87) and eleven horizontal flow gaps (39 through 43 and 82 through 87). Figures 26.3-3 and 26.3-10 illustrate the vertical and radial representation of this section of the vessel model. The interface at the top of the downcomer in Vessel Section 7 with the upper head is via the spray nozzles; a loss coefficient is modeled to reflect the flow through this interface.

Channels 40, 41, 42, 82, 83, 84, 85, 86, and 87 each represent one-ninth of the downcomer annulus volume between the vessel inner wall and the core barrel outer wall. Channel 45 is a vertical extension of Channel 35 in vessel Section 6. [

]^{a,c}

and is a vertical extension of Channel 36 from vessel Section 6. Channel 43 is the inner global region and is a vertical extension of Channel 33 from vessel Section 6. Channel 44 is the outer global region and is a vertical extension of Channel 34 from vessel Section 6. There is no vertical flow connection between Channels 43, 44, and 45 to vessel Section 8 above. Channels 40 through 42 and 82 through 87, however, connect vertically to vessel Section 8 via the upper head spray nozzles. Guide tube Channel 46 also connects vertically to vessel Section 8 through the guide tube extension. The eleven gaps in vessel Section 7 are illustrated in Figure 26.3-10.

Vessel Section 8 extends vertically from the top of the upper support plate to the top of the upper guide tube. This section has one vertical cell for five channels (designated 47 through 49, 88, and 89) and six horizontal flow gaps (14 through 16, 44, 88, and 89). Figures 26.3-3 and 26.3-11 illustrate the vertical and radial representation of this section of the vessel model.

The boundary between outer Channels 47, 88, and 89 and inner Channel 48 is formed by the cylinder which intersects the inside of the upper head sphere at the top of the upper guide tube (Figure 26.3-1). Channels 47, 88, and 89 each include one-third of the volume in the upper head outside this boundary while Channel 48 models the volume inside this boundary, excluding the volume of the upper guide tubes. There is no flow into Channel 48 from below since the upper support plate prevents direct flow communication between the upper head and the upper plenum. Channel 49 models the volume inside of the upper guide tubes. There is no flow communication between the fluid inside the upper guide tube enclosure and Channel 48 in Section 8 of the vessel.

Vessel Section 9 models the vertical section of the vessel extending from the top of the upper guide tubes to the inside top of the vessel head. Similar to Section 1 of the vessel, vessel Section 9 is modeled as one channel (50) containing one vertical cell with no horizontal flow gaps (Figures 26.3-3 and 26.3-12). The flow area at the bottom of Channel 50 (vessel Section 9) is equal to the sum of the flow area at the top of Channels 48 and 49 from vessel Section 8.

26.3.1.2 Core Model

Rod 1 is the [

] ^{a,c} It is located in the hot assembly (Channel 13) which is an assembly under a support column with a flow mixer. Rod 2 represents the remaining 263 fuel rods in the hot assembly and has a power equivalent to the hot assembly average fuel rods.

Rod 5 represents the 28 assemblies in the outer low powered region (Channel 10) and contains (28 assemblies) * (264 fuel rods/assembly) fuel rods. The fuel rods in the remaining 128 assemblies are divided up in proportion to the number of assemblies used in Channels 11 and 12 in the core. The guide tubes contain (53 assemblies) * (264 fuel rods/assembly) fuel rods that are represented by fuel rod 3. The OH/SC/FSM channel contains (75 assemblies) * (264 fuel rods/assembly) fuel rods that are represented by fuel rod 4.

The nuclear fuel rods are initialized with internal gas composition, and fuel average temperatures from the PAD5 code (Crede et al., 2013).

[

] ^{a,c}

26.3.1.3 Loop Model

The Beaver Valley Unit 1 loop model is represented by Figures 26.3-14 and 26.3-15. As with the vessel inputs, each component in the one-dimensional loop has various cells to allow for specific changes in geometry along the component. Each component is identified by a module title, a unique component number, and connections to numbered junctions. The three loops are defined using 37 components and 41 junctions. Components and junctions are indicated by rectangles (squares) and circles, respectively, in Figures 26.3-14 and 26.3-15.

Loop 2 is the loop which contains the pressurizer. Component 21 is the hot leg and was modeled with a TEE module. Component 29, the pressurizer (PRIZER module) is connected to the secondary branch of the hot leg TEE. [

] ^{a,c}

The primary side of the steam generator is modeled as Component 22; with the secondary side consisting of several components. TEE Component 122 is the shell of the steam generator secondary side. The feedwater connection is modeled as TEE Component 123, and the downcomer of the steam generator is PIPE Component 124. The feedwater is injected through FILL Component 27, and the steam flows through TEE Component 128 and then exits via either the Main Steam Isolation Valve (VALVE Component 228 and BREAK Component 28) or the Main Steam Safety Valve (VALVE Component 328 and BREAK Component 428). [

] ^{a,c}

Continuing around the loop are the crossover leg (PIPE Component 23) and reactor coolant pump (PUMP Component 24). It is noted that flow stratification is allowed in the loop seal bends via the use of the STRTX input. The Loop 2 cold leg is next, divided into two TEE components in order to model safety injection (FILL Component 73) and accumulator injection (accumulator PIPE component 72). Component 25 is the pump-side cold leg safety injection TEE and Component 26 is the vessel-side cold leg accumulator TEE. The accumulator line is modeled as a VALVE module (Component 71) which simulates the check valve. The accumulator tank itself (Component 72) is modeled with a PIPE component and an associated input which causes an accumulator module to be invoked.

The accumulators and pressurizer components have two junctions, although they only have a single communication path with the RCS. As such, zero FILL Components 129 and 172 are provided as boundary conditions for the junction not in communication with the RCS.

Loop 1 is set up much the same way except that the hot leg (Component 11) is modeled as a PIPE module in the absence of the pressurizer. Loop 3 is modeled the same as Loop 1.

[

] ^{a,c} BREAK Component(s) 4 and/or 6 are used to model containment conditions for the transient (depending on the break type, either one or both of the components are required). [

] ^{a,c}

Finally, thimble bypass is modeled using three separate PIPE modules (loop Components 50-52) connected to the bottom cells of the low power, guide tube, and OH/SC/FSM core channels in vessel Section 3 and the corresponding CCFL channels in vessel Section 4.

26.3.1.4 Emergency Core Cooling Safety Injection Model

The Safety Injection System for Beaver Valley Unit 1 consists of three accumulator tanks, two charging/safety injection pumps, and two low head RHR pumps. Each pump is connected to injection lines which inject directly into each cold leg. The accumulators are modeled to inject at a nominal pressure, a nominal temperature, and a nominal water volume. The pumped safety injection flow is modeled assuming a nominal temperature and the loss of one train of safety injection pumps (one SI and one RHR). The loss of one train of safety injection is considered as the limiting single failure assumption.

[

] ^{a,c}

26.3.2 Beaver Valley Unit 1 Reference Case and Allowable Plant Operating Conditions

The best-estimate methodology establishes a sampling of the distribution of potential uncertainty contributors which occur due to changes in plant or model variables (Section 29). The following paragraphs describe the assumptions in the key LOCA parameters for Beaver Valley Unit 1.

The reference case input values for Beaver Valley Unit 1 are listed in Table 26.3-1. The input values fall under three categories: 1) plant physical description, 2) plant initial operating conditions, and 3) accident boundary conditions. The values used for the reference case for each of these parameters are discussed in the following subsections.

For most of the parameters, the nominal value is assumed for the reference case. For others, a bounding or conservative value is assumed. The uncertainty associated with these parameters is accounted for in the uncertainty analysis, as shown in Section 31.

26.3.2.1 Plant Physical Description

[

] ^{a,c}

4. [

$J^{a,c}$

26.3.2.2 Plant Initial Operating Conditions – Reactor Power

1. **Initial Core Average Linear Heat Rate** – The core power assumed for the Region I reference case is 102 percent of the power level, and for the Region II reference case is 100 percent of an uprated power level (2900 MWt).
2. **Hot Rod Peak Linear Heat Rate** – The total peaking factor (FQ) for the reference case is [$J^{a,c}$].
3. **Hot Rod Average Linear Heat Rate ($F_{\Delta H}$)** – In the reference case, $F_{\Delta H}$ is [$J^{a,c}$].
4. **Hot Assembly Average Linear Heat Rate** – The minimum difference between the power generated in the hot rod and that in the hot assembly average rod is conservatively assumed. The hot assembly average rod is assumed to be [$J^{a,c}$] lower in power than the hot rod.
5. **Hot Assembly Peak Linear Heat Rate** – Consistent with the average linear heat rates, the peaking factor used to calculate the peak linear heat rate generated in the hot assembly average rod is [$J^{a,c}$] lower than the value assumed in the hot rod.
6. **Axial Power Distribution** – The power distributions represented by the power shapes assumed for the reference case are presented in Figure 26.3-16, and correspond to [$J^{a,c}$].
7. **Low-Power Region (PLOW)** – Current and expected core designs for Beaver Valley Unit 1 result in a range of PLOW from [$J^{a,c}$] to [$J^{a,c}$].
 $J^{a,c}$ is selected as the value for the reference case.
8. **Burnup** – The burnup is selected from the time-in-cycle, which is a sampled attribute within the uncertainty analysis. For the reference case, a nominal cycle burnup equal to [$J^{a,c}$] is assumed.

9. **Prior Operating History** – The power distribution assumed to exist at the time of the LOCA is conservatively assumed to have existed since plant startup when determining fission product inventories.
10. **Moderator Temperature Coefficient** – The maximum value specified in the Technical Specifications for hot full power is assumed, to conservatively estimate core reactivity and fission power.
11. **Hot Full-Power Boron Concentration** – A value typical of those used in current cores is assumed.

26.3.2.3 Plant Initial Operating Conditions – Fluid Conditions

1. **Average Fluid Temperature (T_{avg})** – []^{a,c} is used for Beaver Valley Unit 1.
2. **RCS Pressure** – The nominal value (2250 psia) is assumed for the Beaver Valley Unit 1 reference case.
3. **Loop Flowrate** – []^{a,c} loop flow is assumed for the reference case.
4. **Upper Head Temperature (T_{UH})** – The appropriate best estimate value of T_{UH} is assumed.
5. **Pressurizer Level** – The nominal value of pressurizer level is assumed.
6. **Accumulator Water Temperature** – A nominal (midpoint) value within the range established for Beaver Valley Unit 1 is assumed.
7. **Accumulator Pressure** – A minimum value of accumulator pressure is assumed for Region I, and a nominal (midpoint) value of accumulator pressure is assumed for Region II.
8. **Accumulator Water Volume** – A nominal (midpoint) value of accumulator water volume is assumed.
9. **Accumulator Line Resistance** – A best-estimate value of accumulator line resistance is assumed.
10. **Accumulator Boron Concentration** – The Technical Specification minimum value is assumed.

26.3.2.4 Accident Boundary Conditions

1. Break Location – [

] ^{a,c}

6. **Safety Injection Temperature** – Nominal (midpoint) values are assumed.
7. **Safety Injection Delay** – Maximum values consistent with the offsite-power assumption (loss-of-offsite power) are used.
8. **Containment Pressure** – A conservatively low value was used for the reference case.
9. **Single-Failure Assumption** – [

] ^{a,c}

² The approach described in Section 30.4 to determine the [superseded by limitation and condition #15 from the SER.

] ^{a,c} is

26.3.3 Plant Operating Range

The []^{a,c} developed by the best-estimate methodology are valid for a range of plant operating conditions. Several parameters in the reference calculation are at nominal values. The range of variation of the operating parameters is accounted for in the uncertainty analysis.

This is accomplished by assuring that, in the sampling of the attributes for each run []

[]^{a,c} (as demonstrated in Section 31 for Beaver Valley Unit 1). Westinghouse has processes in place with the utilities to ensure that the analyzed ranges bound the plant operation.

Table 26.3-1 Key LOCA Parameters and Scoping Study Values for Beaver Valley Unit 1

a,c

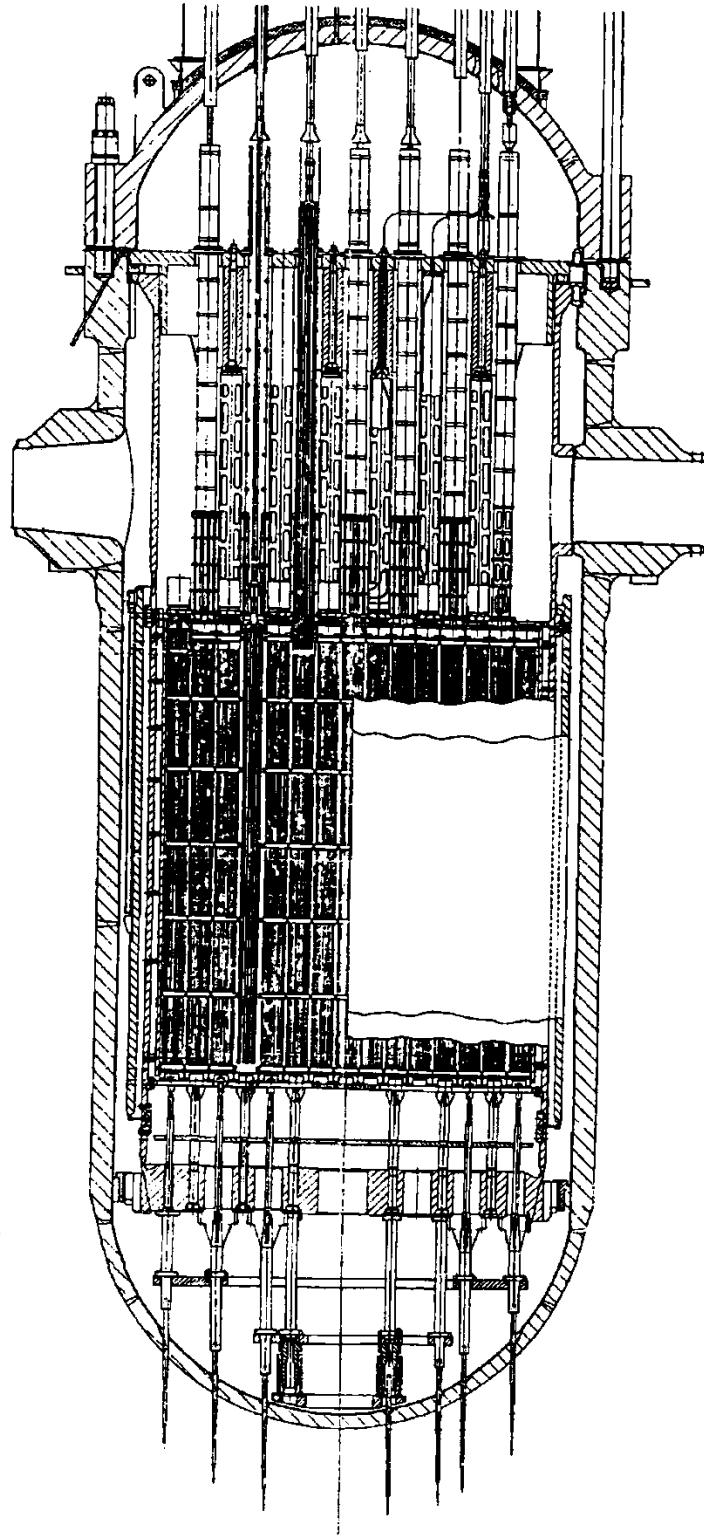


Figure 26.3-1 Beaver Valley Unit 1 Vessel Profile

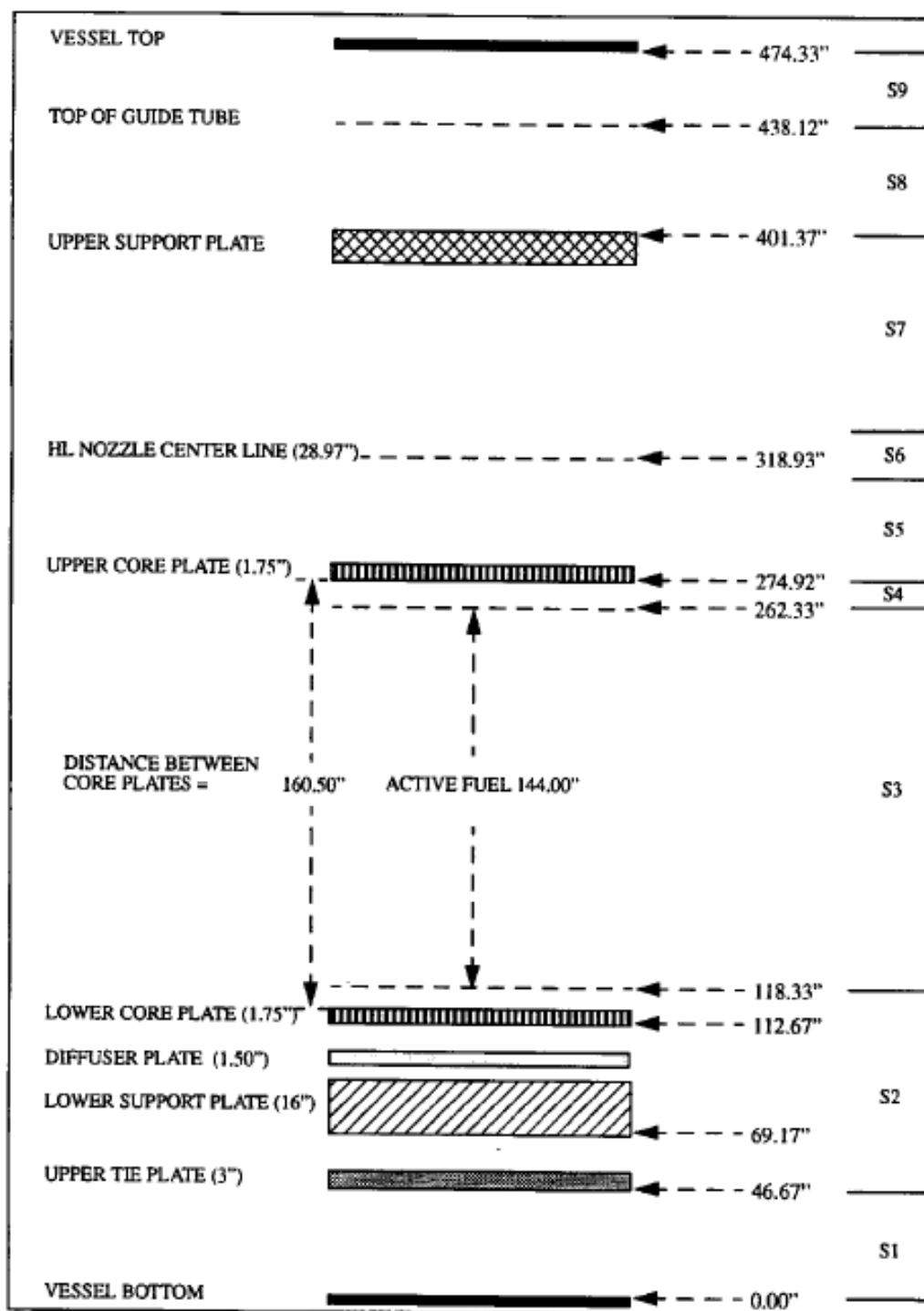


Figure 26.3-2 Beaver Valley Unit 1 Vessel Component Elevations

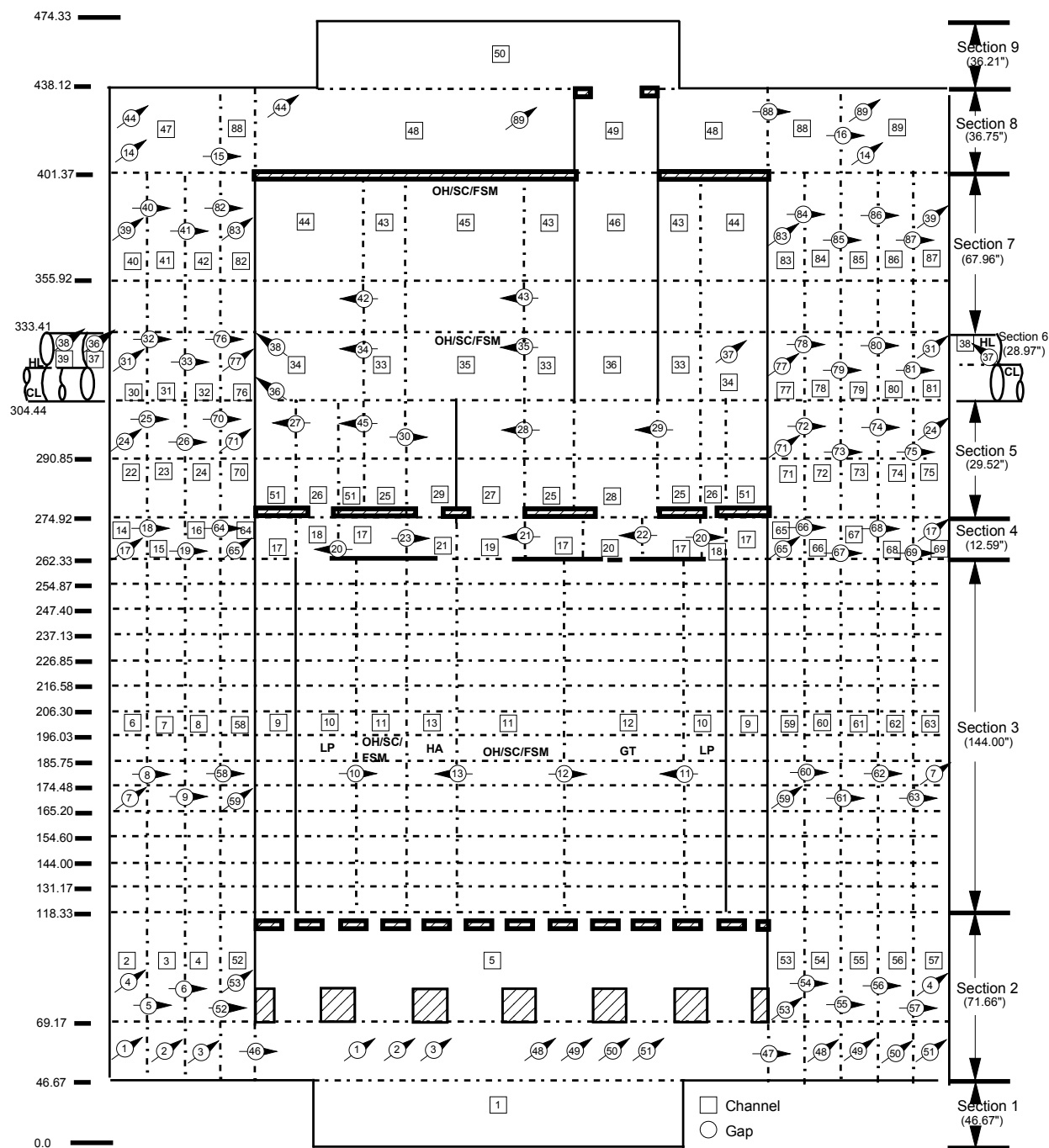
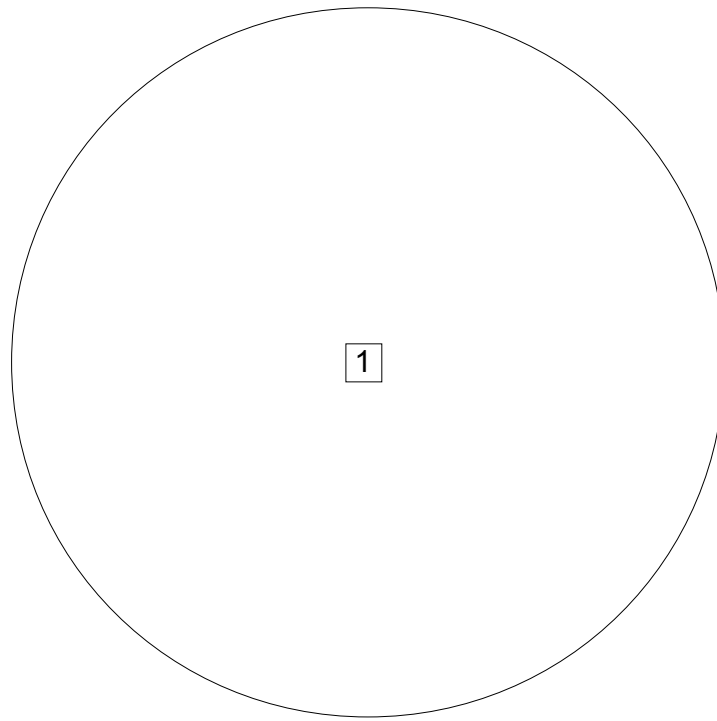
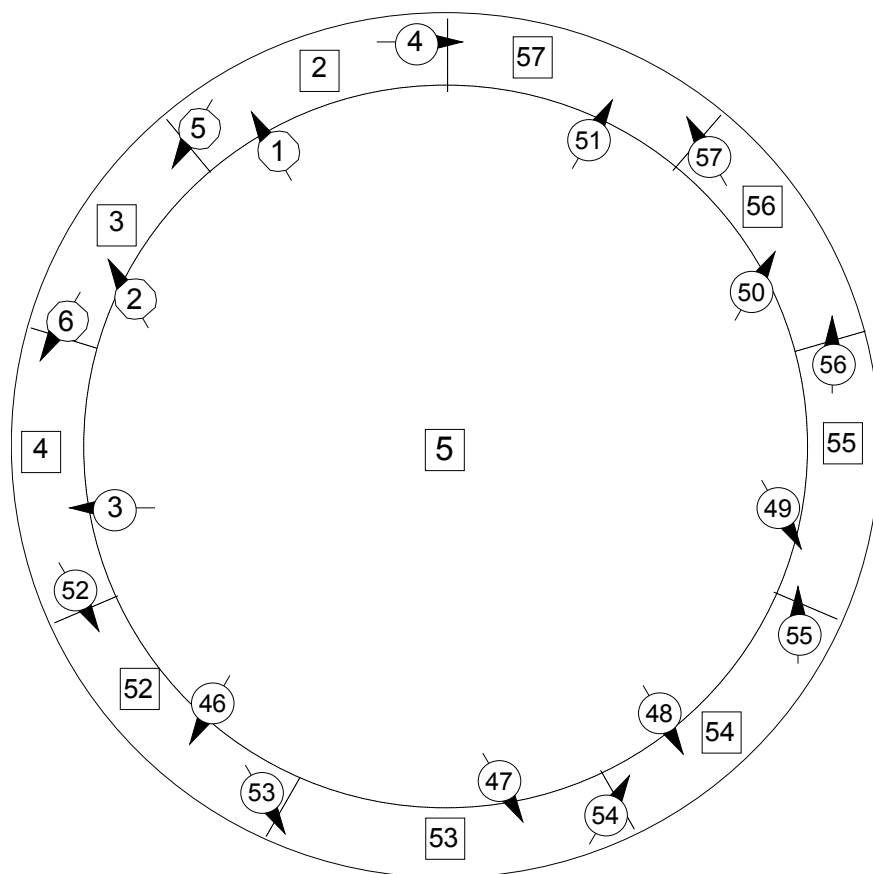


Figure 26.3-3 Beaver Valley Unit 1 Vessel Model Noding Diagram



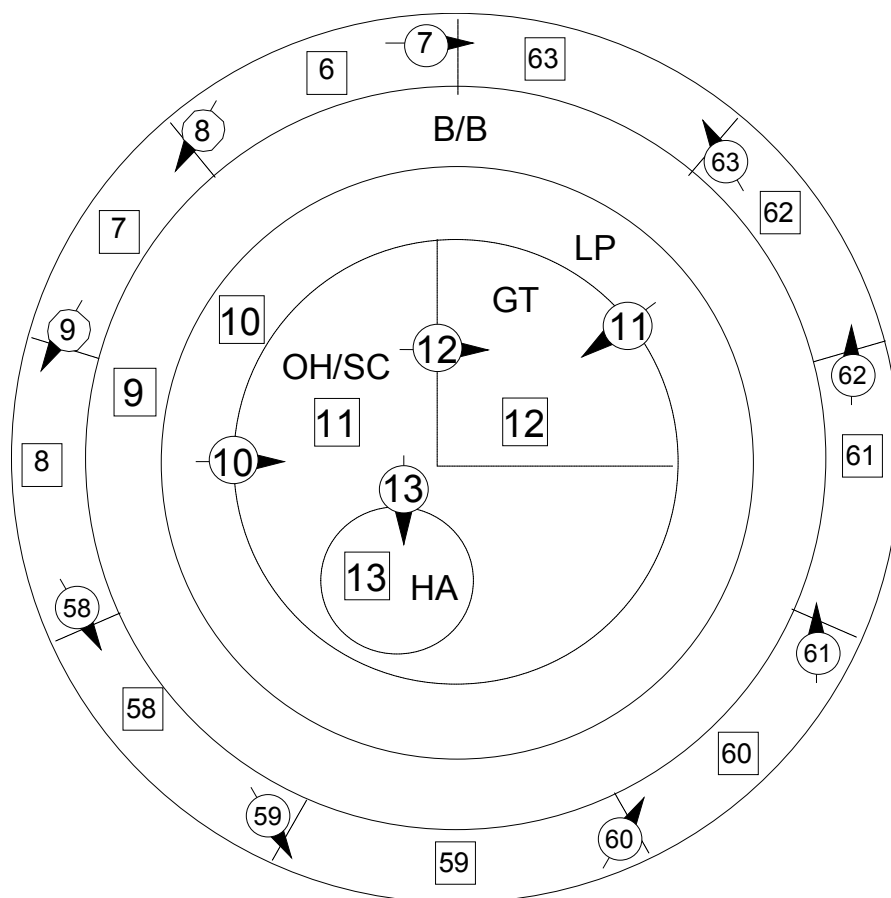
SECTION 1: LOWER HEAD

Figure 26.3-4 Beaver Valley Unit 1 Vessel Section 1



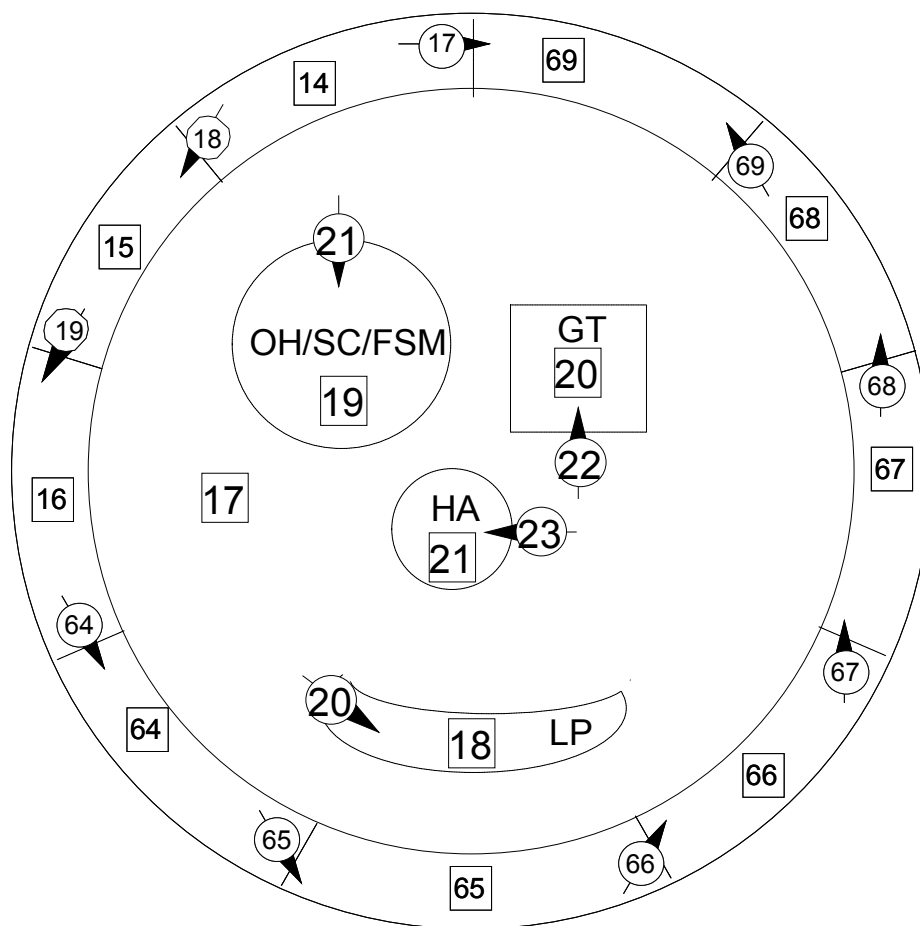
SECTION 2: LOWER PLENUM

Figure 26.3-5 Beaver Valley Unit 1 Vessel Section 2



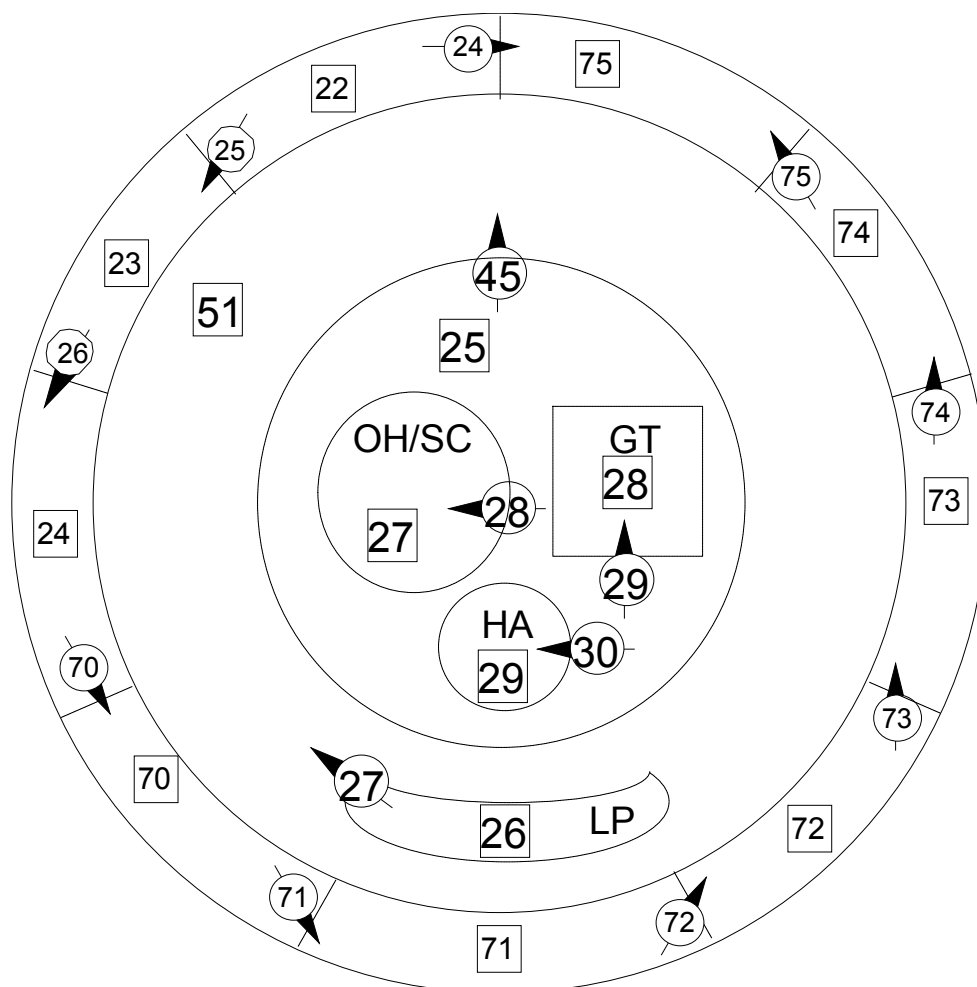
SECTION 3: CORE REGION

Figure 26.3-6 Beaver Valley Unit 1 Vessel Section 3



SECTION 4: CCFL REGION

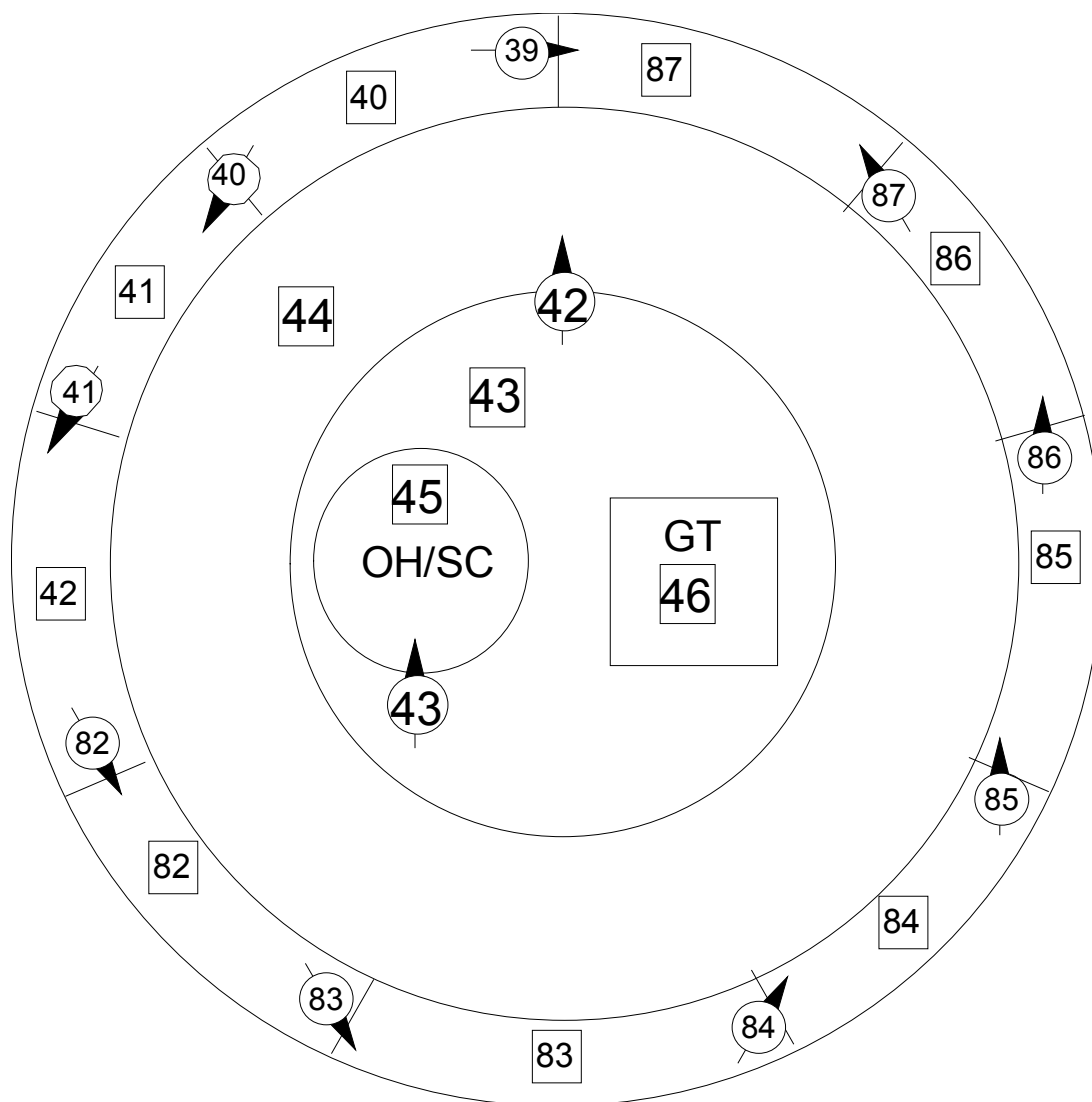
Figure 26.3-7 Beaver Valley Unit 1 Vessel Section 4



SECTION 5: UPPER PLENUM BELOW NOZZLES

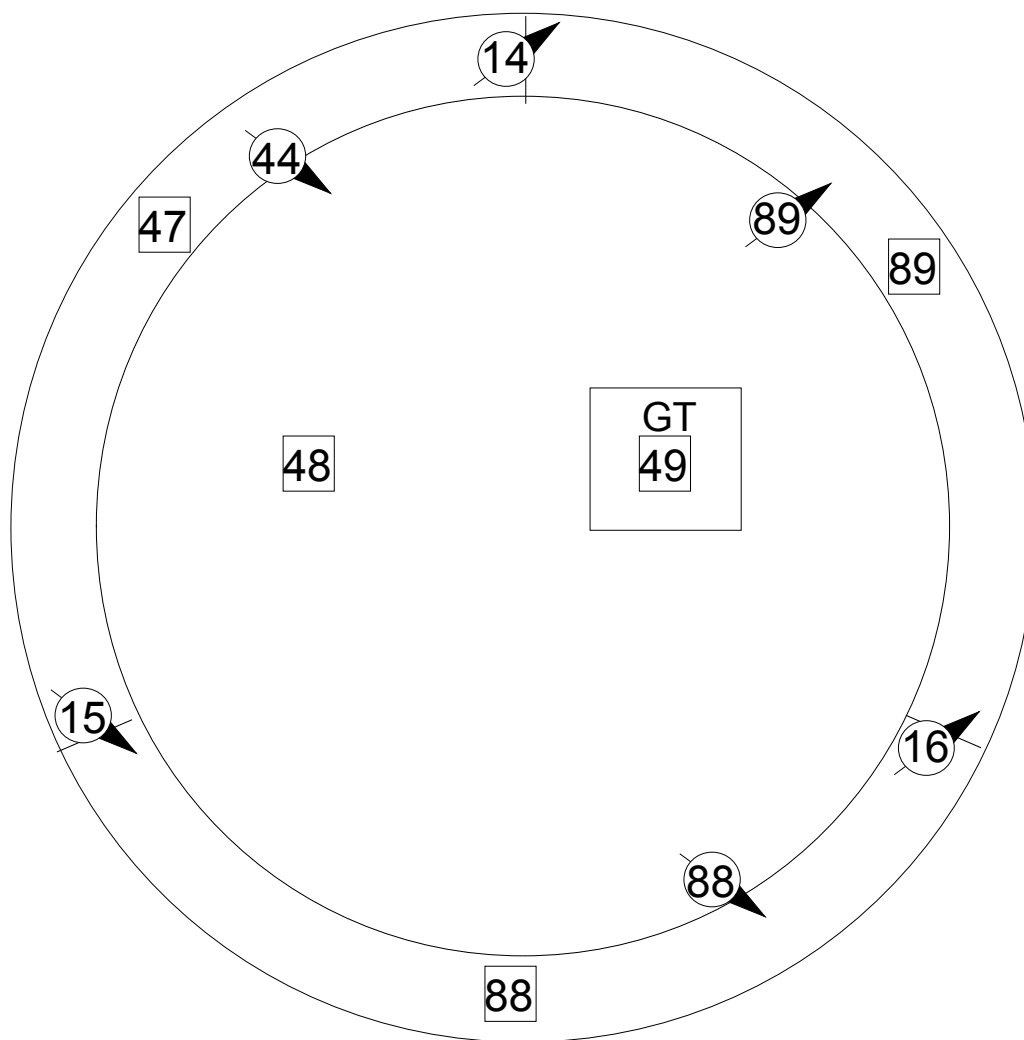
Figure 26.3-8 Beaver Valley Unit 1 Vessel Section 5

Figure 26.3-9 Beaver Valley Unit 1 Vessel Section 6



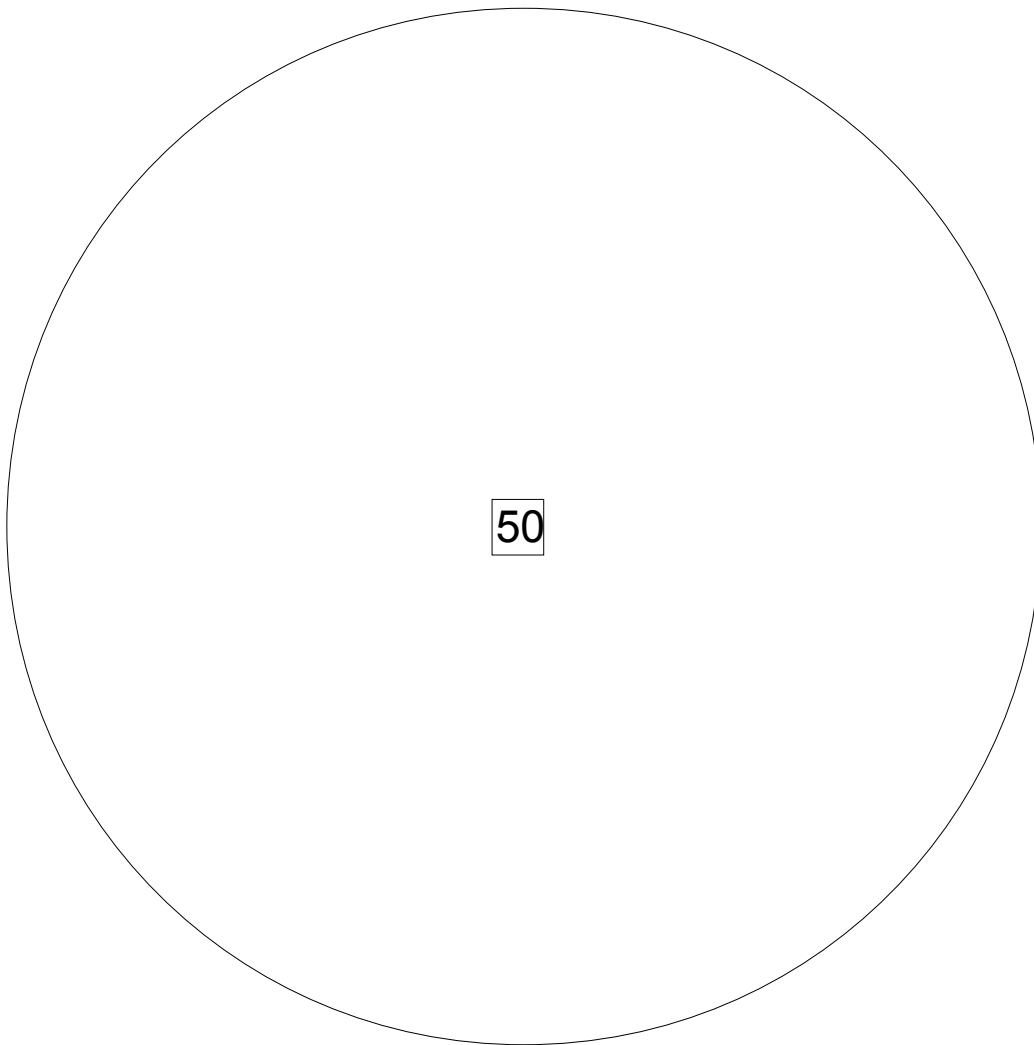
SECTION 7: UPPER PLENUM ABOVE NOZZLES

Figure 26.3-10 Beaver Valley Unit 1 Vessel Section 7



SECTION 8: UPPER HEAD UP TO TOP OF GUIDE TUBES

Figure 26.3-11 Beaver Valley Unit 1 Vessel Section 8



**SECTION 9: UPPER HEAD ABOVE
GUIDE TUBES**

Figure 26.3-12 Beaver Valley Unit 1 Vessel Section 9

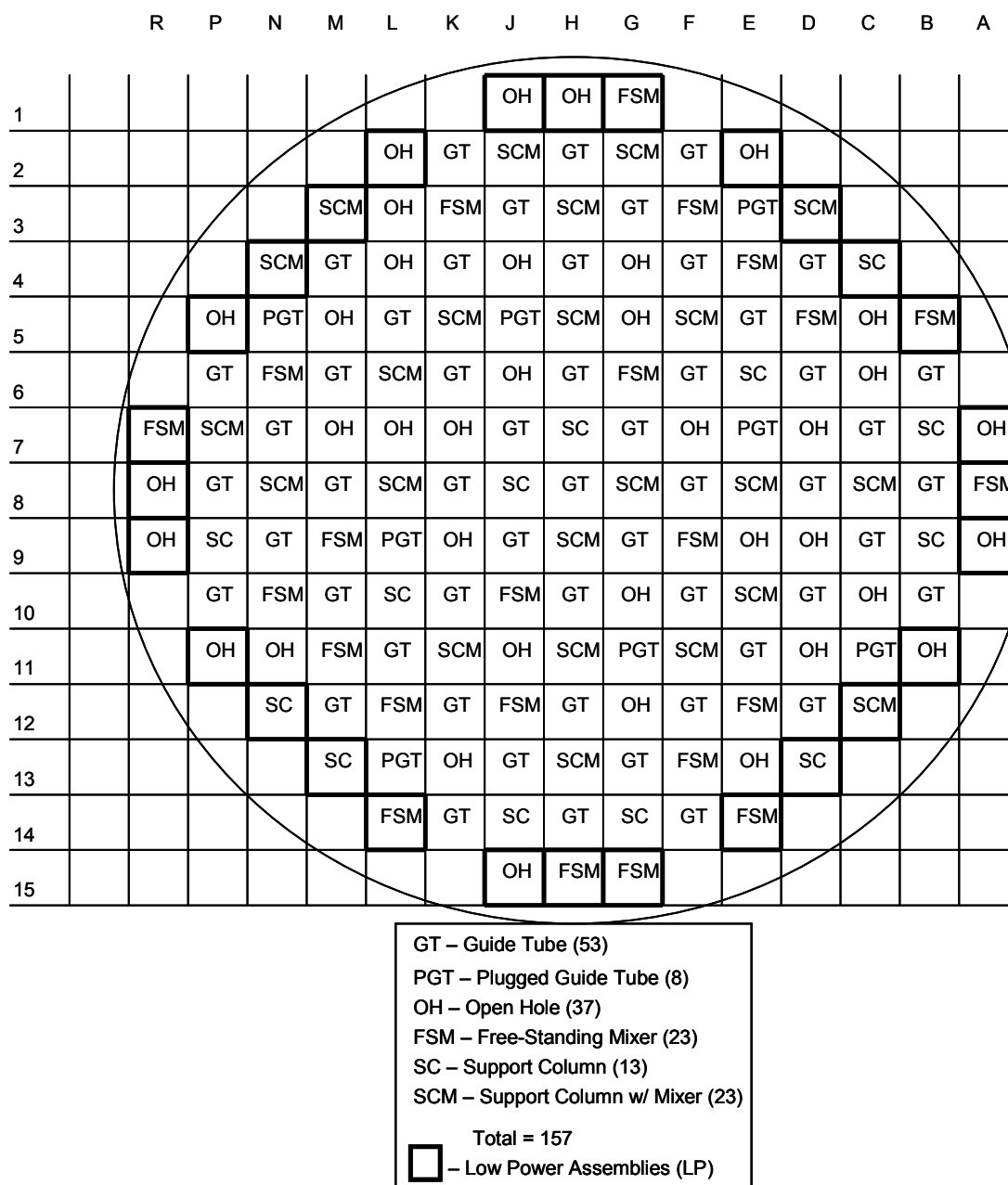


Figure 26.3-13 Beaver Valley Unit 1 Upper Plenum Structure Map

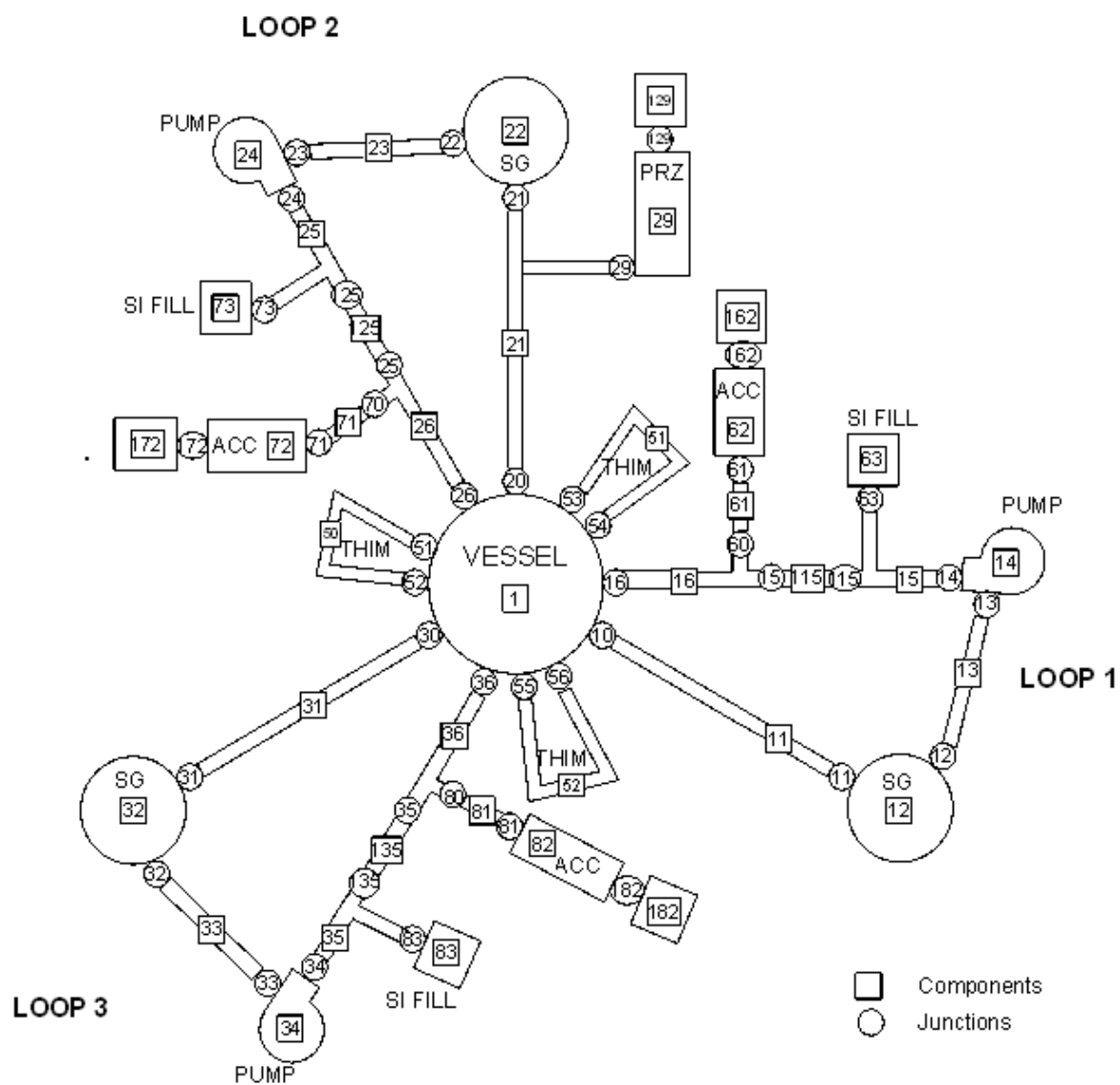


Figure 26.3-14 Beaver Valley Unit 1 Loop Model Noding Diagram

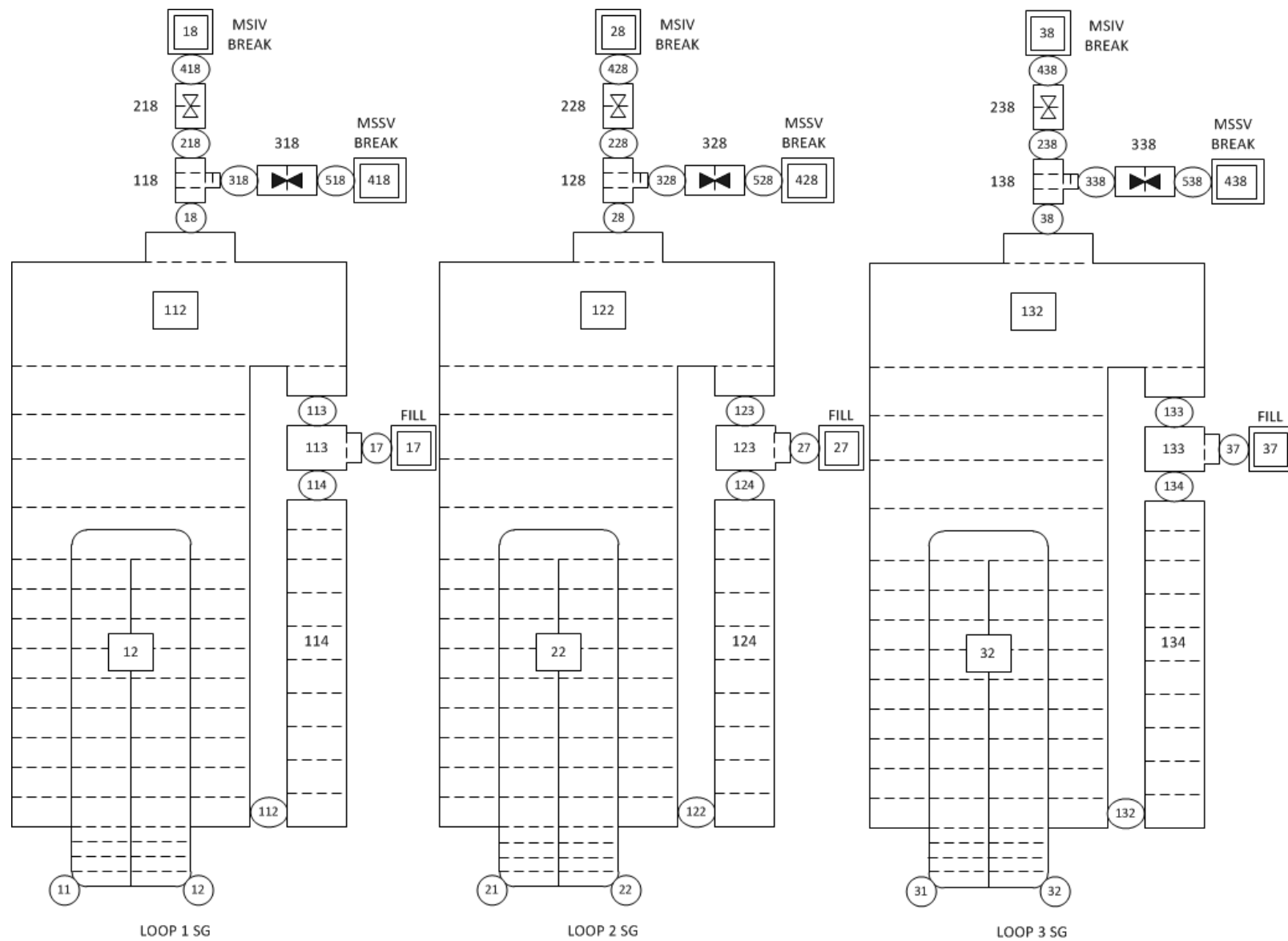


Figure 26.3-15 Beaver Valley Unit 1 Steam Generator Component Noding Diagram

**Figure 26.3-16a Beaver Valley Unit 1 Reference Case Axial Power Distribution for
LBLOCA and IBLOCA**

Figure 26.3-16b Beaver Valley Unit 1 Reference Case Axial Power Distribution for SBLOCA

26.4 STEADY STATE CALCULATION/CALIBRATION

Steady-state acceptance criteria are necessary because the previously-mentioned fluid and core conditions are likely to differ somewhat from plant-to-plant and the degree to which these parameters are matched in the WCOBRA/TRAC-TF2 simulation must be consistent. Table 26.4-1 shows the acceptance criteria used in WCOBRA/TRAC-TF2 for acceptable simulation of plant conditions. A checklist for a number of significant parameters is given below, which utilizes this table to verify whether these variables have reached their acceptable steady-state values.

[

]^{a,c}

[

] ^{a,c}

³ The loop flow rate does not change from case-to-case, but it is checked for each simulation within the run matrix.

Table 26.4-1 Criteria for an Acceptable Steady-State

Notes:
D.V. = Desired Value
C.V. = Calculated Value

a,c

26.5 REFERENCES

1. Bajorek, S. M., et al., March 1998, “Code Qualification Document for Best Estimate LOCA Analysis,” Volume 1 Revision 2, and Volumes 2 through 5, Revision 1, WCAP-12945-P-A (Proprietary).
2. Bordelon, F. M. and Murphy, E. T., 1974, “Containment Pressure Analysis Code (COCO),” WCAP-8327 (Proprietary), WCAP-8306 (Non-Proprietary).
3. Bordelon, F. M., et al., 1974, “Westinghouse Emergency Core Cooling System Evaluation Model – Summary,” WCAP-8339.
4. Bordelon, F. M., et al., 1975, “The Westinghouse ECCS Evaluation Model: Supplementary Information,” WCAP-8471-P-A (Proprietary).
5. Crede, T. M., et al., 2013, “Westinghouse Performance Analysis and Design Model (PAD5),” WCAP-17642-P (Proprietary), WCAP-17642-NP (Non-Proprietary).
6. Shimeck, D. J., March 1988, “COSI SI/Steam Condensation Experiment Analysis,” WCAP-11767 (Proprietary).

27 REFERENCE BREAK SPECTRUM ANALYSIS

27.1 LARGE, INTERMEDIATE, AND SMALL BREAK SPECTRA

The V. C. Summer (CGE) and Beaver Valley Unit 1 (DLW) plant models described in Section 26 are exercised over the full spectrum of break sizes to determine the code's ability to properly capture the phenomena identified in the phenomena identification and ranking table (PIRT) process (Section 2). For each plant, a representative break size is chosen for a small, intermediate, and large break, with a more detailed description of each transient provided in Sections 27.2 (CGE) and 27.3 (DLW). The small and large break reference transients are carried forward into the scoping studies in Section 28. As was historically found and as confirmed in this section, intermediate breaks are not limiting relative to large and small breaks. An intermediate break reference transient is therefore not considered in the scoping studies.

[

$1^{a,c}$

27.1.1 V. C. Summer (CGE) Break Spectra

27.1.1.1 CGE Large Break Spectrum

The phenomena observed following a large break LOCA are generally observed regardless of break size; however, the timing of events and the consequent cladding temperatures will vary. A series of transients typical of large breaks is explored, with all uncertainty parameters at representative (model as coded) values aside from those related to the effective break area, to demonstrate the general sensitivity to break area. The range of effective break areas (EFAs) explored is from $1^{a,c}$ times a nominal double-ended guillotine (DEG, through the use of a discharge coefficient of $1^{a,c}$), or an effective break area of $1^{a,c}$ times the cold leg area, down to a split break with effective break area of 0.5 times the cold leg area.

Figure 27.1.1.1-1 shows the peak cladding temperature for the large break transients. Based on this limited set of cases, [

$1^{a,c}$. The location of the peak cladding temperature (PCT) is more a function of the power shape and the location of flow stagnation during blowdown, and is relatively insensitive to the break size, shown in Figure 27.1.1.1-2.

The effect of increasing break area is primarily to increase the peak magnitude and decrease the duration of the total break flow, shown in Figure 27.1.1.1-3. This directly corresponds with the rate of depressurization (Figure 27.1.1.1-4) where the largest breaks depressurize the most quickly. The faster depressurization for larger breaks allows for an earlier accumulator injection, shown in Figure 27.1.1.1-5, but due to higher emergency core cooling system (ECCS) bypass early in the transient, the total vessel fluid mass is not replaced to the same degree it is for the smaller breaks (Figure 27.1.1.1-6) by the end of refill.

Safety injection flow is shown in Figure 27.1.1.1-7. [

I^{a,c}

Based on the results for the large break spectrum, a nominal DEG with break size twice the cold leg area is chosen as the reference large break and is utilized in the scoping studies in Section 28. The CGE large break reference transient is described in more detail in Section 27.2.1.

Figure 27.1.1.1-1 Hot Rod Peak Cladding Temperature, CGE LBLOCA

Figure 27.1.1.1-2 Hot Rod Peak Cladding Temperature Elevation, CGE LBLOCA

Figure 27.1.1.1-3 Break Flow, CGE LBLOCA

Figure 27.1.1.1-4 RCS Pressure, CGE LBLOCA

Figure 27.1.1.1-5 Accumulator Mass Flow Rate, CGE LBLOCA

Figure 27.1.1.1-6 Vessel Fluid Mass, CGE LBLOCA

Figure 27.1.1.1-7 Safety Injection Flow Rate, CGE LBLOCA

Figure 27.1.1.1-8 Containment Pressure, CGE LBLOCA

27.1.1.2 CGE Intermediate Break Spectrum

Intermediate breaks tend to be non-limiting relative to both large breaks, where significant ECCS bypass prevents efficient core recovery through accumulator injection, and small breaks, where an extended natural circulation phase and vessel depressurization delays accumulator injection such that core uncover may occur. A series of transients is explored here, with effective break areas from approximately 0.35 times the cold leg area for a 16-inch diameter break down to an 8-inch diameter break, equivalent to slightly less than 0.1 times the cold leg area.

Figure 27.1.1.2-1 shows the peak cladding temperature for the intermediate break transients.

[

] ^{a,c}

Figure 27.1.1.2-2 shows a continuation of the trend observed for large breaks, where decreases in effective break area lead to a prolonged period of lower break flow. This is also clear from the depressurization rate, shown in Figure 27.1.1.2-3, and the timing of accumulator injection in Figure 27.1.1.2-4. [

] ^{a,c} The 12-inch break is described in more detail as the intermediate break reference transient in Section 27.2.2.

Figure 27.1.1.2-1 Hot Rod Peak Cladding Temperature, CGE IBLOCA

Figure 27.1.1.2-2 Break Flow, CGE IBLOCA

Figure 27.1.1.2-3 RCS Pressure, CGE IBLOCA

Figure 27.1.1.2-4 Accumulator Mass Flow Rate, CGE IBLOCA

Figure 27.1.1.2-5 Vessel Fluid Mass, CGE IBLOCA

27.1.1.3 CGE Small Break Spectrum

Following a small break LOCA, a relatively long transient ensues in which the timing of the major phenomena and consequently the severity of the cladding heat up are a strong function of break size. The largest of the small breaks will blow down quickly, allowing for an efficient clearing of the loop seals, rapid vessel depressurization, and early accumulator injection, resulting in a transient that is not expected to be limiting as in the case of an intermediate break. In direct contrast, an extremely small break will result in break flow so small that the high head safety injection flows are sufficient to prevent core uncover.

Figure 27.1.1.3-1 shows the break flow void fraction for a range of break sizes from a 2-inch equivalent diameter to a 5-inch break. During blowdown, and until the natural circulation phase ends (Figure 27.1.1.3-2), the break flow is either subcooled liquid or a two-phase mixture. [

] ^{a,c}

All cases demonstrate the top-down draining that is characteristic of small breaks (Figure 27.1.1.3-3). [

] ^{a,c}

Figure 27.1.1.3-5 shows that [

] ^{a,c}

Section 28.2.11 will demonstrate the strong relationship between the number of loop seals that clear, and to what extent, and break size for these small breaks.

The 2.5-inch break is chosen as the small break reference transient and is described in more detail in Section 27.2.3.

Figure 27.1.1.3-1 Break Void Fraction, CGE SBLOCA

Figure 27.1.1.3-2 RCS Pressure, CGE SBLOCA

Figure 27.1.1.3-3 Upper Head Collapsed Liquid Level, CGE SBLOCA

Figure 27.1.1.3-4 Break Flow, CGE SBLOCA

Figure 27.1.1.3-5 Hot Rod Peak Cladding Temperature, CGE SBLOCA

Figure 27.1.1.3-6 Loop 1 Loop Seal Differential Pressure, CGE SBLOCA

Figure 27.1.1.3-7 Loop 2 Loop Seal Differential Pressure, CGE SBLOCA

Figure 27.1.1.3-8 Loop 3 Loop Seal Differential Pressure, CGE SBLOCA

27.1.2 Beaver Valley Unit 1 (DLW) Break Spectra

27.1.2.1 DLW Large Break Spectrum

The phenomena observed following a large break LOCA are generally observed regardless of break size; however, the timing of events and the consequent cladding temperatures will vary. A series of transients typical of large breaks is explored, with all uncertainty parameters at a representative (model as coded) value aside from those related to the effective break area, to demonstrate the general sensitivity to break area. The range of break areas explored is from $[]^{a,c}$ times a nominal DEG (through the use of a discharge coefficient of $[]^{a,c}$), or an effective break area of $[]^{a,c}$ times the cold leg area, down to a split break with effective break area of 0.5 times the cold leg area.

Figure 27.1.2.1-1 shows the peak cladding temperature for the large break transients. For DLW, it appears that $[]^{a,c}$.

The location of the PCT is more a function of the power shape and the location of flow stagnation during blowdown, and is relatively insensitive to the break size, shown in Figure 27.1.2.1-2.

The effect of break area is primarily to increase the magnitude and decrease the duration of the total break flow, shown in Figure 27.1.2.1-3. This directly corresponds with the rate of depressurization (Figure 27.1.2.1-4) where the largest breaks depressurize the most quickly, as expected. The faster depressurization for larger breaks allows for earlier accumulator injection, shown in Figure 27.1.2.1-5, but due to ECCS bypass the total vessel fluid mass is not replaced (Figure 27.1.2.1-6).

Safety injection flow is shown in Figure 27.1.2.1-7. $[]^{a,c}$

$[]^{a,c}$

Based on the results for the large break spectrum, a break size of twice the cold leg area is chosen as the reference large break and is utilized in the scoping studies in Section 28. The DLW large break reference transient is described in more detail in Section 27.3.1.

Figure 27.1.2.1-1 Hot Rod Peak Cladding Temperature, DLW LBLOCA

Figure 27.1.2.1-2 Hot Rod Peak Cladding Temperature Elevation, DLW LBLOCA

Figure 27.1.2.1-3 Break Flow, DLW LBLOCA

Figure 27.1.2.1-4 RCS Pressure, DLW LBLOCA

Figure 27.1.2.1-5 Accumulator Mass Flow Rate, DLW LBLOCA

Figure 27.1.2.1-6 Vessel Fluid Mass, DLW LBLOCA

Figure 27.1.2.1-7 Safety Injection Flow Rate, DLW LBLOCA

Figure 27.1.2.1-8 Containment Pressure, DLW LBLOCA

27.1.2.2 DLW Intermediate Break Spectrum

Intermediate breaks have historically been shown to be non-limiting relative to both large breaks, where significant ECCS bypass prevents efficient core recovery through accumulator injection, and small breaks, where an extended natural circulation phase and vessel depressurization delays accumulator injection such that core uncover may occur. A series of transients is explored here, from a 16-inch diameter break with effective break area of approximately 0.34 times the cold leg area down to a 6-inch diameter break, equivalent to slightly less than 0.05 times the cold leg area.

Figure 27.1.2.2-1 shows the peak cladding temperature for the intermediate break transients.

[

] ^{a,c}

Figure 27.1.2.2-2 shows a continuation of the trend observed for large breaks, where decreases in effective break area lead to a prolonged period of lower break flow. This is also clear from the depressurization rate, shown in Figure 27.1.2.2-3, and the timing of accumulator injection in Figure 27.1.2.2-4. [

] ^{a,c}

The 12-inch break is described in more detail as the intermediate break reference transient in Section 27.3.2.

Figure 27.1.2.2-1 Hot Rod Peak Cladding Temperature, DLW IBLOCA

Figure 27.1.2.2-2 Break Flow, DLW IBLOCA

Figure 27.1.2.2-3 RCS Pressure, DLW IBLOCA

Figure 27.1.2.2-4 Accumulator Mass Flow Rate, DLW IBLOCA

Figure 27.1.2.2-5 Vessel Fluid Mass, DLW IBLOCA

27.1.2.3 DLW Small Break Spectrum

Following a small break LOCA, a relatively long transient ensues in which the timing of the major phenomena and consequently the severity of the cladding heat up are a strong function of break size. The largest of the small breaks will blow down quickly, allowing for an efficient clearing of the loop seals, rapid vessel depressurization, and early accumulator injection, resulting in a transient that is not expected to be limiting as in the case of an intermediate break. In direct contrast, an extremely small break will result in break flow so small that the high head safety injection flows are sufficient to prevent core uncover.

Figure 27.1.2.3-1 shows RCS depressurization following a range of break sizes from a 2-inch equivalent diameter to a 5-inch break. [

] ^{a,c}

All cases demonstrate the top-down draining that is characteristic of small breaks (Figure 27.1.2.3-2).

[

] ^{a,c}

Figure 27.1.2.3-4 shows that [

] ^{a,c} Section 28.2.11 will demonstrate the strong relationship between the number of loop seals that clear, and to what extent, and break size for these small breaks.

The 3-inch break is chosen as the small break reference transient and is described in more detail in Section 27.3.3.

Figure 27.1.2.3-1 RCS Pressure, DLW SBLOCA

Figure 27.1.2.3-2 Upper Head Collapsed Liquid Level, DLW SBLOCA

Figure 27.1.2.3-3 Break Flow, DLW SBLOCA

Figure 27.1.2.3-4 Hot Rod Peak Cladding Temperature, DLW SBLOCA

Figure 27.1.2.3-5 Loop 1 Loop Seal Differential Pressure, DLW SBLOCA

Figure 27.1.2.3-6 Loop 2 Loop Seal Differential Pressure, DLW SBLOCA

Figure 27.1.2.3-7 Loop 3 Loop Seal Differential Pressure, DLW SBLOCA

27.2 V. C. SUMMER (CGE) REFERENCE TRANSIENTS

27.2.1 CGE Large Break Reference Transient Description

The CGE large break reference transient used the conditions listed in Table 26.2-1. The reference large break is a nominal double-ended guillotine break of the cold leg pipe with uncertainty attributes at representative (model as coded) values. A conservatively low containment pressure is calculated according to the mass and energy release [^{a,c}].

The large break LOCA transient can be divided into time periods in which specific phenomena are occurring. A convenient way to divide the transient is in terms of the various heatup and cooldown phases that the hot assembly undergoes. For each of these phases, specific phenomena and heat transfer regimes are important, as discussed below.

1. Critical Heat Flux (CHF) Phase

In this phase, the break flow is subcooled, the discharge rate is high, the core flow reverses, the fuel rods go through departure from nucleate boiling (DNB), and the cladding rapidly heats up while core power shuts down. Figure 27.2.1-1 shows the maximum cladding temperature in the core for all the fuel rods, as a function of time, and Figure 27.2.1-2 shows the PCT location as a function of time for the hot rod.

The regions of the RCS with the highest initial temperatures (upper core, upper plenum, and hot legs) begin to flash during this period. This phase is terminated when the water in the lower plenum and downcomer begin to flash. The mixture level swells and the intact loop pumps, still rotating in single-phase liquid, push this two phase mixture into the core. As the fluid in the cold leg reaches saturation conditions, the discharge flow rate at the break decreases sharply (Figures 27.2.1-3 and 27.2.1-4).

2. Upward Core Flow Phase

Heat transfer is improved as the two-phase mixture is pushed into the core. The break discharge rate is reduced because the fluid is saturated at the break. Figures 27.2.1-3 and 27.2.1-4 show the break flowrate from the vessel and pump sides of the break, respectively. This phase ends as the lower plenum mass is depleted (Figure 27.2.1-5), the loops become two-phase, and the pump head degrades.

3. Downward Core Flow Phase

The break flow begins to dominate and pulls flow down through the core as the pump head degrades due to increased voiding. Figure 27.2.1-6 shows the vapor mass flow rate near the PCT elevation. While liquid and entrained liquid flows also provide cooling, the vapor flow entering the top of the core best illustrates this phase of core cooling. This period may be enhanced by flow from the upper head. Once the system has depressurized to the accumulator pressure (Figure 27.2.1-7 provides the system pressure transient), the accumulators begin to inject cold

water into the intact cold legs (Figure 27.2.1-8). During this period, due to steam upflow in the downcomer, a portion of the injected ECCS (Emergency Core Cooling System) water is calculated to be bypassed around the downcomer and out the break. As the system pressure continues to fall (Figure 27.2.1-7), the break flow and consequently the downward core flow are reduced. The system pressure approaches the containment pressure at around 20-25 seconds.

During this phase, the core begins to heat up as the system approaches containment pressure (Figure 27.2.1-9) and the vessel begins to fill with ECCS water (Figures 27.2.1-10, 27.2.1-11, and 27.2.1-12).

4. Refill Phase

The core continues to heat up as the lower plenum fills with ECCS water. Figure 27.2.1-5 shows the lower plenum liquid level. This phase is characterized by a rapid increase in cladding temperatures at all elevations due to the lack of liquid and steam flow in the core region. This phase ends when the ECCS water enters the core and entrainment begins, with a resulting improvement in heat transfer.

Figures 27.2.1-8 and 27.2.1-13 show the liquid flows from the intact loop accumulators and the safety injection on one of the intact loops, respectively. As water fills the lower plenum, the refill phase ends. A repressurization, which occurs as the accumulators discharge nitrogen, can be seen in the reduction in pumped flow.

5. Reflood Phase

During the early reflood phase, the accumulators begin to empty and nitrogen enters the system (Figure 27.2.1-8). The nitrogen surge forces water into the core, which then boils, causing system repressurization, and the lower core region begins to quench. The repressurization is illustrated by the RCS pressure (Figure 27.2.1-7). During this time, core cooling may increase due to vapor generation and liquid entrainment, but conversely the early reflood pressure spike results in loss of mass out the broken cold leg.

The pumped ECCS water aids in the filling of the downcomer throughout the reflood period. Figure 27.2.1-11 and Figure 27.2.1-12 show the core and downcomer collapsed liquid levels, respectively. Figure 27.2.1-10 shows the vessel fluid mass. As the quench front progresses further into the core, the PCT location moves to a higher elevation (Figure 27.2.1-2).

As the transient progresses, continued injection of pumped ECCS water refills the core, removes the vessel metal mass stored energy and core decay heat, and leads to an increase in the vessel fluid mass. All rods are quenched before approximately []^{a,c} after the break (Figure 27.2.1-1).

Figure 27.2.1-1 Peak Cladding Temperatures, CGE LBLOCA Reference Transient

Figure 27.2.1-2 Hot Rod Peak Cladding Temperature Elevation, CGE LBLOCA Reference Transient

Figure 27.2.1-3 Vessel Side Break Flow, CGE LBLOCA Reference Transient

Figure 27.2.1-4 Pump Side Break Flow, CGE LBLOCA Reference Transient



Figure 27.2.1-5 Lower Plenum Collapsed Liquid Level, CGE LBLOCA Reference Transient

Figure 27.2.1-6 Vapor Mass Flow Rate in Hot Assembly Near PCT Elevation, CGE LBLOCA Reference Transient

Figure 27.2.1-7 RCS Pressure, CGE LBLOCA Reference Transient

Figure 27.2.1-8 Accumulator Mass Flow Rate, CGE LBLOCA Reference Transient

Figure 27.2.1-9 Containment Pressure, CGE LBLOCA Reference Transient

Figure 27.2.1-10 Vessel Fluid Mass, CGE LBLOCA Reference Transient

Figure 27.2.1-11 Core Collapsed Liquid Levels, CGE LBLOCA Reference Transient

Figure 27.2.1-12 Downcomer Collapsed Liquid Level, CGE LBLOCA Reference Transient

Figure 27.2.1-13 Safety Injection Flow, CGE LBLOCA Reference Transient

27.2.2 CGE Intermediate Break Reference Transient Description

The CGE intermediate break reference transient used the conditions listed in Table 26.2-1. The reference intermediate break is a split break of the cold leg pipe with uncertainty attributes at representative (model as coded) values and a break area consistent with a 12-inch diameter hole. A conservatively low containment pressure is calculated according to the mass and energy release [

] ^{a,c}

As stated in Section 2.3.1.3, an intermediate break is classified by a monotonic depressurization, or a lack of pressure stabilization associated with small breaks, and a lack of significant ECCS bypass brought about by steam upflow in the downcomer in large breaks. As a result, effective core recovery is expected early in the transient due to largely uninhibited accumulator flow. Historically, intermediate breaks have been shown to be non-limiting as a consequence. The intermediate break LOCA transient can be divided into time periods in which specific phenomena are occurring, as discussed below.

1. Blowdown/Depressurization

Initially, the break flow is high and single phase at the beginning of the blowdown phase (Figures 27.2.2-1 and 27.2.2-2). Break flow reduces as the flow to the break becomes two-phase, and consequently the depressurization rate also decreases (Figure 27.2.2-3). Flashing in the vessel results from the RCS depressurization, and collapsed liquid levels in the core and downcomer drop (Figures 27.2.2-4 and 27.2.2-5). [

] ^{a,c}

2. Accumulator Injection

Once the RCS pressure reaches the accumulator check valve pressure setpoint, accumulator flow rapidly refills the majority of the lost vessel inventory (Figures 27.2.2-8 and 27.2.2-9). ECCS bypass is low, as the core and downcomer fill with nearly the entire volume of the accumulator liquid. After the accumulators have emptied, ECCS injection is reduced to a minimal amount corresponding with the high-head safety injection (HHSI) system (Figure 27.2.2-10). This results in a period of vessel fluid mass depletion through boiling within the vessel, as the HHSI is not sufficient to make up for the break flow, which continues as the vessel depressurizes.

3. SI Injection

This phase begins as the low-head safety injection (LHSI) system is initiated (Figure 27.2.2-10). The RCS continues to depressurize, resulting in a continually increasing amount of SI flow injection from the LHSI system. Vessel fluid inventory depletion is halted nearly immediately as the total injected flow becomes greater than that lost through the break (Figure 27.2.2-11).

Figure 27.2.2-1 Break Flow, CGE IBLOCA Reference Transient

Figure 27.2.2-2 Void Fraction at the Break, CGE IBLOCA Reference Transient

Figure 27.2.2-3 RCS Pressure, CGE IBLOCA Reference Transient

**Figure 27.2.2-4 Core Collapsed Liquid Levels, CGE IBLOCA Reference Transient
(2=Low Power, 3=OH/SC/FSM, 4=Guide Tube, 5=Hot Assembly)**

Figure 27.2.2-5 Downcomer Collapsed Liquid Levels, CGE IBLOCA Reference Transient

Figure 27.2.2-6 Peak Cladding Temperatures, CGE IBLOCA Reference Transient

Figure 27.2.2-7 Vapor Flowrate in the Hot Assembly, CGE IBLOCA Reference Transient

Figure 27.2.2-8 Accumulator Mass Flow Rate, CGE IBLOCA Reference Transient

Figure 27.2.2-9 Vessel Fluid Mass, CGE IBLOCA Reference Transient

Figure 27.2.2-10 Safety Injection Flow, CGE IBLOCA Reference Transient

Figure 27.2.2-11 Safety Injection and Break Flow, CGE IBLOCA Reference Transient

27.2.3 CGE Small Break Reference Transient Description

The CGE small break reference transient used the conditions listed in Table 26.2-1. The reference small break is a split break of the cold leg pipe with uncertainty attributes at representative (model as coded) or limiting values and a break area consistent with a 2.5-inch diameter hole. [

] ^{a,c}

The small break LOCA transient can be divided into time periods in which specific phenomena are occurring, as discussed below.

1. Blowdown

The rapid depressurization of the RCS coincides with single-phase liquid flow through the break as shown in Figure 27.2.3-1. Following the reactor trip, initiated on a low-low pressurizer pressure setpoint, high pressure safety injection flow begins after the setpoint is reached with some delay (Figure 27.2.3-2). Phase separation begins in the upper head, upper plenum, and hot legs near the end of this period until the entire RCS eventually reaches saturation, ending the rapid depressurization [

] ^{a,c}.

2. Natural Circulation

This quasi-equilibrium phase persists until [^{a,c} as the RCS pressure remains slightly above the secondary side pressure (Figure 27.2.3-3). The system drains from the top down (Figure 27.2.3-4), and while significant mass is continually lost through the break (Figure 27.2.3-5), the vapor generated in the core is trapped in the upper regions by the liquid remaining in the crossover leg loop seals. [

] ^{a,c}

3. Loop Seal Clearance

As the system drains, the liquid level in the downhill side of the pump suction piping becomes depressed to the bottom of the loop seal, allowing the steam trapped during the natural circulation phase to vent to the break (Figures 27.2.3-8, 27.2.3-9, and 27.2.3-10). The break flow and the flow through the RCS loops become primarily vapor (Figure 27.2.3-1). [

] ^{a,c}

4. Boil-Off

With a vapor vent path established, the RCS depressurizes at a rate determined by the critical flow, which continues to be primarily single phase (Figures 27.2.3-3 and 27.2.3-1). [

] ^{a,c}

5. Core Recovery

The RCS pressure continues to fall, and once it reaches that of the accumulator check valve setpoint, the introduction of additional ECCS water (Figure 27.2.3-11) replenishes the vessel inventory (Figure 27.2.3-12) and recovers the core mixture level. Depressurization continues as a result of break flow and condensation, and the transient is declared over as the break flow becomes less than the total injected flow (Figure 27.2.3-13).

Figure 27.2.3-1 Void Fraction at the Break, CGE SBLOCA Reference Transient

Figure 27.2.3-2 Safety Injection Flow, CGE SBLOCA Reference Transient

**Figure 27.2.3-3 RCS and Steam Generator Secondary Side Pressure, CGE SBLOCA
Reference Transient**

Figure 27.2.3-4 Upper Head Collapsed Liquid Level, CGE SBLOCA Reference Transient

Figure 27.2.3-5 Break Flow, CGE SBLOCA Reference Transient

**Figure 27.2.3-6 Core Collapsed Liquid Levels, CGE SBLOCA Reference Transient
(2=Low Power, 3=OH/SC/FSM, 4=Guide Tube, 5=Hot Assembly)**

Figure 27.2.3-7 Hot Rod Cladding Temperature, CGE SBLOCA Reference Transient

Figure 27.2.3-8 Loop 1 Loop Seal Differential Pressure, CGE SBLOCA Reference Transient

Figure 27.2.3-9 Loop 2 Loop Seal Differential Pressure, CGE SBLOCA Reference Transient

Figure 27.2.3-10 Loop 3 Loop Seal Differential Pressure, CGE SBLOCA Reference Transient

Figure 27.2.3-11 Accumulator Mass Flow Rate, CGE SBLOCA Reference Transient

Figure 27.2.3-12 Vessel Fluid Mass, CGE SBLOCA Reference Transient

Figure 27.2.3-13 Safety Injection and Break Flow, CGE SBLOCA Reference Transient

27.3 BEAVER VALLEY UNIT 1 (DLW) REFERENCE TRANSIENTS

27.3.1 DLW Large Break Reference Transient Description

The DLW large break reference transient used the conditions listed in Table 26.3-1. The reference large break is a nominal double-ended guillotine break of the cold leg pipe with uncertainty attributes at representative (model as coded) values. [

]^{a,c}

The large break LOCA transient can be divided into time periods in which specific phenomena are occurring. A convenient way to divide the transient is in terms of the various heatup and cooldown phases that the hot assembly undergoes. For each of these phases, specific phenomena and heat transfer regimes are important, as discussed below.

1. Critical Heat Flux (CHF) Phase

In this phase, the break flow is subcooled, the discharge rate is high, the core flow reverses, the fuel rods go through departure from nucleate boiling (DNB), and the cladding rapidly heats up while core power shuts down. Figure 27.3.1-1 shows the maximum cladding temperature in the core for all the fuel rods, as a function of time, and Figure 27.3.1-2 shows the PCT location as a function of time for the hot rod.

The regions of the RCS with the highest initial temperatures (upper core, upper plenum, upper head, and hot legs) begin to flash during this period. This phase is terminated when the water in the lower plenum and downcomer begin to flash. The mixture level swells and the intact loop pumps, still rotating in single-phase liquid, push this two phase mixture into the core. As the fluid in the cold leg reaches saturation conditions, the discharge flow rate at the break decreases sharply (Figures 27.3.1-3 and 27.3.1-4).

2. Upward Core Flow Phase

Heat transfer is improved as the two-phase mixture is pushed into the core. The break discharge rate is reduced because the fluid is saturated at the break. Figures 27.3.1-3 and 27.3.1-4 show the break flowrate from the vessel and pump sides of the break, respectively. This phase ends as the lower plenum mass is depleted (Figure 27.3.1-5), the loops become two-phase, and the pump head degrades.

3. Downward Core Flow Phase

The break flow begins to dominate and pulls flow down through the core as the pump head degrades due to increased voiding. Figure 27.3.1-6 shows the vapor mass flow rate near the PCT elevation. While liquid and entrained liquid flows also provide cooling, the vapor flow entering the top of the core best illustrates this phase of core cooling. This period may be enhanced by flow from the upper head. Once the system has depressurized to the accumulator pressure (Figure 27.3.1-7 provides the system pressure transient), the accumulators begin to inject cold

water into the intact cold legs (Figure 27.3.1-8). During this period, due to steam upflow in the downcomer, a portion of the injected ECCS (Emergency Core Cooling System) water is calculated to be bypassed around the downcomer and out the break. As the system pressure continues to fall (Figure 27.3.1-7), the break flow and consequently the downward core flow are reduced. The system pressure approaches the containment pressure at around 20-25 seconds.

During this phase, the core begins to heat up as the system reaches containment pressure (Figure 27.3.1-9) and the vessel begins to fill with ECCS water (Figures 27.3.1-10, 27.3.1-11, and 27.3.1-12).

4. Refill Phase

The core continues to heat up as the lower plenum fills with ECCS water. Figure 27.3.1-5 shows the lower plenum liquid level. This phase is characterized by a rapid increase in cladding temperatures at all elevations due to the lack of liquid and steam flow in the core region. This phase ends when the ECCS water enters the core and entrainment begins, with a resulting improvement in heat transfer.

Figures 27.3.1-8 and 27.3.1-13 show the liquid flows from the intact loop accumulators and the safety injection on one of the intact loops, respectively. The repressurization, which occurs as the accumulator discharges nitrogen, can be seen in the reduction in pumped flow.

5. Reflood Phase

During the early reflood phase, the accumulators begin to empty and nitrogen enters the system (Figure 27.3.1-8). The nitrogen surge forces water into the core, which then boils, causing system repressurization, and the lower core region begins to quench. The repressurization is illustrated by the RCS pressure (Figure 27.3.1-7). During this time, core cooling may increase due to vapor generation and liquid entrainment, but conversely the early reflood pressure spike results in loss of mass out the broken cold leg.

The pumped ECCS water aids in the filling of the downcomer throughout the reflood period. Figure 27.3.1-11 and Figure 27.3.1-12 show the core and downcomer collapsed liquid levels, respectively. Figure 27.3.1-10 shows the vessel fluid mass. As the quench front progresses further into the core, the PCT location moves to a higher elevation (Figure 27.3.1-2).

[

] ^{a,c}

As the transient progresses, continued injection of pumped ECCS water refills the downcomer and core, removes the vessel metal mass stored energy and core decay heat, and leads to an increase in the vessel fluid mass. [

] ^{a,c}

Figure 27.3.1-1 Peak Cladding Temperatures, DLW LBLOCA Reference Transient

Figure 27.3.1-2 Hot Rod Peak Cladding Temperature Elevation, DLW LBLOCA Reference Transient

Figure 27.3.1-3 Vessel Side Break Flow, DLW LBLOCA Reference Transient

Figure 27.3.1-4 Pump Side Break Flow, DLW LBLOCA Reference Transient

Figure 27.3.1-5 Lower Plenum Collapsed Liquid Level, DLW LBLOCA Reference Transient

Figure 27.3.1-6 Vapor Mass Flow in Hot Assembly Near PCT Elevation, DLW LBLOCA Reference Transient

Figure 27.3.1-7 RCS Pressure, DLW LBLOCA Reference Transient

Figure 27.3.1-8 Accumulator Mass Flow Rate, DLW LBLOCA Reference Transient



Figure 27.3.1-9 Containment Pressure, DLW LBLOCA Reference Transient

Figure 27.3.1-10 Vessel Fluid Mass, DLW LBLOCA Reference Transient

Figure 27.3.1-11 Core Collapsed Liquid Levels, DLW LBLOCA Reference Transient

Figure 27.3.1-12 Downcomer Collapsed Liquid Level, DLW LBLOCA Reference Transient



Figure 27.3.1-13 Safety Injection Flow, DLW LBLOCA Reference Transient

27.3.2 DLW Intermediate Break Reference Transient Description

The DLW intermediate break reference transient used the conditions listed in Table 26.3-1. The reference intermediate break is a split break of the cold leg pipe with uncertainty attributes at representative (model as coded) values and a break area consistent with a 12-inch diameter hole. [

] ^{a,c}

As stated in Section 2.3.1.3, an intermediate break is classified by a monotonic depressurization, or a lack of pressure stabilization associated with small breaks, and a lack of significant ECCS bypass brought about by steam upflow in the downcomer in large breaks. As a result, effective core recovery is expected early in the transient due to largely uninhibited accumulator flow. Historically, intermediate breaks have been shown to be non-limiting as a consequence. The intermediate break LOCA transient can be divided into time periods in which specific phenomena are occurring, as discussed below.

1. Blowdown/Depressurization

Initially, the break flow is high and single phase at the beginning of the blowdown phase (Figures 27.3.2-1 and 27.3.2-2). Break flow reduces as the flow to the break becomes two-phase, and consequently the depressurization rate also decreases (Figure 27.3.2-3). Flashing in the vessel results from the RCS depressurization, and collapsed liquid levels in the core and downcomer drop (Figures 27.3.2-4 and 27.3.2-5). [

] ^{a,c}

2. Accumulator Injection

Once the RCS pressure reaches the accumulator check valve pressure setpoint, accumulator flow rapidly refills the majority of the lost vessel inventory (Figures 27.3.2-8 and 27.3.2-9). ECCS bypass is low, as the core and downcomer fill with nearly the entire volume of the accumulator liquid. After the accumulators have emptied, ECCS injection is reduced to a minimal amount corresponding with the HHSI system (Figure 27.3.2-10). This results in a period of vessel fluid mass depletion through boiling within the vessel, as the HHSI is not sufficient to make up for the break flow, which continues as the vessel depressurizes.

3. SI Injection

This phase begins as the LHSI system is initiated (Figure 27.3.2-10). The RCS continues to depressurize, resulting in a continually increasing amount of SI flow injection from the LHSI system. Continued boiling in the vessel leads to a reduction in downcomer and core liquid levels (Figures 27.3.2-4 and 27.3.2-5) and in total vessel inventory (Figure 27.3.2-9), resulting in a second heatup. Around 400 seconds after the break, vessel fluid inventory depletion is halted as the total injected flow becomes greater than that lost through boiling (Figure 27.3.2-11), and the second heatup is mitigated.

Figure 27.3.2-1 Break Flow, DLW IBLOCA Reference Transient

Figure 27.3.2-2 Void Fraction at the Break, DLW IBLOCA Reference Transient

Figure 27.3.2-3 RCS Pressure, DLW IBLOCA Reference Transient

**Figure 27.3.2-4 Core Collapsed Liquid Levels, DLW IBLOCA Reference Transient
(2=Low Power, 3=OH/SC/FSM, 4=Guide Tube, 5=Hot Assembly)**

Figure 27.3.2-5 Downcomer Collapsed Liquid Levels, DLW IBLOCA Reference Transient

Figure 27.3.2-6 Peak Cladding Temperatures, DLW IBLOCA Reference Transient

Figure 27.3.2-7 Vapor Flowrate in Hot Assembly Channel, DLW IBLOCA Reference Transient

Figure 27.3.2-8 Accumulator Mass Flow Rate, DLW IBLOCA Reference Transient

Figure 27.3.2-9 Vessel Fluid Mass, DLW IBLOCA Reference Transient

Figure 27.3.2-10 Safety Injection Flow, DLW IBLOCA Reference Transient

Figure 27.3.2-11 Safety Injection and Break Flow, DLW IBLOCA Reference Transient

27.3.3 DLW Small Break Reference Transient Description

The DLW small break reference transient used the conditions listed in Table 26.3-1. The reference small break is a split break of the cold leg pipe with uncertainty attributes at representative (model as coded) or limiting values and a break area consistent with a 3-inch diameter hole. [

] ^{a,c}

The small break LOCA transient can be divided into time periods in which specific phenomena are occurring, as discussed below.

1. Blowdown

The rapid depressurization of the RCS coincides with single-phase liquid flow through the break as shown in Figure 27.3.3-1. Following the reactor trip, initiated on a low-low pressurizer pressure setpoint, high pressure safety injection flow begins after the setpoint is reached with some delay (Figure 27.3.3-2). Phase separation begins in the upper head, upper plenum, and hot legs near the end of this period until the entire RCS eventually reaches saturation, ending the rapid depressurization slightly above the steam generator secondary side pressure near the main steam safety valve (MSSV) setpoint [

] ^{a,c}.

2. Natural Circulation

This quasi-equilibrium phase persists [

] ^{a,c} as the RCS pressure remains slightly above the secondary side pressure (Figure 27.3.3-3). The system drains from the top down (Figure 27.3.3-4), and while significant mass is continually lost through the break (Figure 27.3.3-5), the vapor generated in the core is trapped in the upper regions by the liquid remaining in the crossover leg loop seals. [

] ^{a,c}

3. Loop Seal Clearance

As the system drains, the liquid level in the downhill side of the pump suction piping becomes depressed to the bottom of the loop seal, allowing the steam trapped during the natural circulation phase to vent to the break (Figures 27.3.3-8, 27.3.3-9, and 27.3.3-10). The break flow and the flow through the RCS loops become primarily vapor (Figure 27.3.3-1), [

] ^{a,c}. Relief of a static head imbalance allows for a quick but temporary recovery of liquid levels in the core (Figure 27.3.3-6).

4. Boil-Off

With a vapor vent path established, the RCS depressurizes at a rate determined by the critical flow, which continues to be primarily single phase (Figures 27.3.3-3 and 27.3.3-1). [

] ^{a,c}

5. Core Recovery

The RCS pressure continues to fall, and once it reaches that of the accumulator check valve setpoint, the introduction of additional ECCS water (Figure 27.3.3-11) replenishes the vessel inventory (Figure 27.3.3-12) and recovers the core mixture level. The transient is declared over as the break flow is compensated for with injected flow (Figure 27.3.3-13).

Figure 27.3.3-1 Void Fraction at the Break, DLW SBLOCA Reference Transient

Figure 27.3.3-2 Safety Injection Flow, DLW SBLOCA Reference Transient

Figure 27.3.3-3 RCS and Steam Generator Secondary Side Pressure, DLW SBLOCA Reference Transient

Figure 27.3.3-4 Upper Head Collapsed Liquid Level, DLW SBLOCA Reference Transient

Figure 27.3.3-5 Break Flow, DLW SBLOCA Reference Transient

**Figure 27.3.3-6 Core Collapsed Liquid Levels, DLW SBLOCA Reference Transient
(2=Low Power, 3=OH/SC/FSM, 4=Guide Tube, 5=Hot Assembly)**

Figure 27.3.3-7 Hot Rod Cladding Temperature, DLW SBLOCA Reference Transient

Figure 27.3.3-8 Loop 1 Loop Seal Differential Pressure, DLW SBLOCA Reference Transient

Figure 27.3.3-9 Loop 2 Loop Seal Differential Pressure, DLW SBLOCA Reference Transient

Figure 27.3.3-10 Loop 3 Loop Seal Differential Pressure, DLW SBLOCA Reference Transient

Figure 27.3.3-11 Accumulator Mass Flow Rate, DLW SBLOCA Reference Transient

Figure 27.3.3-12 Vessel Fluid Mass, DLW SBLOCA Reference Transient

Figure 27.3.3-13 Safety Injection Flow and Break Flow, DLW SBLOCA Reference Transient

28 SCOPING AND SENSITIVITY STUDIES

In this section, the pilot plant models for V. C. Summer (CGE) and Beaver Valley Unit 1 (DLW) are exercised using the WCOBRA/TRAC-TF2 code to determine the effect of variations in key Loss-of-Coolant Accident (LOCA) parameters on the small and large break reference transients from Section 27. As was shown in Section 27, breaks typically classified as intermediate in size are less limiting than small and large breaks, and therefore are not considered in these scoping studies. The intent of the studies is to exercise the WCOBRA/TRAC-TF2 plant models, evaluate the effects of parameters of interest to demonstrate reasonable behavior, and to determine the appropriate treatment of several parameters for the plant analysis. For those parameters for which the treatment is determined within this section, a summary of those methodology decisions supported by scoping studies is provided below.

Offsite Power Availability

Section 28.1.2 shows that [

] ^{a,c}

Limiting Offsite Power Scenario

[

] ^{a,c}

Operator Action

The availability of offsite power affects [

] ^{a,c}

Limiting Operator Action

[

] ^{a,c}

¹ The approach described in Section 30.4 to determine the [^{a,c} is superseded by limitation and condition #15 from the safety evaluation report (SER).

Accumulator Elevation

Section 28.1.5 shows that [

] ^{a,c}

Limiting Accumulator Elevation

[

] ^{a,c}

Break Location

Section 28.2.6 shows that [

] ^{a,c}

Limiting Break Location

[

] ^{a,c}

Break Orientation

The Rig-of-Safety Assessment (ROSA) break orientation study in Section 21.7 showed [

] ^{a,c}

Limiting Split Break Orientation

[

] ^{a,c}

Steam Generator Tube Plugging

Section 28.1.6 demonstrates [

] ^{a,c} and Section 28.2.9 [

] ^{a,c}

Limiting Steam Generator Tube Plugging

[

] ^{a,c}

28.1 LARGE BREAK SCOPING STUDY RESULTS

28.1.1 Axial Power Distributions – LBLOCA

As part of the uncertainty analysis, the axial power distribution []^{a,c} The CGE LBLOCA reference transient of Section 27.2.1 and the DLW LBLOCA reference transient of Section 27.3.1 both assumed a top-skewed power distribution, which is expected to be more limiting for a nominal double-ended guillotine break due to the timing of the PCT during reflood with an upward-progressing quench front. A sensitivity case is examined for each plant where the axial power distribution is skewed more toward the bottom of the core.

28.1.1.1 V. C. Summer (CGE)

Figure 28.1.1-1 shows the axial power distribution used for this sensitivity compared with the reference transient. Figure 28.1.1-2 shows []

[]^{a,c}

In addition to affecting PCT and PCT locations during blowdown, []

[]^{a,c}

28.1.1.2 Beaver Valley Unit 1 (DLW)

Overall, the behavior observed here is similar to that shown in the CGE sensitivity. Figure 28.1.1-7 shows the axial power distribution used for this sensitivity compared with the reference transient. Figure 28.1.1-8 shows []

[]^{a,c}

The nature of early reflood is again affected by the power distributed in the lower elevations, []

[]^{a,c}

28.1.1.3 Conclusions

The axial power distribution affects cladding temperatures throughout the transient, [$J^{a,c}$] as described in Section 29.4.1.2.

Figure 28.1.1-1 Axial Power Distribution, CGE Axial Power Distribution Sensitivity

Figure 28.1.1-2 Rod 1 Peak Cladding Temperatures, CGE Axial Power Distribution Sensitivity

Figure 28.1.1-3 Peak Cladding Temperature Location, CGE Axial Power Distribution Sensitivity

Figure 28.1.1-4 Lower Plenum Collapsed Liquid Level, CGE Axial Power Distribution Sensitivity

Figure 28.1.1-5 Hot Assembly Collapsed Liquid Level, CGE Axial Power Distribution Sensitivity

Figure 28.1.1-6 Vessel Fluid Mass, CGE Axial Power Distribution Sensitivity

Figure 28.1.1-7 Axial Power Distribution, DLW Axial Power Distribution Sensitivity

Figure 28.1.1-8 Peak Cladding Temperatures, DLW Axial Power Distribution Sensitivity

Figure 28.1.1-9 Peak Cladding Temperature Location, DLW Axial Power Distribution Sensitivity

Figure 28.1.1-10 Lower Plenum Collapsed Liquid Level, DLW Axial Power Distribution Sensitivity

Figure 28.1.1-11 Hot Assembly Collapsed Liquid Level, DLW Axial Power Distribution Sensitivity

Figure 28.1.1-12 Vessel Fluid Mass, DLW Axial Power Distribution Sensitivity

28.1.2 Offsite Power Availability – LBLOCA

The availability of offsite power affects the timing of the reactor coolant pump trip and the initiation of safety injection flow following a large break LOCA. With a LOOP, there is an extended delay in safety injection. Also with LOOP, the RCP trip is modeled [

] ^{a,c}

28.1.2.1 V. C. Summer (CGE)

With a LOOP, there is extended delay in safety injection, which for V. C. Summer results in a delay time of [^{a,c} with OPA (Figure 28.1.2-1). For the LOOP case, Figure 28.1.2-2 shows the pump coastdown in the intact loops, while Figure 28.1.2-3 shows the predicted acceleration of the pump in the broken loop.

For this case, [

] ^{a,c}

28.1.2.2 Beaver Valley Unit 1 (DLW)

For Beaver Valley Unit 1, the delay in safety injection resulting from a LOOP is [^{a,c} with OPA (Figure 28.1.2-7). For the LOOP case, Figure 28.1.2-8 shows the pump coastdown in the intact loops, while Figure 28.1.2-9 shows the acceleration of the pump in the broken loop.

For the DLW reference transient, [

] ^{a,c}

28.1.2.3 Conclusions

Since the availability of offsite power leads to some competing effects that affect the magnitude of blowdown cooling, the behavior of the liquid surge following refill, and the conditions leading to potential downcomer and lower plenum boiling, [

$J^{a,c}$

² The approach described in Section 30.4 to determine the [$J^{a,c}$] is superseded by limitation and condition #15 from the safety evaluation report (SER).

a,c

Figure 28.1.2-1 Safety Injection Flow, CGE Offsite Power Availability Sensitivity

a,c

Figure 28.1.2-2 Intact Loop Pump Speed, CGE Offsite Power Availability Sensitivity

a,c

Figure 28.1.2-3 Broken Loop Pump Speed, CGE Offsite Power Availability Sensitivity

a,c

Figure 28.1.2-4 Accumulator and Safety Injection Flow Rates, CGE Offsite Power Availability Sensitivity

Figure 28.1.2-5 Hot Assembly Vapor Mass Flow Rate, CGE Offsite Power Availability Sensitivity

Figure 28.1.2-6 Peak Cladding Temperatures, CGE Offsite Power Availability Sensitivity

Figure 28.1.2-7 Safety Injection Flow, DLW Offsite Power Availability Study

a,c

Figure 28.1.2-8 Intact Loop Pump Speed, DLW Offsite Power Availability Study

Figure 28.1.2-9 Broken Loop Pump Speed, DLW Offsite Power Availability Study

Figure 28.1.2-10 Peak Cladding Temperature, DLW Offsite Power Availability Study

Figure 28.1.2-11 Hot Assembly Vapor Mass Flow Rate, DLW Offsite Power Availability Study

a,c

Figure 28.1.2-12 Accumulator and Safety Injection Flow Rates, DLW Offsite Power Availability Sensitivity

a,c

Figure 28.1.2-13 Lower Plenum Collapsed Liquid Level, DLW Offsite Power Availability Study

28.1.3 Time Step and Convergence Criteria Studies – LBLOCA

The large break spectra, including double-ended guillotine (DEG) breaks and split breaks, are executed here using a modified upper limit on the time step (DTMAX) during the blowdown/refill (prior to 100 seconds after break initiation) and reflood portions of the transient. The reference DTMAX strategy consists of []^{a,c}. The decrease and increase explored in this study is shown in Table 28.1.3-1.

28.1.3.1 V. C. Summer (CGE)

Table 28.1.3-2 presents the peak cladding temperatures as calculated with the original and modified DTMAX. The thirteen large break transients from the LBLOCA break spectrum analysis (see Section 27.1.1.1; note that not all thirteen cases are presented there) were examined. The largest PCT difference seen when reducing the DTMAX limit []

[]^{a,c}

The vessel fluid mass, PCT, and time step for the two cases showing the largest PCT difference, run010 and run008, are shown in Figure 28.1.3-1 through Figure 28.1.3-4. For both cases, []

[]^{a,c}

28.1.3.2 Beaver Valley Unit 1 (DLW)

Table 28.1.3-3 presents the results of the DTMAX sensitivity study applied to the DLW LBLOCA break spectrum of Section 27.1.2.1. The largest absolute difference from a DTMAX []

[]^{a,c}

Figure 28.1.3-5 through Figure 28.1.3-8 show the vessel mass and PCT for the two cases with the largest PCT difference. []

[]^{a,c}

28.1.3.3 Conclusions

The use of DTMAX upper limits on time step size []

[]^{a,c}. The choice of DTMAX for the plant is discussed further in Section 29.3.3.

Table 28.1.3-1 DTMAX Values used in LBLOCA Timestep Sensitivity

a,c

Table 28.1.3-2 PCT Results When Varying DTMAX, CGE LBLOCA Sensitivity

a,c

a,c

[illegible]

a,c

Figure 28.1.3-1 Vessel Fluid Mass, run010 of CGE Timestep Sensitivity Study (DTMAX)

a,c

Figure 28.1.3-2 Peak Cladding Temperature, run010 of CGE Timestep Sensitivity Study (DTMAX)

Figure 28.1.3-3 Vessel Fluid Mass, run008 of CGE Timestep Sensitivity Study (DTMAX)

a,c

Figure 28.1.3-4 Peak Cladding Temperature, run008 of CGE Timestep Sensitivity Study (DTMAX)

Figure 28.1.3-5 Vessel Fluid Mass, run004 of DLW Timestep Sensitivity Study (DTMAX)

Figure 28.1.3-6 Peak Cladding Temperature, run004 of DLW Timestep Sensitivity Study (DTMAX)

Figure 28.1.3-7 Vessel Fluid Mass, run010 of DLW Timestep Sensitivity Study (DTMAX)

Figure 28.1.3-8 Peak Cladding Temperature, run010 of DLW Timestep Sensitivity Study (DTMAX)

28.1.4 Break Path Resistance – LBLOCA

To demonstrate that [

] ^{a,c}

Table 28.1.4-1 Scenarios for Break Path Resistance Sensitivity Study								

] ^{a,c}

28.1.4.1 V. C. Summer (CGE)

[

] ^{a,c}

28.1.4.2 Beaver Valley Unit 1 (DLW)

[

] ^{a,c}

28.1.4.3 Conclusions

For a double-ended guillotine break, it has been shown that [

] ^{a,c} For a nominal split break with half the break area as the
DEG break, [

] ^{a,c}

a,c

Figure 28.1.4-1 [

] ^{a,c}

a,c

Figure 28.1.4-2 [

] ^{a,c}

a,c

Figure 28.1.4-3 []^{a,c}

a,c

Figure 28.1.4-4 []^{a,c}

a,c

Figure 28.1.4-5 []^{a,c}

a,c

Figure 28.1.4-6 [

] a,c

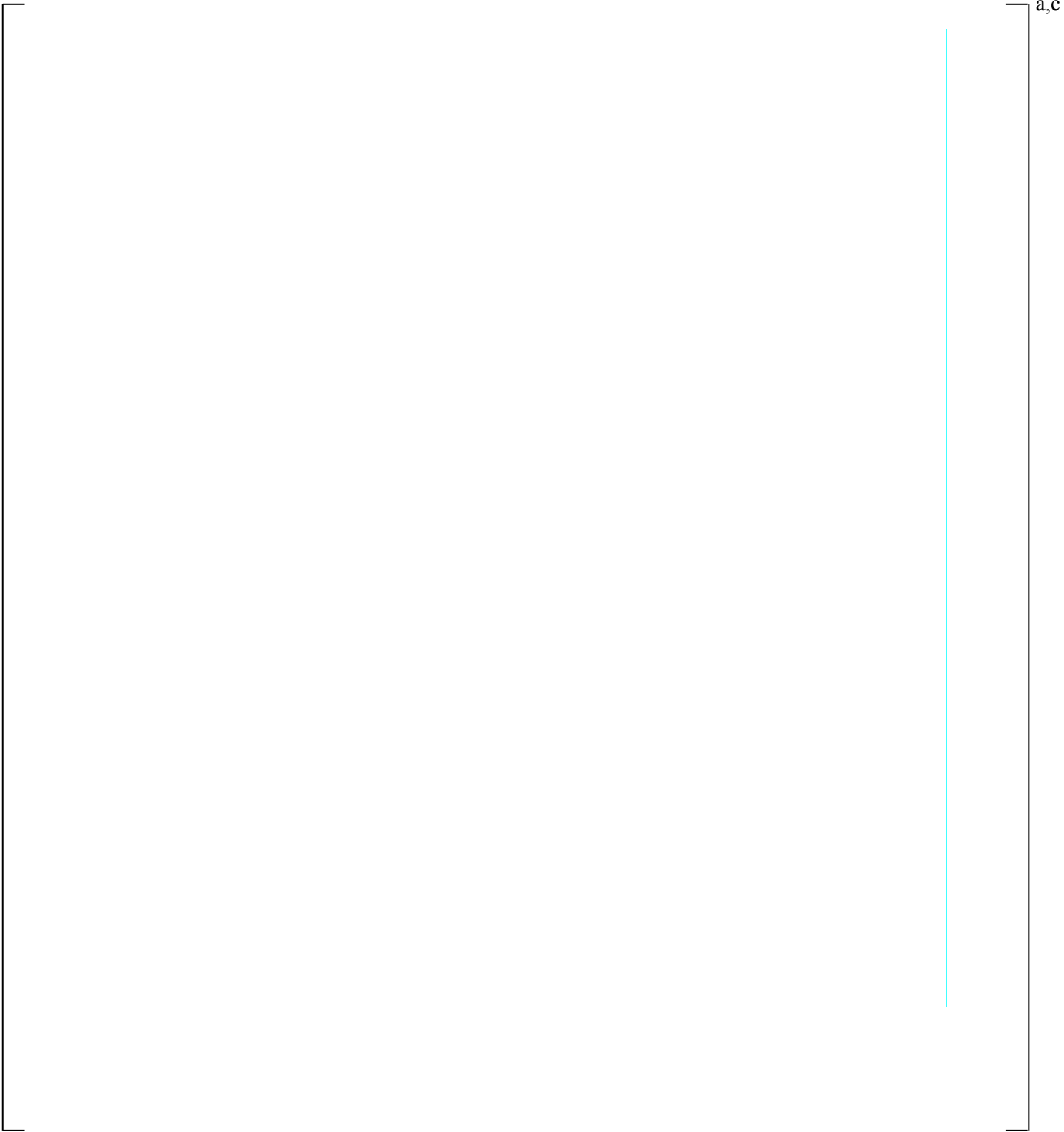


Figure 28.1.4-7 []^{a,c}

a,c

Figure 28.1.4-8 []^{a,c}

a,c

Figure 28.1.4-9 []^{a,c}

a,c

Figure 28.1.4-10 [] ^{a,c}

a,c

Figure 28.1.4-11 [

] a,c

a,c

Figure 28.1.4-12 [

] ^{a,c}

a,c

Figure 28.1.4-13 [

] ^{a,c}

a,c

Figure 28.1.4-14 [] ^{a,c}

a,c

Figure 28.1.4-15 [

] ^{a,c}

a,c

Figure 28.1.4-16 [

] ^{a,c}

a,c

Figure 28.1.4-17 [

] ^{a,c}

a,c

Figure 28.1.4-18 [

] a,c

a,c

Figure 28.1.4-19 [

]a,c

a,c

Figure 28.1.4-20 [

] ^{a,c}

a,c

Figure 28.1.4-21 [

] ^{a,c}

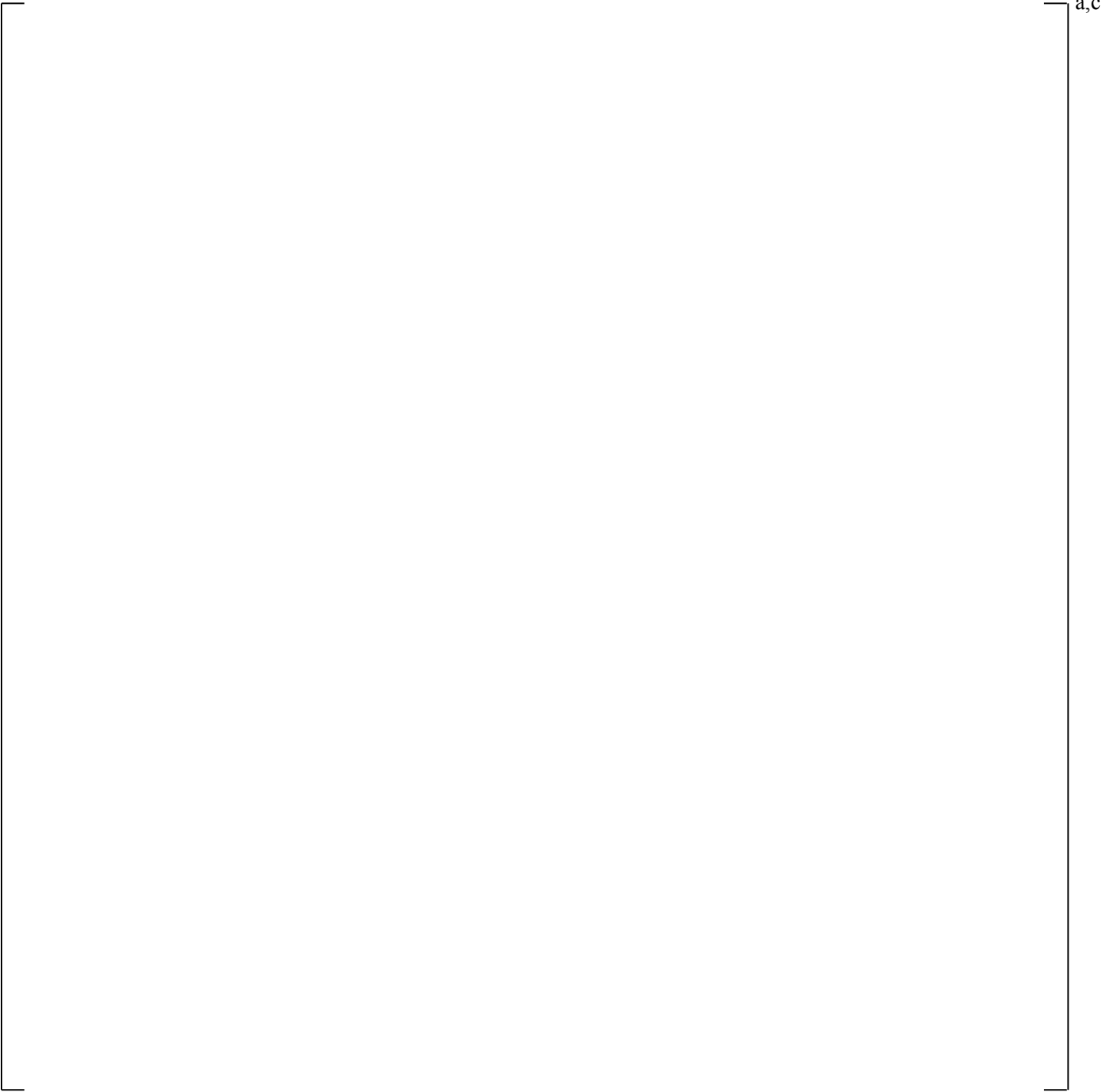


Figure 28.1.4-22 []^{a,c}

a,c

Figure 28.1.4-23 []^{a,c}

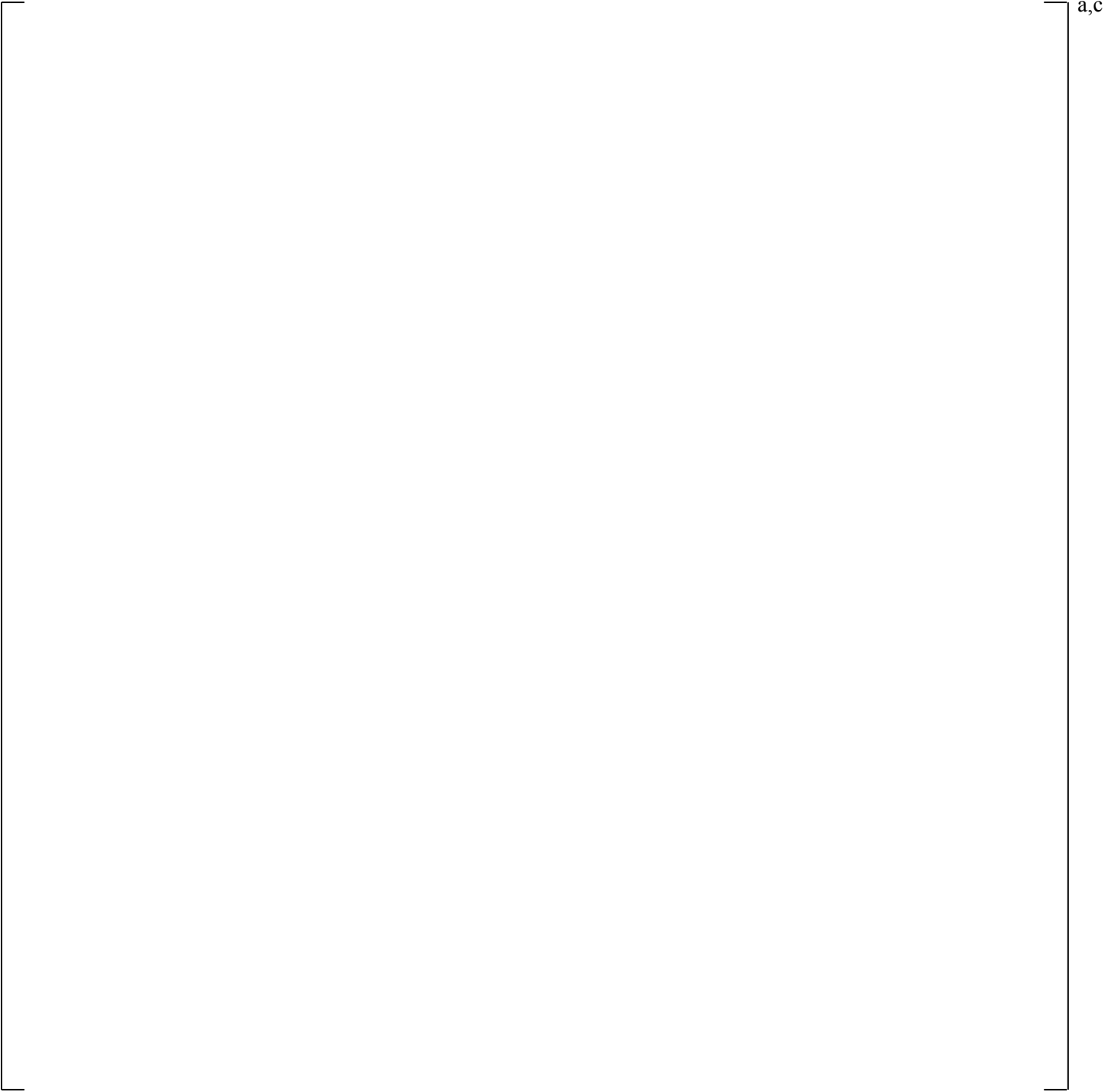


Figure 28.1.4-24 []^{a,c}

a,c

Figure 28.1.4-25 [

] a,c

a,c

Figure 28.1.4-26 []^{a,c}

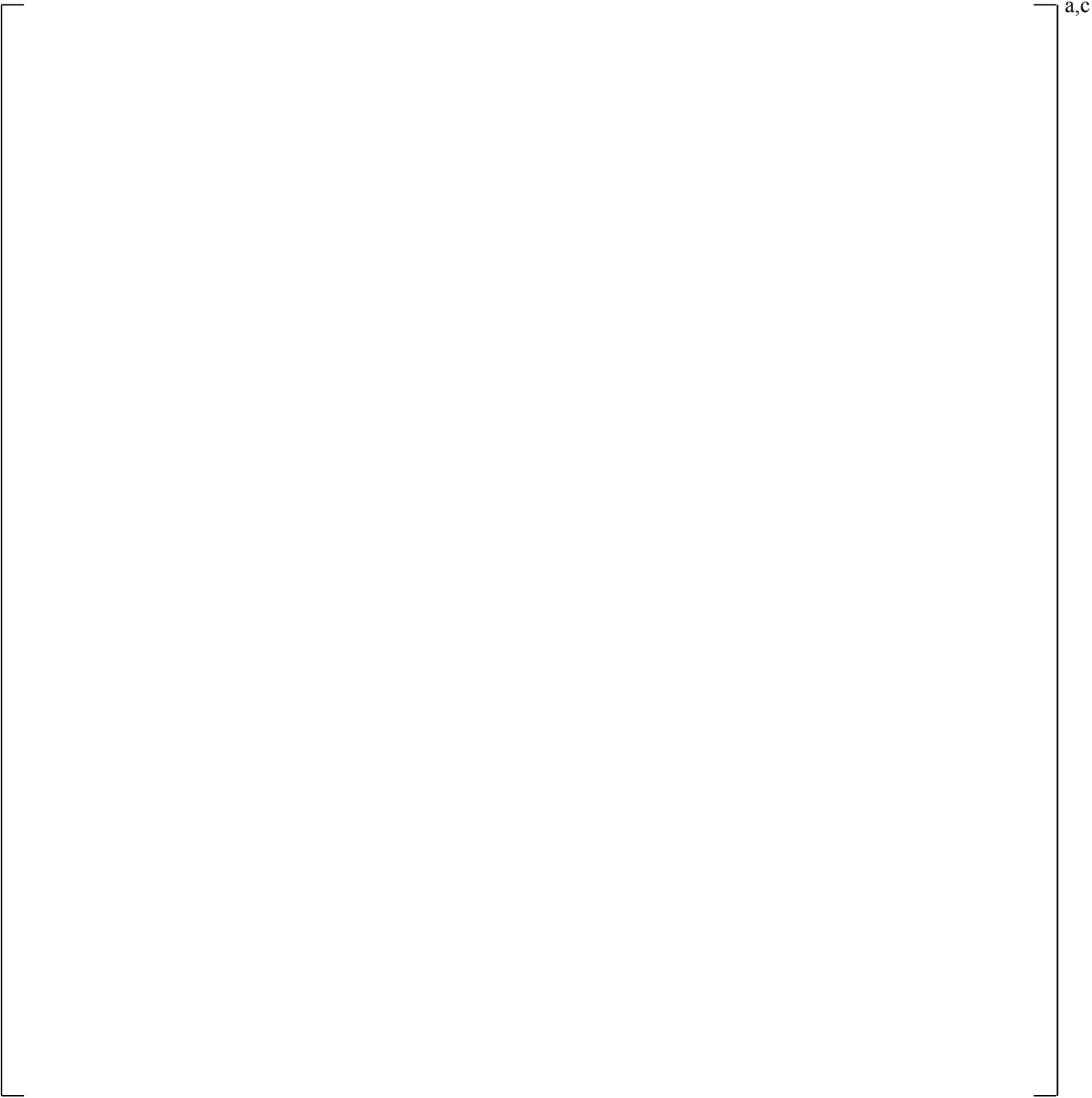


Figure 28.1.4-27 []^{a,c}

a,c

Figure 28.1.4-28 [

] a,c

a,c

Figure 28.1.4-29 [

] ^{a,c}

a,c

Figure 28.1.4-30 [

] ^{a,c}

a,c

Figure 28.1.4-31 [

] ^{a,c}

a,c

Figure 28.1.4-32 [

] a,c

a,c

Figure 28.1.4-33 [

] a,c

a,c

Figure 28.1.4-34 [

] ^{a,c}

a,c

Figure 28.1.4-35 [

] ^{a,c}

a,c

Figure 28.1.4-36 [

] ^{a,c}

28.1.5 Treatment of Accumulator Elevation – LBLOCA

In many plants, the elevation of the accumulators relative to the cold leg is loop-specific. For a large break LOCA, the initiation of accumulator injection is accompanied by a high degree of ECCS bypass, but a significant amount of accumulator liquid penetrates into the lower plenum during the refill phase.

[

] ^{a,c}

28.1.5.1 V. C. Summer (CGE)

The CGE large break LOCA reference transient from Section 27.2.1 is executed [

] ^{a,c}. The length of the accumulator line (fL/D) was preserved in all cases. For CGE, two accumulators are [

] ^{a,c}. The elevations for this study were chosen to represent large but representative values that could be expected in a plant application.

It is expected that the dominance of ECCS bypass during blowdown and early refill will cause differing behavior, as a function of effective break size, in consideration to the accumulator elevation. A nominal double-ended guillotine break is explored along with breaks using a discharge coefficient (CD) of

[

] ^{a,c} to evaluate this effect.

Figure 28.1.5-1 shows the PCT for the Low, Nominal, and High accumulator elevation cases [

] ^{a,c}

Figure 28.1.5-4 shows the PCT for the various arrangements [

] ^{a,c}

The effect of accumulator elevation for a break with a discharge coefficient of [

] ^{a,c}

28.1.5.2 Conclusions

There exists, for a given effective break area and its associated blowdown and ECCS bypass characteristics, an optimum accumulator design. Varying the elevation and consequently the timing of accumulator injection can affect the degree to which accumulator liquid fills the lower plenum. For large breaks, it has been shown [

] ^{a,c}

a,c

Figure 28.1.5-1 []^{a,c}

a,c

Figure 28.1.5-2 [] ^{a,c}

a,c

Figure 28.1.5-3 [

] ^{a,c}

a,c

Figure 28.1.5-4 [

] ^{a,c}

a,c

Figure 28.1.5-5 [

] ^{a,c}

a,c

Figure 28.1.5-6 [

] ^{a,c}

a,c

Figure 28.1.5-7 [

]^{a,c}

a,c

Figure 28.1.5-8 [

]a,c

a,c

Figure 28.1.5-9 [

] ^{a,c}

28.1.6 Steam Generator Hydraulics: Tube Plugging – LBLOCA

For a large break, the additional resistance through the steam generator tubes as a result of tube plugging has two primary effects. First, it affects the relative break path resistance during blowdown, altering the conditions in the core regarding stagnation and flow reversal. Second, it inhibits steam venting during reflood, aggravating the steam binding phenomenon and reducing the rate at which the vessel fills with liquid.

Steam generator tube plugging (SGTP) levels of 0%, 10%, and 20% are examined here for a nominal DEG break in V. C. Summer. Additional break sizes are examined for the SGTP sensitivity for Beaver Valley Unit 1, as well, with SGTP levels of 0% and 22%.

28.1.6.1 V. C. Summer (CGE)

Cooling during blowdown occurs slightly later, which results in a slightly higher blowdown PCT, when the tube plugging level [

] ^{a,c}

28.1.6.2 Beaver Valley Unit 1 (DLW)

[

] ^{a,c}

[

] ^{a,c}

28.1.6.3 Conclusions

The effects of tube plugging for a large break LOCA are to [

] ^{a,c}

a,c

Figure 28.1.6-1 [

]a,c

a,c

Figure 28.1.6-2 []^{a,c}

a,c

Figure 28.1.6-3 []^{a,c}

a,c

Figure 28.1.6-4 [

] ^{a,c}

a,c

Figure 28.1.6-5 [

] ^{a,c}

a,c

Figure 28.1.6-6 [

] ^{a,c}

a,c

Figure 28.1.6-7 [

] ^{a,c}

a,c

Figure 28.1.6-8 [

] ^{a,c}

a,c

Figure 28.1.6-9 []^{a,c}

a,c

Figure 28.1.6-10 [

] ^{a,c}

a,c

Figure 28.1.6-11 []^{a,c}

a,c

Figure 28.1.6-12 [

] ^{a,c}

a,c

Figure 28.1.6-13

[

] ^{a,c}

28.2 SMALL BREAK SCOPING STUDY RESULTS

28.2.1 Small Break Reference Transient

The purpose of the small break scoping study is to obtain the effects of various plant conditions and modeling approaches that can potentially manifest sensitivity to the transient behavior. A demonstration of reasonable variation in the transient results commensurate with the change would confirm the expected predictive capability of the FULL SPECTRUM LOCA (FSLOCA) evaluation model (EM).

28.2.1.1 V. C. Summer (CGE)

For V. C. Summer, the [

] ^{a,c}

28.2.1.2 Beaver Valley Unit 1 (DLW)

For Beaver Valley Unit 1, the [

] ^{a,c}

28.2.2 Axial Power Distributions – SBLOCA

As part of the uncertainty analysis, [

] ^{a,c}. The CGE and DLW SBLOCA

reference transients assumed top-skewed power distributions, which are expected to be more limiting for a small break as a result of higher power in the region of potential core uncover. A sensitivity case is examined for each plant where the axial power distribution is skewed more toward the bottom.

28.2.2.1 V. C. Summer (CGE)

The 2.5-inch break with power skewed more toward the bottom (Figure 28.2.2-1) results in [

] ^{a,c}

28.2.2.2 Beaver Valley Unit 1 (DLW)

For DLW, the bottom-skewed case (Figure 28.2.2-10) results in [

]^{a,c}

28.2.2.3 Conclusions

The axial power distribution affects cladding temperatures throughout the transient, [^{a,c} as described in Section 29.4.1.2.

a,c

Figure 28.2.2-1 [

] a,c

a,c

Figure 28.2.2-2 [

] ^{a,c}

a,c

Figure 28.2.2-3 [

] a,c

a,c

Figure 28.2.2-4 [

] a,c

Figure 28.2.2-5 [

] a,c

a,c

Figure 28.2.2-6 [

] ^{a,c}

a,c

Figure 28.2.2-7 [

] ^{a,c}

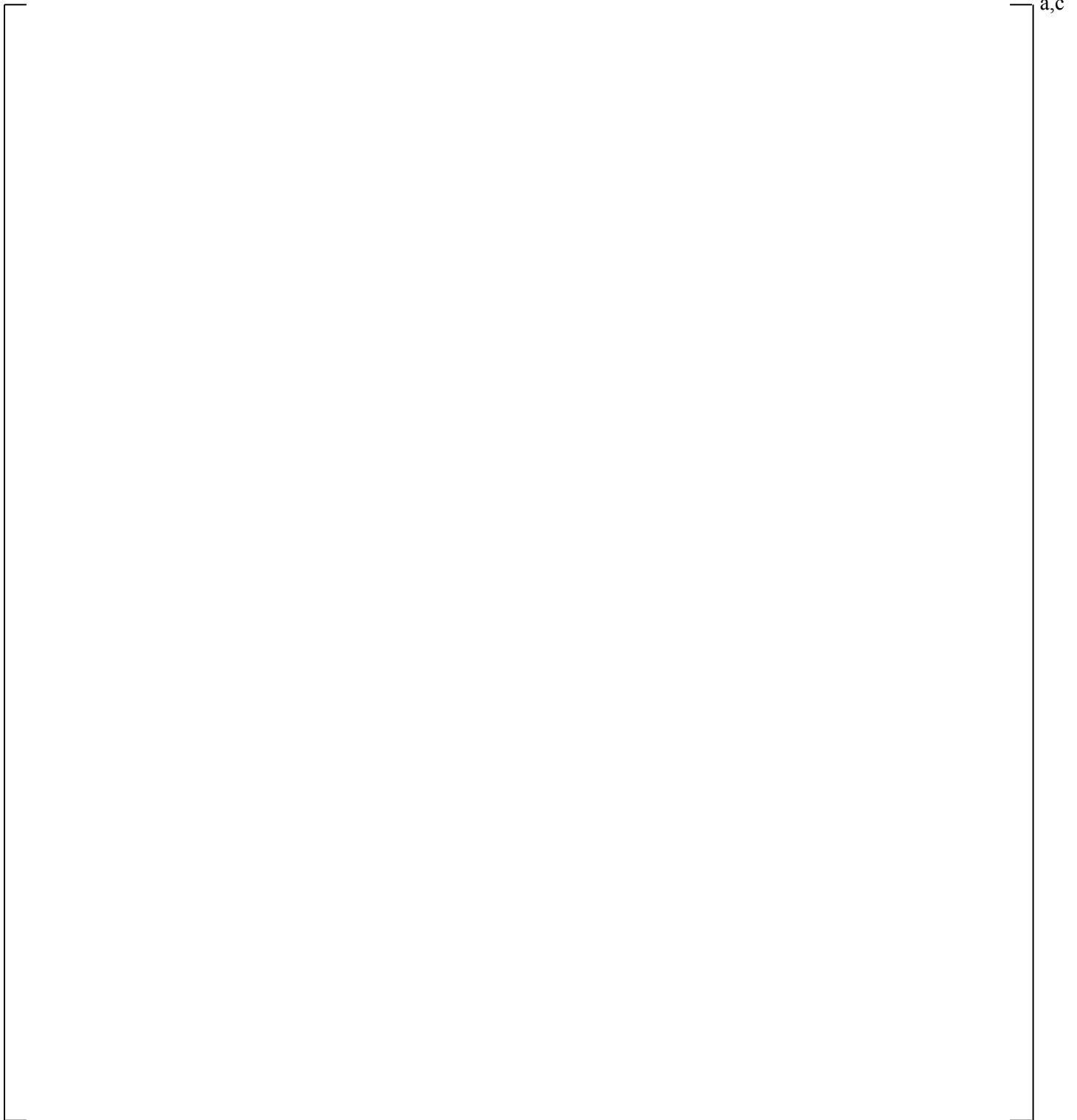


Figure 28.2.2-8 [

] ^{a,c}

a,c

Figure 28.2.2-9 [

] a,c

Figure 28.2.2-10

[

] ^{a,c}

Figure 28.2.2-11 [

] ^{a,c}

a,c

Figure 28.2.2-12 [

] ^{a,c}

a,c

Figure 28.2.2-13 [

] a,c

a,c

Figure 28.2.2-14 [

] ^{a,c}

a,c

Figure 28.2.2-15 [

] ^{a,c}

a,c

Figure 28.2.2-16 [

] ^{a,c}

a,c

Figure 28.2.2-17 [

] a,c

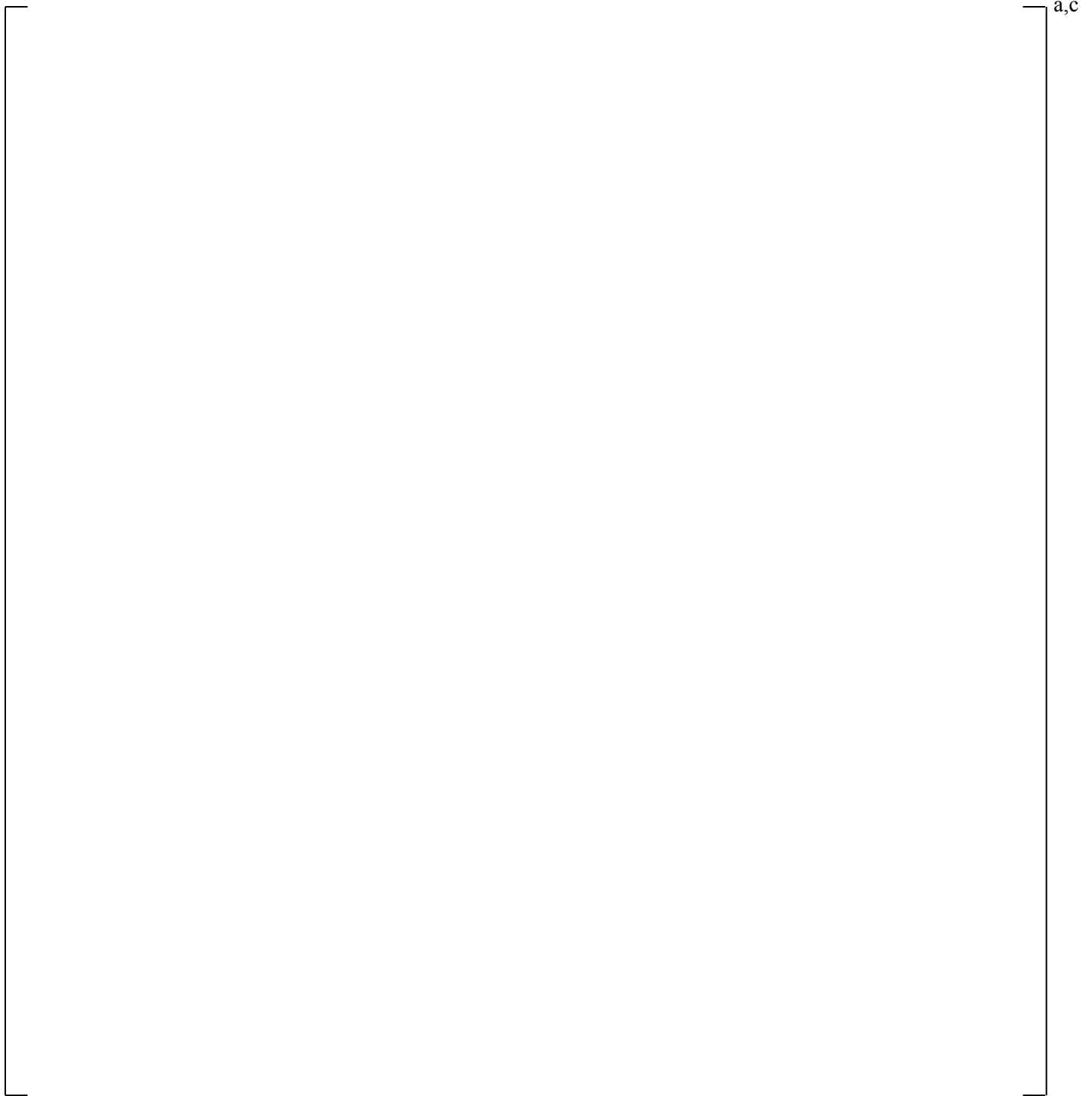


Figure 28.2.2-18 [

] ^{a,c}

28.2.3 Initial and Accident Boundary Conditions and Offsite Power – SBLOCA

In a small break LOCA, the loss-of-offsite power has two main effects. The delay in safety injection is increased due to the diesel generator startup, and the pumps are [

] ^{a,c}. With a loss-of-offsite power, the delayed SI results in a longer period of time when the vessel inventory is lost without being replaced by high head safety injection (HHSI) flow, although the HHSI flow is relatively small in magnitude early in the transient compared to the break flow due to the high RCS pressure. When offsite power is available, continued pump operation can work to pump more flow toward the break, depleting vessel inventory at a greater rate than otherwise would occur for a given break size. For small breaks, however, the continued pump operation can also maintain the positive flow in the broken cold leg, impeding flow reversal and reducing the total flow out the break.

28.2.3.1 Offsite Power Availability: V. C. Summer (CGE)

[

] ^{a,c}

28.2.3.2 Offsite Power Availability: Beaver Valley Unit 1 (DLW)

In addition to the 3-inch diameter SBLOCA reference transient, a 3.2-inch diameter case is also explored here.

[

] ^{a,c}

For a slightly larger break (3.2 inch diameter) [

] ^{a,c}

28.2.3.3 Offsite Power Availability: Conclusions

The availability of offsite power is observed to [

] ^{a,c}

28.2.3.4 Operator Action

The reactor coolant pumps trip very early in the transient for the LOOP case, while the [

] ^{a,c}

a,c

Figure 28.2.3-1 []^{a,c}

a,c

Figure 28.2.3-2 []^{a,c}

a,c

Figure 28.2.3-3 [

] ^{a,c}

a,c

Figure 28.2.3-4 [

] ^{a,c}

a,c

Figure 28.2.3-5 [

] a,c

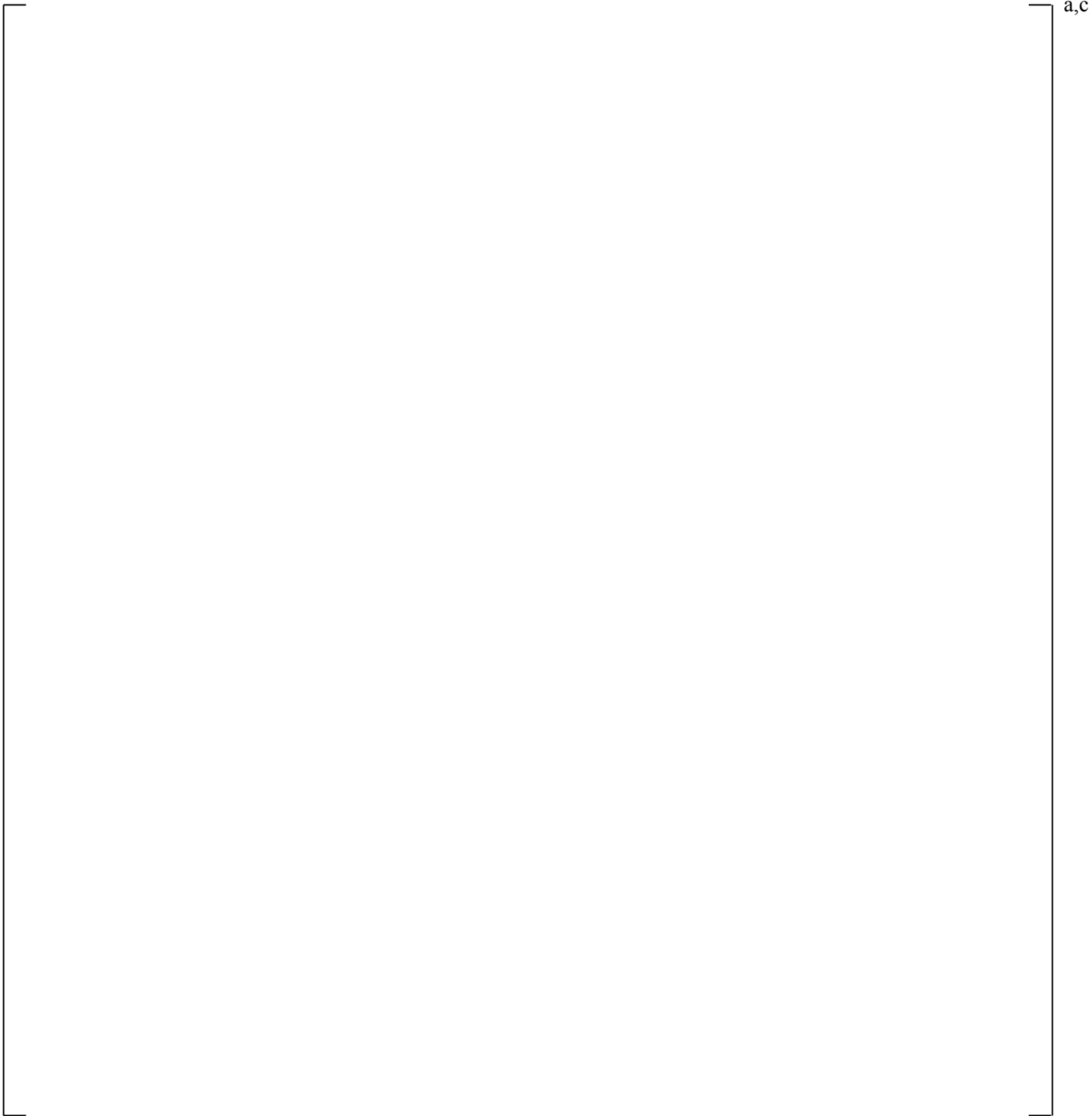


Figure 28.2.3-6 [

] ^{a,c}

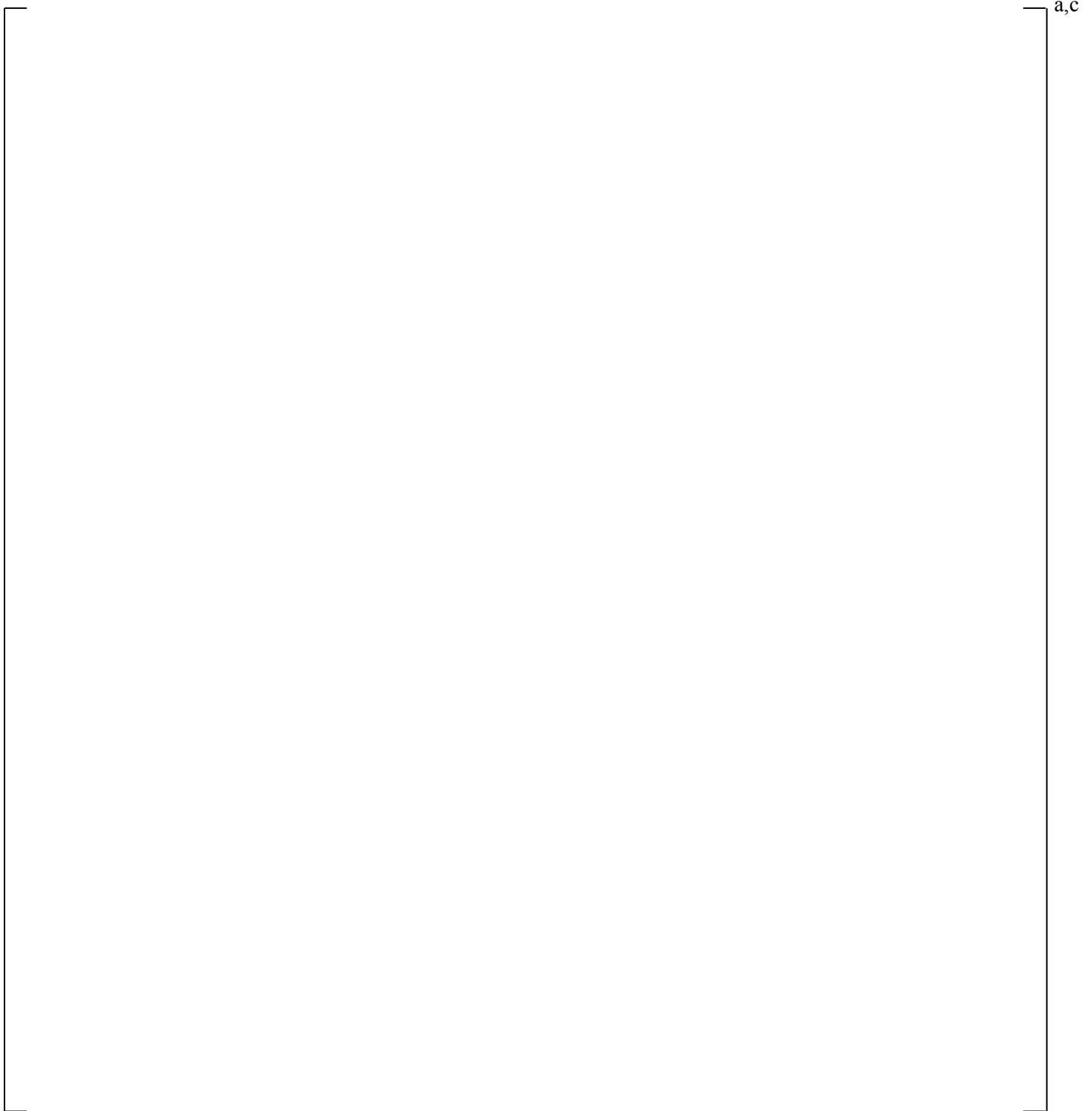


Figure 28.2.3-7 [

] ^{a,c}

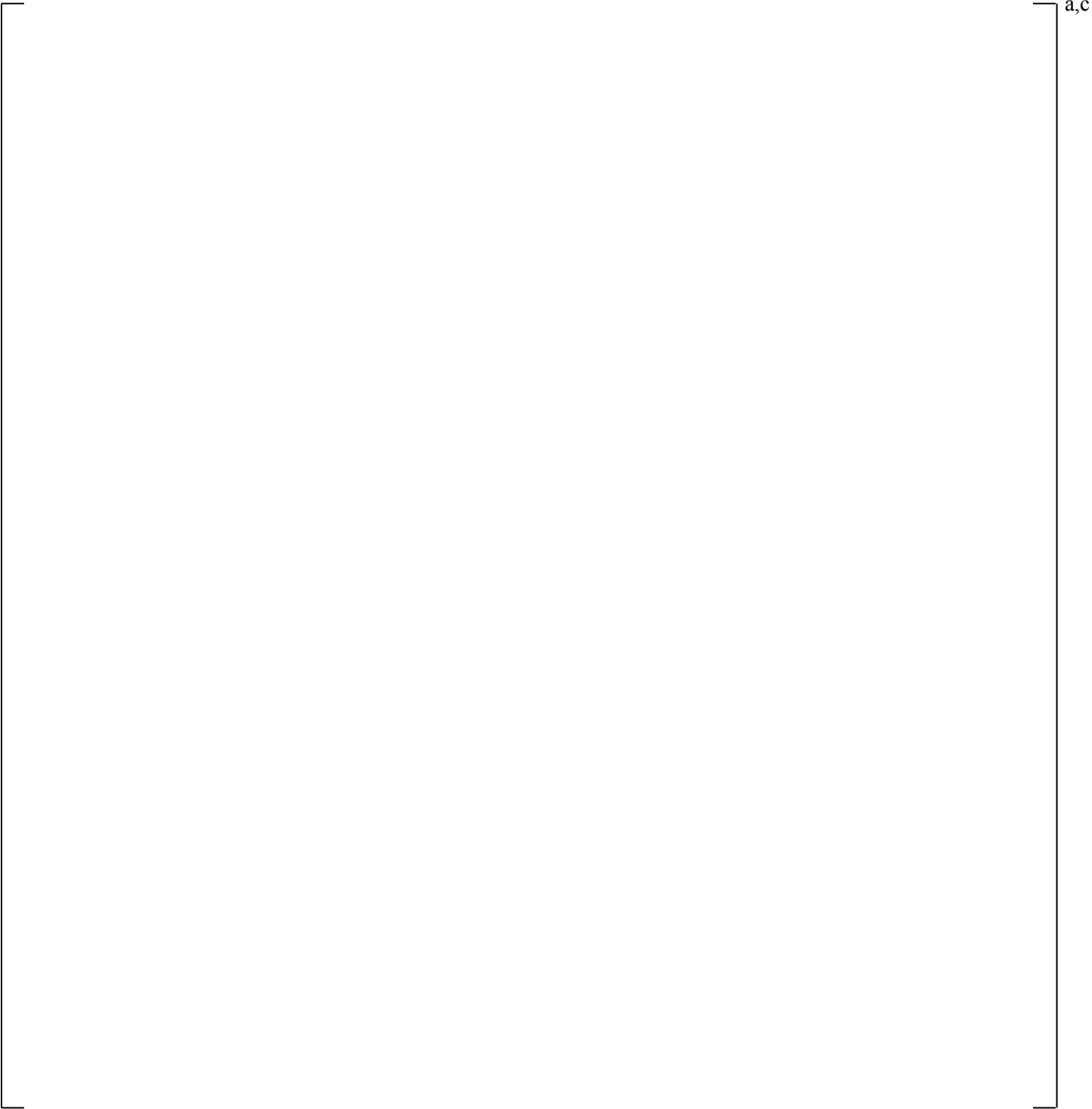


Figure 28.2.3-8 []^{a,c}

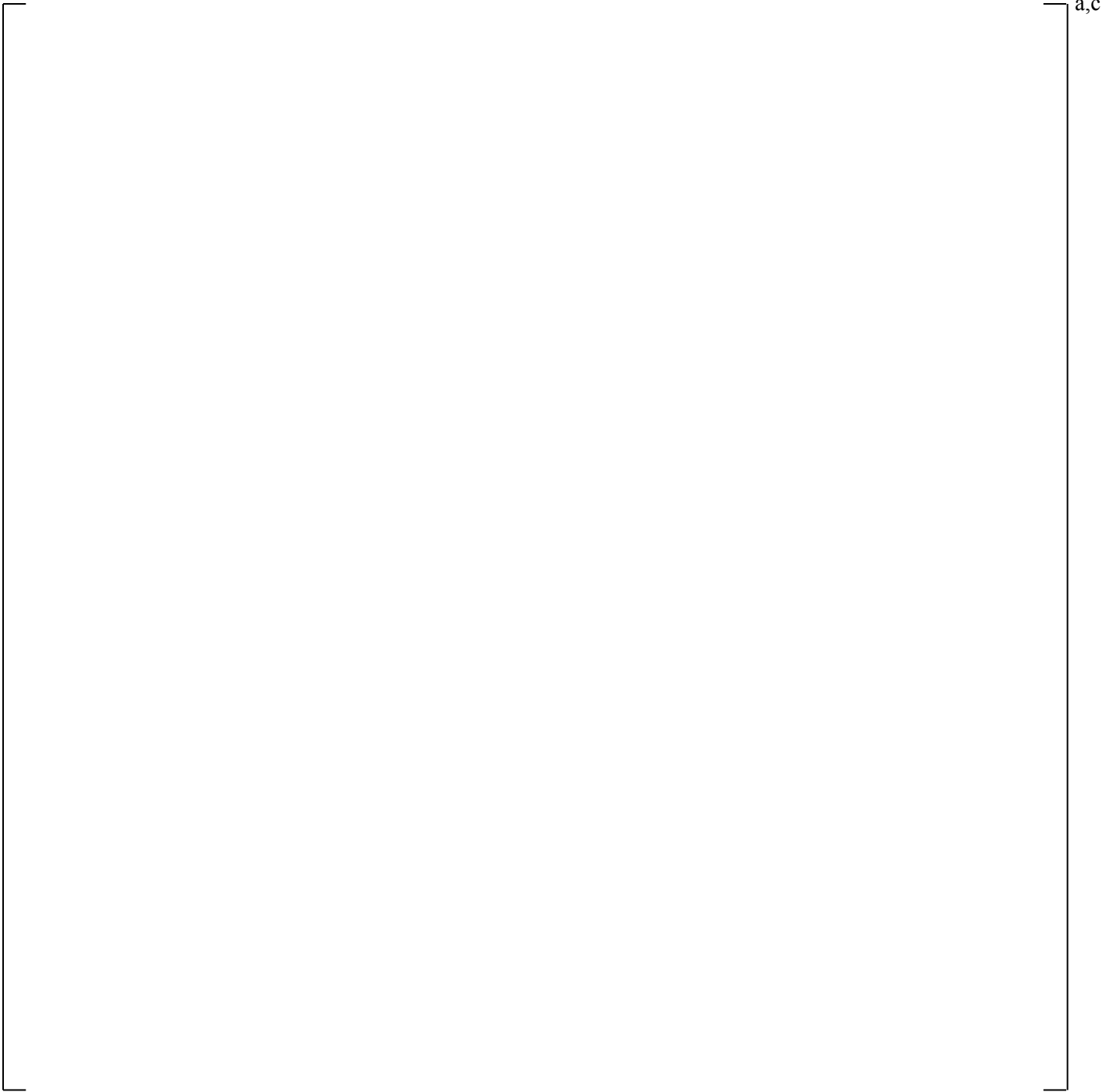


Figure 28.2.3-9 []^{a,c}

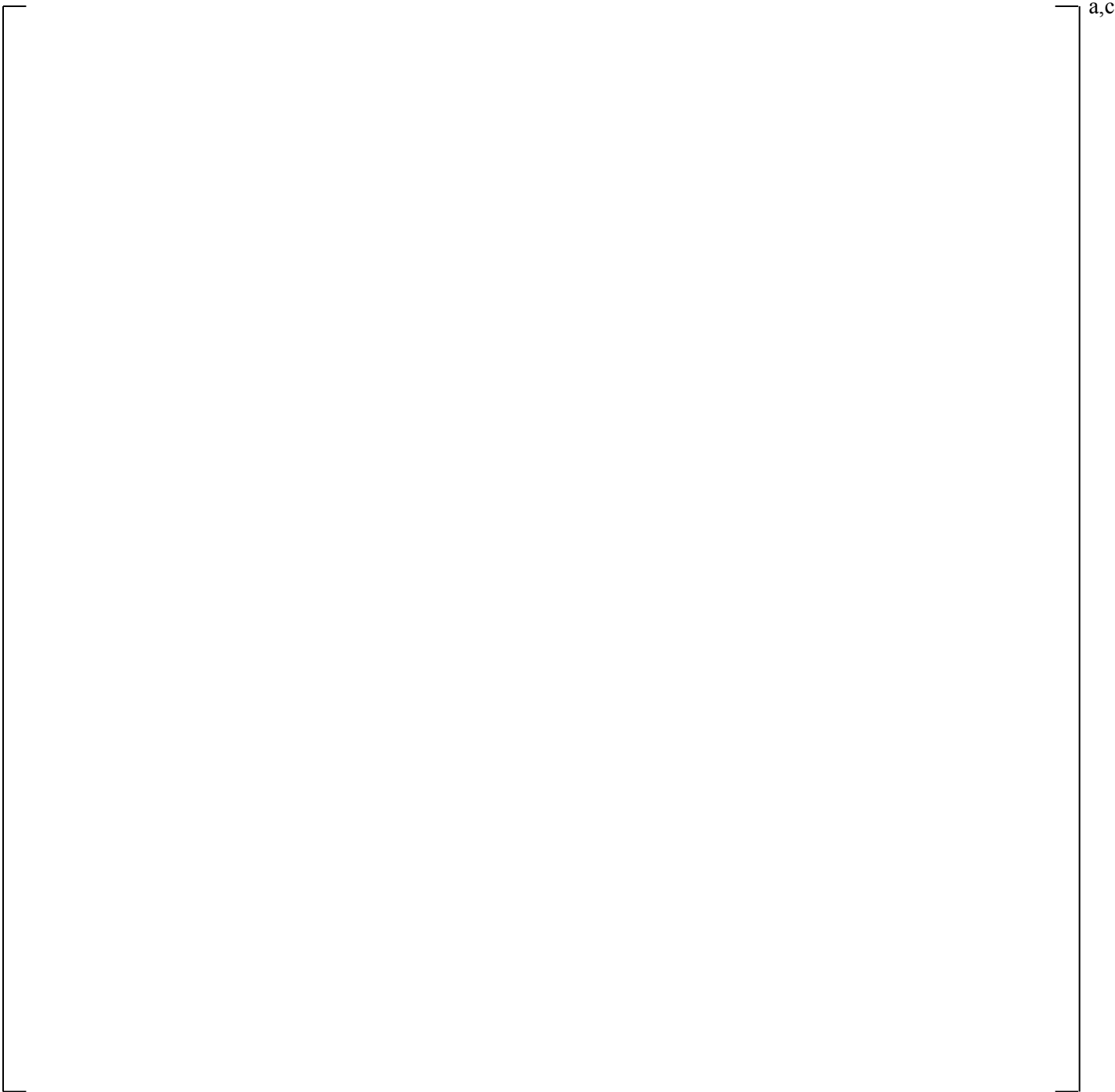


Figure 28.2.3-10 []^{a,c}

a,c

Figure 28.2.3-11 [

] ^{a,c}

a,c

Figure 28.2.3-12 [

] ^{a,c}

a,c

Figure 28.2.3-13

[

] ^{a,c}



Figure 28.2.3-14 [

] ^{a,c}

a,c

Figure 28.2.3-15 []^{a,c}

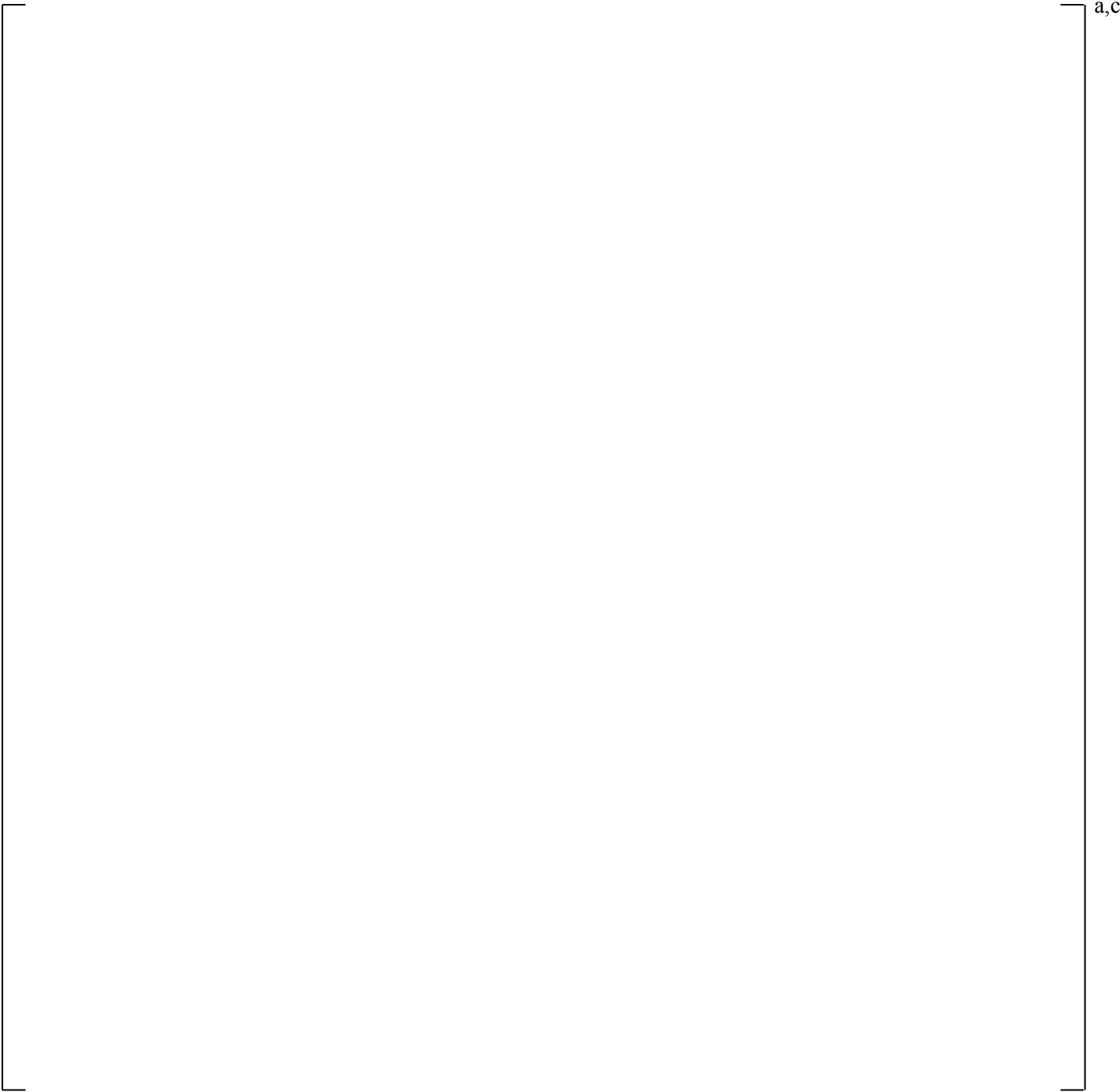


Figure 28.2.3-16 []^{a,c}

a,c

Figure 28.2.3-17

a,c



Figure 28.2.3-18 [

] ^{a,c}

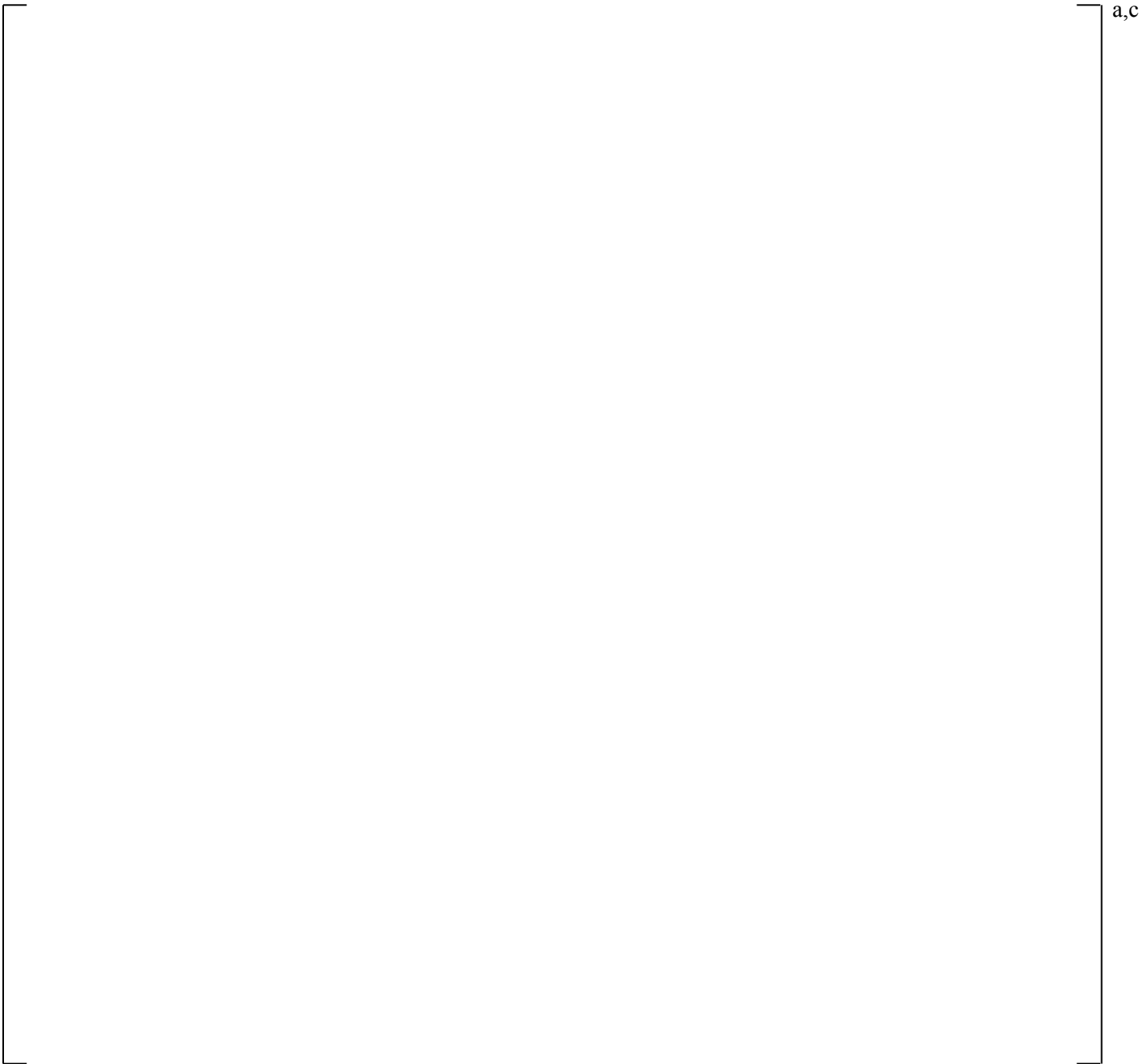


Figure 28.2.3-19 []^{a,c}

a,c

Figure 28.2.3-20 []^{a,c}

28.2.4 Time Step and Convergence Criteria Studies – SBLOCA

The reference transients for CGE and DLW are executed here using a modified upper limit on the time step (DTMAX). The reference DTMAX strategy uses []^{a,c}

28.2.4.1 V. C. Summer (CGE)

Figure 28.2.4-1 shows []

[]^{a,c}

28.2.4.2 Beaver Valley Unit 1 (DLW)

Similar to CGE, []

[]^{a,c}

28.2.4.3 Conclusions

Changes in DTMAX upper limits []

DTMAX for the plant is discussed further in Section 29.3.3.

[]^{a,c} The choice of

a,c

Figure 28.2.4-1 [

] ^{a,c}

a,c

Figure 28.2.4-2 []^{a,c}

a,c

Figure 28.2.4-3 [

] ^{a,c}

a,c

Figure 28.2.4-4 [

] ^{a,c}

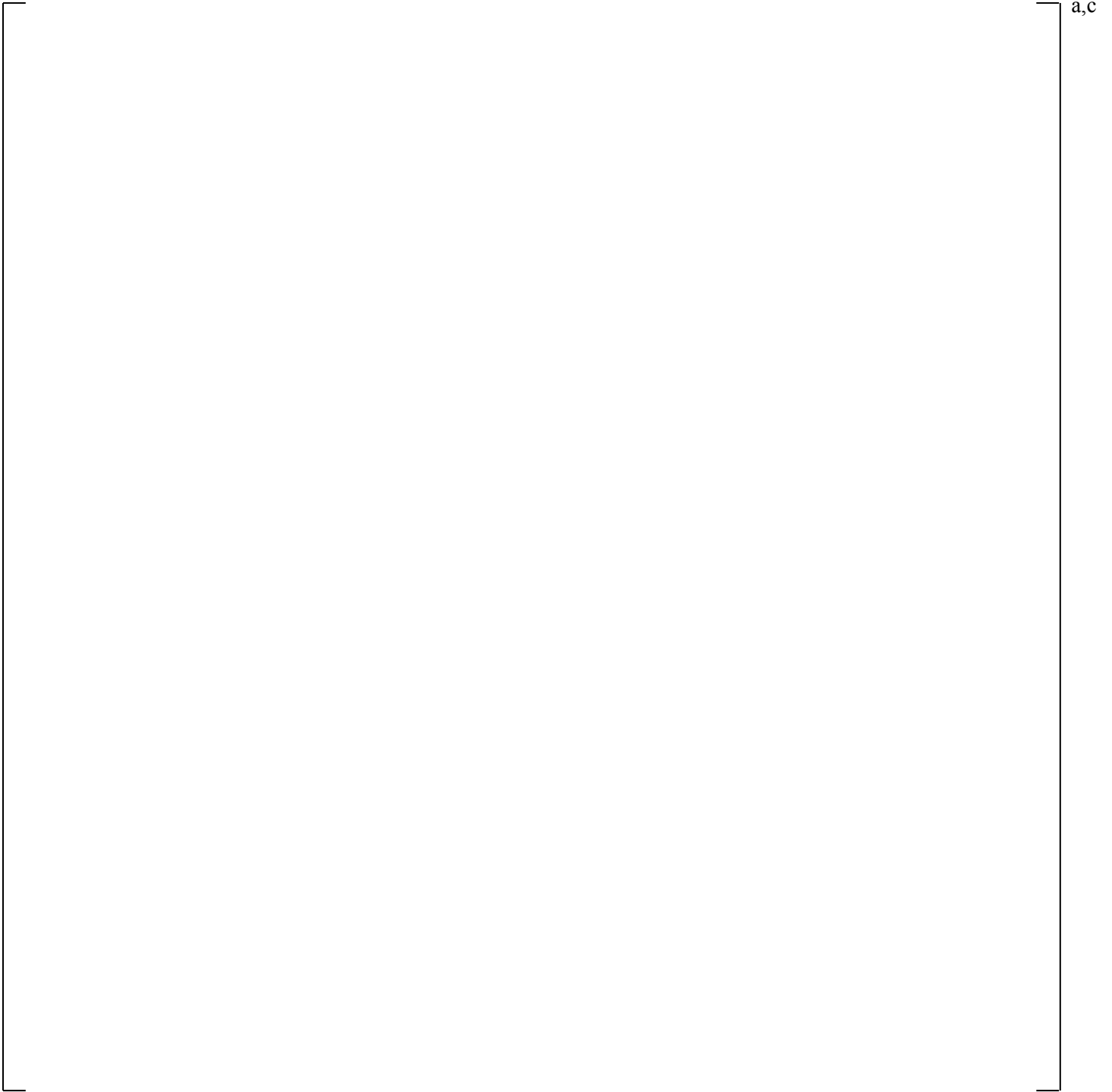


Figure 28.2.4-5 [

] ^{a,c}

a,c

Figure 28.2.4-6 [

] ^{a,c}

28.2.5 Treatment of Accumulator Elevation – SBLOCA

In many plants, the elevation of the accumulators relative to the cold leg is loop-specific. For a small break LOCA, the initiation of accumulator injection is an important event that refills the vessel, bringing about core recovery and effectively ending the transient. [

] ^{a,c}

28.2.5.1 V. C. Summer (CGE)

The CGE small break LOCA reference transient from Section 28.2.1 is executed [

] ^{a,c}

28.2.5.2 Conclusions

Based on these results, it is expected that [

] ^{a,c}

a,c

Figure 28.2.5-1 [

] ^{a,c}

a,c

Figure 28.2.5-2 []^{a,c}

a,c

Figure 28.2.5-3

a,c

28.2.6 Break Location in the Accumulator and SI Lines – SBLOCA

For all breaks in the cold leg, [

] ^{a,c}

28.2.6.1 Beaver Valley Unit 1 (DLW)

[

] ^{a,c}

28.2.6.2 Conclusions

[

] ^{a,c}

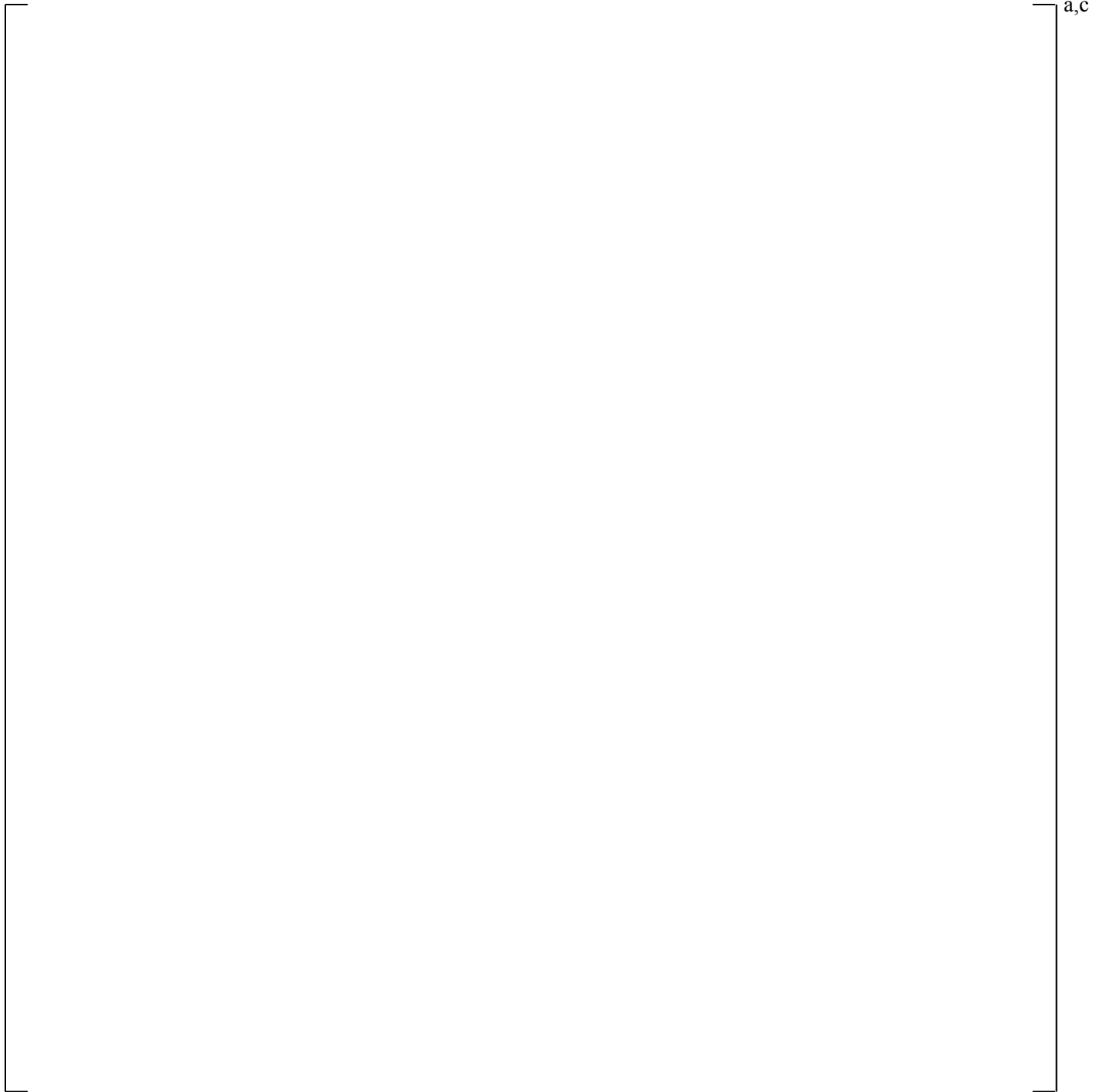


Figure 28.2.6-1 [

] ^{a,c}

a,c

Figure 28.2.6-2 [

] ^{a,c}

a,c

Figure 28.2.6-3 [

] ^{a,c}



a,c

Figure 28.2.6-4 [

] ^{a,c}

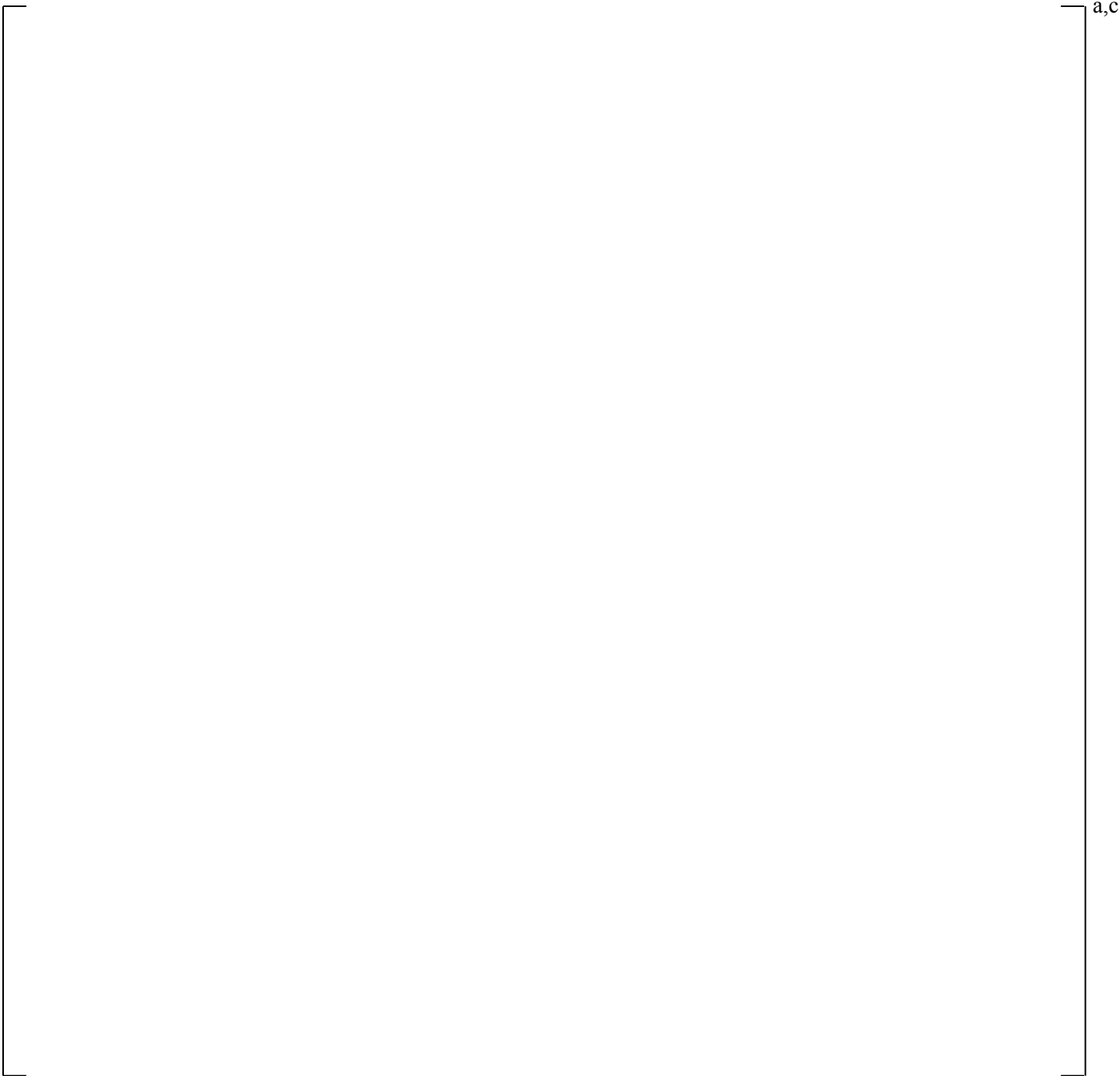


Figure 28.2.6-5 [

] ^{a,c}

a,c

Figure 28.2.6-6 [

] ^{a,c}

a,c

Figure 28.2.6-7 [

] ^{a,c}

a,c

Figure 28.2.6-8 [

] ^{a,c}

a,c

Figure 28.2.6-9 [

] ^{a,c}

28.2.7 Break Orientation Studies – SBLOCA

Similar to tests in the ROSA facility (see Section 21.7), a series of simulations is performed here to evaluate the plant response to a break oriented at the bottom, side, and top of the broken cold leg. The offtake model that accounts for such geometry upstream of the break is described in Section 5.13.

28.2.7.1 V. C. Summer (CGE)

The influence of break orientation on RCS pressure (Figure 28.2.7-1) and core collapsed liquid levels (Figure 28.2.7-2) [

] ^{a,c}

28.2.7.2 Beaver Valley Unit 1 (DLW)

Figure 28.2.7-7 and Figure 28.2.7-8 show that, for DLW, the influence of break orientation on RCS pressure and core collapsed liquid levels [

] ^{a,c}

28.2.7.3 Conclusions

[

] ^{a,c}

Figure 28.2.7-1 [

]^{a,c}

a,c

Figure 28.2.7-2 [

] ^{a,c}

a,c

Figure 28.2.7-3

[

] ^{a,c}

a,c

Figure 28.2.7-4 []^{a,c}

a,c

Figure 28.2.7-5 [

] ^{a,c}

a,c

Figure 28.2.7-6 []^{a,c}

a,c

Figure 28.2.7-7 []^{a,c}

a,c

Figure 28.2.7-8 [

] ^{a,c}

a,c

Figure 28.2.7-9 []^{a,c}

a,c

Figure 28.2.7-10 [

] ^{a,c}

a,c

Figure 28.2.7-11 [

] ^{a,c}

a,c

Figure 28.2.7-12 [

] ^{a,c}

a,c

Figure 28.2.7-13 [

] ^{a,c}

a,c

Figure 28.2.7-14 [

] a,c

a,c

Figure 28.2.7-15 [

] ^{a,c}

28.2.8 Interfacial Drag in the Core (Level Swell) – SBLOCA

The effect of [

] ^{a,c}

28.2.8.1 V. C. Summer (CGE)

[

] ^{a,c}

28.2.8.2 Beaver Valley Unit 1 (DLW)

[

] ^{a,c}

28.2.8.3 Conclusions

Interfacial drag in the core affects core liquid levels, steam venting, and PCT. [

] ^{a,c}



Figure 28.2.8-1 [

] ^{a,c}

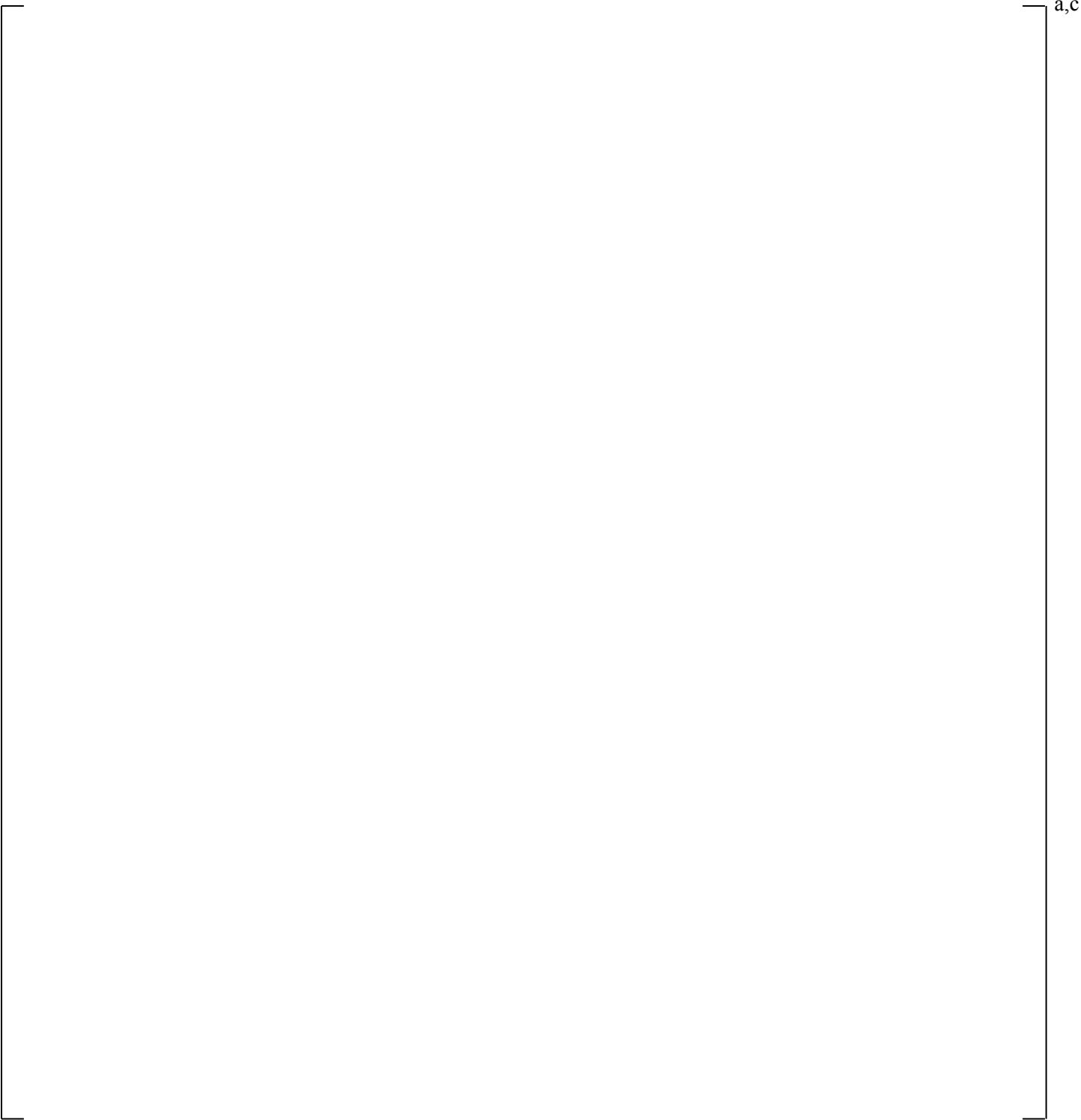
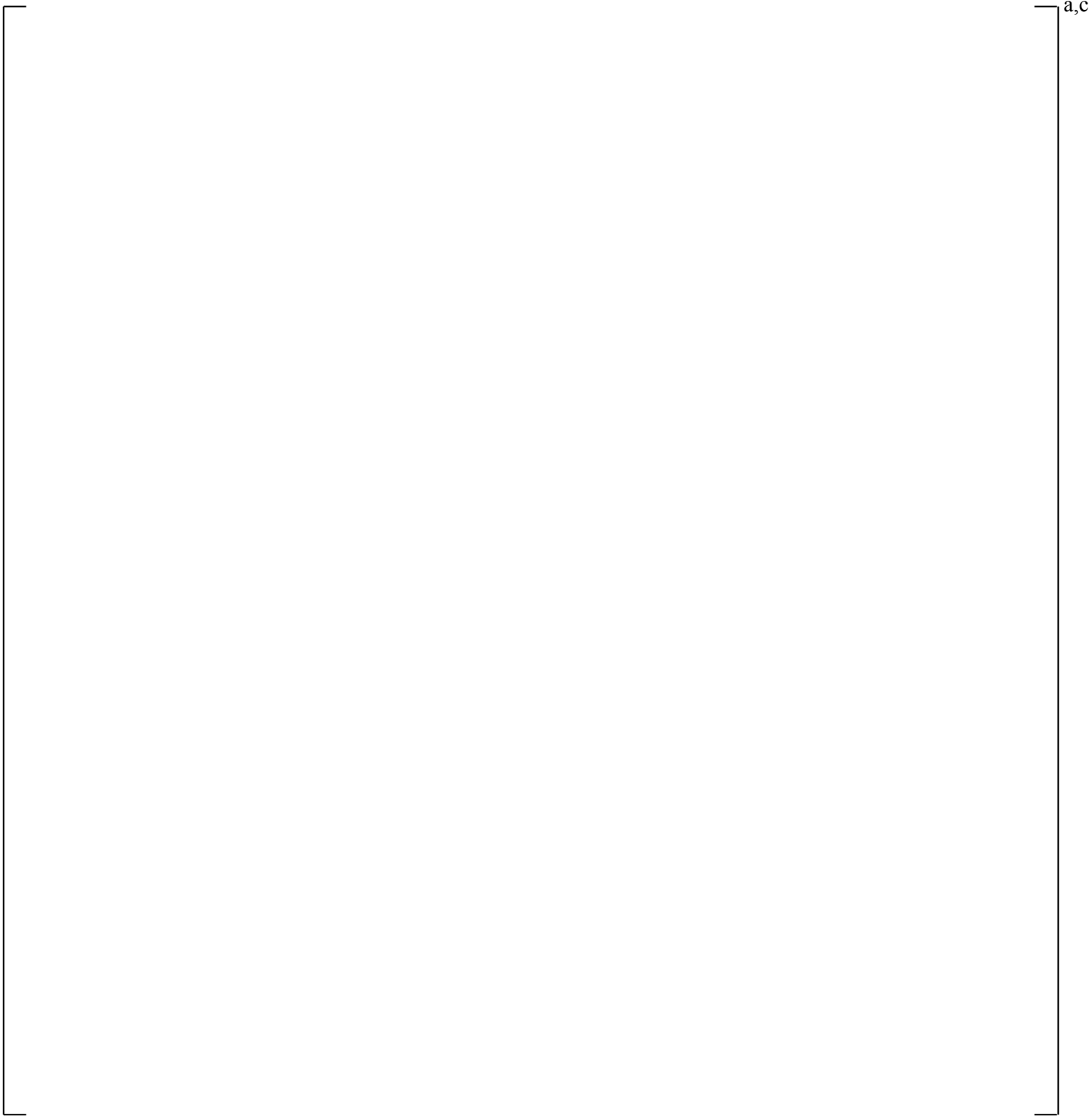


Figure 28.2.8-2 [

] ^{a,c}



a,c

Figure 28.2.8-3 [

] ^{a,c}



Figure 28.2.8-4 [

] ^{a,c}

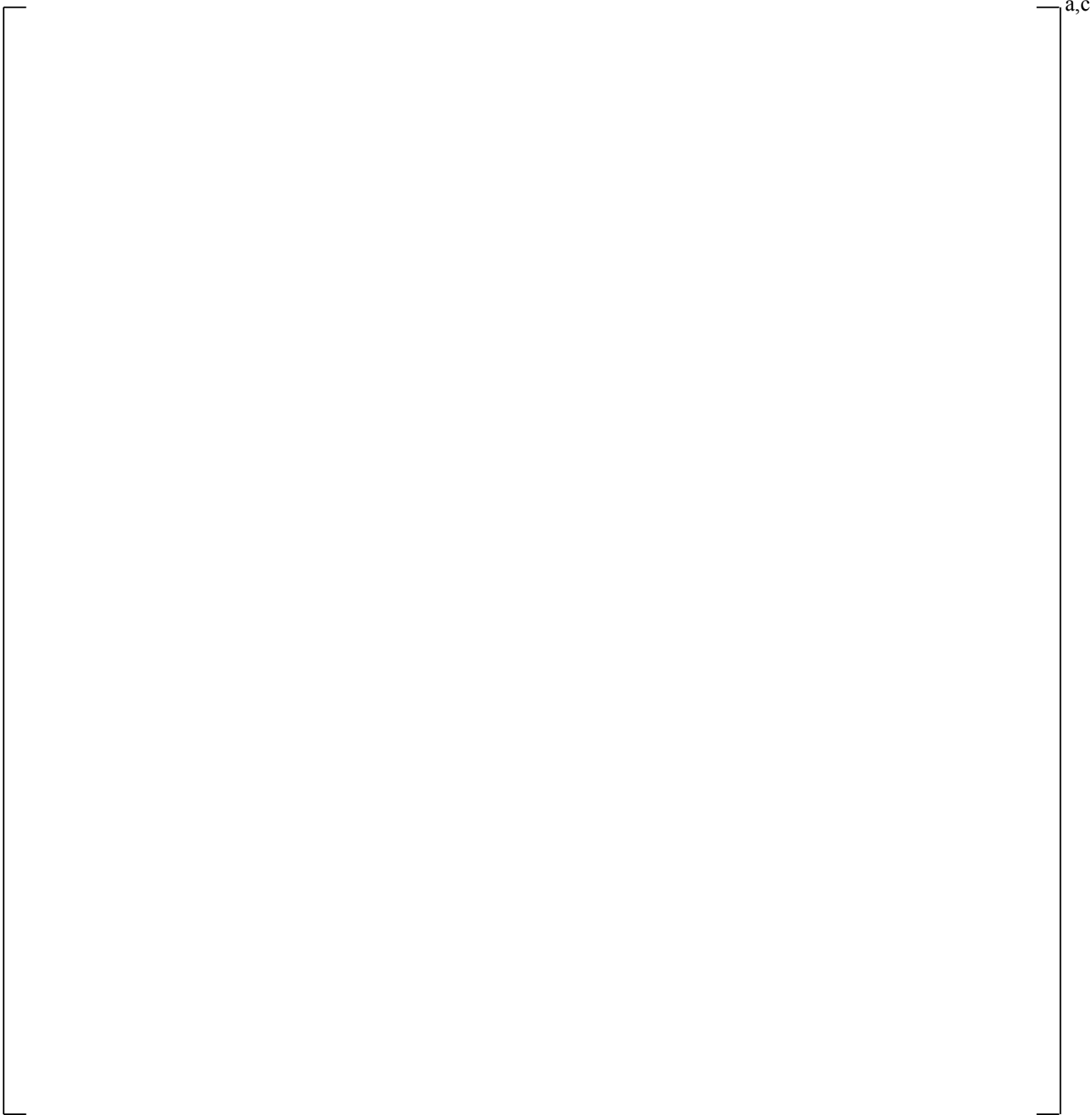


Figure 28.2.8-5 [

] ^{a,c}

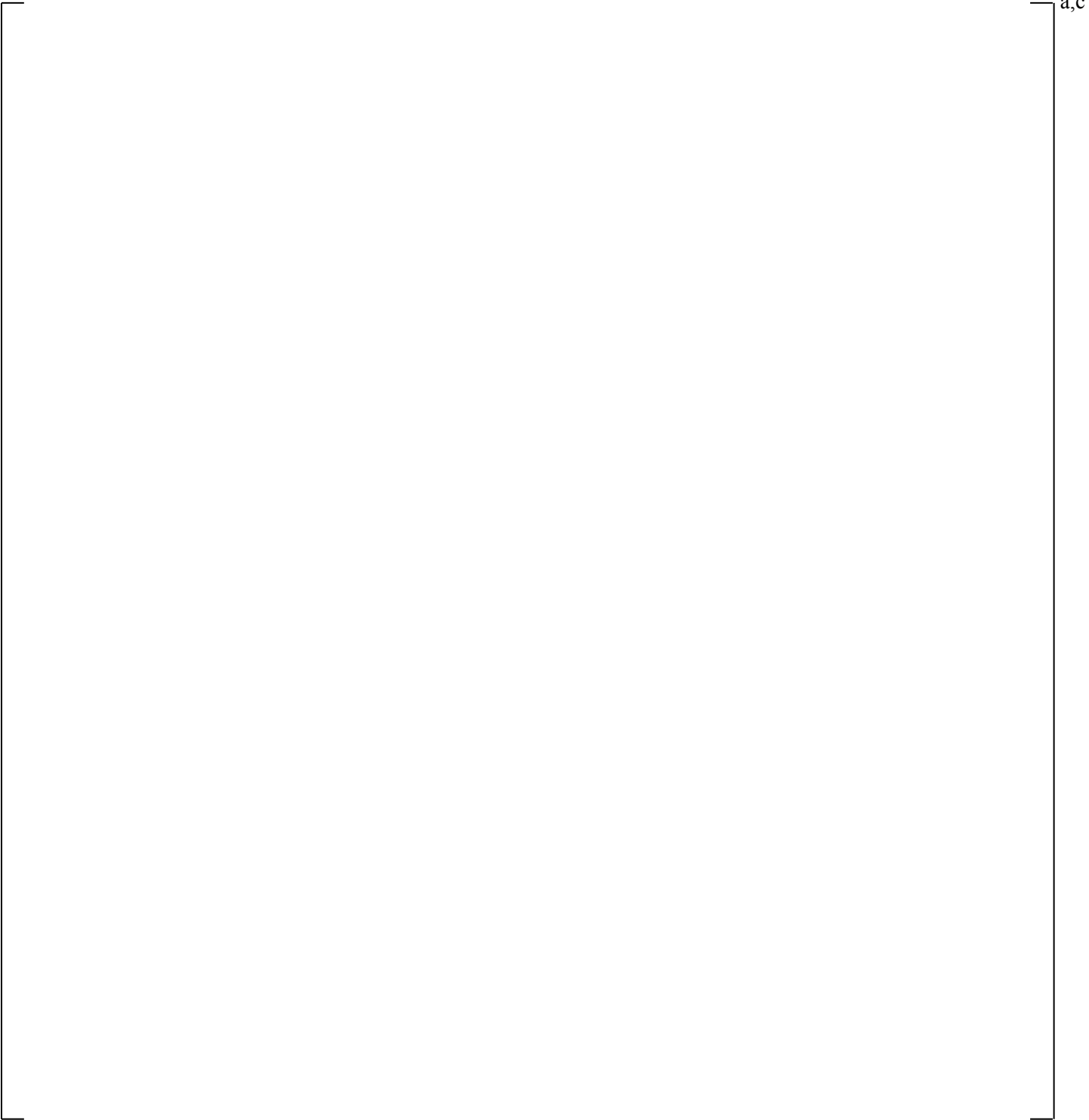
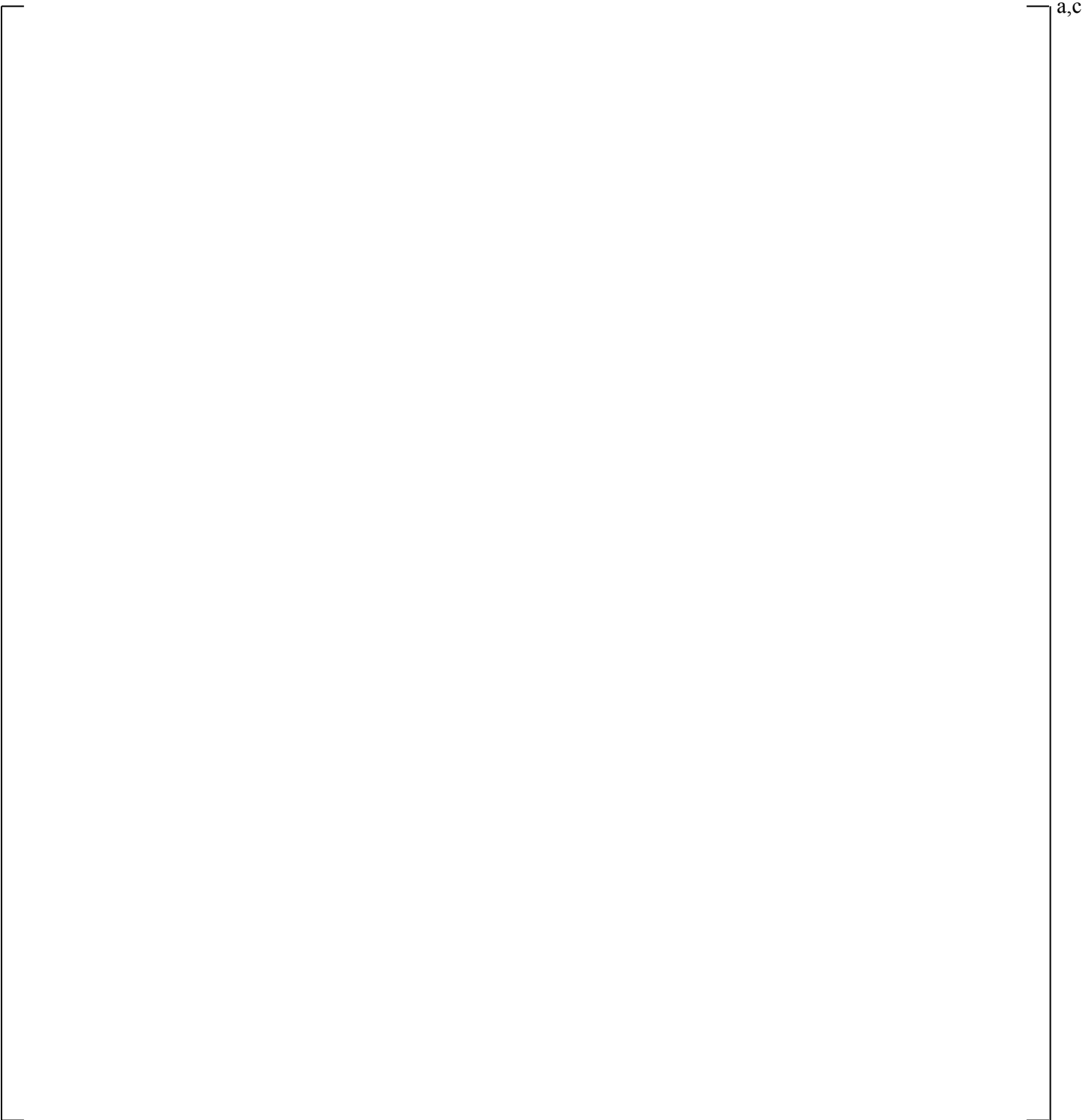


Figure 28.2.8-6 [

] ^{a,c}



a,c

Figure 28.2.8-7 [

] ^{a,c}

a,c

Figure 28.2.8-8 [

] ^{a,c}

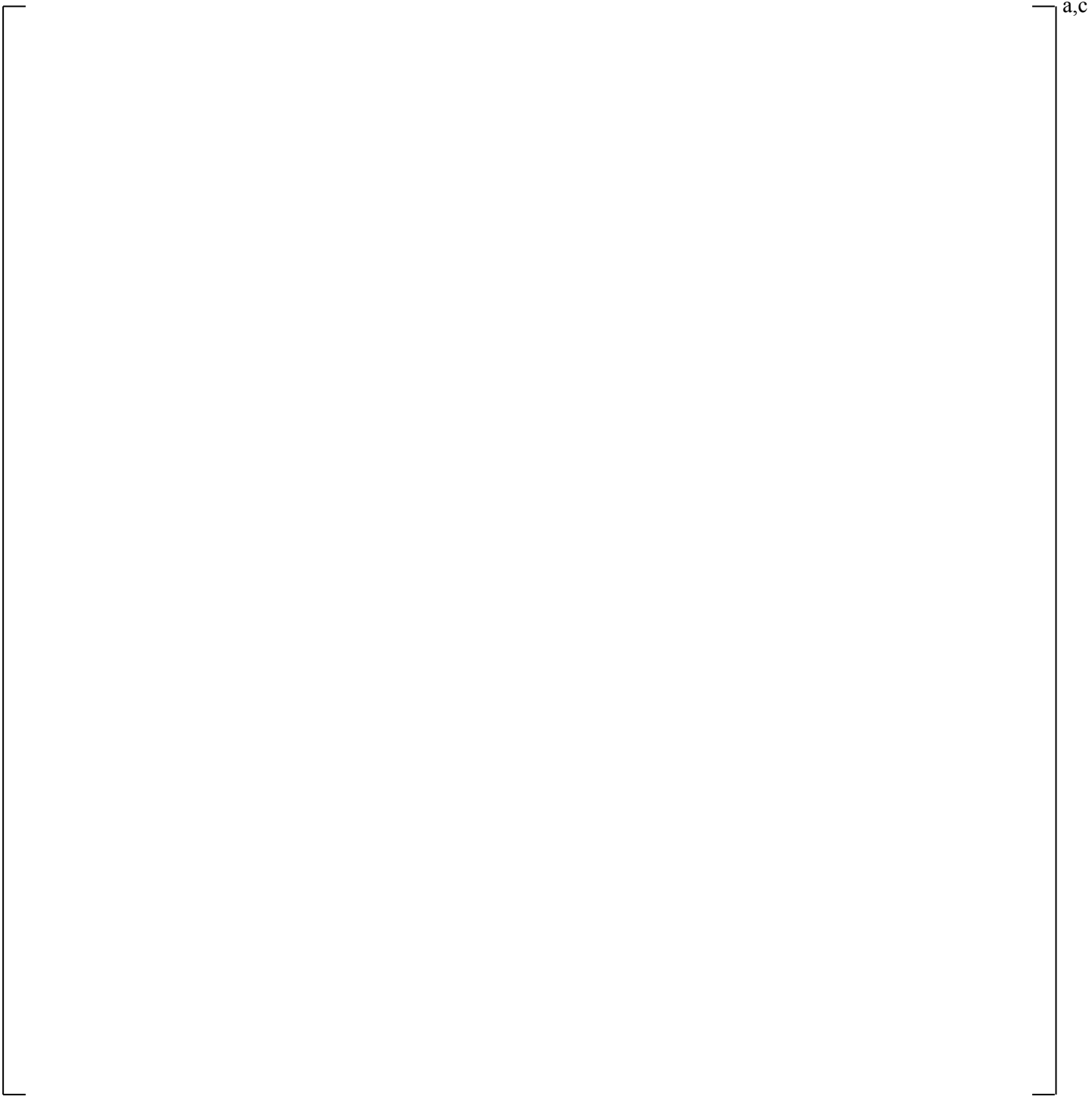


Figure 28.2.8-9 []^{a,c}

a,c

Figure 28.2.8-10 [

] ^{a,c}

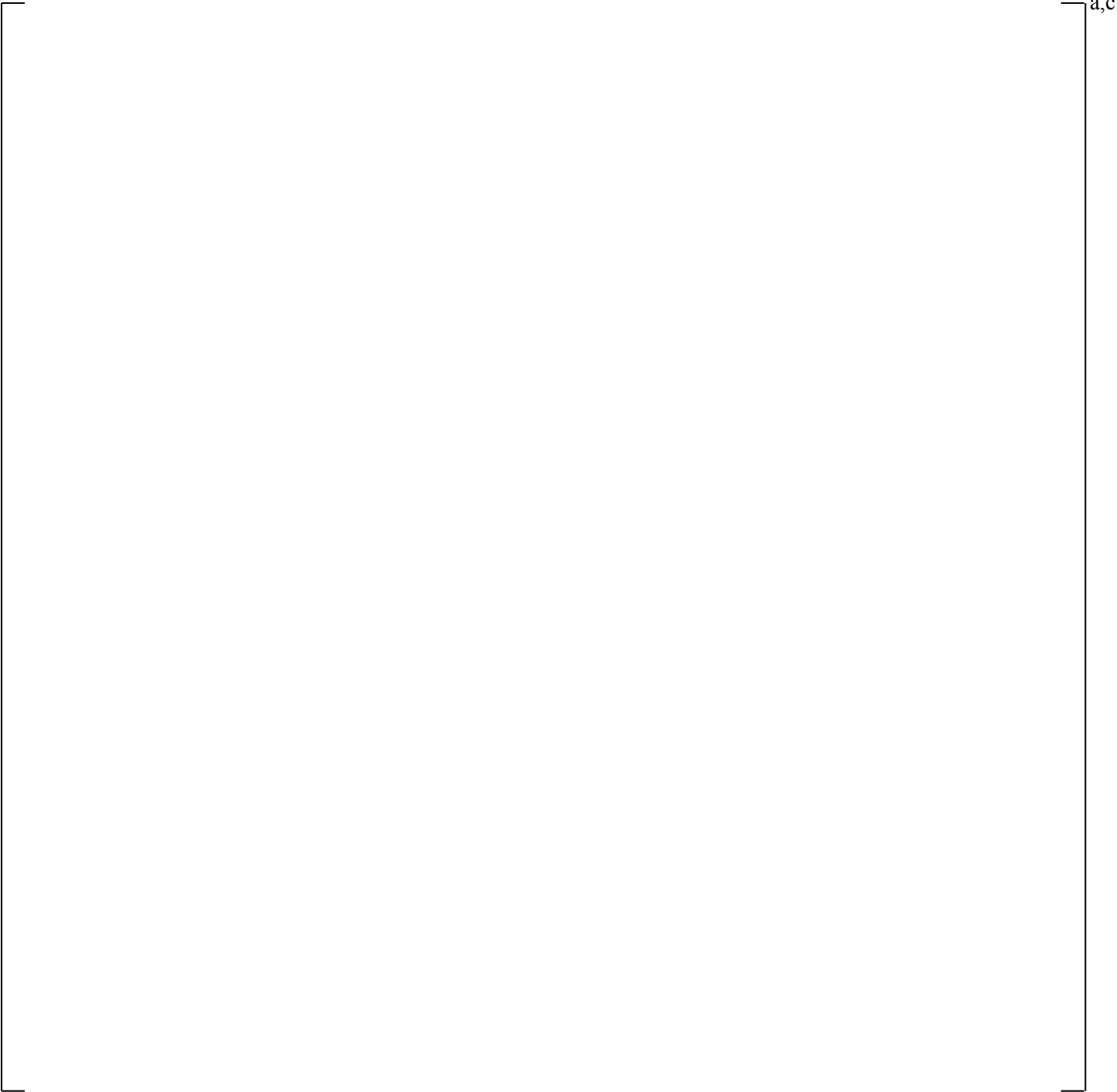


Figure 28.2.8-11 []^{a,c}

a,c

Figure 28.2.8-12 [

] a,c

a,c

Figure 28.2.8-13 [

] a,c

a,c

Figure 28.2.8-14 [

]a,c

a,c

Figure 28.2.8-15

a,c

a,c

Figure 28.2.8-16

a,c

28.2.9 Steam Generator Hydraulics: Tube Plugging – SBLOCA

For a small break, tube plugging affects the steam venting and condensation as a result of reduced flow and heat transfer area. A sensitivity study is performed here to assess the main effects assuming tube plugging levels of 0%, 10%, and 20%.

28.2.9.1 V. C. Summer (CGE)

Table 28.2.9-1 summarizes the PCT results for various break sizes indicating that, although the effect of tube plugging for SBLOCA is small, the typical trend is slightly higher PCT with higher tube plugging.

The result of increasing the tube plugging level is a lower heat transfer area in the steam generators and a potentially lower condensation rate. The vapor generation from the core is the same for all cases, and [

] ^{a,c}

28.2.9.2 Conclusions

Although not a dominant contributor to PCT, [

] ^{a,c}

a,c

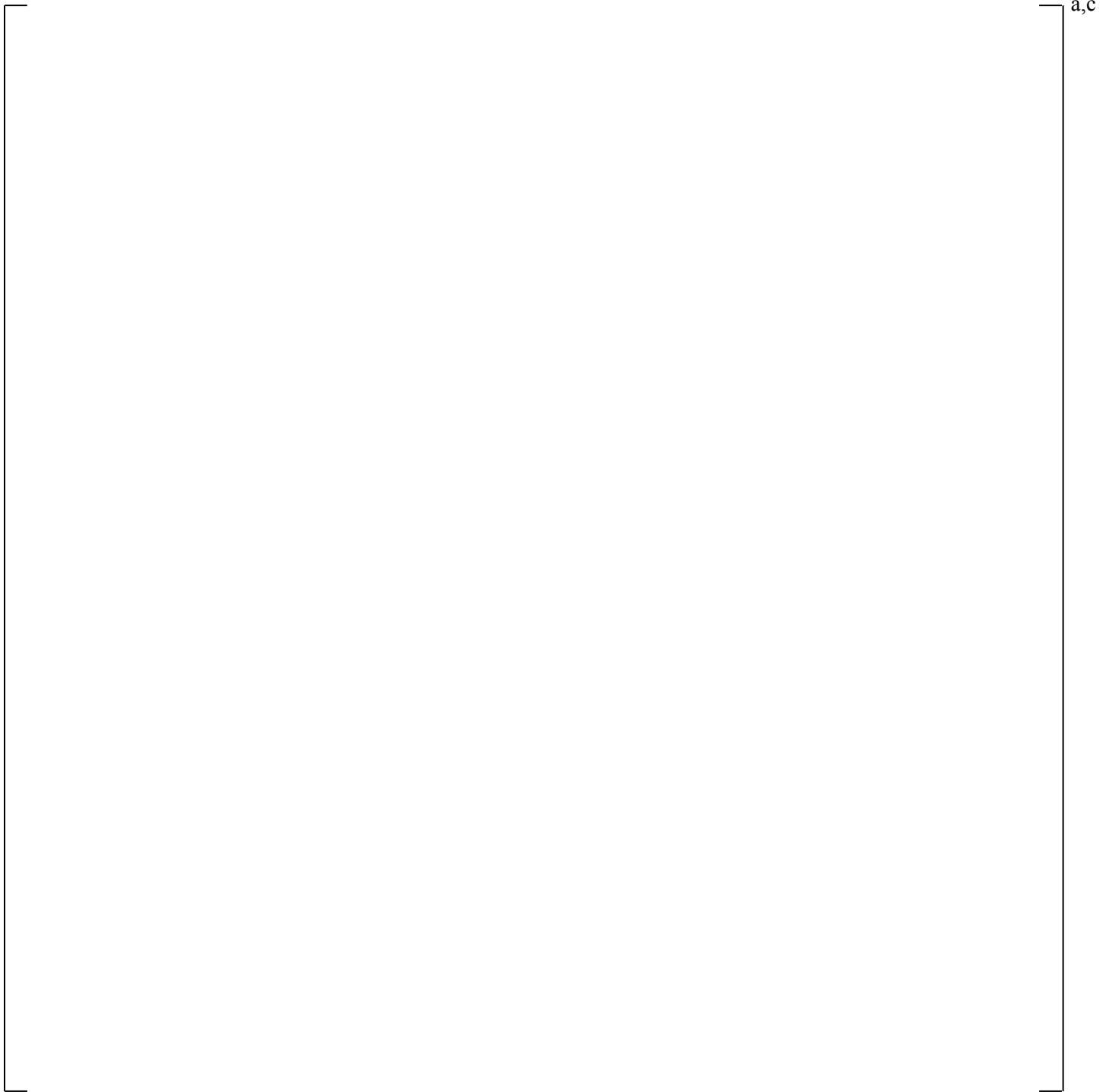


Figure 28.2.9-1 [

] ^{a,c}

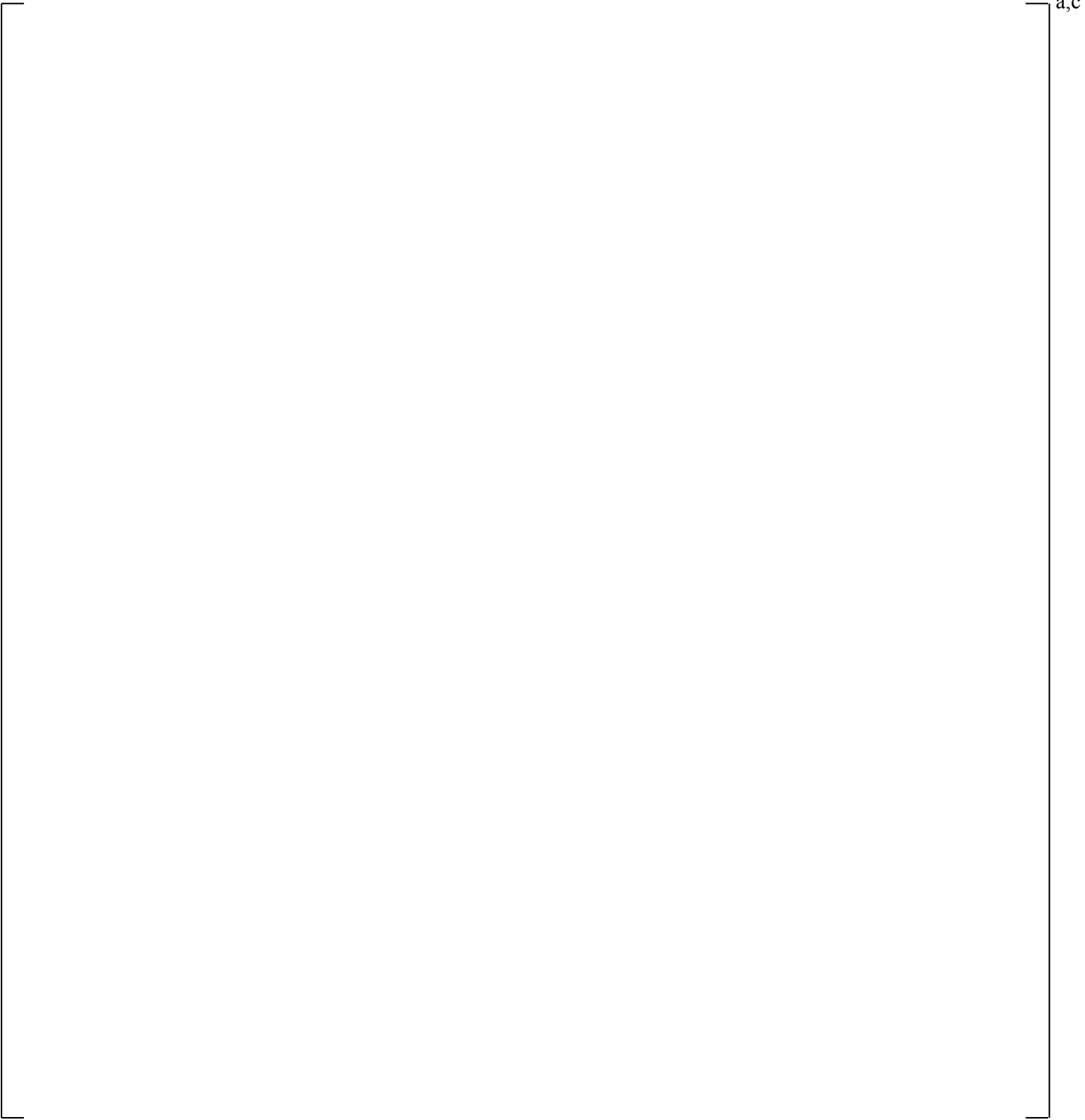


Figure 28.2.9-2 [

] ^{a,c}

a,c

Figure 28.2.9-3 [

] a,c

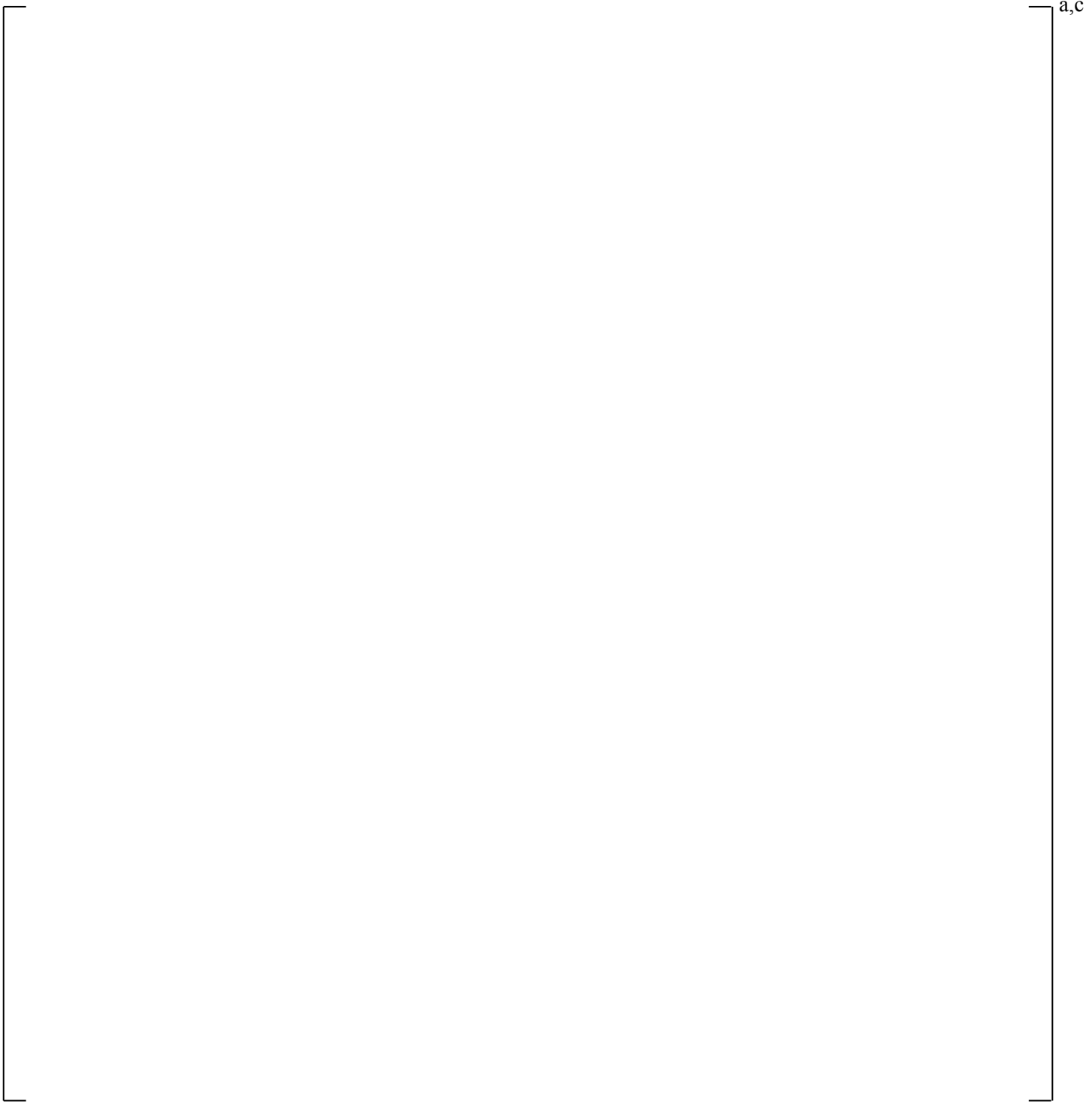


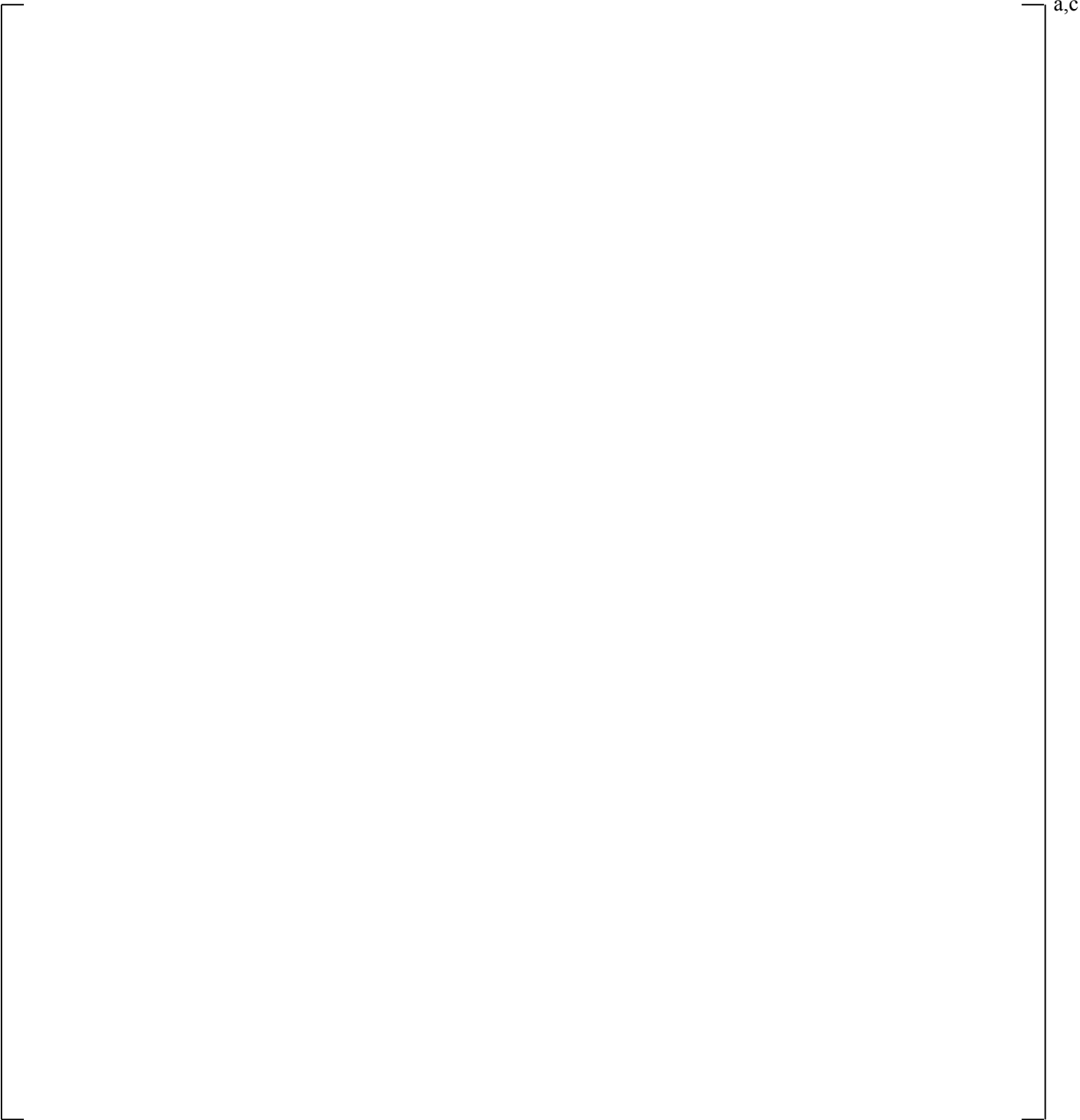
Figure 28.2.9-4 [

] ^{a,c}

a,c

Figure 28.2.9-5 [

] ^{a,c}



a,c

Figure 28.2.9-6 []^{a,c}



Figure 28.2.9-7 [

] ^{a,c}

a,c

Figure 28.2.9-8 []^{a,c}

a,c

Figure 28.2.9-9 [

] a,c

a,c

Figure 28.2.9-10 []^{a,c}

a,c

Figure 28.2.9-11 [

] ^{a,c}

a,c

Figure 28.2.9-12 [

]a,c

28.2.10 Steam Generator Hydraulics: Interfacial Drag – SBLOCA

A sensitivity study is performed to determine the effect of interfacial drag in the steam generator tubes following a small break LOCA. [

] ^{a,c}

28.2.10.1 V. C. Summer (CGE)

[

] ^{a,c}

28.2.10.2 Beaver Valley Unit 1 (DLW)

[

] ^{a,c}

28.2.10.3 Conclusions

As described in Section 29.1.12, the code prediction of steam generator heat transfer, condensation, and counter-current flow limitation (CCFL) effects is reasonable, [

] ^{a,c}

a,c

Figure 28.2.10-1 [

] ^{a,c}

a,c

Figure 28.2.10-2 [

] ^{a,c}

a,c

Figure 28.2.10-3 [

] ^{a,c}

a,c

Figure 28.2.10-4 [

] ^{a,c}

a,c

Figure 28.2.10-5 [

] ^{a,c}

a,c

Figure 28.2.10-6 [

] ^{a,c}

a,c

Figure 28.2.10-7 [] ^{a,c}

Figure 28.2.10-8

[

] ^{a,c}

a,c

Figure 28.2.10-9 [

] ^{a,c}

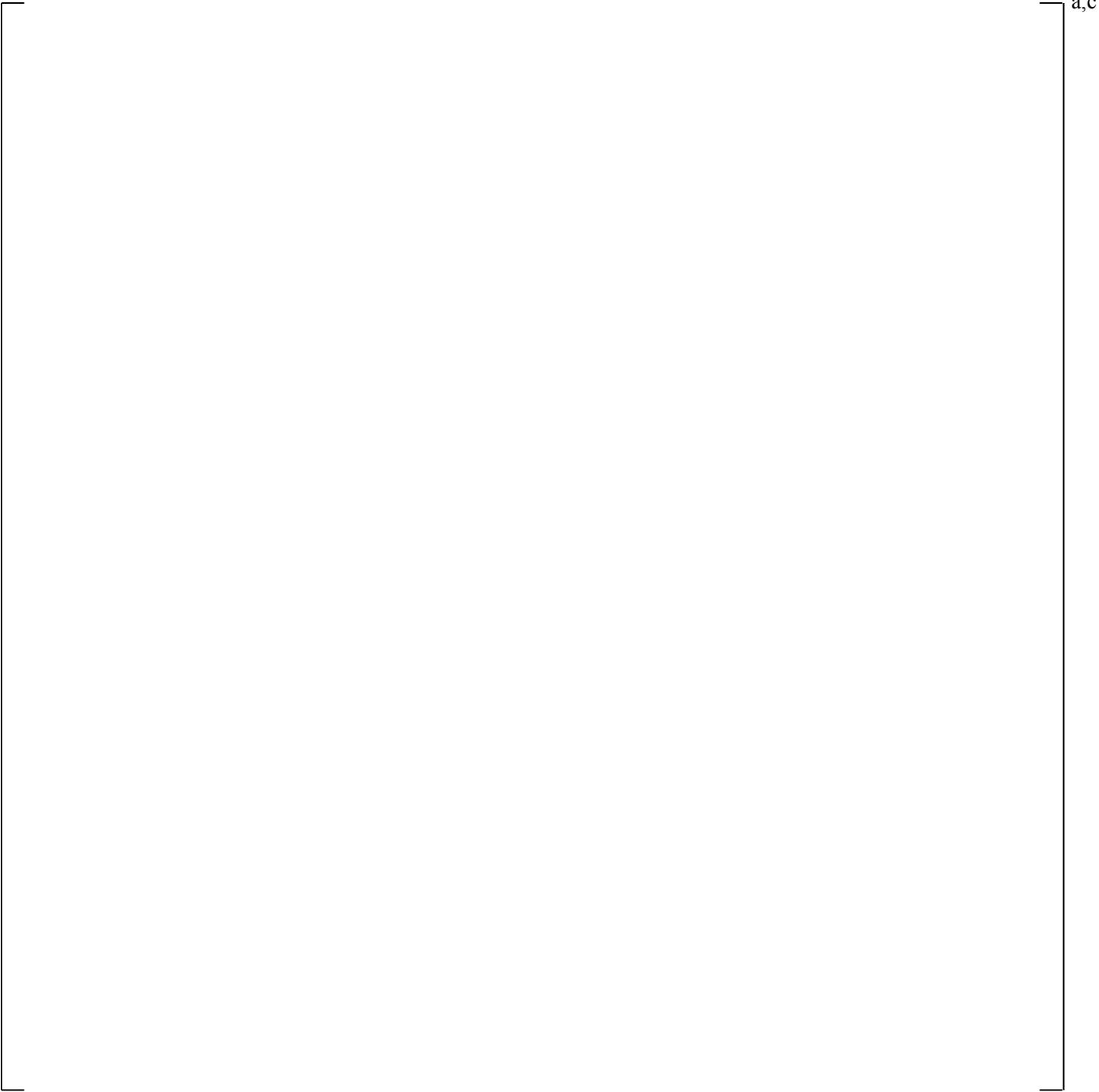


Figure 28.2.10-10 [

]^{a,c}

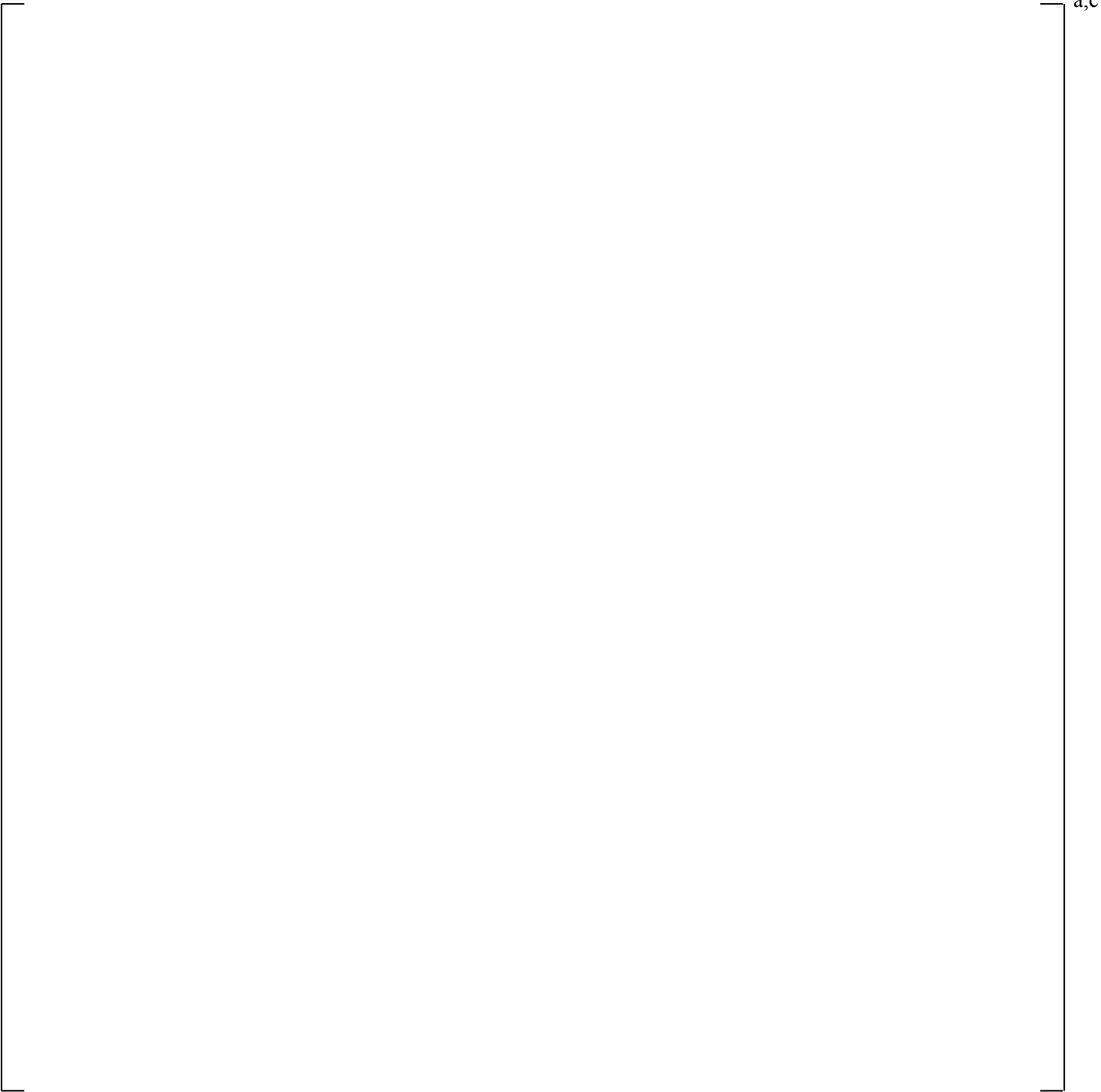


Figure 28.2.10-11 [

]^{a,c}

a,c

Figure 28.2.10-12 [

] ^{a,c}

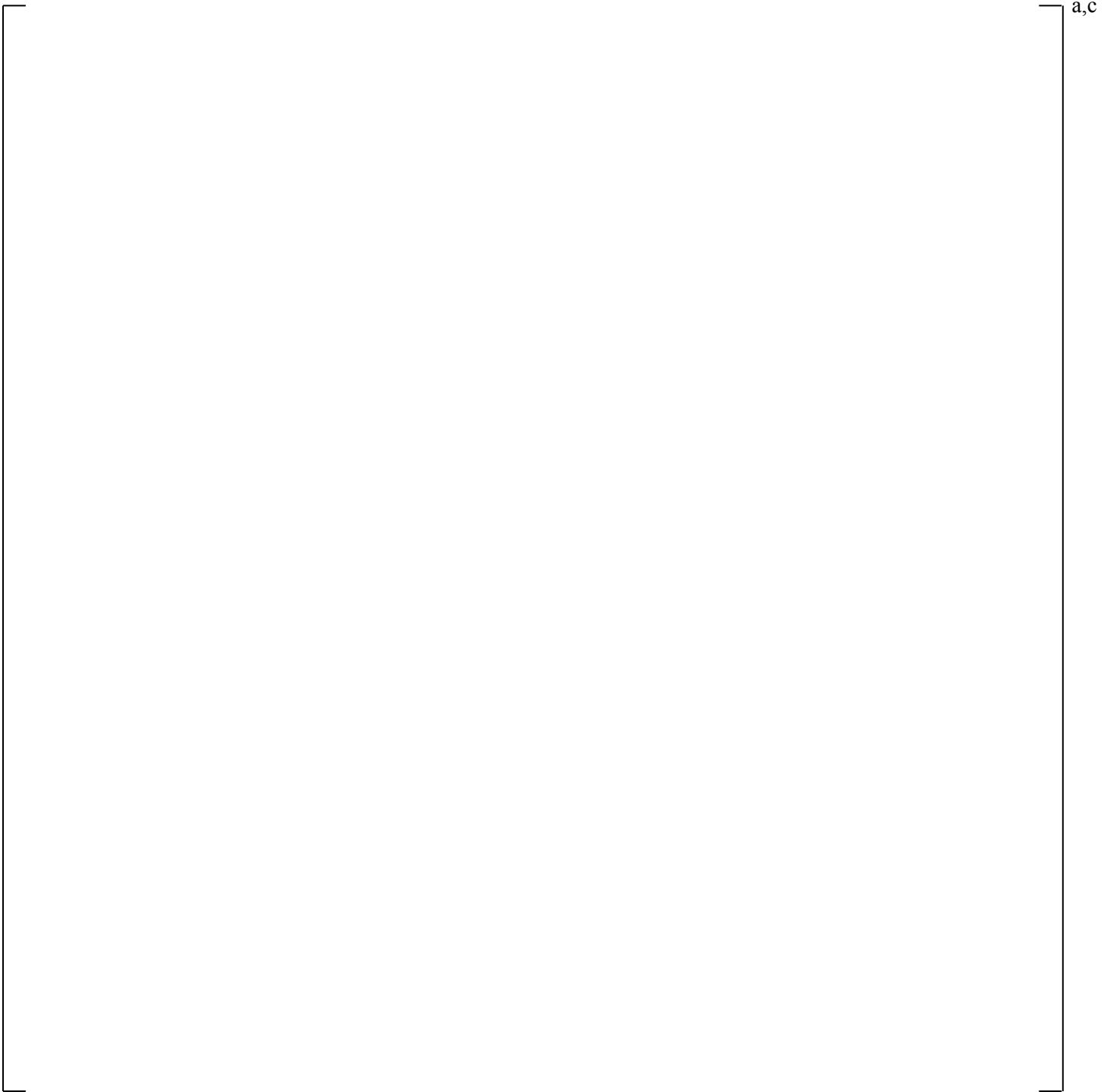


Figure 28.2.10-13 [

] ^{a,c}

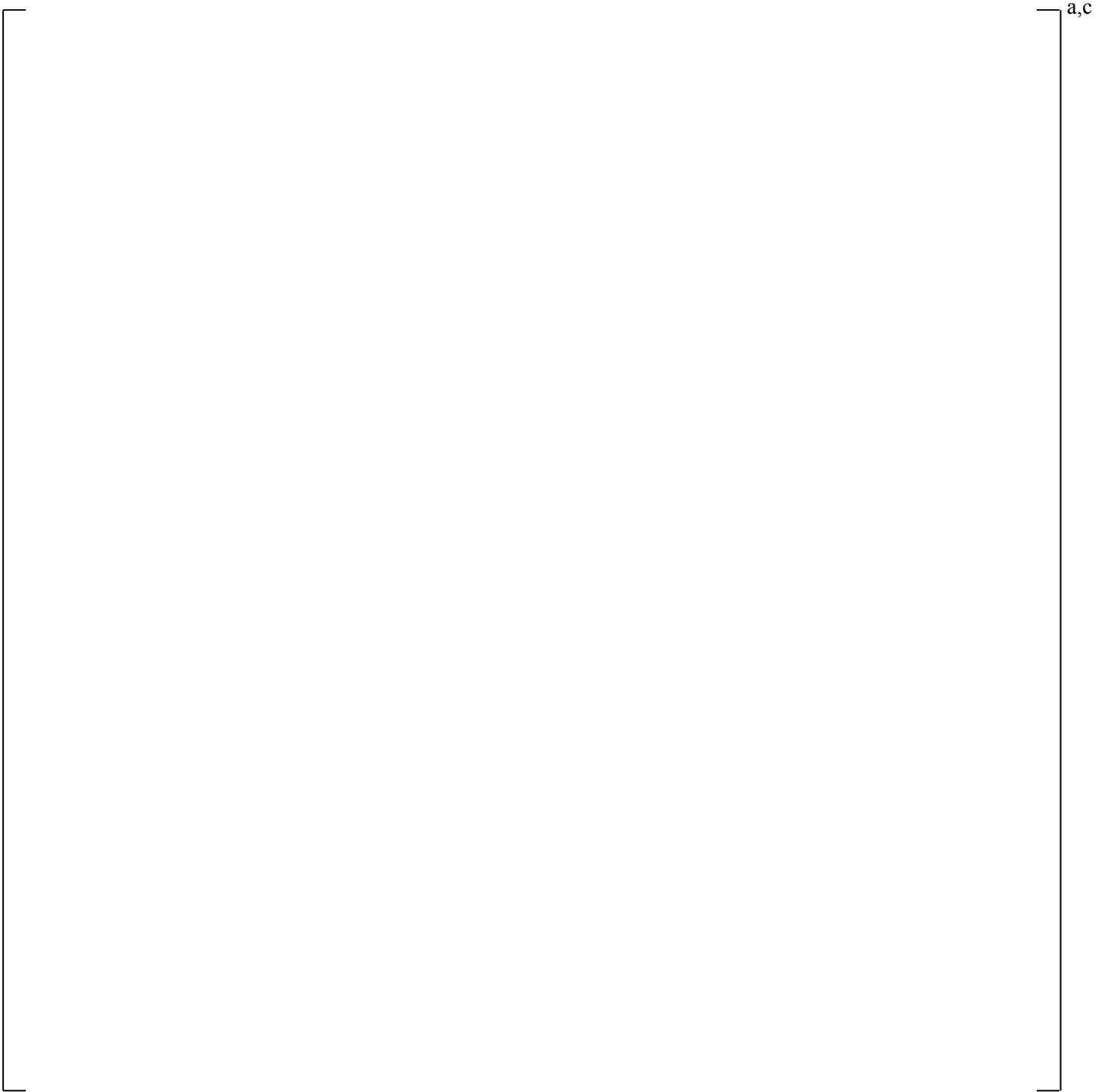


Figure 28.2.10-14 [

]^{a,c}

a,c

Figure 28.2.10-15 [

] ^{a,c}

a,c

Figure 28.2.10-16 [

] ^{a,c}

28.2.11 Loop Seal Clearance – SBLOCA

Section 18 provides a general description of the loop seal clearance, identified as an important phenomenon in modeling small break LOCAs.

A range of small breaks is explored for Beaver Valley Unit 1 (DLW) [

] ^{a,c} At the extremes, a small break resulting in break flow less than the maximum charging flow will never clear the loop seals, while a large break LOCA will effectively clear all the loop seals during blowdown.

[

] ^{a,c}

Further discussion of the treatment of uncertainty in loop seal clearing is provided in Section 29.1.11.

28.2.11.1 References

1. Lee, et al., 1983, "Phenomenological Uncertainty During Loop Seal Steam Venting in a Small Break Cold Leg LOCA of a PWR," ASME 83-HT-104.

a,c

Figure 28.2.11-1 [

] ^{a,c}

a,c

Figure 28.2.11-2 [

] ^{a,c}

a,c

Figure 28.2.11-3 [

] ^{a,c}

a,c

Figure 28.2.11-4 [

] ^{a,c}

a,c

Figure 28.2.11-5 [

] ^{a,c}

a,c

Figure 28.2.11-6 [

] ^{a,c}

a,c

Figure 28.2.11-7 []^{a,c}

28.2.12 Horizontal Stratified Flow (HS_SLUG) – SBLOCA

As discussed in Section 29.1.7, [

The flow stratification in the RCS piping and in the loop seal is expected to affect the venting and loop seal clearance following a small break LOCA. Here, the reference transients for CGE and DLW are executed using [

] ^{a,c}

] ^{a,c}

28.2.12.1 V. C. Summer (CGE)

[

] ^{a,c}

28.2.12.2 Beaver Valley Unit 1 (DLW)

[

] ^{a,c}

[

] ^{a,c}

28.2.12.3 Conclusions

The impact of the variation of HS_SLUG on the severity of heatup in SBLOCA transients [

] ^{a,c} as described in Section 29.1.7.

Table 28.2.12-1 Flow Regime Flags	
Flag	Flow Regime
1	Bubbly or Slug
2	Stratified ($\alpha < 0.5$)
2.5	Wavy Dispersed ($\alpha < 0.5$)
3	Churn (Transition)
4	Stratified ($0.5 < \alpha < 0.75$)
4.5	Wavy-Dispersed ($0.5 < \alpha < 0.75$)
5	Annular/Mist
6	Stratified ($0.75 < \alpha$)
6.5	Wavy-Dispersed ($0.75 < \alpha$)

Table 28.2.12-2 [] ^{a,c}			

a,c

Table 28.2.12-3 [] ^{a,c}			

a,c

a,c

Figure 28.2.12-1 [

] ^{a,c}

a,c

Figure 28.2.12-2 [

] ^{a,c}

a,c

Figure 28.2.12-3 [

] ^{a,c}

a,c

Figure 28.2.12-4 [

] ^{a,c}

a,c

Figure 28.2.12-5 [

] ^{a,c}

a,c

Figure 28.2.12-6 [

] ^{a,c}

a,c

Figure 28.2.12-7 [

] ^{a,c}

a,c

Figure 28.2.12-8 [

] ^{a,c}

a,c

Figure 28.2.12-9 [

] ^{a,c}

a,c

Figure 28.2.12-10 [

] a,c

a,c

Figure 28.2.12-11 [

] a,c

a,c

Figure 28.2.12-12 [

] ^{a,c}

a,c

Figure 28.2.12-13 []^{a,c}

a,c

Figure 28.2.12-14 [

] ^{a,c}

29 ASSESSMENT OF UNCERTAINTY ELEMENTS

The list of dominant phenomena was identified by the Phenomena Identification and Ranking Table (PIRT) discussed in Section 2. The PIRT included all processes covering the scenarios that span the full spectrum of break sizes. A summary of the important phenomena was provided in Section 2.3.3. The code models associated with such phenomena were then assessed against an independent dataset comprised of separate effect tests (SETs), integral effect tests (IETs) and numerical thought problems. This was the subject of Sections 12 through 23. Section 24 provides analysis and assessment of potential compensating errors in those code models.

The code assessment exercise leads to the determination and quantification of model biases and uncertainties (Evaluation Model Development and Assessment Process (EMDAP) Step 20). Consistent with the Code Scaling, Applicability and Uncertainty (CSAU) roadmap, the uncertainty has to be ultimately propagated or convoluted statistically during the plant analysis. The statistical procedure used to propagate the uncertainties is the subject of Section 30.

The FULL SPECTRUM Loss-of-Coolant Accident (FSLOCA) analysis is [

] ^{a,c}

[

] ^{a,c}

The purpose of this section is to summarize the methodology for the treatment of the uncertainty contributors associated with the code capability of representing phenomena and processes identified as highly important by the PIRT. In general, the uncertainty parameters fall into three categories:

1. Nominal without Uncertainty¹ – The nominal value of the parameter is used without consideration of uncertainty when the variation in the parameter is tightly controlled, such as pressurizer level, or when the sensitivity of the transient to the value of the parameter is negligible, such as auxiliary feedwater flow. An example of a model treated as nominal without uncertainty is the offtake model (Section 29.1.1.1).
2. Bounded (or Bounding) – A conservative value of the parameter is used when the parameter varies gradually as a function of operating history, when the sensitivity of the transient to variations in the parameter is small, or when the effort to develop and justify a detailed uncertainty treatment is judged to exceed the benefits of doing so. Bounded plant parameters are discussed in Section 29.3.1. An example of a parameter treated as conservative but not explicitly bounded is the containment pressure, and an example of a phenomenon treated in a bounding manner is steam binding.
3. Nominal with Uncertainty¹ – The uncertainty parameters in this category are sampled for each transient calculation within the uncertainty analysis. The FSLOCA methodology includes three categories of uncertainty contributors to the overall uncertainty assessment. These are the thermal-hydraulic model uncertainties, the power-related parameter uncertainties, and the initial and boundary condition uncertainties. The uncertainty distribution of these parameters may be uniform, normal, or an actual cumulative distribution.

Tables 29-1 through Table 29-5 provide the list of the uncertainty contributors or elements that are explicitly considered in the FSLOCA methodology. [

] ^{a,c}

-
1. The nominal value is defined as: either the average of the minimum and maximum values or the median for a parameter with a uniform distribution; the mean of a normal distribution; the 50th percentile value of an actual cumulative distribution; or determined from an unbiased (without uncertainty) or biased (with uncertainty), as-coded correlation

The uncertainty contributors [

The objective of Section 29.1 is to develop and justify the probability density function (PDFs) associated with such key parameters.]^{a,c}

While a PDF was developed and justified for most of the models, in some instances a bounding approach was judged to be adequate for the purpose of the uncertainty analysis. This was the case when a complete characterization of the individual model biases and uncertainty could not be pursued, because of the complexity of the process, and/or because limitations in experimental data caused the effort of developing a detailed uncertainty treatment for each individual component to exceed the benefit of doing so. In those circumstances, the objective of the exercise was to demonstrate that the biases associated with that specific complex phenomenon, albeit not quantified, are conservative with respect to engineering figures of merit in the context of a realistic but still conservative LOCA simulation. In those cases, the validity of the approach was also supported by compensating error analyses (Section 24). [

] ^{a,c}

The analysis of the uncertainty on the break flow is [

] ^{a,c} The discussion of the break model methodology deserves a section itself, and Section 29.2 is dedicated to this topic.

Core power related parameters are listed in Table 29-4. The time in cycle is the first parameter selected since many fuel related parameters are a function of burnup. The methodology is presented in Section 29.4.1.

Uncertainties associated with the fuel rod models are listed in Tables 29-3a, 29-3b and 29-4. Some of these parameters are characterized as local uncertainties since the effect is postulated to mainly affect the local PCT or MLO and the effect on the global T/H response is expected to be minimal. [

] ^{a,c}

All the other uncertainty parameters are associated with the plant parameters listed in Table 29-5. Section 29.3.2 is dedicated to the topic.

Section 29.5 provides a review of the PIRT and summarizes the conclusions from the perspective of model biases and uncertainty of all phenomena ranked high (H). This corresponds to EMDAP Step 20. Finally, Section 29.6 addresses experimental accuracy in the context of Step 9 of the EMDAP roadmap.

Table 29-1 Uncertainty Elements – Break Location, Type, Orientation and Area Sampling Methodology⁽¹⁾

Parameter	Distribution

a,c

Table 29-2 Uncertainty Elements – Thermal-Hydraulic Models

Parameter	Distribution and Treatment	Basis

a,c

Table 29-3a Uncertainty Elements – Local Models []^{a,c}

Parameter	Distribution	Basis for Distribution

a,c

Table 29-3b Burst Strain for []^{a,c}

a,c

Table 29-4 Uncertainty Elements – Power-Related Parameters Defined in Section 29.4.1

Parameter	Distribution	Basis for Distribution

a,c

Table 29-5 Uncertainty Elements - Initial and Boundary Conditions Considered in Uncertainty Methodology Defined in Section 29.3.2

Parameter	Distribution	Range of Variation

a,c

29.1 GENERATION OF MODEL UNCERTAINTY PARAMETERS AND RANGING DISTRIBUTIONS

The purpose of this section is to document the development of the bias and uncertainty distributions (PDFs) for the ranging parameters associated with the global models. Key controlling parameters (or multipliers) on selected closure relationships have been coded in WCOBRA/TRAC-TF2 to permit the explicit ranging of such uncertainties. For a small set of phenomena, a conservative approach was instead chosen to bound the bias and uncertainty of the associated models. For less influential but complex phenomena a nominal value without uncertainty was judged to be adequate. The justification of these decisions is the subject of the following subsections.

29.1.1 Break Flow – []^{a,c}

The assessment of the break flow model is presented in Section 12. A total of []^{a,c} were used for the determination of bias and uncertainty associated with the critical flow model prediction used in WCOBRA/TRAC-TF2. The main results are summarized in Section 12.5.2.

The model has the tendency to []

[]^{a,c}

To account for the uncertainty of the break flow model, in each of the break spectrum transient calculations the break flow calculated by the code is ranged by applying discharge coefficients CD1 and CD2. The application of discharge coefficient is accomplished by modifying the break flow area and more details on implementation is provided in Sections 29.2.4 and 29.2.5 for double-ended guillotine (DEG) and split breaks, respectively. Here, for the purpose of defining the uncertainty analysis methodology, []

[]^{a,c}

Once the break type and break area are selected, as discussed in Section 29.2.3, the uncertainty of the break flow model is treated by independently sampling a value [

]^{a,c}

Sensitivity studies on the effect of []^{a,c} on the small break LOCA transient were performed with the Rig-of-Safety Assessment IV (ROSA-IV) 5% side break test SB-CL-18, Section 21.

Detailed discussion of the []^{a,c} sensitivity results is presented in Section 21.12. The sensitivity calculations showed that the []^{a,c} multiplier has a pronounced effect on the calculated loss of inventory through the break discharge from the very beginning of the transient. This effect propagates throughout the entire transient and has a fairly significant effect on the loop seal clearance timing and the calculated peak cladding temperature during the loop seal clearance and the boil-off period as well; see Figures 21.12-3, 21.12-4, and 21.12-18 in Section 21.12.

The results of the []^{a,c} sensitivity calculations, documented in Section 21.13, show some effect on the loop seal clearance period; higher []^{a,c} tends to somewhat delay the core level recovery following the loop seal clearance depression. However, the effect of the []^{a,c} multiplier on the transient is much more pronounced after the loop seal clearance. With higher []^{a,c} multiplier, the system depressurizes faster and boil-off heatup occurs earlier. Also with higher []^{a,c} the peak cladding temperature is calculated to turn around earlier due to the sooner initiation of accumulator injection; see Figure 21.13-19 in Section 21.13.

a,c

Figure 29.1.1-1 [

] ^{a,c}

a,c

Figure 29.1.1-2 [

] a,c

a,c

Figure 29.1.1-3 [

] ^{a,c}

a,c

Figure 29.1.1-4 [

] ^{a,c}

29.1.1.1 Break Flow – Offtake and Pull-Through Behavior

When the flow in the cold leg is stratified, the vapor pull-through (break below stratified interface)/liquid entrainment (break above stratified interface) phenomenon is especially important in determining the flow quality upstream of the break. This phenomenon is called offtake entrainment and is discussed in Section 12.7. The uncertainty associated with the offtake model could be an additional contributor to the break flow uncertainty. Note that this effect is only relevant for smaller break sizes.

[

] ^{a,c}

Figure 29.1.1-5 Branchline Quality Versus Mainline Liquid Level for Horizontal Configuration

Figure 29.1.1-6 Branchline Quality Versus Mainline Liquid Level for Downward-Vertical Configuration

29.1.2 Broken Cold-Leg Nozzle Flow Resistance (KN) and Broken Loop Pump Resistance

The flow resistance through the broken loop cold leg nozzle was found to be of high importance during the blowdown phase of a large break LOCA in the PIRT (Section 2.3.2.14). The broken loop flow resistance, of which the pump resistance is a large contributor, was ranked high in the PIRT for large breaks (Section 2.3.2.9). This section assesses the uncertainty associated with the cold leg nozzle and broken loop pump resistance. These two large contributors to relative break path resistance, in combination with the influence from break discharge coefficient uncertainty, [

] ^{a,c}

29.1.2.1 Broken Cold-Leg Nozzle Flow Resistance (KN)

The uncertainty in the flow resistance through the broken loop nozzle is characterized here. Table 29.1.2-1 shows the experimental database used to establish the value and range for this parameter. The effect of geometry was established by evaluating data from full-scale Upper Plenum Test Facility (UPTF) tests (Section 19).

The UPTF pressure drop data (Section 19.3.5.10) was used to extract a loss coefficient (KN) by subtracting out velocity and friction effects. The way in which the loss coefficient is used at the ID/3D junction in WCOBRA/TRAC-TF2 is as a total pressure loss coefficient. For application to the ID/3D junction, the data is evaluated as a total loss coefficient by subtracting the friction pressure drop.

The UPTF range of conditions relative to PWR is shown in Table 29.1.2-1, with the pressure loss data provided in Table 19.3-15. [

] ^{a,c}

$$\left[\quad \quad \quad \right]^{a,c} \quad (29.1.2.1-1)$$

An additional data point is available from estimates made of the pressure loss during reflood in the Cylindrical Core Test Facility (CCTF) (Akimoto et al., 1984). These estimates indicate a pressure loss coefficient of approximately 0.5, which is well within the range of the UPTF test data. The CCTF range of conditions relative to the UPTF and PWR ranges is shown in Table 29.1.2-1.

[

] ^{a,c}

29.1.2.2 Broken Loop Pump Resistance

For large breaks, the pump flow resistance contributes to the overall loop resistance, which together with the broken cold leg nozzle resistance affects the flow reversal and stagnation in the core. For smaller breaks, the influence of flow resistance through the pump and its effect on flow to the break is at most of medium importance during the natural circulation and loop seal clearing periods. Therefore, the ranging of the broken loop pump resistance is considered for the uncertainty analysis with the expectation that such ranging will be relevant or have an effect only for larger breaks.

The pump model was developed from 1/3-scale Westinghouse pump data (Section 20.2), and assessed against four Loss-of-Fluid Test (LOFT) facility tests (Section 22). In two of the tests, the pumps continued to rotate, while in the other two tests, the pumps were allowed to coast down. The two-phase test data extend well beyond the range expected to occur in a PWR. This can be seen in Figure 20.2-6, which shows the WCOBRA/TRAC-TF2 pump head curves and the test data in non-dimensional (homologous) form.

Recall from Section 10.4 that the homologous curves plot the normalized head/normalized speed squared ratio (H/α^2) against the normalized flow/normalized speed ratio (ϕ/α), where the normalization is to pump rated head, flow, and speed. In Figure 20.2-6, two-phase data are available over a normalized flow range []^{a,c}. It was found (Section 20.2) that the uncertainty in two-phase pump head was significant when the pump was in dissipative (i.e., forward flow producing a pressure drop through the pump) operation. Pumping mode data was therefore used to determine the degradation multiplier, and it was found that predictions were largely insensitive to the nature of the degradation multiplier curve. The uncertainty in the pump will therefore be accounted for using the uncertainty in the dissipative (single phase) data.

From Figures 20.2-3 and 20.2-4 of Section 20.2, the uncertainty range of $(H/H_R)/(Q/Q_R)^2$ is determined to be []^{a,c}

The approach on the ranging of $(H/H_R)/(Q/Q_R)^2$ is considered to be applicable to both small and large break LOCA scenarios. To evaluate the impact of these decisions for a small break, a sensitivity calculation was performed with the ROSA-IV test SB-CL-18, Section 21.14. The ROSA-IV sensitivity performed therein was not a sensitivity on the $(H/H_R)/(Q/Q_R)^2$ adder, but simply looks at the sensitivity on the results when the pump resistance at zero rotation point in the homologous curve (resistance when pump velocity is equal to zero) is reduced by 50%. The ROSA-IV sensitivity results presented in Section 21.14 show that the impact is small. Since during the critical time for a small break (boil-off) the pumps will most likely operate close to locked rotor conditions, this shows that ranging of the $(H/H_R)/(Q/Q_R)^2$ is expected to have a negligible effect on the results.

Table 29.1.2-1 Nozzle Loss Coefficient Assessment Data Base			
Parameter	Test Range		PWR Range
	UPTF	CCTF	
Geometry: Vessel/Nozzle	Full Scale	1/20 Scale	Full Scale
Pressure (psia)	120 – 40	30	2250 – 40
Vapor Fraction	1.0	0-1	0-1

29.1.3 Delivery and Bypassing of ECC – Bounding Approach

The delivery and bypassing of ECC water is a phenomenon which is only important during a large break (LB) scenario. The ECC bypass (counter-current flow limitation (CCFL)) models in WCOBRA/TRAC-TF2 were assessed in Section 19.3 using UPTF full-scale data. In particular, the UPTF Test 6 series looks at ECC bypass during the blowdown period and UPTF Test 25A investigates steam-water interaction (entrainment) during reflood.

The assessment showed that the models as coded adequately predict the ECC delivery and bypassing with a moderately conservative bias that does not warrant an explicit consideration of the uncertainties.

29.1.4 Condensation in the Downcomer

The model for condensation in the downcomer annulus was assessed against full-scale UPTF data in Section 19.3.5 (UPTF Test 6 series). Condensation efficiencies were estimated by MPR (1990) and calculated with two methods which provided an upper and lower bound for the uncertainty range.

Table 19.3-8 compares the predicted average condensation efficiency from WCOBRA/TRAC-TF2, and the condensation efficiency calculated in the MPR report by two methods described in Section 19.3.5.8. The ratio of experimental to predicted efficiency was calculated as shown, [

$$]^{a,c}.$$

The effect of condensation in the downcomer annulus was ranked High only during the refill phase of a large break LOCA (LBLOCA) scenario, therefore [

$$]^{a,c}.$$

A sensitivity analysis was performed where the UPTF 6 test series was simulated by varying the downcomer condensation multiplier, XC, in Section 19.3.5.8, considering values of 0.0, 0.4, 1.0, and 1.1 to examine the effect of the condensation multiplier. Results are shown in Tables 19.3-9 and 19.3-10 and Figures 19.3-128 and 19.3-129, where, in general, [

$$]^{a,c}.$$

A sensitivity study was performed with XC=0.4 for the UPTF Test 25A in Section 19.3.11. It was observed that [

$$]^{a,c}.$$

The overall assessment on the downcomer condensation during refill phase indicates that [

$$]^{a,c}.$$

29.1.5 Interfacial Drag in the Core Region []^{a,c}

From the PIRT, prediction of the mixture level swell and tracking of the mixture level are important in the later stages of a small break or intermediate break LOCA. [

] ^{a,c}

In a small break LOCA, as more liquid is boiled away the mixture level can eventually drop into the core. While good cooling can be maintained below the mixture level, dryout occurs above the mixture level. Heat transfer above the mixture level is limited to convection and thermal radiation to steam. Everything else being the same, the PCT and MLO in the period when the core is uncovered will increase as the mixture level decreases because steam enthalpy rise starts from the location of the mixture level upward. The location of the mixture level is defined as the ‘dryout’ point, or the point where there is a sharp reduction in total heat transfer and most of the heat is transferred to the steam.

The location of the mixture level also determines the steam flow rate in the uncovered portion of the core, since boiling can only occur below in the two-phase region. The steam generation decreases with the magnitude of the core uncover. As the steam flow decreases in the uncovered portion of the core, this will further increase the steam temperature and enthalpy rise.

For a given mass inventory (or core collapsed liquid level) the location of the mixture level depends on the phenomenon characterized as level swell. The level swell is defined in Section 13. The mixture level swell is a function of the interfacial drag between the vapor and liquid in the two-phase region. The exact location of the dryout point also depends on other factors which are not strictly related to the swell in the two-phase region. A sharp mixture level exists when the annular film flow regime cannot develop (low bundle power and corresponding low vapor superficial velocity which are typical of the boil-off phase in a small break LOCA scenario). At higher power, critical heat flux (CHF) can occur at a lower void fraction and below the two-phase mixture level. Also the CHF model and the hydraulic mesh resolution play a role in exactly defining the location of the dryout point. Higher linear heat rates are more typical of the later phase in intermediate and large break LOCA scenarios. Under those conditions an annular film flow regime is expected to dominate in the upper region of the core.

There are several closure relationships used to calculate the interfacial drag in the various flow regimes below the two-phase mixture level. [

] ^{a,c} The interfacial drag in the small bubble regime [] ^{a,c} in a rod bundle channel is calculated from Equation 5-74:

$$\left[\right]^{a,c}$$

$$j^{a,c} = \left[\frac{1}{\left(\frac{1}{j_{a,c}^{a,c}} \right)} \right]$$

The interfacial drag in the small-to-large bubble regime $j^{a,c}$ is calculated from Equation 5-76:

$$j^{a,c} = \left[\frac{1}{\left(\frac{1}{j_{a,c}^{a,c}} \right)} \right]$$

$$j^{a,c} = \left[\frac{1}{\left(\frac{1}{j_{a,c}^{a,c}} \right)} \right]$$

$$j^{a,c} = \left[\frac{1}{\left(\frac{1}{j_{a,c}^{a,c}} \right)} \right]$$

Since the interfacial drag multiplier is applied to both interfacial drag components prior to this calculation, the overall calculation is consistent and will include the effects of the multiplier.

As described by Equations 5-78a and 5-78b, the transition from small-to-large bubble flow regime

$$j^{a,c}$$

As such, the interfacial drag multiplier is inherent in the transition from small-to-large bubble flow regime and will include the effects of the multiplier.

$$j^{a,c} \text{ The interfacial drag in the film/drop regime}$$

$j^{a,c}$ is calculated from Equation 5-85:

$$j^{a,c} = \left[\frac{1}{\left(\frac{1}{j_{a,c}^{a,c}} \right)} \right]$$

1001

$$\left. \begin{array}{c} \text{---} \\ \text{---} \end{array} \right] \text{a,c}$$
 $\mathbf{l}^{\mathbf{a,c}}$

[

 $\mathbf{l}^{\mathbf{a,c}}$ $\mathbf{l}^{\mathbf{a,c}}$

[

The Full-Length Emergency Core Heat Transfer (FLECHT) Separate-Effects and System-Effects Tests (SEASET) test 31504 (described in Section 14.2.3.1) is taken as a representative test of rod heat transfer under prototypical LBLOCA reflood conditions. The WCOBRA/TRAC-TF2 simulation of this test is addressed in Section 15.6.1.1.2. Figures 29.1.5-3 and 29.1.5-4 show results from a YDRAG sensitivity analysis performed for FLECHT-SEASET test 31504. []^{a,c}

[]^{a,c}

Similarly, a sensitivity study for YDRAG was performed with ROSA-IV test SB-CL-18 to examine its effect in an integral small break LOCA test simulation. In two simulations of the SB-CL-18 test, the YDRAG parameter in the core channels was ranged between []^{a,c} The results of this sensitivity are discussed in Section 21.15. []

[]^{a,c}

Figure 29.1.5-1 Predicted Versus Measured Level Swell for the G-1 and G-2 Boil-off Simulations with []^{a,c}

a,c

Figure 29.1.5-2 Predicted Versus Measured Level Swell for the G-2 Boil-off Simulations with
[]^{a,c}

a,c

Figure 29.1.5-3 Differential Pressure in the Test Bundle for [
FLECHT-SEASET Test 31504

] ^{a,c},

Figure 29.1.5-4 Quench Profile for [
Test 31504

] ^{a,c}, FLECHT-SEASET

29.1.6 Cold Leg Condensation (KCOSI)

The cold leg condensation by the cold liquid injected from the emergency core cooling system (ECCS) is an important phenomenon during both small and large break LOCAs (see PIRT in Section 2). [

] ^{a,c} A special cold leg condensation model was developed in Section 6.3.6 to predict the cold leg condensation heat transfer rate when the cold leg is expected to be [

] ^{a,c}.

The cold leg condensation model was assessed against SBLOCA SETs: Westinghouse Condensation on Safety Injection (COSI), Framatome COSI, and ROSA IV SB-CL-05 in Section 17; and LBLOCA SETs: UPTF 8A and 25A in Sections 17 and 19. The comparison with experimental results shows that the code is able to predict condensation rates within a reasonable range of uncertainty for a SBLOCA.

[

] ^{a,c}

A cold leg condensation multiplier (KCOSI) was added in the code to allow a ranging capability for the cold leg condensation model for the purpose of the uncertainty analysis. In the code, the nominal-as-coded cold leg condensation heat transfer rate is calculated from Equation 6-236a:

$$\left[\text{Equation 6-236a} \right]^{a,c}$$

where the Nusselt number is predicted using Equation 6-236. The cold leg condensation multiplier is applied to the above equation directly, such that the cold leg condensation heat transfer rate is calculated as:

$$\left[\text{Equation 6-236a} \right]^{a,c}$$

The uncertainty on the cold leg condensation model for Region I was determined using the data from the Westinghouse horizontal COSI tests and the Framatome COSI tests [

] ^{a,c}

A KCOSI sensitivity was performed with the ROSA-IV 5% side break test SB-CL-05. Detailed discussion of the sensitivity results is presented in Section 21.17. [

] ^{a,c}

29.1.7 Horizontal Stratified Flow Regime Transition Boundary (HS_SLUG)

In WCOBRA/TRAC-TF2, a transition criterion from the stratified flow regime to the non-stratified flow regime was developed by combining [^{a,c} (Section 4.4.5). Figure 4-17 compared the transition criterion with various test data at different pressures, and different pipe diameters. [

] ^{a,c}

The horizontal stratified flow regime transition boundary multiplier, HS_SLUG, is then introduced to adjust the critical relative velocity for horizontal stratified flow. The multiplier is represented by the symbol C_{hs_slug} in Equation 4-117. The discussion in Section 4 suggests an HS_SLUG uncertainty range of 0.5 to 1.5. For the purpose of the PWR uncertainty analysis for Region I, HS_SLUG is biased high (HS_SLUG=1.5) to maximize the stratified flow regime range to increase the tendency to stratify, and thus retain more liquid in the cross-over legs following loop seal clearance. For Region II a random value of HS_SLUG is sampled with [^{a,c}

A sensitivity study of the effect of the HS_SLUG multiplier on the small break LOCA transient were performed with selected ROSA-IV tests and as part of the plant scoping analyses. Detailed discussions of these sensitivities are documented in Sections 21.16 and 28.2.12. Based on the results from the HS_SLUG sensitivity calculations presented in Section 21.16, it is concluded that the effect of the HS_SLUG ranging would have [

] ^{a,c}

29.1.8 Minimum Film Boiling Temperature (T_{min})

The minimum film boiling temperature (T_{min}) represents the minimum temperature at which vapor can maintain a stable film around the heated surface, preventing liquid from wetting the surface. Below this temperature, liquid can contact the heated surface intermittently and partial wetting is possible. T_{min} is used to define the boundary between the transition boiling heat transfer regime and the film boiling regimes. In WCOBRA/TRAC-TF2, T_{min} is estimated by a simple correlation or in some instances set to a constant value in order to determine the applicable heat transfer regime, and then to select a set of heat transfer correlations appropriate for that regime.

It must be recognized that T_{\min} is not a property or a unique value for a given geometry. The minimum film boiling temperature is the result of two competing processes: liquid evaporation and the conduction of heat to the wall surface. Evaporation of the liquid determines the repulsive force that acts on the liquid, which can be in the form of droplets or an inverted annular column. When the evaporation rate is high, it can prevent the liquid from making contact with the heated surface. If contact between the liquid and the wall does occur, the rate at which heat is conducted to the surface determines if the liquid is quickly thrown off the wall, or if the contact can be sustained. Conduction within and along the wall is affected by its material properties as well as its internal geometry and initial temperature distribution.

Figures 29.1.8-1 and 29.1.8-2 illustrate two situations encountered in the quenching of nuclear fuel rods. Figure 29.1.8-1 shows a situation typical of the blowdown cooling phase, in which liquid is distributed in a dispersed droplet field and the subcooling is equal to or nearly zero. In this case, droplets approach the wall with a normal velocity caused by turbulent motion in the bulk fluid. Unequal evaporation on the wall-facing and fluid-facing sides of the droplet causes a repulsive force to act on the droplet. Drop-wall contact depends on the magnitudes of the repulsive force and the initial droplet momentum towards the wall. This process is described by Ganic and Rohsenow (1977) who calculated a continuous post-CHF boiling curve by considering a force balance on a droplet entering a boundary layer. T_{\min} in their analysis was the surface temperature when the heat flux reached a minimum.

The more complex situation typical of bottom reflood is shown in Figure 29.1.8-2, in which the liquid is in the form of an inverted annular column. In this case, wave phenomena on the surface of the liquid column must be considered. Unlike the droplet situation in Figure 29.1.8-1, the inverted annular column is much more difficult to characterize. It can consist not only of relatively large waves as shown in the figure, but also include “ripples” superimposed on the primary waves. The complexity of the inverted annular column was investigated by Vijaykumar and Dhir (1992), who used a holographic interferometer to examine the wave structures that can occur. Liquid-wall contact still depends on the relative magnitudes of the wave momentum towards the wall and the repulsive force due to evaporation. Baum (1977) developed a model for transition and film boiling that considered the forces acting on a wave near a heated wall, but T_{\min} was not a major consideration.

In both Figures 29.1.8-1 and 29.1.8-2, the “wall” is the fuel rod cladding, which is made of zircaloy, and is separated from the fuel pellet by a thin gap. The gap acts as a resistance to conduction from the heat source to the clad. Thus, as liquid nears contact with the clad, the effect of the gap on the transient conduction from the pellet to the cladding needs to be accounted for in determining the limit at which energy can be made available to evaporate the liquid. The material property effect was examined by Dhir, Duffey, and Catton (1981), who found that zircaloy quenched faster than stainless steel.

From a consideration of the physical processes involved in rewetting, it is apparent that details of the heat transfer process must be known locally if T_{\min} is to be accurately determined. While numerous correlations have been proposed for T_{\min} , none have gained wide acceptance due to the large uncertainty in their estimates compared to data. The major cause of the large uncertainty is twofold. First, few of the available methods have attempted to determine T_{\min} based on all of the fundamental processes, which limits their applicability. Second, while there is considerable data for T_{\min} , none of the available databases included nor systematically examined parameters that must be known on a local basis. Most databases include parameters such as pressure, mass flux, and inlet subcooling, but few contain information on local parameters such as void fraction, droplet size, heat flux, cladding oxidation, and axial temperature.

gradient. In addition, most data for T_{\min} were obtained for solid heater rods with stainless steel cladding as opposed to zircaloy cladding rods with a gap between the pellet and the cladding as is the case in a nuclear rod. Therefore, the available data must be examined in order to identify an appropriate T_{\min} value for an individual rod.

[

$J^{a,c}$

The T_{\min} model used in WCOBRA/TRAC-TF2 is described in Section 7, which is derived from a model suggested by Henry (1974). Dispersed flow film boiling (DFFB) simulations were performed in Section 15.5, and reflood simulations were performed in Section 15.6. Since T_{\min} defines when the rods may rewet during blowdown or quench during reflood, quench temperature comparisons are performed for select tests simulated in Sections 15.5 and 15.6. The method for determining the quench temperatures is [

$J^{a,c}$

Figure 29.1.8-7a provides a comparison of predicted versus measured quench temperatures at several elevations from the G-1 Blowdown experiments simulated in Section 15.5. The data values are the average of all the thermocouples located within the inner channel modeled by WCOBRA/TRAC-TF2. As can be seen from the figure, [

$J^{a,c}$

Figures 29.1.8-8 through 29.1.8-10 provide a comparison of predicted versus measured quench temperatures for the FLECHT experiments (SEASET, low flooding rate, Skewed) simulated in Section 15.6. The data values are the individual thermocouples located within the inner channel modeled by WCOBRA/TRAC-TF2. As can be seen from the figures, WCOBRA/TRAC-TF2 tends to [

$J^{a,c}$

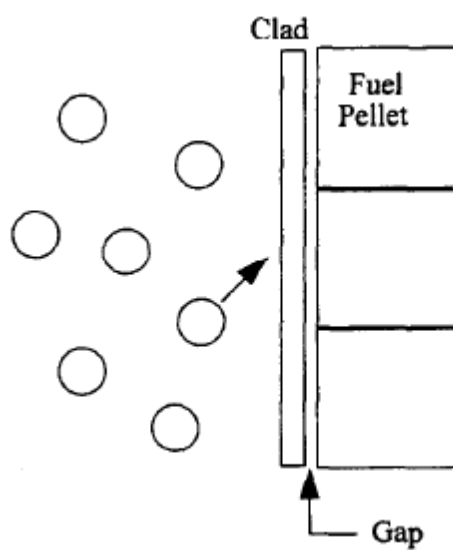


Figure 29.1.8-1 Dispersed Flow Cooling

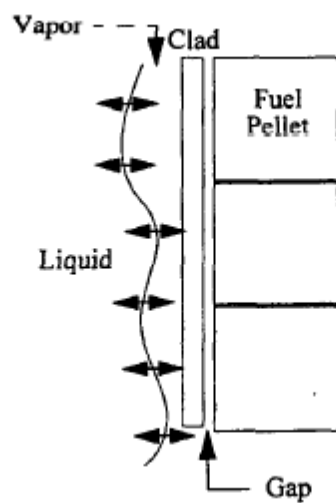


Figure 29.1.8-2 Inverted Annular Cooling

Figure 29.1.8-3 Histogram of T_{\min} Values Based on G-1 and G-2 Test Data [

]^{a,c}

a,c

Figure 29.1.8-4 T_{\min} Variation with Re (From Appendix N, Boyack et al., 1989)

a,c

Figure 29.1.8-5 T_{\min} Variation with Pressure (From Appendix N, Boyack et al., 1989)

a,c

Figure 29.1.8-6 Method for Determining Quench Temperature [

] ^{a,c}

a,c

Figure 29.1.8-7a Predicted vs. Measured Quench Temperatures from G-1 Blowdown Simulations

a,c

Figure 29.1.8-7b Predicted vs. Measured Quench Temperatures from G-1 Blowdown Simulations with TMIN Set to Homogeneous Nucleation Temperature

a,c

Figure 29.1.8-8 Predicted vs. Measured Quench Temperatures from FLECHT SEASET Forced Reflood Test Simulations

a,c

Figure 29.1.8-9 Predicted vs. Measured Quench Temperatures from FLECHT Low Flooding Rate Forced Reflood Test Simulations

a,c

Figure 29.1.8-10 Predicted vs. Measured Quench Temperatures from FLECHT Skewed Forced Reflood Test Simulations

29.1.9 Steam Binding and Entrainment – Bounding Approach

Simulations of the FLECHT forced reflood tests (Section 19.5) indicate that the WCOBRA/TRAC-TF2 predictions are in good agreement with data regarding carryover, while CCTF Test 62 simulation (Section 19.6) indicates that WCOBRA/TRAC-TF2 tends to over-predict the amount of entrainment from the core. For forced reflood tests (FLECHT), this leads to a slightly higher predicted heat transfer but slower quench front progression. For gravity reflood tests such as CCTF Test 62, however, the excess entrainment results in an over-prediction of steam binding, which reduces the flooding rate and causes an under-prediction of core heat transfer. In addition, the comparisons with UPTF Test 29B showed that when the conditions at the entrance to the upper plenum are known, WCOBRA/TRAC-TF2 under-predicts the mass retained in the upper plenum, therefore over-predicting the amount of water entrained into the loops. Based on the CCTF Test 62 gravity reflood and UPTF Test 29B predictions, it is concluded that a conservative bias already exists in the calculations with regards to core entrainment/de-entrainment and the resulting steam-binding effects, and an additional bias or uncertainty treatment is not required.

29.1.10 Non Condensable Gases/Accumulator Nitrogen – Bounding Approach

This refers to the impact of the accumulators' nitrogen discharge into the RCS at the end of the accumulators' blowdown. The main effects are the compression at the top of the downcomer as a result of nitrogen discharge into the cold leg and downcomer and condensation suppression in the loops and downcomer as a result of the presence of non-condensable gas.

The effect of accumulator nitrogen on the PWR reflood transient is evaluated in Section 20.1.4 by comparing ACHILLES and LOFT simulations with the respective test measurements. Comparisons with ACHILLES test data indicated that WCOBRA/TRAC-TF2 reasonably predicted the impact of nitrogen flow into the downcomer and the resulting in-surge of water into the core with the tendency to under-predict the downcomer pressurization and the subsequent core cooling effect.

Comparisons with LOFT L2-5 showed that the prediction of liquid discharge, the initial RCS pressurization, and the reflood/quench behavior was in good agreement with the measurement, though the code tended to under-predict the pressurization and the subsequent core cooling effect. The break flow increase due to the out-surge of liquid following the pressurization was over-predicted.

Based on the above comparison, the tendency to conservatively predict downcomer pressurization and the resulting effect on the heat transfer during the initial in-surge of water into the core leads to the conclusion that the effects of accumulator nitrogen injection will be reasonably calculated in a PWR LOCA transient without the need to explicitly account for this uncertainty in the analysis.

29.1.11 Uncertainty in Loop Seal Clearance Phenomenon

The loop seal (LS) starts to clear when the level formed in the downhill side of the pump suction piping reaches the top of the horizontal pipe. The timing of the onset is determined by the break flow, the vapor generation rate (boil-off rate) in the core, the condensation rate in the steam generator tubes, and the bypass flow rate. Once the clearing commences, because of the significant volume of vapor accumulated in the inner vessel, a relatively high vapor flow is maintained for a significant period of time such that a significant fraction or all of the liquid in the loop seal is swept to the cold leg. At larger break sizes, the vapor volumetric flow is large enough to clear the loop seal in multiple loops.

After a stable loop seal clearing, which may include a partially cleared loop, the remaining liquid in the cross-over leg (pump suction) affects the hydraulic resistance and thus the steam venting capacity following loop seal clearance.

The UPTF loop seal test is a quasi-steady state experiment. The test provides important full-scale single loop seal clearing separate effect data in a prototypic PWR geometry with well-defined boundary conditions. The assessment of the WCOBRA/TRAC-TF2 model against the UPTF loop seal test is discussed in Section 18. The conclusions from the assessment in Section 18 are [

]^{a,c}. Since horizontal stratification can affect the residual liquid mass after the loop seal clears and the pressure drop across the loop seal, a HS_SLUG sensitivity study is performed with the [

study is []^{a,c}. Figure 29.1.11-1 shows a comparison of the []^{a,c} The value chosen to

]^{a,c}.

For the purpose of a reasonable treatment of the uncertainty associated with the loop seal clearing event during a small break LOCA, [

]^{a,c}

[

] ^{a,c}

a,c

Figure 29.1.11-1 Residual Liquid Level from UPTF Loop Seal HS_SLUG Study

a,c

Figure 29.1.11-2 Break Spectrum Studies (3-loop PWR) Segregated Based on the Number and Which Loop Seals Clear

29.1.12 Steam Generator Thermal-Hydraulics

There are two important phenomena associated with the steam generator thermal-hydraulics which are significant for the purpose of modeling a small break LOCA scenario:

1. The primary-to-secondary heat transfer and condensation in U-tubes.
2. The flow regime, in particular the CCFL in the primary side.

29.1.12.1 Primary to Secondary Heat Transfer and Condensation Reflux

The primary to secondary side heat transfer was assessed based on the results of the simulation of the natural circulation test ST-NC-02, Section 21.9. Based on the results, it was concluded that, [

] ^{a,c}

29.1.12.2 Counter-current Flow Limitation (CCFL)

Assessment of the code's capability to predict counter-current flow in a small break LOCA was performed with calculated counter-current flow results extracted from simulations of a number of ROSA-IV LSTF tests, documented in more detail in Section 21.10. The overall effect of CCFL calculated at the steam generator U-tubes, hot leg elbow region and the upper core plate was evaluated in Sections 21.10.1, 21.10.2, and 21.10.3, respectively. The major conclusion made therein is that [

] ^{a,c}.

29.2 BREAK LOCATION, TYPE (SPLIT VS. DEGCL) AND SPLIT BREAK AREA

The objective of the Westinghouse FULL SPECTRUM LOCA methodology is to cover the spectrum of LOCA scenarios that are initiated by an instantaneous rupture of a RCS pipe. The break type considered is either a double-ended guillotine, defined as a complete severance of the pipe resulting in unimpeded flow from either end, or a split break, defined as a partial tear. The break size considered for a split break includes any break size such that break flow is beyond the capacity of the normal charging pumps up to and including a break flow area two times the cold leg pipe area.

Note that guidelines for acceptable method for the break modeling are provided in the Regulatory Position 3.1 – Second Paragraph, of Regulatory Guide 1.157. The main criteria are repeated here and divided in the following three paragraphs:

1. *“The calculations performed should be representative of the spectrum of possible break sizes from the full double-ended break of the largest pipe to a size small enough that it can be shown that smaller breaks are of less consequence than those already considered.”*
2. *“The analyses should also include the effects of longitudinal splits in the largest pipes, with the split area equal to twice the cross-sectional area of the pipe.”*
3. *“The range of break sizes considered should be sufficiently broad that the system response as a function of break size is well enough defined so that interpolations between calculations, without considering unexpected behavior between the break sizes, may be made confidently.”*

While it is acknowledged that RG 1.157 was written with focus on a Large Break LOCA scenario, there is not a reason that prevents the extension of these principles to cover the entire spectrum of break sizes and scenarios.

Section 2.3.1 provides further clarification on the LOCA scenario considered by the Westinghouse FSLOCA methodology. In particular with regard to the break location, any break is located always (conservatively) in a cold leg, while all other piping locations have been identified as being less limiting. Section 29.2.1 discusses []^{a,c}.

Break orientation relative to the cold leg (top, side or bottom) is another attribute that is expected to have some influence on the break flow via vapor pull-through (bottom) or entrainment offtake (top). This is known to have some effect, especially for relatively small break sizes.

The ROSA-IV program considered the effect of break orientation by running experiments of bottom, side, and top breaks. []

] ^{a,c}

[

] ^{a,c}

In summary the break uncertainty attributes in the methodology are postulated to be the following:

[

] ^{a,c}

The uncertainty on the break flow model is discussed in Section 29.1.1. The overall break modeling methodology is discussed here.

29.2.1 [] ^{a,c}

[

] ^{a,c}

29.2.2 Determination of the Minimum Break Area (A_{min})

Consistent with the FSLOCA EM scenario definition, the minimum break area should correspond to a break flow rate which can be compensated by the charging pump flow (i.e., charging pumps can maintain system inventory and pressure). Based on results from the plant break spectrum studies presented in Sections 27.1.1.3 and 27.1.2.3, core uncover is not expected for break diameters less than [

] ^{a,c}

29.2.3 Break Type and Split Break Area Uncertainty Methodology

Herein a methodology position for the treatment of the break type and, for a split break, the break area is developed.

One key difference between the previous LBLOCA methodology (ASTRUM EM, Nissley et al., 2005) and the FSLOCA methodology is that the FSLOCA methodology extends the break area spectrum considered in the analysis to cover the full range from what is historically defined as small breaks to large breaks including break sizes previously not analyzed and classified as intermediate breaks.

The approved approach in the ASTRUM EM (Nissley et al., 2005) considers both the break type (Split vs. DEGCL) and, for Split breaks, the break area as random variables during the Monte Carlo sampling procedure. The break type is first selected (with a 50/50 chance of Split vs. DEGCL) and for the split breaks, the area is uniformly sampled between [

] ^{a,c}.

For the treatment of break area in the FSLOCA EM the following two approaches were first considered:

Option 1 – [

] ^{a,c}

Option 2 – [

] ^{a,c}

[

] ^{a,c}

29.2.3.1 [

] ^{a,c}

[

] ^{a,c}

[

] ^{a,c}

29.2.3.2 [

] ^{a,c}

[

] ^{a,c}

29.2.3.3 Break Area Sampling Conclusion

The approach discussed herein provides an adequate coverage of all possible LOCA scenarios. [

] ^{a,c}

The uncertainty on the break flow rate prediction is treated as discussed in Section 29.1.1. The modeling methodology and treatment of model uncertainty for DEGCL and split breaks are described in Sections 29.2.4 and 29.2.5 respectively.

Table 29.2.3-1 [] ^{a,c}		
Parameter	Bias Value	Basis

a,c

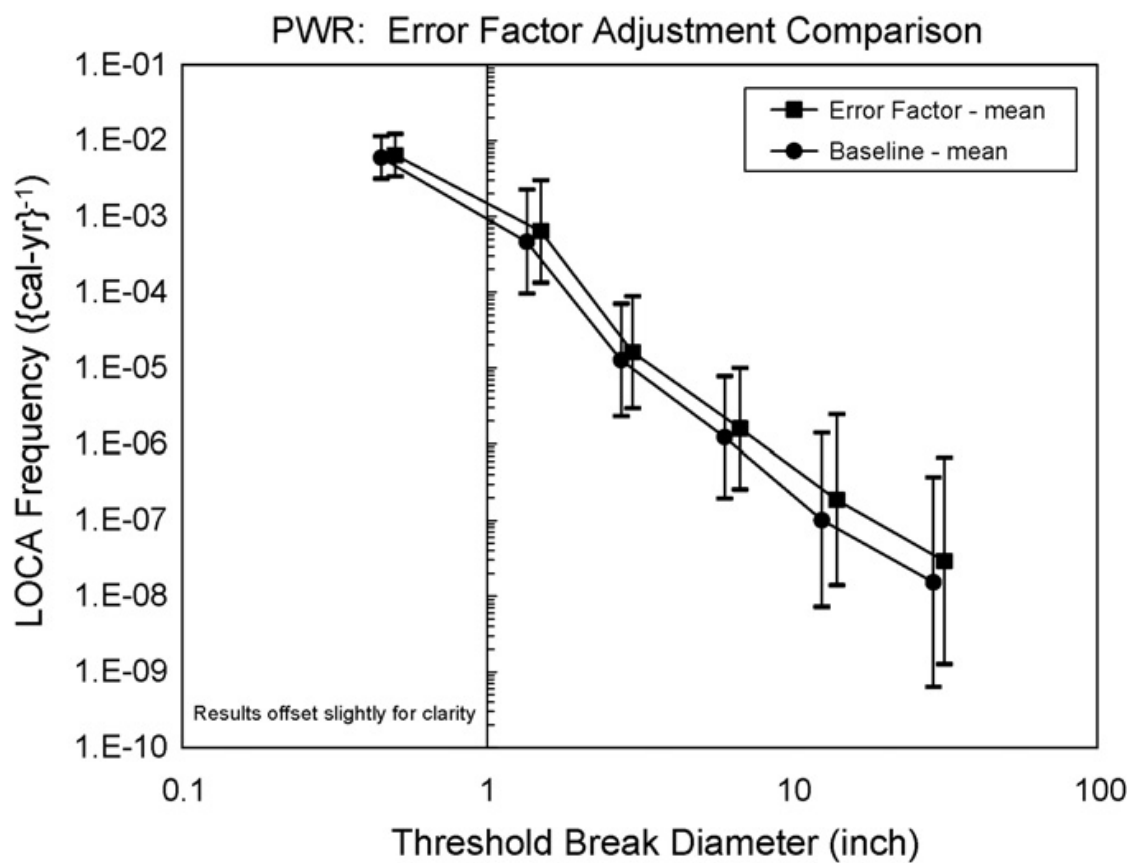


Figure 29.2.3-1 LOCA Frequency Evaluation Obtained using Expert Elicitation Presented by Tregoning, et al. (2007)

29.2.4 Modeling of DEGCL Breaks and Break Flow Uncertainty

The cold-leg double-ended guillotine break is modeled as shown in Figure 29.2.4-1. [

]^{a,c}

Discharge Coefficient Uncertainty Strategy

The guillotine break analysis requires explicit accounting for the uncertainties in break discharge flow. [

]^{a,c}

The values of [

]^{a,c}

Justification of CD Strategy

To confirm that this modeling approach achieved the desired change in flowrate, the same changes were made to the pipe model used to simulate the Marviken Test 6 experiment. The results are shown in Section 12.5.4.4, where Figure 12.5-12b confirms that discharge coefficients of 0.8 and 1.2 result in an observed 20% reduction and increase in break flow, respectively.

Figure 29.2.4-1 DEGCL Break Noding Scheme

Figure 29.2.4-2 Guillotine Break Noding Used in WCOBRA/TRAC-TF2

29.2.5 Modeling of Split Breaks and Break Flow Uncertainty

The size of a double ended guillotine break is fixed and equal to twice the cold leg cross sectional area. Therefore, any break which is smaller than twice the cold leg area is considered a split break. A large split break is possible only if the split is longitudinal. However, since there is no physical evidence that would indicate how such break types would appear (if they could in fact occur), the break geometry must be postulated.

Discharge Coefficient and Break Area Uncertainty Strategy

The nodding scheme of a broken cold leg pipe for a split break is shown in Figure 29.2.5-1. [

] ^{a,c}

As in the guillotine break, the code calculates the appropriate pressure drop using the TRAC momentum equations until the cell next to the break is reached. The acceleration to the throat where the flow is assumed to choke is calculated by the critical flow model.

[

] ^{a,c}

[

] ^{a,c}

Figure 29.2.5-1 Split Break Noding Scheme

a,c

Figure 29.2.5-2 Split Break Noding Used in WCOBRA/TRAC-TF2

a,c

Figure 29.2.5-3 Demonstration of CD1/CD2 Application for SPLIT Breaks

29.2.6 Compliance with Regulatory Guide 1.157 on Break Type and Size

Regulatory Guide (RG) 1.157 states the Nuclear Regulatory Commission's (NRC's) regulatory position on the break type and size for the requirement for best-estimate LOCA (BELOCA) analysis. In this section, the compliance of the revised BELOCA sampling methodology for break type and size to RG 1.157 is examined. The following statements are found in RG 1.157:

Regulatory Position 3.1 – Second Paragraph

“The calculations performed should be representative of the spectrum of possible break sizes from the full double-ended break of the largest pipe to a size small enough that it can be shown that smaller breaks are of less consequence than those already considered. The analyses should also include the effects of longitudinal splits in the largest pipes, with the split area equal to twice the cross-sectional area of the pipe. The range of break sizes considered should be sufficiently broad that the system response as a function of break size is well enough defined so that interpolations between calculations, without considering unexpected behavior between the break sizes, may be made confidently.”

Regulatory Position 3.4.1

“In analyses of hypothetical LOCAs, a spectrum of possible break sizes should be considered, as indicated in Regulatory Position 3.1. The discharge flowrate should be calculated with a critical flowrate model that considers the fluid conditions at the break location, upstream and downstream pressures, and break geometry. The critical flow model should be justified by comparison to applicable experimental data over a range of conditions for which the model is applied. The model should be a best-estimate calculation, with uncertainty in the critical flowrate included as part of the uncertainty evaluation. Best-estimate models will be considered acceptable provided their technical basis is demonstrated with appropriate data and analyses.”

Regulatory Position 3.15

“Break flow may be greatly influenced by the location and specific geometry of the break. For a break in a horizontal pipe containing stratified flow, the quality of the break flow will be a strong function of the assumed location of the break on the pipe (e.g., top or bottom). Small break loss-of-coolant accident calculations should, therefore, include various assumed break locations in the spectrum of breaks analyzed.”

Considering Regulatory Position 3.1, strict compliance with this position has been demonstrated in Section 29.2.3 by [

] ^{a,c}

Considering Regulatory Position 3.4.1, the worst location of the break that results in the highest PCT and MLO was found [

] ^{a,c}

Considering the remarks specific to small break LOCAs in Regulatory Position 3.15, the specific geometry of the break cannot be determined. Therefore, the [

] ^{a,c} In addition, the orientation of the break was explored in the context of the ROSA experiments and WCOBRA/TRAC-TF2 simulations (Section 21.7), and PWR plant scoping studies (Section 28.2.7). Break orientations on the top, side, and bottom of the pipe were considered. [

] ^{a,c}

29.3 REVIEW OF PLANT SCOPING STUDIES AND UNCERTAINTY IN PLANT INPUT PARAMETERS

A review of the uncertainty associated with plant specific inputs and the treatment of those uncertainties in the FSLOCA methodology is discussed in this section. The plant input parameters and modeling approach were introduced in Section 26. Section 28 presented PWR sensitivity studies performed to identify or confirm the ranging required of potential contributors to uncertainty. A summary of the results is provided at the beginning of Section 28.

The plant input parameters treated in a bounding nature (Section 29.3.1) or as an uncertainty parameter (Section 29.3.2) are discussed in this section.

29.3.1 Bounded Parameters

The previous Westinghouse realistic LBLOCA EM (ASTRUM EM, Nissley et al., 2005) included the use of “confirmatory studies” to determine the limiting value of the following parameters for the reference transient:

- Offsite power availability
- Steam generator tube plugging level (maximum vs. minimum)
- Relative power of peripheral assemblies (maximum vs. minimum)

and, in some cases,

- Average fluid temperature in the reactor coolant system (maximum vs. minimum, if the plant being analyzed has an allowable range for the nominal value)

In addition, the confirmatory studies served to derive an appropriate (conservatively low) containment backpressure for use in the uncertainty analysis.

The limiting hot assembly location was also determined from a detailed examination of the upper plenum geometry. The location of the hot assembly is mainly important during a LBLOCA. A similar procedure to identify the limiting location is followed in the FSLOCA EM and the location is used consistently in both Region I and Region II analyses.

The “confirmatory” approach was originally developed for the Code Qualification Document (CQD) EM (Bajorek et al., 1998), which used response surfaces based on limited parametric studies of the global system response to dominant parameters. In the CQD EM, the reference transient played a major role in that the effect of variations in the dominant parameters was expressed as a difference in the PCT relative to the reference transient PCT.

In the ASTRUM EM (Nissley et al., 2005), the reference transient had much less significance. The confirmatory studies were still used to determine the limiting value of the above parameters and to derive an appropriate containment backpressure, but the use of non-parametric order statistics eliminated the use of the reference transient in the statistical combination of uncertainties; the reference transient PCT had no direct influence on the analysis.

With the introduction of the FULL SPECTRUM LOCA EM, the method used to treat the above parameters has been re-examined. The treatment of each of these parameters in the FULL SPECTRUM LOCA EM is as described below.

Offsite Power Availability

The treatment of offsite power availability is an integral part of the FULL SPECTRUM LOCA uncertainty methodology. [

] ^{a,c} Details of the Region II treatment are described in
Section 30.4².

Steam Generator Tube Plugging Level

[

] ^{a,c}

² The approach described in Section 30.4 to determine the [^{a,c} is superseded by limitation and condition #15 from the safety evaluation report (SER).

Relative Power of Peripheral Assemblies

Standard core design practice is to minimize neutron leakage from the reactor core by placing assemblies on the periphery that have already been irradiated for at least one cycle. The average power of the peripheral assemblies typically varies by only a small amount from cycle to cycle. Furthermore, historical studies have shown that power in the peripheral assemblies (PLOW) has a limited impact on analysis results. Core physics predictions for the plant being analyzed will be reviewed, [

] ^{a,c}

Average Fluid Temperature in the Reactor Coolant System

If the plant being analyzed has an allowable range for the nominal value, the entire range will be sampled in the uncertainty analysis for both Region I and Region II. Uncertainty in the measurement will also be included to augment the range beyond that of the allowable range for the nominal.

Containment Backpressure

[

] ^{a,c}

29.3.2 Initial and Boundary Conditions (Ranged Parameters)

The following are the parameters selected to describe the primary fluid conditions (RCS and ECCS), as discussed in Section 25.2.2.2.

- a. Average fluid temperature
- b. Pressurizer pressure
- c. Loop flowrate
- d. Upper head fluid temperature
- e. Pressurizer level
- f. Accumulator water temperature
- g. Accumulator pressure
- h. Accumulator water volume
- i. Accumulator line resistance
- j. Accumulator boron concentration

The range of variation of the operating parameters is accounted for in the uncertainty analysis. This is accomplished by assuring that, in the sampling of the attributes for each run (Section 31), the normal operating range is bounded. Table 29-5 presents the list of parameters that are statistically sampled in a typical analysis.

Items (a) and (b) are ranged according to measurement uncertainty. Item (c) tends to be well-controlled and measured, so the nominal thermal design flow is used. Item (d) is implicitly ranged through its relationship with the average fluid temperature, discussed in Section 25.2.2.2. Because pressurizer level, Item (e) is tightly controlled relative to the average fluid temperature, it is also ranged consistently with variations in RCS average temperature.

Parameters related to the accumulator, items (f) through (i), are ranged according to plant-specific data. Specific to the line resistance, accumulator blowdown tests have been performed at dozens of plants as part of the standard plant startup testing. Standard procedures are to perform these tests for each RCS loop. The uncertainty of the line resistances measured in these tests is estimated to be about []^{a,c}. For those plants for which measured accumulator line resistances are not readily available, it is considered acceptable to use the calculated resistance as the nominal value. Westinghouse calculates accumulator line resistances using the charts in (Crane, 1969). Comparisons of pre-test calculations and test results were made for a number of plants. Table 29.3.2-1 shows that the calculations typically over-predict the measurements, conservative for large breaks in that the prediction of lower plenum and downcomer refill is delayed. For the ACHILLES test facility, the uncertainty estimated for the accumulator line resistance was 10% (Table 2.2 of Holmes, 1991). [

] ^{a,c}

As described in Section 25.2.2.2, while accumulator boron concentration, Item (j), is not likely to have a significant effect on the LOCA PCT, it is modeled at its nominal value without uncertainty to ensure that recriticality does not occur in the short-term following a LOCA. [

] ^{a,c}

Those uncertainty treatments are consistent in both the Region I and Region II uncertainty analyses.

Table 29.3.2-1 Comparison of Measured and Calculated Accumulator Line Resistances

a,c

29.3.3 Uncertainty Associated with Maximum Time Step Size

In WCOBRA/TRAC-TF2, a maximum allowable time step size is set by the user through the DTMAX input. In addition to the numerical convergence criteria covered in Section 3.6.5.3, the DTMAX input, in combination with the analogous minimum time step size input DTMIN, defines for the code the range of allowable time step size. The size of the time step employed by the code is then determined for each time step by the promotional and inhibitive algorithms described in Section 3.6.5.3, with a general tendency to promote (increase) the time step for increased computational efficiency. In the DTMAX range typically used to achieve reliable numerical convergence in the plant analyses, the maximum time step limit is often more restrictive than the limits imposed by the convergence criteria. As a result, WCOBRA/TRAC-TF2 uses DTMAX as the time step throughout significant portions of the transient.

The effect of the choice of DTMAX was demonstrated for UPTF Test 6 in Section 19.3.5.9. Varying DTMAX []^{a,c} did not result in a clear effect on the ECC penetration delay, and conservatism relative to the test data was observed for all DTMAX values.

A sensitivity of the CCTF Test 62 prediction in Section 19.6.6 showed that an increase in DTMAX to []^{a,c} had negligible impact on the predictions, and the overall conservatism regarding cladding temperatures at the upper elevations was preserved.

The impact of DTMAX on reflood heat transfer predictions was also investigated using the FLECHT SEASET test series as described in Section 15.8. It was observed that varying DTMAX []^{a,c} had minimal impact on the PCT and quench front progression for the lowest and highest flooding rate tests.

Section 28.1.3 presents a DTMAX sensitivity study of the V. C. Summer and Beaver Valley Unit 1 reference large break spectra. It is observed there that DTMAX values []^{a,c}

Section 28.2.4 presents a DTMAX study of the reference small break spectra. DTMAX values []^{a,c} are not observed to introduce significant bias or additional uncertainty.

[]^{a,c} a Monte Carlo uncertainty analysis is implemented to combine the uncertainties and predict an upper bound to the 95th quantile PCT, MLO, and core-wide oxidation (CWO) (see Section 30). For any given transient, there exists inherent uncertainty in phenomena (e.g., initial surge for LBLOCA), the prediction for which is observed to differ somewhat depending on the choice of DTMAX. In the analysis, a choice of DTMAX is made and is applied in all transients. []^{a,c}

29.4 CORE AND FUEL ROD MODEL UNCERTAINTIES

29.4.1 Initial Reactor State Uncertainties

29.4.1.1 Time in Cycle

[

] ^{a,c}

Hot Rod Burnup

[

] ^{a,c}

[

] ^{a,c}

[

] ^{a,c}

Hot Assembly Rod Burnup

[

] ^{a,c}

Core Balance Rods Burnup

[

] ^{a,c}

In summary, [

] ^{a,c}

29.4.1.2 Reactor Core Power Distributions and Global Uncertainties

Reactor core power distributions are characterized by radial and axial power distributions, as discussed in Section 25.2.1. The steady-state radial distribution is established by core loading pattern, fuel enrichment, fixed burnable poisons, etc., and is not subject to wide variation during normal operation (Section 25.2.1.1). The maximum of the radial distribution is defined by $F_{\Delta H}$ (hot rod average power divided by the core average rod average power). Predictions of $F_{\Delta H}$ are accurate to within [^{a,c} at > 95 percent probability (Section 25.2.1.3). [

] ^{a,c}

Steady-state axial distributions are established by core loading pattern and burnup. The axial distribution tends to vary widely as a result of changes in reactor power, xenon transients, boron or control rods. The maximum of the radial distribution times maximum of the axial distribution is F_Q (maximum linear heat rate divided by the core average linear heat rate). Transients are simulated in the core design process, yielding a wide range of possible power distributions and F_Q values. As described in Section 25, [

] ^{a,c}

Plants operate in “baseload” (i.e., full power, control rods out) nearly all the time. In baseload operation, F_Q varies slowly with time. However, the Technical Specifications allow for transient operation. Figure 29.4.1-4 shows the effect of a typical load follow maneuver on peaking factor ($F_Q \times \text{power}$), for a plant with a Technical Specification F_Q limit of [^{a,c}. In the Westinghouse FSLOCA methodology, [

] ^{a,c}

[

] ^{a,c}

[

] ^{a,c}

[

] ^{a,c}

Other sources of uncertainty in the power related parameters involve: 1) the accuracy with which the power distribution in the hot assembly and remainder of the core can be defined; 2) the accuracy with which the power at the hot spot (most limiting elevation of the hot rod) can be defined, including local uncertainties. The latter is addressed in Section 29.4.2.

The following contributors are considered, [

] ^{a,c}.

- Radial power distribution
- Total peaking factor and axial power distribution
- Initial core power level
- Decay heat
- Gamma redistribution

Radial Power Distribution

The hot assembly and core radial power distribution is modeled by defining the following variables:

- Hot rod average relative power, $F_{\Delta H}$. The hot rod average relative power, $F_{\Delta H}$ will be ranged according to its calculational uncertainty. This global uncertainty (without assembly radial peaking), as shown in Table 25.2-2, has a standard deviation equal to [] ^{a,c} of the nominal value.

- Hot assembly average power is [$P_{HA}^{a,c}$] lower than hot rod $F_{\Delta H}$, [$P_{HR}^{a,c}$]
- Power in the assemblies in the core periphery, as a percent of average assembly power ([$P_{HA}^{a,c}$] are typical lower and upper bounds). Variations in this parameter will have a small effect on the power of the core average rods surrounding the hot assembly. [$P_{HA}^{a,c}$]

Total Peaking Factor and Axial Power Distribution

As previously discussed, the axial power distribution is [$P_{HA}^{a,c}$]. The initial power generation rate, as a function of elevation, is specified for the hot rod by the initial axial and radial power distributions (peaking factors F_Q and $F_{\Delta H}$) on the hot rod. The uncertainty associated with the total peaking factor F_Q (Tables 25.2-2 and 25.2-3) can be divided into two components; one closely coupled to the uncertainty in the hot assembly power, and one associated only with local uncertainties and therefore independent of the hot assembly. Since there is a fixed radial power distribution in the assembly, a fluctuation in the hot assembly power results in a similar fluctuation in the hot rod. This situation is illustrated in Figure 29.4.1-12. Fluctuations in the hot assembly rod are assumed to also affect the thermal-hydraulics (i.e., they affect the heat transfer coefficient boundary condition), and so the uncertainties are considered in the global thermal-hydraulic solution accordingly. [$P_{HA}^{a,c}$]

[$P_{HA}^{a,c}$]

Initial Core Power, Decay Heat, Gamma Redistribution

The remaining variables, core average power, gamma redistribution, and decay heat, contribute additional uncertainty to the peak linear heat rate. The uncertainty in core power ($AFLUX_0$, [$P_{HA}^{a,c}$]) was quantified in Section 25.2.1.3. Increases (decreases) in $AFLUX$ result in proportional increases (decreases) in rod powers for all rods as described in Section 25.2.1.4.

Uncertainty in decay heat is considered through the application of ANSI/ANS 5.1-1979 Standard (DH, normal distribution). See also Section 9.7. [$P_{HA}^{a,c}$]

[$P_{HA}^{a,c}$]

[

] ^{a,c}

Table 29.4.1-1 [] ^{a,c}	

a,c

Figure 29.4.1-1 Maximum Rod Average Power at a Given Rod Burnup at Various Times During a Typical Cycle



Figure 29.4.1-2 | **a,c**

**Figure 29.4.1-3 Fuel Pellet Average Temperatures as a Function of Rod Average Burnup
for 0.422-inch Outer Diameter Fuel**

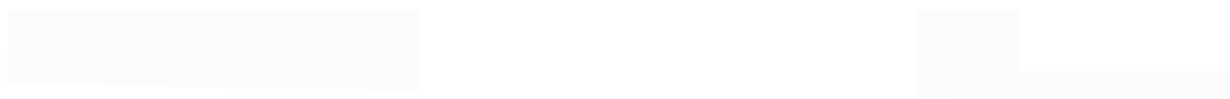


Figure 29.4.1-4 Effect of Load Follow on F_Q

a,c

Figure 29.4.1-5 [

] a,c

a,c

Figure 29.4.1-6 [

] ^{a,c}

a,c

Figure 29.4.1-7 [

] ^{a,c}

a.c

Figure 29.4.1-8 [

] ^{a,c}

Figure 29.4.1-9 Example Bottom Skewed Axial Power Distribution [
]^{a,c}

a,c

Figure 29.4.1-10 Example Top Skewed Axial Power Distribution [
]^{a,c}

a,c

Figure 29.4.1-11 [

] ^{a,c}

a,c

Figure 29.4.1-12 [

]^{a,c}

29.4.2 Hot Rod Local Models Uncertainty

Beside the uncertainty in hot rod local power discussed in the previous section, several other uncertainty contributors in the fuel rod models and heat transfer from the rod to the fluid contribute to the local hot spot uncertainty.

The fuel rod modeling was presented in Sections 8.3 through 8.6. These included the fuel conduction model, the pellet-cladding gap conductance model, the fuel rod deformation model, the cladding reaction with water or steam models, and []^{a,c}. The heat transfer from the fuel rod to the fluid was discussed in Section 7 and its assessment is provided in Sections 14 and 15.

The discussion in Sections 7 and 8 focuses on the models as coded, while here the discussion is expanded to describe the treatment of the uncertainty associated with those models.

In particular, the following contributors are considered:

- Hot rod peaking factor
- Hot rod radial peaking, manufacturing tolerances, and rod bow uncertainties
- []^{a,c}
- []^{a,c}
- Cladding burst temperature
- Cladding burst strain
- []^{a,c}
- Zirconium-water reaction
- Fuel relocation
- Convective heat transfer coefficient from the rod to the fluid

Models are considered ‘local’ when the effect of the uncertainty in those models has an effect limited to local processes, such as the local cladding temperature or local cladding oxidation, while the impact of such uncertainties on the ‘global’ thermal-hydraulic process is negligible. The hot rod peaking factor uncertainty reflects the power difference between the hot rod and the hot assembly rod. The additional uncertainty related to hot rod radial peaking, manufacturing tolerances, and rod bow is captured by the local linear heat rate uncertainty. []

[]^{a,c} The uncertainties in the cladding burst

temperature, the cladding burst strain, []^{a,c}, Zirconium-water reaction, fuel relocation, and convective heat transfer coefficient are incorporated into []^{a,c}.

In the previous ASTRUM EM (Nissley et al., 2005) the WCOBRA/TRAC solution was followed by the execution of a one-dimensional conduction code (HOTSPOT) [

] ^{a,c}

HOTSPOT is essentially a one-dimensional conduction code used to resolve the heat conduction []^{a,c}. Driven by boundary conditions on the fluid side calculated with WCOBRA/TRAC, HOTSPOT was used to simulate the transient conduction []^{a,c}. The models in HOTSPOT were consistent with the corresponding models in WCOBRA/TRAC.

[

] ^{a,c}

The uncertainty methodology for the heat transfer coefficients will be discussed in more detail in Section 29.4.3. The FSLOCA EM for modeling the hot assembly rods was discussed in Section 8 and is briefly summarized here:

[

] ^{a,c}

[

] ^{a,c}

29.4.2.1 [

] ^{a,c}

[

] ^{a,c}

[

] ^{a,c}

Fuel Internal Heat Generation – Local Uncertainty

As discussed in Section 29.4.1.2, the uncertainty in total peaking factor F_Q is comprised of components that are global in nature, and hence are closely coupled with hot assembly power, and components that are local in nature. The local uncertainties, which do not affect the global thermal-hydraulic solution, are accounted for [^{a,c}. From Tables 25.2-2 and 25.2-3, the local uncertainties in the local heat generation arise from the combination of [^{a,c}. The total standard deviation (σ) can be expressed as:

$$\left[\begin{array}{c} \text{ } \\ \text{ } \end{array} \right]^{a,c} \quad (29.4.2-1)$$

[

] ^{a,c} The local uncertainty amounts to:

$$\left[\begin{array}{c} \text{ } \\ \text{ } \end{array} \right]^{a,c} \quad (29.4.2-2)$$

where,

[

] ^{a,c}

Cladding Burst Temperature

The rupture criteria for Zircaloy-4 cladding and ZIRLO[®] cladding introduced in Section 8.4.1 are applicable for both the hot assembly rod and [^{a,c}.

Cladding burst is calculated by monitoring the stress on the cladding and using the cladding rupture correlations to predict the rod burst as described in Section 8.4. The cladding burst temperature can be correlated fairly well as a function of hoop stress for ZIRLO[®] cladding as shown in Figure 8-19 in Section 8.4. Figure 29.4.2-1 is a replication of Figure 8-19 with a band of [^{a,c} of the calculated burst temperature shown. The [^{a,c}.

The []^{a,c} uncertainty range on cladding burst temperature (Fahrenheit) is used for both Zircaloy-4 and ZIRLO[®] cladding. The ZIRLO[®] cladding data shown in Figure 29.4.2-1 actually indicates a smaller uncertainty than the assumed []^{a,c}. These data were obtained by Westinghouse using a consistent testing method. The zircaloy data from Powers and Meyer (1980), which were used to develop the zircaloy burst temperature and burst strain models in Section 8.4.1, show scatter more consistent with the []^{a,c} range (Figure 1 of Powers and Meyer, 1980). This is believed to be at least partly attributable to the variety of testing methods used to obtain the Zircaloy-4 data. Although it is believed that the ZIRLO[®] cladding testing methods are as valid as those in Powers and Meyer, there may be some uncertainty due to the testing method, and the larger uncertainty for both cladding materials is used.

[

] ^{a,c}

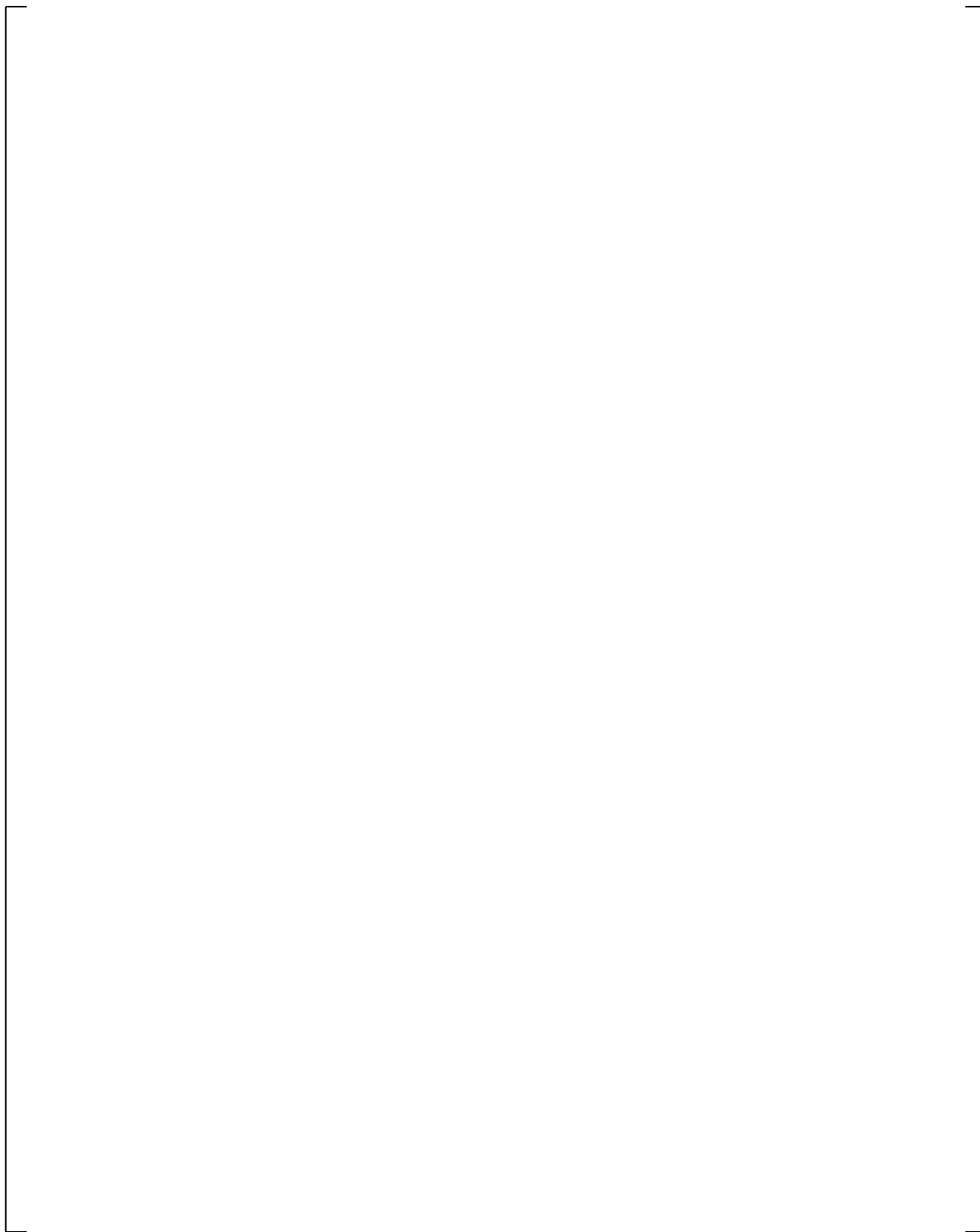


Figure 29.4.2-1 ZIRLO® Cladding Burst Temperature Data and Correlation

Cladding Burst Strain

The burst strain discussed in Section 8.4, as shown in Figures 8-18 and 8-20 for the respective Zircaloy-4 and ZIRLO[®] cladding, is applied to the hot assembly rod. However, the data in Figures 8-18 and 8-20 show wide scatter. Burman (1980) discussed how burst occurs randomly at “hot spots” which are the results of a wide range of azimuthal temperature gradients around the cladding. Burman also argued that in fuel rods these gradients can be larger due to random contact of the pellet against the cladding, which then causes smaller burst strains to occur.

For the cladding burst strain of the []^{a,c}, Figures 29.4.2-2 and 29.4.2-3 revisit the data of maximum burst strain as a function of burst temperature for the Zircaloy-4 and ZIRLO[®] cladding at different heatup rates to identify the influence of heat up rate. In both cases, the scatter is very large for both alpha phase and beta phase, and low uncertainty for the alpha/beta transition region is observed. Thus, three burst temperature ranges are identified: []

[]^{a,c} Figures 29.4.2-4 to 29.4.2-6 show the Zircaloy-4 burst data in the form of histograms for burst temperature ranges []^{a,c}, indicating the frequency of occurrence of a particular burst strain within a range of burst temperatures. []

[]^{a,c} except for the difference in the transition temperature. The effect of heatup rate on cladding strain is evident []

[]^{a,c}

[

$$\left[\begin{array}{c} \\ \end{array} \right]^{a,c} \quad \left[\begin{array}{c} \\ \end{array} \right]^{a,c} \quad (29.4.2-3)$$

[

$$\left[\begin{array}{c} \\ \end{array} \right]^{a,c} \quad \left[\begin{array}{c} \\ \end{array} \right]^{a,c} \quad (29.4.2-4)$$

$$\left[\begin{array}{c} \\ \end{array} \right]^{a,c} \quad \left[\begin{array}{c} \\ \end{array} \right]^{a,c} \quad (29.4.2-5)$$

[

$$\left[\begin{array}{c} \\ \end{array} \right]^{a,c} \quad \left[\begin{array}{c} \\ \end{array} \right]^{a,c} \quad (29.4.2-6)$$

[

] ^{a,c}

a,c

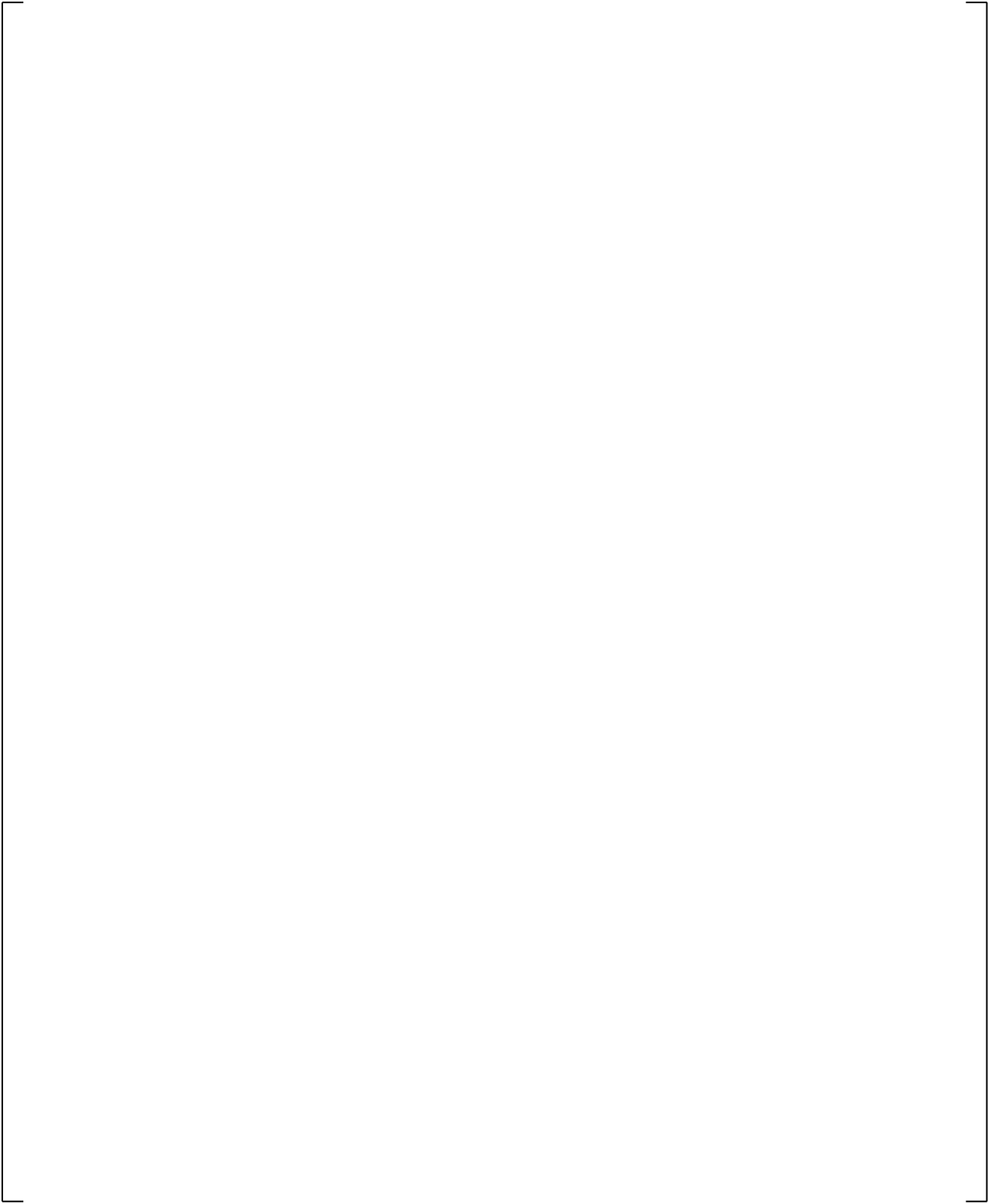


Figure 29.4.2-2 [

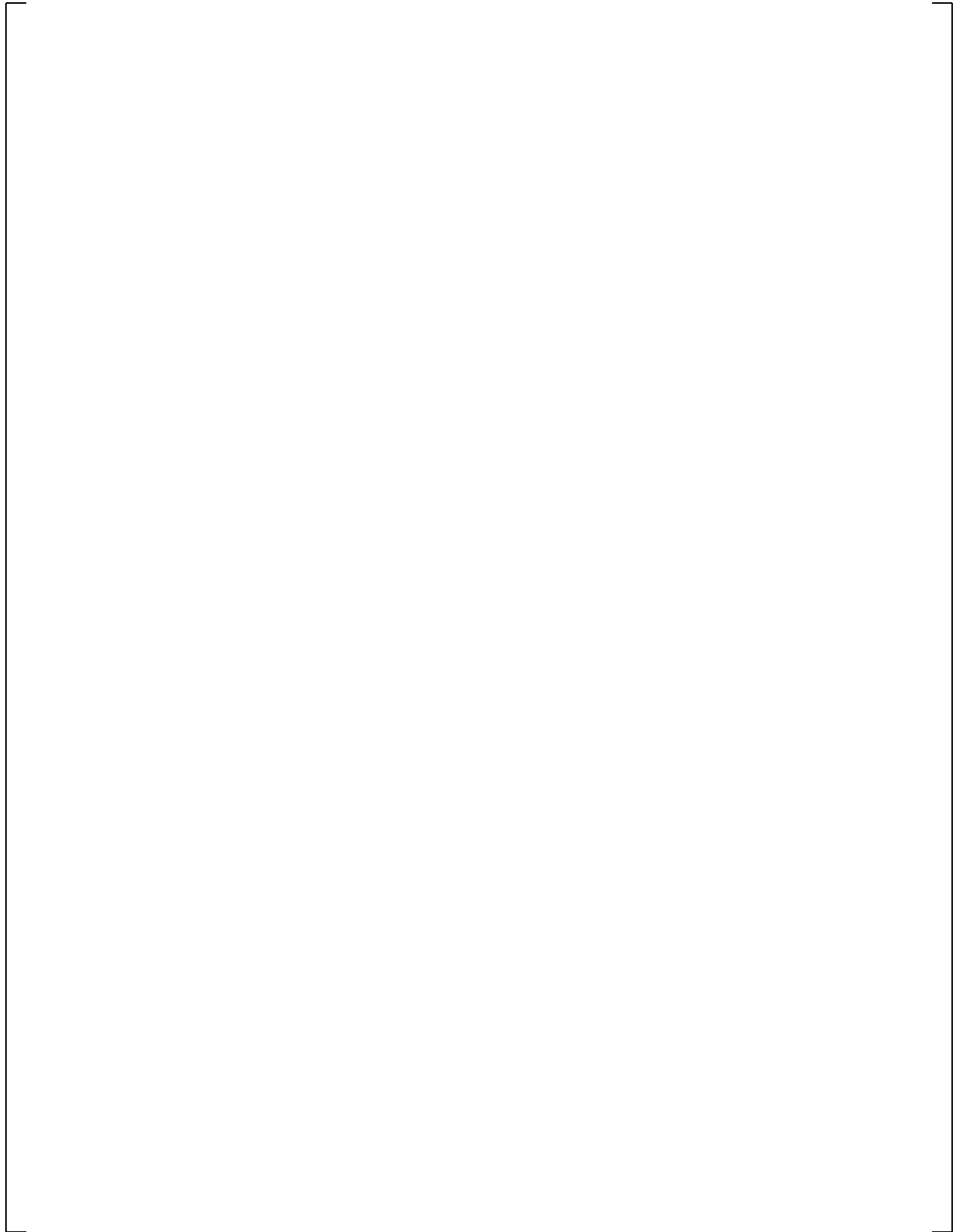
] ^{a,c}

a,c

Figure 29.4.2-3 [

]^{a,c}

a,c

**Figure 29.4.2-4 [****]^{a,c}**

a,c

Figure 29.4.2-5 [

] ^{a,c}

a,c

Figure 29.4.2-6 [

]^{a,c}

a,c

Figure 29.4.2-7 [

]^{a,c}

a,c

0

Figure 29.4.2-8 [

] a,c

Figure 29.4.2-9 [

] ^{a,c}

a,c

Figure 29.4.2-10 [] ^{a,c}

Fuel Relocation Following Burst

The phenomenon of fuel relocation following cladding burst was discussed in Section 8.6.1. The fuel density at the burst region of []^{a,c} is measured by the packing fraction. The packing fraction is the ratio of the volume of fuel within the burst region to the total volume within the burst region. INEL (Broughton, 1981) studied data from several sources and used several measurement methods. In addition, NNC performed additional analyses using photographs of the fuel cross sections. These data are summarized in Table 29.4.2-1. A plot of this data versus burst strain (Figure 29.4.2-11) appears to confirm []

[]^{a,c}. From these different measurement methods, the uncertainty on packing fraction was estimated.

The numbers of occurrences as a function of packing fractions are plotted in Figure 29.4.2-12. The range was calculated by taking the difference between the maximum and minimum value, and dividing by the average value. A histogram of the data is shown in Figure 29.4.2-12. []

[]^{a,c}

Table 29.4.2-1 Packing Fractions Using Various Measurements				
Burst Strain Percent	Packing Fractions Percent (Various Measurement Methods)			
29	79	70	66	65
35	63	70	42	63
42	71	67	59	58
47	71	—	62	—
48	62	70	61	74
74	66	—	52	—



Figure 29.4.2-11 []^{a,c}



Figure 29.4.2-12 Distribution of Packing Fraction Data

Zirconium-Water Reaction and its Uncertainty

The zirconium-water reaction rate calculations are performed using methods described in Section 8.5.

When [

] ^{a,c} from

Cathcart and Pawel (1977). The prediction interval at 95 percent probability for this equation was calculated from the data using the following equation (Draper and Smith, 1981):

$$Y + t(95\%, n-2) \left[1 + \frac{1}{n} + \frac{(X - \bar{X})^2}{\sum (X_i - \bar{X})^2} \right]^{1/2} s \quad (29.4.2-7)$$

Where $t(95\%, n-2)$ is the 95th percentage point of a t-distribution with $n-2$ degrees of freedom, to account for sample size, \bar{X} is the average of the X values, and s^2 is the residual mean square of the data around the reaction equation line. The equation above is the prediction interval for the next “point estimate” of the reaction rate; the uncertainty interval for the prediction of the mean of the data is smaller (the equation is similar to that above except that the 1 is missing).

The “uncertainty” cited in [

] ^{a,c} A model is assumed of the form:

$$\ln(\delta^2 / 2) = A + B(1 / T(K)) \quad (29.4.2-8)$$

The regression output is shown in Table 29.4.2-2b. The output shows that the constants A and B are:

[
] ^{a,c}

These numbers compare to those in Table A2 of Cathcart and Pawel:

$$\begin{aligned} A &= -1.70986 \\ B &= -20100 \end{aligned}$$

[

] ^{a,c}

$$\begin{aligned}
 & \left[\begin{array}{c} \\ \\ \\ \end{array} \right]^{a,c} \\
 & \left[\begin{array}{c} \\ \\ \\ \end{array} \right]^{a,c} \\
 & \left[\begin{array}{c} \\ \\ \\ \end{array} \right]^{a,c} \\
 & \left[\begin{array}{c} \\ \\ \\ \end{array} \right]^{a,c} \\
 & \left[\begin{array}{c} \\ \\ \\ \end{array} \right]^{a,c}
 \end{aligned}$$

Pre-Accident Corrosion

NRC Information Notice (IN) 98-29 (Roe, 1998) provides clarification that the 10 CFR 50.46(b)(2) maximum local oxidation criterion of 17% “includes both pre-accident oxidation and oxidation occurring during a LOCA.” In the FSLOCA uncertainty methodology, therefore, ‘MLO’ results are the sum of the two. At high rod average burnup, the uncertainty in pre-accident corrosion can become important when comparing the total calculated MLO against the 17% limit.

The approved corrosion models for ZIRLO[®] and Optimized ZIRLO[™] cladding (Garde et al., 2013) are incorporated into the PAD5 code as described in Section 3.3.1 of Crede et al. (2013). The corrosion models were developed based on rod oxide measurements collected from cladding material in post-irradiation exams (PIEs), including data from operating plants. A calibration database was used to develop the model forms and for the determination of the final model coefficients, and a separate validation database was used to independently validate the models.

The corrosion model uncertainties were determined as a function of predicted thickness in order to cover 95% of the data over the entire measurement range. The actual uncertainty equation bounds more than 95% of the calibration data set.

To address IN 98-29 in the FSLOCA EM, [

$$]^{a,c}$$

Table 29.4.2-2a Zircaloy Rate Constants (Total Oxygen)				
T(°C)	$\delta^2/2=OX$	1/T(K)=X	(X-XBAR)²	LN(OX)=Y
1050	4.720E-08	0.000755	1.109E-08	-16.8689
1101	8.070E-08	0.000727	5.968E-09	-16.3325
1153	1.390E-07	0.000701	2.573E-09	-15.7888
1203	2.180E-07	0.000677	7.274E-10	-15.3388
1253	3.300E-07	0.000655	2.280E-11	-14.9242
1304	5.080E-07	0.000634	2.694E-10	-14.4928
1352	7.690E-07	0.000615	1.235E-09	-14.0782
1404	1.130E-06	0.000596	2.940E-09	-13.6933
1454	1.640E-06	0.000578	5.109E-09	-13.3208
1504	2.280E-06	0.000562	7.704E-09	-12.9913
NTESTS:		XBAR:	$\Sigma(X-XBAR)^2$:	
10		0.000650	3.764E-08	

Table 29.4.2-2b []^{a,c}	

a,c

[illegible]

a,c

Figure 29.4.2-13 [**]**^{a,c}

Figure 29.4.2-14 [**]**^{a,c}

29.4.2.2 Initial Calibration of the Steady-State Condition for the Nuclear Rods

The initial fuel temperature and rod internal pressure for Westinghouse PWRs and CE PWRs are calibrated against the NRC-approved version of the PAD5 fuel performance code (Crede et al., 2013, as-submitted). The calibration of initial fuel temperature is performed for [$T^{a,c}$] in FSLOCA.

The initial stored energy in the fuel is a direct function of the pellet average (radial) fuel temperature which is called TFUEL. The initial fuel temperature is a function of the local linear heat rate and burnup.

[

$$[\begin{matrix} & & T^{a,c} & \\ & [& &]^{a,c} \\ & & L^{a,c} & \end{matrix}]^{a,c} \quad (29.4.2-9)$$

$$[\begin{matrix} & & & \\ & [& &]^{a,c} \\ & & L^{a,c} & \end{matrix}]^{a,c} \quad (29.4.2-10)$$

[

$T^{a,c}$

[

[

[

[

] ^{a,c}

[

] ^{a,c}

] ^{a,c}

] ^{a,c}

(29.4.2-11)

(29.4.2-12)

] ^{a,c}

29.4.3 Fuel Rod: Uncertainty on Heat Transfer to the Fluid

The methodology for uncertainty propagation considers, in addition to fuel rod model and minimum film boiling temperature uncertainties, the local variation in heat transfer from the nuclear rod to the fluid. There are several heat transfer regimes that affect the cladding temperature during a postulated LOCA accident, which depend on the fluid conditions as well as the cladding temperature itself. Models are included in the code to characterize each heat transfer regime, as described in Section 7. During a simulation, models are properly selected depending on the local flow regime, void fraction and surface temperature. Such models have been derived from a large data base which describes the fundamental heat transfer processes. The heat transfer package is then validated and assessed against prototypical data which was intended to recreate conditions expected in the reactor core during an accident, as discussed in Sections 14 and 15.

[

29.4.3.1 Heat Transfer Multipliers for [

[

] ^{a,c}

[

] ^{a,c}

(29.4.3-1)

[

] ^{a,c}

[

] ^{a,c}

(29.4.3-2)

[

] ^{a,c}

[

$$\left[\frac{h_a}{h_c} \right]^{a,c} \quad (29.4.3-3)$$

29.4.3.2 Heat Transfer Multipliers for [

] ^{a,c}

[

$$\left[\frac{h_a}{h_c} \right]^{a,c} \quad (29.4.3-4)$$

[

$$\left[\frac{h_a}{h_c} \right]^{a,c} \quad (29.4.3-5)$$

[

$$\left[\frac{h_a}{h_c} \right]^{a,c} \quad (29.4.3-6)$$

or,

$$\left[\frac{h_a}{h_c} \right]^{a,c} \quad (29.4.3-7)$$

[

$]^{a,c}$

29.4.3.3 Heat Transfer Multipliers for [

$]^{a,c}$

[

$]^{a,c}$

[

$]^{a,c}$

(29.4.3-8)

where,

[

$]^{a,c}$

(29.4.3-9)

(29.4.3-10)

and,

[

$]^{a,c}$

(29.4.3-11)

[]^{a,c}
(29.4.3-12)

[

]^{a,c}

[]^{a,c}
(29.4.3-13)

[

]^{a,c}

[

 $]^{a,c}$

[

 $]^{a,c}$

(29.4.3-14)

29.4.3.4 Hot Rod versus [**$]^{a,c}$ Heat Transfer Coefficient Application**

[

 $]^{a,c}$

[

] ^{a,c}

29.4.3.5 Effect of Rod-to-Rod Radiation Heat Transfer

Section 15 documents the assessment of the WCOBRA/TRAC-TF2 heat transfer logic for several rod bundle heat transfer experiments. Given the limited size of the experimental test sections, the presence of the housing and any thimbles and unheated rods may affect the overall heat transfer by enhancing the radiation heat flux from the rod to the cooler housing, thimble and/or rod (termed rod-to-rod radiation herein). Such phenomenon cannot be neglected in the overall heat transfer assessment.

[

] ^{a,c}

[illegible]

Figure 29.4.3-1 [] ^{a,c}**Figure 29.4.3-2** [] ^{a,c}



Figure 29.4.3-3 Heat Transfer Coefficient vs. Time from FLECHT 31805, 6 ft

a,c

Figure 29.4.3-4 Predicted vs. Measured Heat Transfer Coefficients from Forced Reflood Tests

a,c

Figure 29.4.3-5 [

] a,c

a,c

Figure 29.4.3-6 FLECHT 31203 6-ft Elevation Cladding Temperature Comparison for
[]^{a,c} Heat Transfer Multiplier of []^{a,c}

a,c

Figure 29.4.3-7 FLECHT 31203 6-ft Elevation Cladding Temperature Comparison for
[]^{a,c} Heat Transfer Multiplier of []^{a,c}

a,c

Figure 29.4.3-8 FLECHT 31203 8-ft Elevation Cladding Temperature Comparison for
[]^{a,c} Heat Transfer Multiplier of []^{a,c}

a,c

Figure 29.4.3-9 FLECHT 31203 8-ft Elevation Cladding Temperature Comparison for
[]^{a,c} Heat Transfer Multiplier of []^{a,c}

Figure 29.4.3-10 FLECHT 31203 10-ft Elevation Cladding Temperature Comparison for
[]^{a,c} Heat Transfer Multiplier of []^{a,c}

Figure 29.4.3-11 FLECHT 31203 10-ft Elevation Cladding Temperature Comparison for
[]^{a,c} Heat Transfer Multiplier of []^{a,c}

a,c

Figure 29.4.3-12 FLECHT 31504 6-ft Elevation Cladding Temperature Comparison for
[]^{a,c} Heat Transfer Multiplier of []^{a,c}

a,c

Figure 29.4.3-13 FLECHT 31504 6-ft Elevation Cladding Temperature Comparison for
[]^{a,c} Heat Transfer Multiplier of []^{a,c}

a,c

Figure 29.4.3-14 FLECHT 31504 8-ft Elevation Cladding Temperature Comparison for
[]^{a,c} Heat Transfer Multiplier of []^{a,c}

a,c

Figure 29.4.3-15 FLECHT 31504 8-ft Elevation Cladding Temperature Comparison for
[]^{a,c} Heat Transfer Multiplier of []^{a,c}

a,c

Figure 29.4.3-16 FLECHT 31504 10-ft Elevation Cladding Temperature Comparison for
[]^{a,c} Heat Transfer Multiplier of []^{a,c}

a,c

Figure 29.4.3-17 FLECHT 31504 10-ft Elevation Cladding Temperature Comparison for
[]^{a,c} Heat Transfer Multiplier of []^{a,c}

a,c

Figure 29.4.3-18 FLECHT 31805 6-ft Elevation Cladding Temperature Comparison for
[]^{a,c} Heat Transfer Multiplier of []^{a,c}

a,c

Figure 29.4.3-19 FLECHT 31805 6-ft Elevation Cladding Temperature Comparison for
[]^{a,c} Heat Transfer Multiplier of []^{a,c}

a,c

Figure 29.4.3-20 FLECHT 31805 8-ft Elevation Cladding Temperature Comparison for
[]^{a,c} Heat Transfer Multiplier of []^{a,c}

a,c

Figure 29.4.3-21 FLECHT 31805 8-ft Elevation Cladding Temperature Comparison for
[]^{a,c} Heat Transfer Multiplier of []^{a,c}

a,c

Figure 29.4.3-22 FLECHT 31805 10-ft Elevation Cladding Temperature Comparison for
[]^{a,c} Heat Transfer Multiplier of []^{a,c}

a,c

Figure 29.4.3-23 FLECHT 31805 10-ft Elevation Cladding Temperature Comparison for
[]^{a,c} Heat Transfer Multiplier of []^{a,c}

29.5 EVALUATION MODEL BIASES AND UNCERTAINTY (EMDAP STEP 20)

According to the Regulatory Guide 1.203, a singular uncertainty statement on the overall uncertainty results can only be achieved when the individual uncertainty contributions are determined. The procedure used to obtain the convolution of such uncertainties is the subject of Section 30. The development of the individual uncertainty contributors, ranges, and probability density functions has been the objective of this section.

The uncertainty contributors are divided in two main categories:

1. The first main category is the uncertainty associated with the code capability of representing phenomena and processes identified as highly important by the PIRT. The capability is established by assessing the code against SET/IET experiments that were designed to simulate such processes. The combined uncertainty will reflect the degree to which the individual models, correlations and methods used within the code represent the physical phenomena, the uncertainty associated with the use of such models, and the uncertainty associated with the experimental data itself and applicability of the data to PWRs.
2. The second main category is the uncertainty associated with the input boundary and initial conditions and all those parameters that define the plant state at the time of the postulated LOCA event, as well as the uncertainty associated with the break location, break type and size, etc. This uncertainty is not the result of the code capability of simulating the LOCA event, but rather the uncertainty associated with the LOCA scenario event itself.

The purpose of this section is to summarize the methodology for the treatment of the uncertainty contributors contained mainly in the first category. This is in line with the intent of Step 20 of the EMDAP, which asks for the determination of the EM biases and uncertainty. Since the process started by identifying the important phenomena with the PIRT, it is useful here to structure the review following the PIRT (Section 2), by describing how each of the phenomena was considered in the uncertainty methodology.

29.5.1 Fuel Rod

Stored Energy

Uncertainties in the initial stored energy of the hot rod and hot assembly are large. There is a wide range of possible peaking factors and power distributions that are allowed by the Technical Specifications. For a given power distribution, [

^{a,c} have been considered in the uncertainty methodology by explicitly ranging them as part of the uncertainty methodology. The treatment of the contributing uncertainty parameters is shown in Table 29-3a.

Cladding Oxidation

The metal-water reaction rate is ranged based on uncertainty estimates obtained from experimental data. This uncertainty is treated as a local uncertainty – see Table 29-3a for the numerical values.

[]^{a,c}

Decay Heat

The decay heat uncertainties from the American National Standards Institute/American Nuclear Society (ANSI/ANS) 5.1-1979 standard are applied as described in Section 9.7. []

[]^{a,c} The uncertainty treatment is shown in Table 29-4.

Cladding Deformation (Burst Strain, Relocation)

These processes were ranked []

[]^{a,c}
The uncertainty on cladding burst strain and temperature are obtained from the data scatter. The fuel pellet fragments packing fraction after relocation is also identified as an uncertainty contributor. Numerical values are provided in Table 29-3a and Table 29-3b.

29.5.2 Core

Critical Heat Flux (CHF)

Assessments of the CHF predictions are discussed in Sections 13, 15 and 22. As discussed in Section 13, for boil-off conditions characteristic of a SBLOCA transient, the []

[]^{a,c}

As discussed in Sections 15 and 22, for the blowdown condition encountered in LBLOCA scenarios, the []

[]^{a,c}

The treatment of the contributing uncertainty parameters is summarized in Table 29-2.

Post-Critical Heat Flux (CHF) Heat Transfer

Uncertainties in the post-CHF heat transfer are accounted for by ranging $I^{a,c}$ are based on the assessments of Sections 15 and 29.4.3, and the uncertainty treatment is shown in Table 29-3a.

Rewet/ T_{min}

The effects of the uncertainty on rewet/ T_{min} on the post-CHF heat transfer in a large or intermediate break LOCA are discussed in Section 29.1.8. For small breaks, the uncovered portion of the rod is in single-phase vapor which is the only source of cooling until the mixture level passes through. The advancement of the mixture level determines the rod re-wetting. The uncertainty treatment is shown in Table 29-2.

Three-Dimensional (3D) Flow/Core Natural Circulation

The importance of correctly predicting the distribution of the downflow from the upper plenum to the core is high (H) for large breaks during the blowdown period. Uncertainties in these parameters are accounted for by choosing the limiting hot assembly location based on consideration of the hardware in the upper plenum, and the resulting flow distribution during the downward core flow period of blowdown. Multidimensional effects are also captured by the core nodalization scheme, which uses 4 separate assembly groupings (hot assembly, assemblies on core periphery, interior assemblies located under guide tube assemblies, and interior assemblies located under other structures).

Void Generation/Void Distribution

During a small break, the void generation and distribution determine the location of the mixture level and the portion of core that uncovers for a given liquid inventory. The interfacial drag is the parameter controlling the void fraction in the two-phase region. The process is assigned a high (H) importance during the loop seal clearing, boil-off, and core recovery periods. For intermediate breaks, for similar considerations, this process is assigned a high (H) ranking during the accumulator injection and SI injection phases. The code has been assessed in these regards in an extreme core uncover condition in the simulation of the Semiscale test (Section 23.1.2) with satisfactory results. $I^{a,c}$

The uncertainty is treated as discussed in Section 29.1.5, and summarized in Table 29-2.

In a large break LOCA, during blowdown, different considerations apply but void distribution/generation is also ranked high (H) following the multiple channel flow discussion above (see the ranking rationale for 3D Flow/Natural Circulation above). The amount and timing of liquid and vapor downflow the core receives from the upper plenum depends on the hardware and geometry directly above a particular core region. The geometry of the upper internals in the upper plenum is explicitly modeled, and the core regions under particular hardware are explicitly modeled to account for different downflow behavior. The ability of the code to calculate voiding and flow under blowdown conditions was assessed indirectly by simulating the LOFT tests (Section 22.5), $I^{a,c}$

[

]^{a,c} (see *Flow Reversal/Stagnation* discussion below).

Entrainment/De-entrainment

This is highly (H) important during the accumulator injection period of intermediate breaks and the reflood period in large breaks. Comparisons with FLECHT and CCTF data indicate that WCOBRA/TRAC-TF2 overpredicts the amount of entrainment from the core. For forced reflood tests, the entrainment was accurately predicted to modestly over-predicted. For gravity reflood tests such as CCTF, excess entrainment results in an over-prediction of steam binding, which reduces the flooding rate and causes an under-prediction of core heat transfer. In addition, the comparisons with UPTF tests showed that when the conditions at the entrance to the upper plenum are known, WCOBRA/TRAC-TF2 underpredicts the mass retained in the upper plenum, therefore overpredicting the amount of water entrained into the loops. Based on the gravity reflood and UPTF test predictions, it is concluded that a conservative bias already exists in the calculations for core entrainment/de-entrainment, and an additional bias or uncertainty is not required.

Flow Reversal/Stagnation

This phenomenon was assigned high (H) only during the blowdown phase of a large break LOCA. Uncertainties in the blowdown flow reversal and stagnation affect the time and magnitude of the blowdown PCT, and the core-wide cooling during blowdown. Uncertainties are accounted for by varying break flowrate, via sampling of break type, split-break area, and the application of break flow multipliers based on the assessment of the critical flow model. Ranging of the broken cold-leg nozzle resistance and pump resistance also affects the flow reversal and stagnation as demonstrated in Section 28.1.4. The interactions between the stagnation point and the location of peak nuclear power are accounted for by ranging the core axial power distribution as well. The treatment of the contributing uncertainty parameters is summarized in Table 29-2.

29.5.3 Upper Head

Draining/Flashing/Mixture Level

The liquid inventory in the upper head initially drains through the guide tubes, until the depressurization causes flashing in this region. For large breaks, the initial depressurization is rapid and the upper head inventory can be a significant contributor to the removal of initial core stored energy. This process is therefore highly ranked in blowdown. It is considered not applicable for later periods due to depletion of inventory. The initial upper head liquid temperature is calibrated during the steady-state calculation. Upper head liquid temperature uncertainty is considered by varying the temperature based on the ranging of vessel average temperature.

Venting

Later in a LOCA transient, steam generated in the core will either be vented through the hot legs, the hot leg nozzle gaps, or the upper head. The ability to vent steam through the upper head is strongly dependent on the flow area of the spray nozzles, which is the flow path connecting the upper head and the downcomer. Venting has a high importance during the loop seal clearing period when it relieves some of the core two-phase level depression. Sensitivity studies of the effect of spray nozzle bypass on the small break LOCA transient were performed with both the ROSA-IV and Semiscale test simulations. The Semiscale simulations indicate that the code appropriately captures the impact of variations in bypass capacity. The overall conclusion from the results presented in Section 21.11 for ROSA-IV and from the Semiscale simulations is that [

]^{a,c}

Initial Fluid Temperature

The initial fluid temperature in the upper head region will be either equal to the cold leg temperature, or close to the hot leg temperature, depending on the spray nozzle flow area. This will affect the timing at which flashing occurs in the upper head, causing the flow through the guide tubes to switch from single phase liquid to a two-phase mixture. For large breaks, the initial depressurization is rapid and the upper head inventory can be a significant contributor to the removal of initial core stored energy. The timing of flashing in the upper head has a significant effect on the downflow cooling of the core. This process is therefore highly ranked in blowdown. For the uncertainty, see a similar discussion under *Draining/Flashing/Mixture Level*.

29.5.4 Upper Plenum

Hot Assembly Location

Refer to the discussion of core 3D flow in Section 29.5.2.

Entrainment/De-entrainment/Phase Separation

The entrainment/de-entrainment in the upper plenum was ranked high (H) only for two-loop plants with UPI. The applicability of the FSLOCA EM to that type of plant is outside the scope of this report, other than the PIRT (Section 2), which sets the basis for applicability to UPI plants. For 3- and 4-loop plants with cold-leg injection, refer to the discussion of core entrainment/de-entrainment in Section 29.5.2.

Hot Leg-Downcomer Gap Flow

Small gaps exist at the interface of the core barrel and the hot leg nozzles. These are the leakage paths that exist between the hot leg nozzles and upper downcomer region during all operating modes. For small breaks, these leakage paths are expected to have high importance during the loop seal clearing period when they provide alternative paths from the upper plenum to the cold leg break location to vent steam and relieve some two-phase level depression. The ROSA sensitivity study in Section 21.11 shows that []^{a,c}.

29.5.5 Steam Generator

Primary Side Heat Transfer/Condensation in U-tubes

This refers to the heat transfer processes on the primary side of the steam generator (SG) tubes. If condensation occurs, it affects the amount of vapor present and the resistance to flow through the generator. For small breaks, during the blowdown period, the U-tube heat transfer from the primary to the secondary system is important and was ranked high (H), and during the loop seal clearance period the process was ranked high (H) because of the effect of condensation. The primary-to-secondary heat transfer and condensation is calculated with a conservative bias by the code as discussed in Section 29.1.12. There is no need to explicitly treat uncertainties for this phenomenon.

The effect of reduced heat transfer area due to steam generator tube plugging is []^{a,c}.

Flow Regime/CCFL

This refers to the flow regime in the primary side of the steam generator, and in particular the hydraulic processes on the primary side in the SG tubes that lead to liquid holdup on the uphill side and voiding at the top of the U-tube. The potential for CCFL in the tubes and the impact of CCFL predictions on the transient was judged to be of high (H) importance during the loop seal clearing period. Based on the results of the ROSA-IV simulations with enforcement of CCFL at key locations (upper core plate, hot leg elbow/SG inlet, and steam generator U-tubes), the code calculations have been concluded to be biased in a conservative direction (see Section 29.1.12.2).

Steam Binding

This process becomes important when high liquid entrainment from the upper plenum is carried into the steam generator U-tubes, while the SG is acting as a heat source. The vaporization of the liquid leads to pressure increase and a reduction of the core inlet flow rate. The steam binding is highly important (H) only during the reflood period of a large break as it affects the venting path resistance and thus the reflood in the core. Refer to the discussion of core entrainment/de-entrainment in Section 29.5.2. The effects of steam binding in combination with the steam generator tube plugging are []^{a,c} (see the introductory summary in Section 28 and Section 28.1.6.2).

Primary Flow Resistance (Two-Phase DP)

The two-phase pressure drop through the SG primary side was rated high (H) for the loop seal clearing part of a small break LOCA transient and during the blowdown period of a large break LOCA when the SG flow resistance affects the overall loop resistance, which in turn affect the flow reversal and stagnation in the core. It was also rated medium (M) during the natural circulation phase of a SBLOCA and during the reflood phase of a LBLOCA. The resistance through the steam generator is maximized via the assumption of maximum tube plugging, and a conservative CCFL limit on the uphill side of the tubes. This is conservative relative to venting steam from the core. The ranging of flow reversal and stagnation in the core is addressed via sampling the break area, discharge coefficient, pump loss, broken cold leg nozzle loss, and axial power distribution (see Section *Flow Reversal/Stagnation* discussion in 29.5.2).

29.5.6 Pump Suction Piping/Loop Seal

Horizontal Stratification

The prediction of the horizontal stratified flow regime in the loop seal piping was assigned a high (H) ranking in the loop seal clearance period of a small break LOCA. The uncertainty on the flow regime transition in and out from horizontal stratified flow (or wavy-dispersed) is treated as discussed in Section 29.1.7 (HS_SLUG). [

]^{a,c} The uncertainty treatment of the controlling parameter (HS_SLUG) is shown in Table 29-2.

Entrainment/Flow Regime/Interfacial Drag

This refers to the entrainment of liquid from the stratified layer at the bottom of the horizontal section of loop seal piping, and the carryout of this liquid from the region.

For small breaks a high (H) ranking was assigned for the loop seal clearance period when entrainment and interfacial drag determine the efficacy of clearing. The modeling of the uncertainty in the loop seal clearing phenomenon; i.e., the timing of loop seal clearing and the flow resistance through the loop seal region after clearing is [

]^{a,c} as discussed in Section 29.1.11.

29.5.7 Pump

Coastdown Performance

This item refers to the effect the pump has on the flow between the time when the pump is tripped and when the impeller completes its coastdown. Note that the effects of pump friction/windage losses are included in this process. For large breaks, the coastdown performance is important since the pumping capability (in concert with the break flow) impacts the presence or absence of upflow into the core. These parameters are also the dominant factors in determining the timing of flow reversal in the core, and therefore the coastdown performance is ranked consistently with flow reversal in the core. The process is ranked high (H) during blowdown. The intact loop pumps are in the pumping mode during the 2-phase

period, and the data in this mode show little scatter (Section 20.2). However, the broken loop pump is in the dissipative mode, where the data scatter is considerable. The uncertainty treatment, therefore, focuses on the broken loop pump resistance uncertainty in the dissipative mode, described in Sections 29.1.2.2 and 20.2. The uncertainty treatment is summarized in Table 29-2.

Flow Resistance

The hydraulic resistance to flow passing through the pump was ranked high for large breaks. During the reflood portion of the transient, the flow resistance is expected to have an effect on the venting path flow resistance, with an effect similar to that discussed above for the steam binding. The ranging of the pump resistance discussed before for the blowdown phase is also applicable to reflect the uncertainty in the pump flow resistance during reflood.

29.5.8 Cold Leg/Safety Injection

Phenomena relative to the flow delivered by accumulator safety injection in the cold leg are discussed here, as well as phenomena relative to the pumped safety injection. Additional discussion regarding the accumulator is contained in Section 29.5.9.

[

$J^{a,c}$

Interfacial Heat Transfer (Condensation)

This is condensation that occurs on and about the stream of subcooled water injected into the cold leg from the pumped SI system and/or the accumulator. For small breaks during the boil-off period and the recovery period, the SI flow to the cold legs is high because the system pressure is lower, so a high (H) ranking was assigned. For the intermediate breaks, condensation was assigned high (H) ranking during the accumulator injection and SI injection phases. For the large breaks, condensation is of the highest relative importance during the refill period. When the ECC water is no longer bypassed in the refill period, the condensation process at the top of the downcomer can increase the downcomer level and therefore helps to induce reflood through the core, promoting cooling. A ranking of high (H) is assigned during this period. A specific condensation model for the SI jet was included in the code (Section 6) and is active in the cold leg in the node connected with the ECC piping when the flow regime is separated flow (i.e., stratified, wavy-dispersed, or annular-mist). The model was shown to be applicable to the full spectrum of breaks and scenarios (Section 17). The uncertainty on the model was developed in Section 29.1.6, and treatment of the uncertainty is summarized in Table 29-2.

³ [

$J^{a,c}$

Non-Condensable Gas Effects

This refers to the effect that nitrogen has on condensation in the cold leg. The rankings for this effect generally follow those assigned for condensation. For intermediate breaks, a high (H) ranking was assigned for the safety injection period to reflect the effect of nitrogen on condensation in the cold leg, which was ranked high during this period for intermediate breaks as discussed above. For the larger breaks, the effects of non-condensable gases are important during the reflood period when the accumulators empty and the nitrogen from the accumulators is released into the primary system. In the PIRT the effect on condensation is considered to have medium (M) importance during the reflood period of a large break LOCA.

The transport of the non-condensable field was added to WCOBRA/TRAC-TF2 and the effect of the non-condensable on the condensation is captured. Given the medium ranking for large break and considering that intermediate breaks are typically not limiting, the model as coded is considered adequate without consideration of uncertainties. Comparisons with ACHILLES test data (see Section 29.1.10) indicated that WCOBRA/TRAC-TF2 tends to underpredict the pressurization of the downcomer and the resulting insurge of water into the core. The tendency to underpredict downcomer pressurization, and the impact on the heat transfer during the initial insurge of water in the core, leads to the conclusion that the effects of accumulator nitrogen will be reasonably calculated and therefore the uncertainty associated with this model is bounded.

Flow Regime

Horizontal stratification was assigned a high (H) ranking in the loop seal clearance, boil-off, and recovery periods, when the two-phase level drops in the cold legs and the break uncovers. The controlling parameter is the transition boundary between horizontally stratified or wavy-dispersed flow and non-stratified flow regimes. The uncertainty on the flow regime transition in and out from horizontal stratified flow (or wavy-dispersed) is treated as discussed in Section 29.1.7 through the biasing or ranging of HS_SLUG (Table 29-2).

Spilling Flow Treatment (Pumped SI)

The treatment of the pumped SI flow in terms of flow spilled at the break versus flow delivered is considered. Spilled flow depends on the break dimension and location on the cold leg. For small breaks, a ranking of high (H) was assigned for the boil-off and recovery periods. A ranking of high was also assigned during the safety injection phase of intermediate break and during the reflood period of a large break LOCA. The uncertainty on the amount of pumped SI flow spilling to containment and its impact to the SI delivered in the RCS is bounded in the analysis as discussed in Section 25.

29.5.9 Accumulator

Injection Flowrate/Line Resistance

This refers to the rate at which liquid is discharged from the accumulator, which depends upon the cover gas expansion coefficient and the hydraulic resistance to accumulator flow in the check valve and in the line connecting the accumulator to the cold leg. The effect of the line resistance was ranked high (H) during the accumulator injection period of intermediate breaks, and during the refill period of large breaks. The uncertainty in the line resistance is ranged in the uncertainty analysis. Numerical values are provided in Table 29-5.

Nitrogen Discharge

The accumulator nitrogen provides the main source of non-condensable gas in the system during the LOCA transient. While the potential effects of non-condensables are discussed elsewhere as applicable, it is recognized that the accumulator cover gas provides the main source of non-condensable gas in the system, and thus ranking should follow consistently. The modeling of this process was assigned a high (H) ranking for intermediate breaks during the safety injection phase. See *Non-Condensable Gas Effects* discussion in Section 29.5.8.

Broken Loop Accumulator Treatment

The accumulator on the broken loop [*Injection* discussion in Section 29.5.8.

] ^{a,c}. See *Cold Leg/Safety*

29.5.10 Downcomer

Condensation

In a large break LOCA condensation in the downcomer affects ECC bypass and the refill and reflood transient. Comparisons with small- and large-scale tests showed that while WCOBRA/TRAC-TF2 predicted reasonable values of condensation efficiency, the range of uncertainty in the data interpretation is large. The condensation in the downcomer is calculated using the nominal model, which demonstrates conservatism regarding the timing of ECC bypass and the beginning of refill. Treatment of uncertainty is discussed in Section 29.1.4, and the numerical value of the controlling parameter (XC) is given in Table 29-2.

Reactor Pressure Vessel Internals/Vessel Wall Stored Energy

This is the effect of the heat release to the fluid from the downcomer metal structures. Heating of the water in the downcomer during reflood eventually causes boiling, which results in level swell, spilling of water out of the broken loop, and a reduction in reflood rate. Comparisons with CCTF Test 62 and UPTF Test 25A hot wall tests indicated that the combined effects of downcomer boiling and entrainment on downcomer level during reflood are well predicted (Figure 19.6-27 and Figures 19.3-175 and 19.3-176 for CCTF and UPTF, respectively). The timing of the onset of downcomer boiling is ranged by varying the accumulator and pumped safety injection water temperatures, based on historical plant data. The severity of the downcomer boiling is influenced by the temperature of the liquid flow into the downcomer, which is well-to-conservatively predicted by WCOBRA/TRAC-TF2 based on the simulations of UPTF Test 8A and UPTF Test 25A.

3D Effects

This refers to multidimensional flow that may occur in the downcomer and its impact on the transient. This is important for Large Break LOCA, where it was ranked high (H) for the refill phase. The FSLOCA methodology is based on relatively detailed modeling of the downcomer's 3D flow by including 3 circumferential nodes (channels) per cold leg. For a 3-loop plant this will result in a downcomer noding with 9 sectors in the circumferential direction. Code model uncertainties were assessed by comparisons with the UPTF ECC bypass test data (Test 6). Those assessments showed that there is a conservative bias, in that ECC bypass is overpredicted, which in turn extends the refill time period in a conservative direction (Section 19.3.5).

Mixture Level/Flashing/Void Fraction

For Small Break LOCA, Mixture Level (as it reflects the collapsed level) was assigned a high (H) ranking for the final three phases of the transient since the downcomer level affects the level in the inner vessel. For Intermediate Break LOCA, the mixture level is assigned a high (H) ranking for the final two phases of the transient since the downcomer level affects the level in the inner vessel. For Large Break LOCA, the downcomer level becomes the only driving force for the core inlet flow during reflood making the ranking high (H) for this phase.

The code's ability to predict the void distribution and mixture level for blowdown/flashing transients slower than a typical large break LOCA was assessed in the General Electric (GE) Vessel Blowdown Tests (Section 23.1.1). That facility contains no internal structures, and has a hydraulic diameter similar to a PWR downcomer. It was confirmed that the code is able to adequately predict the void distribution []^{a,c}.

For large breaks, uncertainties in the flow regimes and void distributions affect the amount of ECC water bypassed at the end of blowdown and the beginning of refill. Code model uncertainties were assessed by comparisons with the UPTF ECC bypass test data (Test 6). Those assessments showed that there is a conservative bias, in that ECC bypass is over-predicted (Section 19.3.5).

Entrainment/De-entrainment

Uncertainties in entrainment/de-entrainment affect the amount of ECC water bypassed at the end of blowdown/beginning of refill and was ranked high (H) in both refill and reflood phases of a large break LOCA. Code model uncertainties were assessed by comparisons with the UPTF ECC bypass test data (Test 6). Those assessments showed that there is a conservative bias, in that ECC bypass is overpredicted (Section 19.3.5). The amount of water entrained from the downcomer and out of the broken loop during reflood is also effectively ranged by varying the break type, flowrate, and broken loop nozzle resistance. Entrainment can also occur during reflood, due to the steam flow from the intact loops. Comparisons with CCTF Test 62 and UPTF Test 25A data indicated that entrainment during reflood is well-to-conservatively predicted (Sections 19.6.5 and 19.3.11). Based on these assessments this uncertainty contributor is bounded in the analysis.

Liquid Level Oscillations

The liquid level in the downcomer during the reflood phase of a large break LOCA is affected by a number of parameters that are ranged, including accumulator and safety injection temperature, accumulator water volume, break type and flowrate, and broken cold-leg nozzle resistance. Manometric oscillations in the downcomer and core are evident during early reflood following a large break LOCA. Such is observed in integral effects tests (CCTF, see Section 19.6), where the oscillatory behavior is captured adequately. The oscillatory core inlet flow during reflood is expected to cause increased cooling (Section 23.2.2.6). The expected improvement in cooling is predicted to be much smaller by WCOBRA/TRAC-TF2 judging from CCTF Test 62 (Section 19.6) and ACHILLES (Section 20.1) test comparisons.

29.5.11 Lower Plenum

Hot-wall Effect (Void Generation or Boiling)

Heating of the water in the lower plenum under SBLOCA conditions and during the reflood phase of a LBLOCA eventually causes boiling, which results in level swell in the downcomer, spilling of water out of the broken loop, and a reduction in reflood rate. The swelling can also increase the level in the core. The boiling in the lower plenum is treated in a best-estimate manner. The timing of the onset of boiling in the lower plenum for the reflood phase of a LBLOCA is ranged by varying the accumulator and pumped safety injection water temperatures, based on historical plant data. See *Reactor Pressure Vessel Internals/Vessel Wall Stored Energy* discussion in Section 29.5.10.

29.5.12 Break

Critical Flow

The break flowrate is varied by [

]^{a,c} The development of the break flow multipliers is described in Section 29.1.1, and the uncertainty distributions for the controlling parameters (CD1,CD2) are given in Table 29-2.

Containment Pressure

A conservatively low containment pressure is used, which eliminates the need for a detailed uncertainty treatment.

Upstream Flow Regime

For small breaks, the upstream flow regime affects the inlet quality at the break depending on the assumed orientation of the break relative to the cold leg (top, side or bottom). Since the break flowrate largely determines the system inventory, a high (H) ranking is assigned to this process for all phases of the small break LOCA transient with exception of blowdown phase. As described in Section 29.2, []^{a,c}.

Cold Leg Nozzle Flow Resistance

The broken cold leg nozzle resistance influences the flow split between the vessel side flow path and the pump discharge side flow path, which then impacts the core flow during the blowdown for a large break LOCA. The flow split in the broken loop is ranged by varying the broken cold-leg nozzle resistance (distribution summarized in Table 29-2), among other parameters, by an amount that accounts for uncertainties in its value (Section 29.1.2). See also *Flow Reversal/Stagnation* discussion in Section 29.5.2.

29.6 EXPERIMENTAL UNCERTAINTIES (EMDAP STEP 9)

As part of the evaluation model development, a large database of experiments was used to compare against code predictions. As stated in Regulatory Guide 1.203, Section 1.2.7:

“It is important to know the uncertainties in the database. These uncertainties arise from measurement errors, experimental distortions, and other aspects of experimentation. If the quantified experimental uncertainties are too large compared to the requirements for evaluation model assessment, the particular data set or correlation should be rejected.”

Throughout this report (Volumes I and II in particular), when information regarding experimental uncertainty was available or could be derived from the data reports and references, it was presented in a way to reflect measurement uncertainties. In some cases, the experimental measurement uncertainty was large and was therefore reflected and accounted for in the uncertainty analysis (see for example Section 17 regarding the safety injection condensation model). However, in some instances no uncertainty information could be found or could be inferred from the references. In those cases the measurement uncertainty is expected to be negligible when compared to the relatively large uncertainty and scatter in the data itself.

29.7 REFERENCES

1. Akimoto, et al., 1984, "Pressure Drop through Broken Cold Leg during Reflood Phase of Loss-of-Coolant Accident of Pressurized Water Reactor," *Journal of Nuclear Science and Technology*, 21[6], pp. 450-465.
2. American Nuclear Society, 1979, "American National Standard for Decay Heat Power in Light Water Reactors," ANSI/ANS-5.1-1979.
3. Anklam, T. M., et al., 1982, "Experimental Investigations of Uncovered-Bundle Heat Transfer and Two-Phase Mixture-Level Swell Under High-Pressure Low Heat-Flux Conditions," NUREG/CR-2456.
4. Bajorek, S. M., et al., 1998, "Code Qualification Document for Best Estimate LOCA Analysis," WCAP-12945-P-A, Volume 1 Revision 2, and Volumes 2 through 5 Revision 1 (Proprietary), and WCAP-14747 (Non-Proprietary).
5. Baum, A. J., 1977, "A Study of Transition and Film Boiling From Vertical Surfaces," Ph. D. Thesis, Carnegie-Mellon University.
6. Bordelon, F. M. and Murphy, E. T., 1974, "Containment Pressure Analysis Code (COCO)," WCAP-8327 (Proprietary), WCAP-8326 (Non-Proprietary).
7. Boyack, B., et al., 1989, "Quantifying Reactor Safety Margins," NUREG/CR-5249.
8. Broughton, J. M., 1981, "PBF LOCA Test Series, Tests LOC-3 and LOC-5 Fuel Behavior Report," NUREG/CR-2073.
9. Burman, D. L., 1980, "Comparison of Westinghouse LOCA Burst Tests Results with ORNL and Other Program Results," Proceedings of a CSNI Specialist Meeting on Safety Aspects of Fuel Behavior in Off-normal and Accident Conditions, September 1 – 4, Espoo, Finland, pp. 251-284.
10. Cathcart, J. V., Pawel, R. E., et al., 1977, "Zirconium Metal-Water Oxidation Kinetics IV – Reaction Rate Studies," ORNL/NUREG-17, Oak Ridge National Laboratory, Oak Ridge, TN.
11. Combustion Engineering, 1981, "C-E ECCS Evaluation Model – Flow Blockage Analysis – ECCS Analysis," Enclosure 1-P-A (Proprietary) and Enclosure 1-NP-A (Non-Proprietary) to LD-81-095.
12. Crede, T. M., et al., 2013, "Westinghouse Performance Analysis and Design Model (PAD5)," WCAP-17642-P (Proprietary), WCAP-17642-NP (Non-Proprietary).
13. Crane Co., 1969, "Flow of Fluids Through Valves, Fittings, and Pipe," Technical Paper No. 410 published by Crane Co.

-
14. Dhira, V. K., Duffey, R. B., and Catton, I., 1981, "Quenching Studies on a Zircaloy Rod Bundle," *ASME J. Heat Transfer*, Vol. 103, pp. 293-299.
 15. Draper, N. and Smith, H., 1981, Applied Regression Analysis, Second Edition, John Wiley and Sons.
 16. Frepoli, C., 2007, "Assessment of Rod-to-Rod Thermal Radiation Heat Transfer Contribution During Reflood in PWR Fuel Assemblies," ICAPP 2007, Nice, France, May 13-18, Paper 7323.
 17. Garde, A., et al., 2013, "Westinghouse Clad Corrosion Model for ZIRLO and Optimized ZIRLO," WCAP 12610-P-A & CENPD-404-P-A, Addendum 2-A (Proprietary), WCAP-14342-A & CENPD-404-NP-A, Addendum 2-A (Non-Proprietary).
 18. Ganic, E. and Rohsenow, W. M., 1977, "Dispersed Flow Heat Transfer," *Int. J. Heat Mass Transfer*, Vol. 20, pp. 855-866.
 19. Henry, R. E., 1974, "A Correlation for the Minimum Film Boiling Temperature," *AIChE Symposium Series*, Vol. 138, pp. 81-90.
 20. Holmes, B. J., 1991, "ISP 25 Comparison Report," AEA-TRS-1043.
 21. Hsieh, T. and Raymond, M., 1976, "Long Term Ice Condenser Containment Code – LOTIC Code," WCAP-8354-P-A, Supplement 1 (Proprietary), WCAP-8355-A, Supplement 1 (Non-Proprietary).
 22. Lanning, D. D., Beyer, C. E., Geelhood, K. J., 2005, "FRAPCON-3 Updates, Including Mixed-Oxide Fuel Properties," Pacific Northwest National Laboratory, NUREG/CR-6534, Vol. 4.
 23. Loftus, M. J., et al., 1980, "PWR FLECHT SEASET Unblocked Bundle, Forced and Gravity Reflood Task, Data Report," NUREG/CR-1532, EPRI NP-1459, WCAP-9699.
 24. Morita, T., et al., 1974, "Power Distribution Control and Load Following Procedures," WCAP-8385-P-A.
 25. MPR, 1990, "Summary of Results From the UPTF Downcomer Separate Effects Tests, Comparison to Previous Scaled Tests, and Application to U.S. Pressurized Water Reactors," MPR Associates, MPR-1163.
 26. Nissley, M. E., et al., 2005, "Realistic Large-Break LOCA Evaluation Methodology Using the Automated Statistical Treatment Of Uncertainty Method (ASTRUM)," WCAP-16009-P-A and WCAP-16009-NP-A.
 27. Powers, D. A. and Meyer, R. O., 1980, "Cladding Swelling and Rupture Models for LOCA Analysis," NUREG/CR-0630.

-
28. Roe, J., 1998, "NRC Information Notice 98-29: Predicted Increase in Fuel Rod Cladding Oxidation."
 29. Schueren, P., 2006, "Optimized ZIRLO™," WCAP-12610-P-A & CENPD-404-P-A, Addendum 1-A.
 30. Shumway, R., 1985, "Return to Nucleate Boiling," *ANS Proceedings National Heat Transfer Conference*, Denver, CO, pp. 372-388.
 31. Spier, E. M., et al., 1988, "Evaluation of Nuclear Hot Channel Factor Uncertainties," WCAP-7308-L-P-A.
 32. Tasaka, K., et al., 1988, "The Results of 5% Small-Break LOCA Tests and Natural Circulation Tests at the ROSA-IV LSTF," *Nuclear Engineering and Design*, 108, pp. 37-44.
 33. Tregoning, Abramson, Scott, and Chokshi, 2007, "LOCA frequency evaluation using expert elicitation," *Nuclear Engineering and Design* 237, pp. 1429-1436.
 34. Vijaykumar, R. and Dhir, V. K., 1992, "An Experimental Study of Subcooled Film Boiling on a Vertical Surface – Hydrodynamic Aspects," *ASME J. Heat Transfer*, Vol. 114 (1), pp. 161-168.
 35. Yoder, et al., 1982, "Dispersed Flow Film Boiling in Rod Bundle Geometry – Steady-State Heat Transfer Data and Correlation Comparisons," NUREG/CR-2435, ORNL-5822.

30 TECHNICAL BASIS OF STATISTICAL PROCEDURES APPLIED IN FULL SPECTRUM LOCA UNCERTAINTY METHODOLOGY

30.1 STATISTICAL METHODOLOGY ROADMAP

A realistic (best-estimate) safety analysis asks for the assessment of uncertainties associated with physical models, data uncertainties, and plant initial and boundary condition variability. The current safety regulations of the United States Nuclear Regulatory Commission (US NRC) are stipulated in the Code of Federal Regulations (CFR) 10 CFR Part 50, Section 50.46. Based on the 10 CFR 50.46 rule, an emergency core cooling system (ECCS) design is required to satisfy prescriptive criteria. The regulation identifies the following five criteria:

1. Peak cladding temperature (PCT) shall be less than 2200°F
2. Maximum local oxidation (MLO) shall be less than 17%
3. Core-wide oxidation (CWO) shall be less than 1% (to limit the maximum amount of hydrogen generated)
4. The core shall maintain a coolable geometry
5. Long term cooling shall be demonstrated

NRC Information Notice 98-29 (Roe, 1998) provides further clarification that the 10 CFR 50.46(b)(2) MLO criterion “includes both pre-accident oxidation and oxidation occurring during a LOCA.” In the FULL SPECTRUM LOCA (FSLOCA) uncertainty methodology, therefore, ‘MLO’ results are the sum of the two.

Code Scaling, Applicability, and Uncertainty (CSAU) Element 3, the sensitivity and uncertainty analysis element, aims to provide a simple Best-Estimate Plus Uncertainty (BEPU) statement (Boyack et al., 1989) that satisfies the first three criteria above. To accomplish this objective, the effects of the important uncertainty contributors are determined. The uncertainty statement is based on the combined effect of the contributors.

The objective of a Loss-of-Coolant Accident (LOCA) analysis is to directly address criteria (b)(1), (b)(2) and (b)(3) of 10 CFR 50.46; the determination of peak cladding temperature, maximum local oxidation, and core-wide oxidation. [

]^{a,c} Criterion (b)(4) (coolable geometry)

is satisfied by meeting the first three criteria, and accounting for grid deformation if calculated to occur in the in-board assemblies. Typically the last criterion (long-term cooling) is satisfied outside the LOCA analysis.

Regarding the treatment of uncertainties within the CSAU framework, the most straightforward approach is to combine the uncertainties with a direct Monte Carlo simulation. The procedure is designed to first generate a sample of the predicted short term LOCA population (which for the FSLOCA evaluation model is designed to be more severe than the expected LOCA response). Then non-parametric statistical inference procedures are applied to develop probabilistic statements based on the predicted LOCA population, which are in turn used to show a high probability of compliance with the 10 CFR 50.46 criteria.

The code (WCOBRA/TRAC-TF2) is the ‘black-box’ which receives as input a set of random values, one for each uncertainty parameter, and outputs the three values that characterize a specific LOCA scenario (PCT, MLO and CWO). [

]^{a,c}

Several cases (scenarios) are executed until the sample size is large enough to represent the population and provide the estimates of the key parameters of interest. The issue is how results are interpreted to demonstrate compliance with the 10 CFR 50.46 requirements.

10 CFR 50.46 states that “[...] *uncertainty must be accounted for, so that, when the calculated ECCS cooling performance is compared to the criteria set forth in paragraph (b) of this section, there is a high level of probability that the criteria would not be exceeded.*” Paragraph (b) of 10 CFR 50.46 contains the list of the acceptance criteria. 10 CFR 50.46 does not explicitly specify how this probability should be evaluated or what its value should be.

Additional clarification as to the US NRC expectations on the acceptable implementation of the “high probability” requirement is provided in Section 4 of Regulatory Guide 1.157 (Best-Estimate Calculations of Emergency Core Cooling System Performance) that states: “*a 95% probability is considered acceptable to the NRC staff [...].*” Further, Regulatory Guide 1.157 introduced the concept of confidence level as a possible refinement to the uncertainty treatment, but did not expand further on this concept.

As statistical methods are implemented to perform LOCA safety analyses, a statistical statement which estimates or bounds the 95th quantile of the population with a 95% confidence level has been suggested by the NRC as acceptable to demonstrate the required “high probability.” In the previous approved Automated Statistical Treatment of Uncertainty Method (ASTRUM, Nissley et al., 2005), the 95th quantile of the joint-distribution of PCT, MLO and CWO is bounded with at least 95% confidence level. The Safety Evaluation Report (SER) of the Westinghouse Best-Estimate Large Break LOCA methodology (ASTRUM) states the following: “*the staff determined that a 95th percentile probability level based on best approximations of the constituent parameter distributions and the statistical approach used in the methodology is appropriately high for this application.*”

Consistent with the previously approved methodology, the 95/95 criterion is also considered for the FSLOCA methodology. [

] ^{a,c}

One key difference between the previous Large Break LOCA methodology (ASTRUM, Nissley et.al, 2005) and the FSLOCA EM is that the FSLOCA methodology extends the break area spectrum considered in the analysis to cover the full range from what is historically defined as Small Breaks (SB) to Large Breaks (LB) including break sizes typically not analyzed and classified as Intermediate Breaks (IB). As discussed in Section 29.2, a simple extension of the ASTRUM approach to smaller break sizes was considered not appropriate because SBLOCA would not be properly considered in the sample by simply extending a uniform probability distribution of the split break sizes in the SB region. A more balanced approach has been developed and was discussed in Section 29.2.

[

] ^{a,c}

[

]^{a,c}

30.2 STATISTICAL SAMPLING APPROACH (MONTE CARLO)

The run matrix is generated by using random numbers. The random numbers are obtained using a generator from Press et al. (1992). This particular generator has a period of approximately 2.3×10^{18} , that is, the series of numbers generated would not be repeated before 2.3×10^{18} random numbers are used. For all practical purposes, this number is quite large and period exhaustion is considered impossible.

In addition, according to Press et al. (1992), the output from this random number generator has passed standard statistical tests intended to detect lack of randomness (especially certain subtle serial correlations).

The random number generator returns a value, RND, between 0 and 1. To alter the range to [a,b] instead, a linear mapping is applied.:

$$\text{VALUE} = a + (b-a) \cdot \text{RND}$$

The generation of normal (Gaussian) random variables is done by first generating RND and then using a rejection method that is efficient for distributions that have symmetric unimodal probability density functions (PDFs).

The random number generator depends on an initial seed to select the starting point in a random sequence. Having such algorithms allows for repeatability of results without compromising randomness. In the analysis, the initial seed is obtained randomly from the configuration control system. This system assigns a random identifier to each run, so that they can be uniquely identified. If the run matrix needs to be repeated or extended, repeatability is ensured by using the same seed.

30.3 NON-PARAMETRIC ORDER-STATISTICS TOLERANCE LIMITS FORMULATION

The consideration of nonparametric tolerance limits was originally presented by Wilks (Wilks, 1941). Wilks showed that for continuous populations, the distribution of $P(i,j)$, the proportion of the population between the i -th and j -th order statistics, is independent of the population sampled.

The assumption of continuity is a rather mild one. In the present context, it means that the probability of getting two runs with precisely the same result is zero. Formally, we require that the cumulative distribution function (CDF) of the outcomes be continuous; the PDF, which is the derivative of the CDF, need not be continuous for the relevant results to hold.

Derivation of non-parametric tolerance limits is presented next. This derivation is based on the non-parametric multivariate tolerance limits formulation first proved by Wald (1943) and more recently adapted by Guba-Makai (Guba, et al., 2003) to the problem of making safety inferences based on the output of models of complex systems. The derivation provided here of the non-parametric tolerance limits follows the formulation by Guba-Makai.

For the sake of simplicity the case with a single output variable y with a probability density function $g(y)$ is considered first. Assume that nothing is known about the probability density function $g(y)$ except that it is continuous. If N runs are carried out with random input(s), then a sample $\{y_1, y_2, \dots, y_N\}$ of the random output y will be obtained.

Two functions $L = L(y_1, y_2, \dots, y_N)$ and $U = U(y_1, y_2, \dots, y_N)$ called tolerance limits can be defined such that:

$$P \left(\int_L^U g(y) dy > \gamma \right) = \beta \quad (30-1)$$

where β represents the probability that a fraction γ of the random output variable y population falls within the tolerance limits U and L .

Now arrange the values y_1, y_2, \dots, y_N in increasing order (the probability of equal values of y occurring is neglected since $g(y)$ has been assumed to be a continuous function), and denote by y_k the k^{th} of these ordered value.

Thus, in particular:

$$y(1) = \min y_k \quad \text{and} \quad y(N) = \max y_k \quad (30-2)$$

$$1 \leq k \leq N \quad \quad \quad 1 \leq k \leq N$$

and let by definition $y(0) = -\infty$ and $y(N+1) = +\infty$.

In this case, for some positive $\gamma < 1$ and $\beta < 1$, it can be demonstrated that there can be constructed two functions $L = L(y_1, y_2, \dots, y_N)$ and $U = U(y_1, y_2, \dots, y_N)$, such that the probability β that

$$\int_L^U g(y) dy > \gamma \quad (30-3)$$

can be determined, as demonstrated in Guba, et al. (2003), as:

$$\beta = 1 - I(\gamma, s - r, N - s + r + 1) = \sum_{j=0}^{s-r-1} \binom{N}{j} \gamma^j (1 - \gamma)^{N-j} \quad (30-4)$$

where,

$$I(\gamma, j, k) = \int_0^\gamma \frac{u^{j-1} (1-u)^{k-1}}{B(j, k)} du \quad (30-5)$$

$$B(j, k) = \frac{(j-1)!(k-1)!}{(j+k-2)!} \quad (30-6)$$

$$0 \leq r < s \leq N, \text{ and } L = y(r), U = y(s)$$

Equation 30-4 can be used to provide an answer to the question “for a given $L = y(r)$ and $U = y(s)$, what is the sampling size N of the output variable y that has to be collected so that there is a probability β that a fraction γ of the random output variable y population falls within the specified tolerance limits U and L ?” It can be observed that Equation 30-4 does not depend on the probability density function $g(y)$ or the number of input variables in the process.

In the particular case that the tolerance limits are selected such that $r = 1$ and $s = N$ (i.e., the maximum and minimum value of the samples $y(k)$ of the output variable y are used to define L and U), the two-sided tolerance level can be obtained as¹:

$$\beta = 1 - \gamma^N - N(1 - \gamma)\gamma^{N-1} \quad (30-7)$$

If interest is limited only to the upper tolerance limit ($r = 0$ and $s = N$),

$$\beta = 1 - \gamma^N \quad (30-8)$$

1. Note that Guba, et al. (2003) Equation 18 contains a typographical error in the definition of β for the two-sided case that is corrected in Equation 30-7.

Guba, et al. (2003) also provides an extension of the single output variable formulation for the case of multiple variables. For this case, some additional definitions are required. Consider an output comprised of p variables, y_1, y_2, \dots, y_p . Let $g(y_1, \dots, y_p)$ be the joint distribution of the output variables and let \underline{Y} be defined as:

$$\underline{Y} = \begin{pmatrix} y_{11} & y_{12} & \dots & y_{1N} \\ y_{21} & y_{22} & \dots & y_{2N} \\ \dots & \dots & \dots & \dots \\ y_{p1} & y_{p2} & \dots & y_{pN} \end{pmatrix} \quad (30-9)$$

Analogous to the single output case, the problem of setting tolerance limits for y_1, \dots, y_p can be formulated as follows: for some given positive values $\gamma < 1$ and $\beta < 1$, there can be constructed two random functions $L_j = L_j(y_1, y_2, \dots, y_N)$ and $U_j = U_j(y_1, y_2, \dots, y_N)$, such that there is a probability β that:

$$\int_{L_1}^{U_1} \dots \int_{L_p}^{U_p} g(y_1, \dots, y_p) dy_1 \dots dy_p > \gamma \quad (30-10)$$

If $g(y_1, \dots, y_p)$ is continuous, it can be assumed that no two elements in \underline{Y} are equal. The sequence of rows in \underline{Y} is arbitrary, reflecting the fact that we number the output variables arbitrarily. Let us consider the first row of the sample matrix and arrange its elements in order of increasing magnitude $y_1(1), y_1(2), \dots, y_1(N)$. Select now between these $y_1(r_1)$ as L_1 and $y_1(s_1) > y_1(r_1)$ as U_1 . Let $i_1, i_2, \dots, i_{s_1-r_1-1}$ stand for the original columns of the elements $y_1(r_1 + 1), y_1(r_1 + 2), \dots, y_1(s_1 - 1)$. Next, the N observed values of the output variable y_2 are considered, and the part $y_{2,i_1}, y_{2,i_2}, \dots, y_{2,i_{s_1-r_1-1}}$ of its elements are arranged in increasing order to obtain $y_2(1), y_2(2), \dots, y_2(s_1 - r_1 - 1)$. Select now between these $y_2(r_2)$ as L_2 and $y_2(s_2) > y_2(r_2)$ as U_2 , where evidently $r_2 \geq r_1$ and $s_2 \leq s_1 - r_1 - 1$. If this process is applied to the end of the sample matrix, a p -dimensional space will be defined:

$$V_p = \{[L_1, U_1] * [L_2, U_2] * \dots * [L_p, U_p]\} \quad (30-11)$$

where,

$$\begin{aligned} L_j &= y_j(r_j) \\ U_j &= y_j(s_j) \end{aligned}$$

$$\begin{aligned} r_j &\geq r_{j-1} \geq \dots \geq r_1, & \text{for } j = 2, \dots, p \\ r_j &< s_j \leq s_{j-1} - r_{j-1} - 1, & \text{for } j = 2, \dots, p \end{aligned}$$

As demonstrated by Guba, et al. (2003), in the case of $p \geq 2$ dependent output variables with continuous joint distribution function $g(y_1, \dots, y_p)$ it is then possible to construct p -pairs of random intervals $[L_i, U_i]$, $i = 1, \dots, p$ such that the probability of the inequality:

$$\int_{L_1}^{U_1} \dots \int_{L_p}^{U_p} g(y_1, \dots, y_p) dy_1 \dots dy_p > \gamma \quad (30-12)$$

is free of $g(y_1, \dots, y_p)$ and is given by

$$P \left(\int_{L_1}^{U_1} \dots \int_{L_p}^{U_p} g(y_1, \dots, y_p) dy_1 \dots dy_p > \gamma \right) = 1 - I(\gamma, s_p - r_p, N - s_p + r_p + 1) \quad (30-13)$$

As demonstrated in Guba, et al. (2003), where $I(\dots, \dots, \dots)$ is the incomplete beta function ratio defined in Equation 30-5 and

$$s_p \leq s_{p-1} - r_{p-1} - 1 \leq s_1 - \sum_{j=1}^{p-1} (r_j + 1) \quad (30-14)$$

$$r_p \geq r_{p-1} \geq r_1 \quad (30-15)$$

In several practical applications, $r_1 = r_2 = \dots = r_p = 1$, and $s_p = N - 2(p - 1)$, and the probability β from Equation 30-13 can be expressed as:

$$\beta = 1 - I(\gamma, N - 2p + 1, 2p) = \sum_{j=0}^{N-2p} \binom{N}{j} \gamma^j (1 - \gamma)^{N-j} \quad (30-16)$$

And for a one sided confidence level ($r_1 = r_2 = \dots = r_p = 0$) and $s_p = N - p + 1$, then²:

$$\beta = 1 - I(\gamma, N - p + 1, p) = \sum_{j=0}^{N-p} \binom{N}{j} \gamma^j (1 - \gamma)^{N-j} \quad (30-17)$$

2. Note that Guba, et al. (2003) Equation 25 contains a typographical error in the definition of β for the single-sided case that is corrected in Equation 30-17.

[

$$\left[\begin{matrix} \text{ } \\ \text{ } \end{matrix} \right]^{a,c} \quad (30-18)$$

where,

$$\left[\begin{matrix} \text{ } \\ \text{ } \end{matrix} \right]^{a,c} \quad (30-19)$$

which can be expanded as follows:

$$\left[\begin{matrix} \text{ } \\ \text{ } \end{matrix} \right]^{a,c} \quad (30-20)$$

Equation 30-18 can be expressed as follows:

$$\left[\begin{matrix} \text{ } \\ \text{ } \end{matrix} \right]^{a,c} \quad (30-21)$$

[

]^{a,c}

However, there are important disadvantages of the distribution-free upper confidence bounds. First, the extreme order statistics generally tend to have high variance, so different sets of computer runs can give

very high upper confidence bounds. The variance of the estimator can be reduced by extending the sample size. The effect of the sample size on the variance of the estimator is discussed next.

30.3.1 Tolerance Intervals and Sample Size

The approach discussed in Section 30.3 is the so-called '*tolerance interval method*.' The procedure is used to determine an upper bound estimate of a given quantile of the population, say the 95th quantile Q_{95} . The k -th estimator/rank (Table 30-1) bounds the proportion $\gamma = 95\%$ of the population for the considered output variables []^{a,c} with at least $\beta = 95\%$ confidence.

Call this estimate $Q_{95/95}$. The procedure is known to be conservative (bounding) and the risk of excessively overestimating the fraction of the population of interest is very high, especially if the estimator is based on the extreme case, rank $k=1$.

[

] ^{a,c}

30.4 [

] ^{a,c}

[

] ^{a,c}

³ The approach described in this section to determine the []^{a,c} is superseded by limitation and condition #15 from the SER.

[

J^{a,c}

30.5 OVERVIEW OF FULL SPECTRUM LOCA STATISTICAL PROCEDURE

Sections 30.3 and 30.4 provided the theoretical basis for the various statistical procedures needed to:

1. Generate a representative sample of the LOCA scenarios population;
2. Analyze the results and infer figures of merit that can satisfy compliance with the 10 CFR 50.46 design criteria.

[

J^{a,c}

[

] ^{a,c}

⁴ The approach described in the following steps to determine the [
] ^{a,c} is superseded by limitation and condition #15 from the SER.

30.6 CONCLUSIONS ON COMPLIANCE WITH 10 CFR 50.46 ACCEPTANCE CRITERIA

The previous sections described the statistical theory used to determine the number of cases required to assure that there is a high probability that the first two acceptance criteria are met, consistent with the 10 CFR 50.46 requirements and Regulatory Guide 1.157 guidance. Further insights on the full compliance with the 10 CFR 50.46 criteria are described below.

30.6.1 []^{a,c}

[

] ^{a,c}

30.6.2 []^{a,c}

[

] ^{a,c}

[

] ^{a,c}

[

] ^{a,c}

30.7 REFERENCES

1. Boyack, B., et al., 1989, "Quantifying Reactor Safety Margins," NUREG/CR-5249.
2. Glaeser, H., et al., 2011, "BEMUSE Phase VI Report, Status report on the area, classification of the methods, conclusions and recommendations," NEA/CSNI/R(2011)4.
3. Guba, A., et al., 2003, "Statistical Aspects of Best Estimate Method-I," *Reliability Engineering and System Safety*, 80, pp. 217-232.
4. Nissley, M.E., et al., 2005, "Realistic Large Break LOCA Evaluation Methodology Using Automated Statistical Treatment of Uncertainty Method (ASTRUM)," WCAP-16009-P-A, Revision 0, and WCAP-16009-P-NP-A, Revision 0 (Non-Proprietary).
5. Press, W. H., et al., 1992, Numerical Recipes in FORTRAN: The Art of Scientific Computing, 2nd Edition, Cambridge University Press, Chapter 7.
6. Roe, J., 1998, "NRC Information Notice 98-29: Predicted Increase in Fuel Rod Cladding Oxidation."
7. Wald, A., 1943, "An Extension of Wilks' Method for Setting Tolerance Limits," *The Annals of Mathematical Statistics*, Vol. 14, pp. 45-55.
8. Wilks, S. S., 1941, "Determination of Sample Sizes for Setting Tolerance Limits," *The Annals of Mathematical Statistics*, Vol. 12, pp. 91-96.

a,c

Table 30-3 Generic Rod Power Census Used for Core-Wide Oxidation Assessment

a,c

31 FULL SPECTRUM LOCA DEMONSTRATION ANALYSIS

The nuclear power plant selected for the demonstration analysis of the FULL SPECTRUM LOCA (FSLOCA) methodology is Beaver Valley Unit 1 (DLW), a three-loop Westinghouse pressurized water reactor.

The development of the plant input model and input parameters were documented in Section 26. In Section 27, this plant model was exercised in the representative loss-of-coolant accident (LOCA) scenarios covering the full spectrum of break sizes to demonstrate that the dominant phenomena identified in the phenomena identification and ranking table (PIRT) (Section 2) were properly captured.

To perform a realistic (best-estimate) safety analysis for an emergency core coolant system (ECCS), the associated uncertainties in the physical models, experimental data and plant initial and boundary conditions needed to first be identified and assessed as outlined in Section 29. With regard to the treatment of the identified uncertainties, Section 30 introduces the approach to combine the identified uncertainties along with the technical basis for doing so.

In this section, the demonstration plant model is exercised using the WCOBRA/TRAC-TF2 code to demonstrate the FSLOCA analysis methodology.

31.1 DEVELOPMENT OF INITIAL MATRIX

As discussed in Section 30, a Monte Carlo simulation is to be carried out to combine the uncertainties and generate a representative sample of LOCA scenarios. The uncertainty attributes sampled include plant initial and boundary conditions and global and local model uncertainty variables (Section 29), and the plant response to a LOCA scenario is computed with the WCOBRA/TRAC-TF2 computer code.

[

] ^{a,c}

¹ [

] ^{a,c}

² The approach described in this paragraph and Section 30.4 of the topical report for Region II is superseded by limitation and condition #15 from the safety evaluation report (SER). However, since the demonstration analysis was executed prior to receipt of the limitations and conditions, the treatment of the Region II offsite power availability did not follow the approved method.

[

] ^{a,c}

Among all the uncertainty attributes, [

] ^{a,c}.

31.1.1 Break Area Ranges³

The break size is [

] ^{a,c}

31.1.2 Plant Operating Range

In Section 29, the uncertainty contributors or parameters that are explicitly considered in the FSLOCA evaluation model (EM) are listed in Tables 29-1 through 29-5. As discussed there, the uncertainty contributors are grouped as:

1. [] ^{a,c}, break type (DEG vs. Split), Split break area (Table 29-1)
2. Thermal-hydraulic (T/H) global models (Table 29-2)
3. Local models for the Dummy Rod (Tables 29-3a and 29-3b)
4. Power related uncertainty parameters (Table 29-4)
5. Initial and boundary conditions (Table 29-5)

Table 31.1-1 summarizes the plant operating range over which the uncertainty evaluation is to be performed for the demonstration plant.

[

] ^{a,c}

³ [

] ^{a,c}

[

] ^{a,c}

Table 31.1-1 Nominal and Uncertainty Range of Plant Specific Uncertainty Contributors			

] ^{a,c}

Table 31.1-2a []^{a,c}

a,c

Table 31.1-2b []^{a,c}

a,c

Table 31.1-2c []^{a,c}

a,c

Table 31.1-3 [] ^{a,c}		

a,c

a,c

Figure 31.1-1 Description of Break Area Regions

31.2 ANALYSIS EXECUTION

Section 30.5 outlines the statistical procedures used to:

1. Generate a representative sample of the LOCA population;
2. Analyze the results and infer figures of merit that address compliance with the Code of Federal Regulation (CFR) 10 CFR 50.46 design criteria.

The purpose of this section is to describe the generation of the LOCA database. The statistical analysis of the results and reporting relative to 10 CFR 50.46 acceptance criteria will be discussed in Section 31.5.

[

30.5.

] ^{a,c} discussed in Section

⁴ The approach described in this paragraph and Section 30.4 of the topical report for Region II is superseded by limitation and condition #15 from the safety evaluation report (SER). However, since the demonstration analysis was executed prior to receipt of the limitations and conditions, the treatment of the Region II offsite power availability did not follow the approved method.

31.2.1 [

] ^{a,c}

[

] ^{a,c}

a,c

Figure 31.2-1 [

] ^{a,c}

a,c

Figure 31.2-2 [

] ^{a,c}

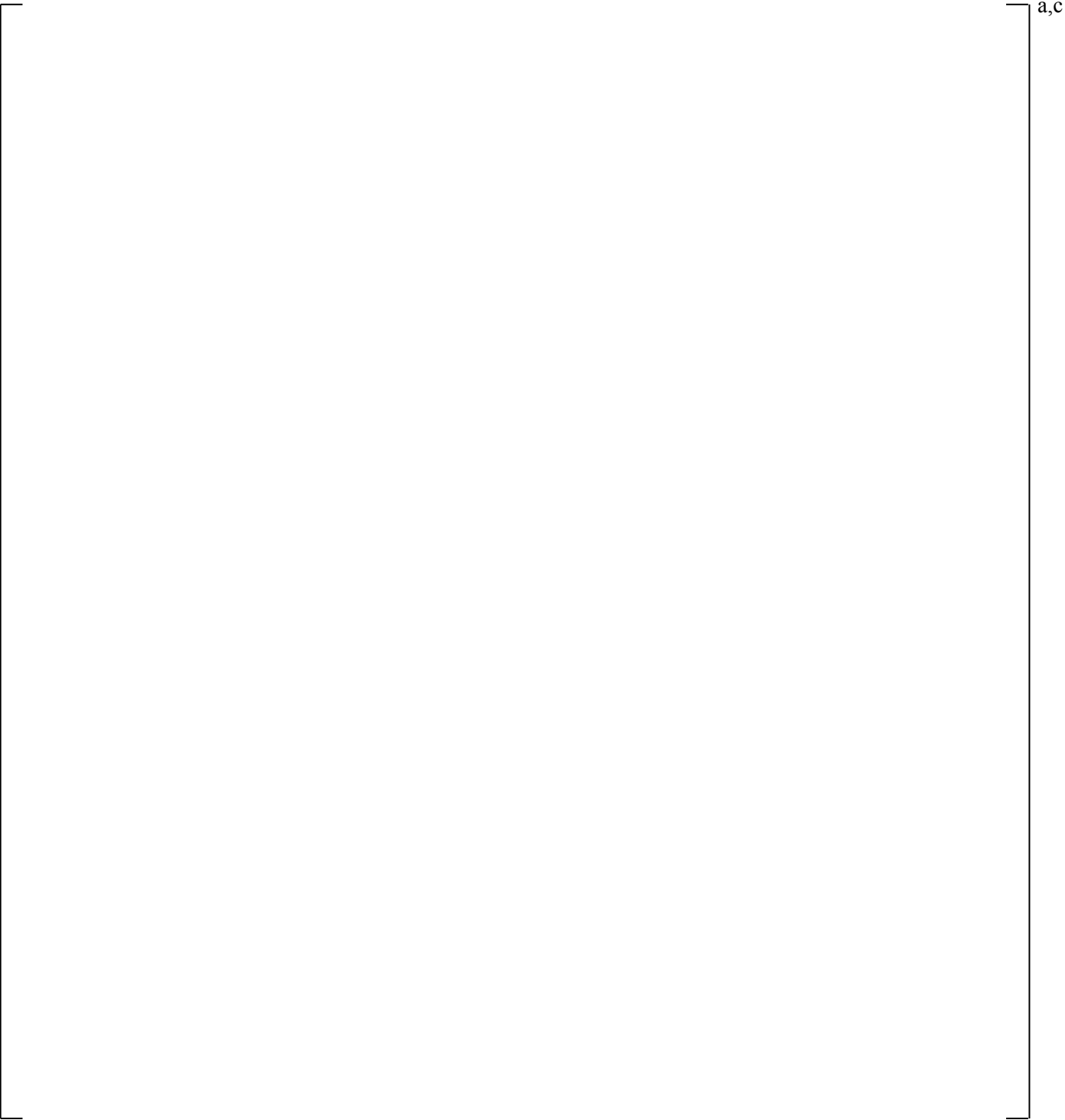


Figure 31.2-3 [

] ^{a,c}

a,c

Figure 31.2-4 [

] a,c

31.2.2 []^{a,c}

[

] ^{a,c}

Table 31.2-2a [] ^{a,c}	

a,c

Table 31.2-2b [] ^{a,c}	

a,c

⁵ The approach described in this section and Section 30.4 of the topical report for Region II is superseded by limitation and condition #15 from the safety evaluation report (SER). However, since the demonstration analysis was executed prior to receipt of the limitations and conditions, the treatment of the Region II offsite power availability did not follow the approved method.

31.2.3 Conclusion

The analysis shows that [

] ^{a,c} Details of the results are provided in Section 31.3.

[

] ^{a,c} Details of the results are provided in Section 31.4.

31.3 ANALYSIS OF RESULTS [] ^{a,c}

[

] ^{a,c}

The predicted PCTs for [] ^{a,c} are provided in Figure 31.3-1 as a function of

[

[

] ^{a,c}

(31-1)

The [

] ^{a,c}

⁶ [

] ^{a,c}

[]^{a,c} Tables 31.3-1a and 31.3-1b provide the uncertainty attributes
and the results for the []^{a,c}

Figure 31.3-3 shows the PCT sensitivity to []

[]^{a,c}

[

] ^{a,c}

a,c

Table 31.3-1a Uncertainty Attributes [] ^{a,c} (cont.)									

Table 31.3-1b Results for [] ^{a,c}									

Figure 31.3-1 [] ^{a,c}

a,c

Figure 31.3-2 [

] ^{a,c}

Figure 31.3-3 [

] a,c

a,c

Figure 31.3-4 [

] ^{a,c}

a,c

Figure 31.3-5 [

]^{a,c}

Figure 31.3-6 [

]^{a,c}

a,c

Figure 31.3-7 []^{a,c}

a,c

Figure 31.3-8 [

] ^{a,c}

a,c

Figure 31.3-9 [

]^{a,c}

Figure 31.3-10 [

]^{a,c}

a,c

Figure 31.3-11 [

] ^{a,c}

a,c

Figure 31.3-12 [

] ^{a,c}

Figure 31.3-13 [

] ^{a,c}

Figure 31.3-14 [

]^{a,c}

a,c

Figure 31.3-15 [

]^{a,c}

a,c

Figure 31.3-16 [**]**^{a,c}

a,c

Figure 31.3-17 [**] a,c**

a,c

Figure 31.3-18 [**]**^{a,c}

a,c

Figure 31.3-19 [**] ^{a,c}**

Figure 31.3-20 [

] ^{a,c}

Figure 31.3-21 [

] ^{a,c}

a,c

Figure 31.3-22 []^{a,c}

31.4 ANALYSIS OF RESULTS []^{a,c}

[

] ^{a,c}

Table 31.4-1a provides the uncertainty attributes for the 10 most limiting []^{a,c} while Table 31.4-1b shows the PCT and MLO results. Figure 31.4-1 shows the influence of the effective break area [

[

] ^{a,c} In the case of a DEG break,

] ^{a,c} Figure 31.4-4 shows the influence of [

] ^{a,c}

[]^{a,c} Appreciable transient oxidation is expected to occur only above approximately []

[]^{a,c}

Figure 31.4-8 shows the peak cladding temperatures []

[]^{a,c} Each case indicates rod quench has occurred by []^{a,c}
 A comparison of the []^{a,c} and the nominal DEG reference transient from Section 27.2.1 is provided in Figure 31.4-9, where the peak cladding temperature for the hot rod is shown []

[]^{a,c}

Section 30.3.1 discusses the concept of tolerance intervals and sample size in the context of order statistics, while Section 30.5 describes []

[]^{a,c} Figure 31.4-11 shows the upper bound predictor of the 95th quantile PCT with 95% confidence (95/95) []

[]^{a,c}

$\neg a, c$

Table 31.4-1a Uncertainty Attributes [] ^{a,c} (cont.)									

Table 31.4-1b Results [] ^{a,c}									

a,c

Figure 31.4-1 [

] ^{a,c}

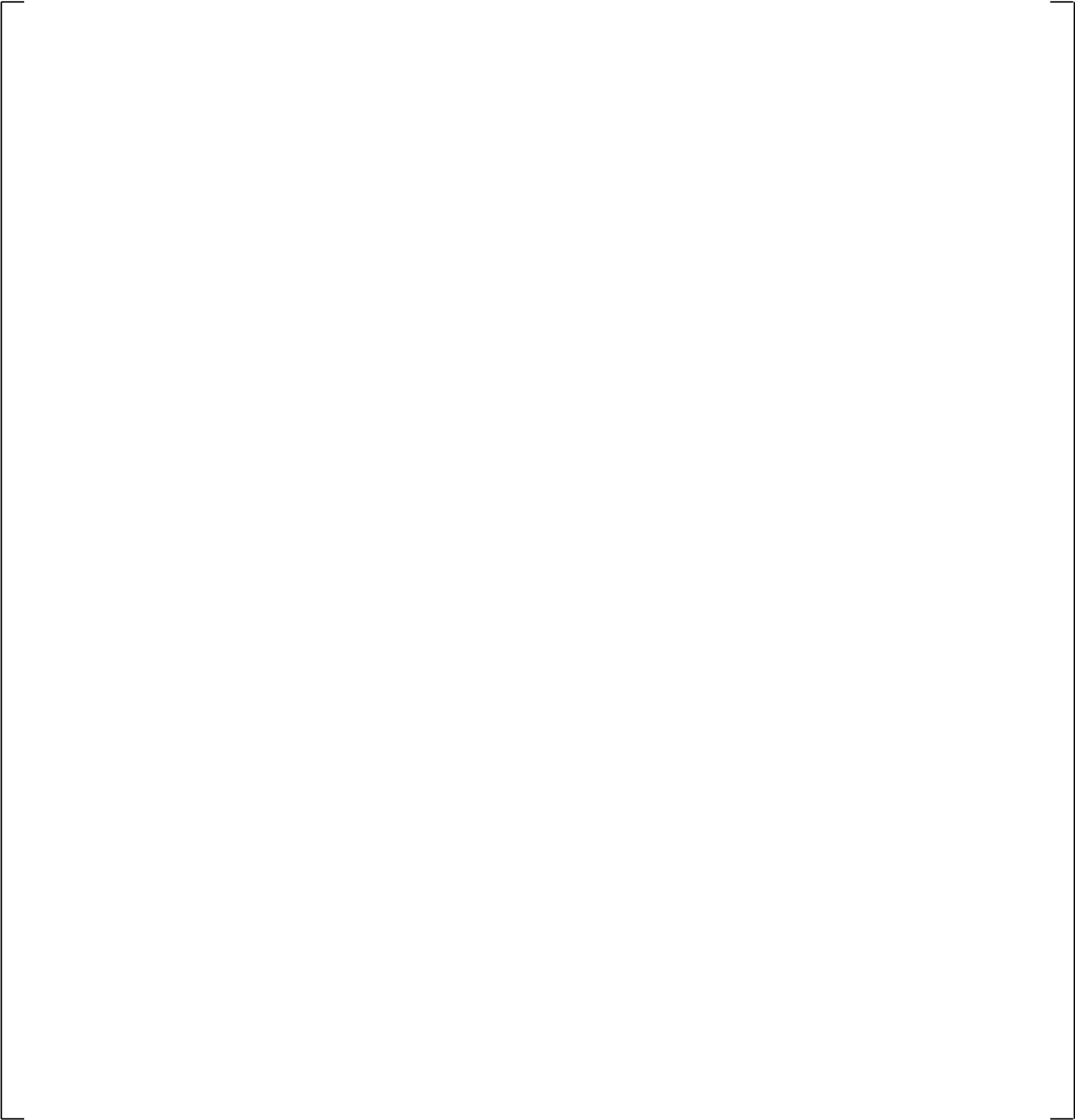


Figure 31.4-2 [

]^{a,c}

Figure 31.4-3 [

] ^{a,c}

a,c

Figure 31.4-4 [

] ^{a,c}

a,c

Figure 31.4-5 [

] a,c

a,c

Figure 31.4-6 [

]a,c

Figure 31.4-7 [

]^{a,c}

a,c

Figure 31.4-8 [

] ^{a,c}

a,c

Figure 31.4-9 [

] ^{a,c}

Figure 31.4-10 [

] ^{a,c}

a,c

Figure 31.4-11 [

] ^{a,c}

31.5 SUMMARY REPORT AND COMPLIANCE WITH 10 CFR 50.46 CRITERIA

The objective of the LOCA safety analysis is to provide upper bound values of PCT, MLO and core-wide oxidation (CWO) that can be directly compared against (b)(1), (b)(2) and (b)(3) of the 10 CFR 50.46 acceptance criteria. It is written that the “[...] *uncertainty must be accounted for, so that, when the calculated ECCS cooling performance is compared to the criteria set forth in paragraph (b) of this section, there is a high level of probability that the criteria would not be exceeded.*”

The method chosen to accomplish such objectives was discussed in Section 30.6. [

] ^{a,c}

As discussed in Section 30.6.2, [

] ^{a,c}

Table 31.5-1 [^{a,c}			

a,c

32 METHODOLOGY SUMMARY

In this section, the FULL SPECTRUM LOCA (FSLOCA) evaluation model (EM) is assessed against applicable regulatory criteria and guidance.

32.1 COMPLIANCE WITH 10 CFR 50.46

1. (i) – This part briefly outlines the requirements for an acceptable evaluation model, and requires that demonstration be provided that the limits of the Code of Federal Regulations (CFR) 10 CFR 50.46 be met with a high degree of probability. Additional details concerning these requirements are spelled out in Regulatory Guides (RG) 1.157 (US Nuclear Regulatory Commission (NRC), 1989) and 1.203 (US Nuclear Regulatory Commission, 2005). Compliance of the best-estimate methodology with these requirements is addressed in detail in the next section.
2. Peak Cladding Temperature – The peak cladding temperature (PCT) is verified to remain below the limit of 2,200°F for Loss-of-Coolant Accidents (LOCAs) of all break sizes, using the methods described in Section 30. A demonstrative application of the method is discussed in Section 31.
3. Maximum Cladding Oxidation – The maximum cladding oxidation (MLO) is verified to remain below the regulatory limit of 17 percent of cladding thickness, using the procedure described in Section 30. Consistent with NRC Information Notice 98-29 (Roe, 1998), MLO is taken as the sum of pre-accident oxidation and the oxidation occurring during the LOCA. A demonstrative application of the method is discussed in Section 31.
4. Maximum Hydrogen Generation – The hydrogen generated in the core, as determined by estimating the total volume of cladding oxidized for the limiting conditions, is verified to be less than the regulatory limit of 0.01 times the maximum theoretical amount, using the procedure described in Section 30. A demonstrative application of the method is discussed in Section 31.
5. Coolable Geometry – Westinghouse reload cores are analyzed using plant-specific or bounding seismic and LOCA loads to confirm that the core remains coolable during the LOCA. This acceptance criterion is met by compliance with acceptance criteria (b)(1), (b)(2), and (b)(3), and showing that grid deformation due to combined seismic and LOCA loads does not extend to the in-board assemblies. Specific calculations are performed if grid deformation occurs in the in-board assemblies to assess the effects of the grid deformation (Section 25.1).
6. Long-Term Cooling – Long-term cooling is dependent on the demonstration of continued delivery of cooling water to the core. The actions, automatic or manual, that are currently in place at these plants to maintain long-term cooling remain unchanged.

The NRC has initiated the formal process to revise the Emergency Core Cooling System (ECCS) acceptance criteria in § 50.46 via issuance of a proposed rule “Performance-Based Emergency Core Cooling Systems Cladding Acceptance Criteria” (FR Vol. 79, No. 56, March 2014), hereafter referred to as 10 CFR 50.46c rulemaking. In its current form, the FSLOCA EM shows compliance with the current 10 CFR 50.46 criteria. Changes to the method will be required to address the 10 CFR 50.46c rulemaking, with the expectation that the Maximum Cladding Oxidation criterion will be replaced with an allowable Equivalent Cladding Reacted (ECR) limit that is based on cladding hydrogen content (along with other considerations). While the present topical report does not address compliance with 10 CFR 50.46c, the analysis framework described in this topical report lends itself to showing eventual compliance with the future rule.

32.2 COMPLIANCE WITH REGULATORY GUIDE 1.203

The FULL SPECTRUM LOCA evaluation model has been developed consistently with RG 1.203 which represents an evolution and extension to the 1989 RG 1.157. RG 1.203 provides guidance on the Evaluation Model Development and Assessment Process (EMDAP). RG 1.203 extends on the regulatory positions of RG 1.157 which has been the basis of previously approved methodologies (2004 Automated Statistical Treatment of Uncertainty Method (ASTRUM) EM, Nissley et al., 2005 and 1996 Code Qualification Document (CQD) EM, Bajorek et al., 1998).

The EMDAP is the process utilized to define the function requirements of the EM, and to guide its assessment such that a decision on the EM adequacy for the purpose of LOCA safety analysis can be made. The EMDAP comprises 4 Elements and a total of 20 Steps which represent the Regulatory Position on the matter.

The mapping of the FSLOCA EM to the EMDAP was provided in Section 1.2. The purpose of this section is to summarize main conclusions relative to compliance with regulatory guide RG 1.203 and aspects of RG 1.157 that are not already considered in RG 1.203.

32.2.1 Regulatory Position 1, “Evaluation Model Development and Assessment Process”

The application envelope of the Westinghouse FULL SPECTRUM LOCA EM is defined in Sections 1 and 2. The scenario being addressed is a postulated loss-of-coolant accident that is initiated by an instantaneous rupture of a reactor coolant system (RCS) pipe in a Pressurized Water Reactor (PWR). The break type considered is either a double-ended guillotine, defined as a complete severance of the pipe resulting in unimpeded flow from either end, or a split break, defined as a partial tear. The break size considered for a split includes any break size such that break flow is beyond the capacity of the normal charging pumps up to and including the area of a double ended guillotine rupture with a break flow area two times the pipe area.

As far as the power plant class is concerned, the Phenomena Identification and Ranking Table (PIRT) developed in Section 2 is intended to be comprehensive and therefore to cover the same power plant class included in the previous methodology (ASTRUM), which included Westinghouse-designed 3- and 4-loop plants with ECCS injection into the cold legs, Westinghouse-designed 2-loop plants with upper plenum injection (UPI), and Combustion Engineering designs.

The FSLOCA EM development followed the EMDAP process of RG 1.203, and the mapping of the development roadmap and documentation to the elements of the EMDAP was provided in Section 1.2. The focus here is in addressing the “EM Adequacy Decision” – Regulatory Position 1.5 of RG 1.203.

Adequacy Decision

The adequacy decision is based on the final assessment of the WCOBRA/TRAC-TF2 code performance. The standard suggested in the Regulatory Position 1.5 was followed here. The High-ranked PIRT phenomena are reviewed in the following table. Some of the processes have been combined to ease the analysis.

For each item, the EM capability is assessed following these standards:

Excellent Agreement – Applies when the code exhibits no deficiencies in modeling a given behavior. Major and minor phenomena and trends are correctly predicted. The calculated results are judged to agree closely with data.

Reasonable Agreement – Applies when the code exhibits minor deficiencies. Overall, the code provides an acceptable prediction. All major trends and phenomena are predicted correctly. Differences between calculated values and data are greater than are deemed necessary for excellent agreement.

Minimal Agreement – Applies when the code exhibits significant deficiencies. Overall, the code provides a prediction that is not acceptable. Some major trends or phenomena are not predicted correctly, and some calculated values lie considerably outside the specified or inferred uncertainty bands of the data.

Insufficient Agreement – Applies when the code exhibits major deficiencies. The code provides an unacceptable prediction of the test data because major trends are not predicted correctly. Most calculated values lie outside the specified or inferred uncertainty bands of the data.

For high-ranked phenomena in PIRT, the standard for acceptability with respect to fidelity is generally “reasonable agreement.” Any phenomena whose assessment is in the Minimum Agreement or Insufficient Agreement category would require conservative treatment in the EM. A conservative treatment for phenomena whose assessments are in Reasonable agreement is sometimes selected when the effort of developing an uncertainty range is not justified.

The assessment summary of high PIRT ranked phenomena and models is tabulated below in Table 32-1. The order of the phenomena groups in the table follows the PIRT given in Table 2-1. In addition to the adequacy rating, the assessments are described, the main assessment findings are provided, and the uncertainty treatment for each phenomenon in the EM is shown.

Table 32-1 Summary of Assessment Results and Uncertainty Treatment for High PIRT Ranked Phenomena

a,c

**Table 32-1 Summary of Assessment Results and Uncertainty Treatment for High PIRT Ranked Phenomena
(cont.)**

a,c

**Table 32-1 Summary of Assessment Results and Uncertainty Treatment for High PIRT Ranked Phenomena
(cont.)**

a,c

**Table 32-1 Summary of Assessment Results and Uncertainty Treatment for High PIRT Ranked Phenomena
(cont.)**

a,c

**Table 32-1 Summary of Assessment Results and Uncertainty Treatment for High PIRT Ranked Phenomena
(cont.)**

a,c

**Table 32-1 Summary of Assessment Results and Uncertainty Treatment for High PIRT Ranked Phenomena
(cont.)**

a,c

**Table 32-1 Summary of Assessment Results and Uncertainty Treatment for High PIRT Ranked Phenomena
(cont.)**

a,c

**Table 32-1 Summary of Assessment Results and Uncertainty Treatment for High PIRT Ranked Phenomena
(cont.)**

a,c

Table 32-1 Summary of Assessment Results and Uncertainty Treatment for High PIRT Ranked Phenomena (cont.)

a,c

**Table 32-1 Summary of Assessment Results and Uncertainty Treatment for High PIRT Ranked Phenomena
(cont.)**

a,c

**Table 32-1 Summary of Assessment Results and Uncertainty Treatment for High PIRT Ranked Phenomena
(cont.)**

a,c

32.2.2 Regulatory Position 2, “Quality Assurance”

Westinghouse quality assurance (QA) procedures were followed for all aspects of methodology development related to documentation and review. User guidance was developed and cited in FSLOCA methodology related calculation notes, independent verification of all FSLOCA methodology related calculations notes was performed, and all records were archived in accordance with Westinghouse requirements. In addition, an independent and interdisciplinary design review team was convened five separate times over the course of the development and once during the licensing of the FSLOCA EM in order to review major components of the methodology and important decisions made during the methodology development.

32.2.3 Regulatory Position 3, “Documentation”

This document is intended to comply with the RG 1.203, Regulatory Position 3 which asks for “Proper documentation to allow appraisal of the EM application to the postulated scenario”. The documentation material is organized in three volumes whose content is summarized in Section 1.3. In the following, compliance with regulatory positions 3.1 through 3.7 is discussed.

Requirements

The FSLOCA EM functional requirements are presented in Section 2, Volume 1 and are consistent with Element 1 of the EMDAP.

Methodology

The computer code WCOBRA/TRAC-TF2 represents the engine of the FSLOCA EM and it is the only computational device. The uncertainty analysis methodology is [

] ^{a,c} Volume III documents the FSLOCA EM methodology. Section 25 is a compilation of the plant sources of uncertainty; Section 26 provides a detailed description of the WCOBRA/TRAC-TF2 model for selected PWRs. Sections 27 and 28 describe the simulation of selected reference transients for the PWRs for the purpose of justifying specific methodology decisions. The uncertainty contributors are then summarized and discussed in Section 29 while Section 30 outlines the methodology used to combine those uncertainties.

Computational Device Description Manuals

The purpose of Volume 1, particularly Sections 3 through 11, is to describe the modeling theory and associated numerical scheme and solution models. Section 3 provides a “Top-Down” review of the computational device (WCOBRA/TRAC-TF2) that starts with the presentation of the governing equations, the discretization and linearization of those equations and the numerical algorithm used to solve the set of equations. The following Sections (from 4 to 11) provide a “Bottom-Up” review of the closure relations, their pedigree, applicability and scalability.

User Manual and User Guidelines

The WCOBRA/TRAC-TF2 User's Manual is a separate document from this topical report. Guidelines on nodding and modeling strategy are discussed in Section 26, Volume 3 of this report for the purpose of ensuring consistency between the nodding scheme used to model the PWRs and that used for the experiments which are used for validation of physical models in the code. Reinforcing nodding consistency to the extent practical between the Separate Effects Tests (SETs), IETs and the PWR ensure that the same conclusions with respect to biases and uncertainties derived from the code and model assessments are applicable to the PWR LOCA simulations for which the EM was designed. Exceptions to the general nodding philosophy are discussed and justified on a case-by-case basis throughout the report.

Scaling Reports

Rather than providing a separate scaling report, scaling considerations are disseminated throughout this report. The scalability of models and correlations are discussed in Volume 1 as part of the "Bottom-Up" review as outlined here under the compliance to Regulatory Position 3.3. Scaling analyses used to support the viability of the experimental database are summarized within each section of Volume 2 (assessment report), for each test facility.

Assessment Reports

Volume 2 (Sections 12 through 24) can be seen as the "WCOBRA/TRAC-TF2 assessment report". Volume 2 discussed the assessment of the code against SETs, IETs and additional component assessments or thought problems. The content of Volume 2 is organized as discussed in Section 1.3. The intent of the assessment purposes (1)-(15) of Regulatory Position 3.6 has been followed. In particular Section 24 provides a compensating error analysis.

Uncertainty Analysis Reports

The FSLOCA EM uncertainty methodology is presented in Volume 3 which is organized as discussed before to comply with Regulatory Position 3.2.

32.2.4 Regulatory Position 4, "General Purpose Computer Programs"

The WCOBRA/TRAC-TF2 code used by Westinghouse for best-estimate LOCA analyses is an improved version of WCOBRA/TRAC which is used in Westinghouse's previously approved best-estimate LBLOCA methodology (or EM) as described in WCAP-16009-P-A (Nissley et al., 2005). The 1D Module of the code was replaced with TRAC-P []^{a,c} which is the basis of the current NRC audit tool TRACE. The models in WCOBRA/TRAC-TF2 are intended to provide realistic calculations of phenomena of importance to the behavior of a PWR during a LOCA transient. These models have been assessed using comparisons of code predictions from several experiments conducted in a number of separate effects test facilities, and three integral test facilities (ROSA, LOFT and CCTF) and full-scale separate effects test (UPTF). The code validation matrix was selected to cover the range of conditions expected during a PWR LOCA transient, to the extent practical. Uncertainty in the experimental data was considered in the overall uncertainty assessment.

32.2.5 Regulatory Position 5, “Graded Approach to Applying the EMDAP Process”

The FSLOCA EM is an evolution of the currently approved methodology (ASTRUM, Nissley et al., 2005); however, a graded approach to the EMDAP process was deemed not practical and justifiable in this case. The extent of the changes and the novelty of including Small Break LOCA scenarios required the application of the full EMDAP process.

32.3 COMPLIANCE WITH REGULATORY POSITION WITH RESPECT TO THE UNCERTAINTY METHODOLOGY

Regulatory Guide 1.203 focuses primarily on the code development and assessment process (EMDAP). Appendix A.3 of RG 1.203 essentially points back to RG 1.157 and the code scaling, applicability, and uncertainty (CSAU) approach as far as the preferred method utilized to combine the uncertainties. It is noted that original CSAU suggested the use of response surfaces as a means of combining uncertainties. However, potential disadvantages are discussed. It is recognized that response surface techniques are limited because of *“the dependency of the number of computer simulations on the number of phenomena or processes determined in the PIRT that may be needed to estimate the total uncertainty. That is, at least two “single parameter change” runs must be made for each required phenomenon or process. In addition, cross-product runs must be made when several of the phenomena or processes have significant covariance. The cross-product runs may involve change runs of two, three, or four parameters to adequately determine the effect of nonindependent phenomena or processes.”*

Such limitations were recognized during the development of the ASTRUM EM (Nissley et al., 2005), and resolved by replacing the response surface step with a direct Monte Carlo sampling of the uncertainty combined with a non-parametric order statistics technique to obtain a high probability statement for compliance with the 10 CFR 50.46 acceptance criteria. [

]^{a,c}

The following section addresses the regulatory positions of RG 1.157 specific to the uncertainty methodology.

32.3.1 Regulatory Position 4, “Estimation of Overall Calculational Uncertainty”

General

The Westinghouse approach to the overall calculational uncertainty has been to separate the uncertainty contributors into two general classifications; the code and models uncertainty contributors, and the plant conditions uncertainty contributors. Each uncertainty contributor is varied simultaneously in the calculations performed for the uncertainty analysis.

The code and models uncertainty contributors account for the uncertainty in predicting the important thermal-hydraulic phenomena identified in the PIRT, and important modeling assumptions. Controlling parameters of the important phenomena are ranged via use of multipliers. Each multiplier is characterized by a Cumulative Distribution Function (CDF) which represents the bias and uncertainty for the corresponding model. Development of the CDFs is discussed in Section 29. The CDFs were developed by performing a systematic assessment of the uncertainty associated with the code prediction relative to the

data. [

] ^{a,c}

The assessment of the thermal-hydraulic models in WCOBRA/TRAC-TF2 used a large number of test comparisons to ensure that estimates of the model uncertainties were well-founded, and included potential scaling effects. Models were grouped in some cases as a package when it was considered more meaningful to validate a specific model package against experiments. For example, the WCOBRA/TRAC-TF2 simulations of the FLECHT reflooding experiments in Sections 14 and 15 were used to validate many aspects of the heat transfer package, including specific heat transfer correlations, the prediction of the minimum film boiling temperature, the entrainment model, the heat flux split between evaporation and superheating, and calculated dispersed droplet flow behavior (drop sizes and velocities). The FLECHT and FLECHT-SEASET tests have sufficient independent sources of data that can be used to validate the computer code such that one is confident that the correct answer is being calculated for the correct reasons. A compensating error analysis is also provided in Section 24.

The plant conditions uncertainty contributors calculations account for the different possible operating conditions and accident initial conditions that the plant could experience. The plant specific sources of uncertainty are discussed in Section 25. Similar to the code model uncertainty contributors, some are explicitly ranged in the uncertainty methodology, others are bounded to ease the analysis when it is not practical or desirable to treat these conditions in a statistical fashion.

10 CFR 50.46 states that “[...] *uncertainty must be accounted for, so that, when the calculated ECCS cooling performance is compared to the criteria set forth in paragraph (b) of this section, there is a high level of probability that the criteria would not be exceeded.*” 10 CFR 50.46 does not explicitly specify how this probability should be evaluated or what its value should be. However, additional clarification as to the US NRC expectations on the acceptable implementation of the “high probability” requirement is provided in Regulatory Position 4.1 that states: “*a 95% probability is considered acceptable by the NRC staff [...]*”. Further, Regulatory Guide 1.157 introduced the concept of confidence level as a possible refinement to the uncertainty treatment, but did not expand further on this concept.

As statistical methods are implemented to perform LOCA safety analyses, a statistical statement which estimates or bounds the 95th quantile of the population with a 95% confidence level has been suggested by the NRC as acceptable to demonstrate the required “high probability.” In the previous approved methodology (ASTRUM, Nissley et al., 2005) the 95th quantile of the joint-distribution of PCT, MLO and core-wide oxidation (CWO) is bounded with at least 95% confidence level. [

] ^{a,c}

Code Uncertainty

The best test of the overall accuracy of the computer code, and the accuracy of individual models, is to compare code predictions to data obtained from a wide range of experiments. Wherever possible, tests performed at full scale or large scale should be used, to eliminate or minimize uncertainties associated with scalability. WCOBRA/TRAC-TF2 was used to simulate several different experiments that capture the same phenomena at different scales. The WCOBRA/TRAC-TF2 validation matrix includes tests with different bundle sizes, rod arrays, lengths, power shapes, and grid types, since the computer code will have to model these effects for different plant designs and conditions. Test rod bundles are prototypical of PWR fuel assemblies. Potential distortions induced by the apparatus and test geometry were addressed in the assessment. An assessment was made of the code's ability to predict PCT with varying power scales. For complex phenomena such as the ECC bypass the code was assessed against full scale data (UPTF test facility). In each case, the code predictions were shown to be conservative at full scale, or they reasonably predicted the phenomenon.

One measure of the accuracy of the code uses the comparisons of the predicted and measured PCTs and time-at-temperature. By selecting experiments with care and by comparing to data other than the measured cladding temperatures, it can be assured that the PCT and oxidation are reasonably predicted for the correct reasons. The possibility of compensating errors being present was investigated. It was concluded that while compensating errors do exist, the net effect is a conservative prediction of a PWR LOCA transient.

While the available integral effects tests are useful for addressing the issues of scalability and compensating errors, there are insufficient data to address the potential for propagation of uncertainties as a LOCA transient progresses. A detailed study of uncertainty propagation requires that the effects be quantified using computer code calculations of a PWR LOCA transient. [

] ^{a,c}

Other Sources of Uncertainty

Initial and Boundary Conditions and Equipment Availability

The treatment of important initial and boundary conditions, and assumptions of the availability of important equipment, are summarized below.

	a,c
--	-----



Fuel Behavior

Uncertainties in the lead fuel rod initial conditions and its behavior during the LOCA transient are explicitly accounted for. These uncertainties include hot rod peaking, initial fuel temperature, cladding burst temperature, burst strain, fuel density after burst due to relocation, and metal-water reaction rates. The treatment of fuel behavior in the Westinghouse methodology is considered to be more complete than that used in the CSAU methodology, in that [

] ^{a,c}

Other Variables

Uncertainties in decay heat and break flowrate are included in the overall uncertainty assessment. The metal-water reaction rate uncertainty is also considered as one of the fuel rod uncertainty parameters, as noted in the Regulatory Position 4.3.2 Compliance Discussion.

Statistical Treatment of Overall Computational Uncertainty

The overall calculational uncertainty statement is determined using a non-parametric statistical method. Uncertainties in [

] ^{a,c}

The FULL SPECTRUM LOCA methodology used by Westinghouse addresses the PCT, maximum cladding oxidation, maximum hydrogen generation, and coolable geometry criteria defined in 10 CFR 50.46(b)(1) through (b)(4). [

] ^{a,c} Coolable geometry is demonstrated by ensuring that the [] ^{a,c} criteria are satisfied, including any effects of combined LOCA and Safe-Shutdown Earthquake (SSE) loads on core geometry.

The Westinghouse methodology used to satisfy the long-term cooling criterion defined in 10 CFR 50.46(b)(5) is unaffected by the use of best-estimate techniques for the short-term transient calculation.

32.4 METHODOLOGY LIMITATIONS

The maximum assembly [

] ^{a,c}

The FULL SPECTRUM LOCA evaluation model cannot be applied for transient times longer than 10,000 seconds following shutdown unless the decay heat model is shown to be acceptable for the analyzed core conditions.

32.5 REFERENCES

1. Bajorek, S. M., et al., 1998, "Code Qualification Document for Best Estimate LOCA Analysis," WCAP-12945-P-A, Appendix C (Proprietary).
2. Nissley, M. E., et al., 2005, "Realistic Large Break LOCA Evaluation Methodology Using Automated Statistical Treatment of Uncertainty Method (ASTRUM)," WCAP-16009-P-A, Revision 0, and WCAP-16009-NP-A, Revision 0 (Non-Proprietary).
3. Roe, J., 1998, "NRC Information Notice 98-29: Predicted Increase in Fuel Rod Cladding Oxidation."
4. USNRC, 1989, "Best-Estimate Calculations of Emergency Core Cooling System Performance," Regulatory Guide 1.157.
5. USNRC, 2005, "Transient and Accident Analysis Methods," Regulatory Guide 1.203.